A PLANT-FRIENDLY MULTIVARIABLE SYSTEM IDENTIFICATION FRAMEWORK BASED ON IDENTIFICATION TEST MONITORING

by

Hyunjin Lee

A Dissertation Presented in Partial Fulfillment
of the Requirements for the Degree
Doctor of Philosophy

ARIZONA STATE UNIVERSITY

December 2006

A PLANT-FRIENDLY MULTIVARIABLE SYSTEM IDENTIFICATION FRAMEWORK BASED ON IDENTIFICATION TEST MONITORING

by

Hyunjin Lee

has been approved

December 2006

APPROVED:

_____, Chair

_____

_____

_____

_____

Supervisory Committee

ACCEPTED:

_____

Department Chair

_____

Dean, Division of Graduate Studies

ABSTRACT

Historically, model development for advanced process control applications has been a major consideration, demanding significant time and effort. The increased use of advanced control systems in industry creates a need for efficient methods for multivariable system identification that systematically refine process knowledge, leading to models that achieve desirable control performance. Moreover, time-varying changes and the aging of process equipment frequently demand model maintenance and control system tuning during the life of process operation. A comprehensive identification test monitoring procedure can aid in resolving this significant model development challenge.

This dissertation presents a plant-friendly identification framework, aimed at developing dynamic models for multivariable systems. The components of the framework include plant-friendly multisine input design, frequency response estimation, control-relevant parameter estimation, and robust loopshaping. These components are implemented in a plant-friendly manner to facilitate industrial implementation.

Deterministic, periodic multisine input signals are developed to perform plant-friendly experimental testing. A series of multisine design guidelines are derived based on *a priori* knowledge to generate a desirable input power spectral density. The use of constrained optimization enforces requirements on manipulated and controlled variables. A control-relevant parameter estimation procedure is formulated for curvefitting frequency responses generated from data into linear Matrix Fractional Description models with Model Predictive Control (MPC)-relevant weightings. The MPC-relevant weights emphasize closed-loop performance requirements in the curvefit. A set of models defined by the curvefitted model and uncertainty bounds are used in a robust loopshaping procedure, based on Structured Singular Value (μ) analysis. Robust stability and performance bounds are computed and used as criteria for defining model adequacy with respect to the end-use control application, and to decide when to halt or continue experimental testing.

The framework provides a viable tool for performing experimental testing and controller design of systems involving strong interaction, ill-conditioning, and gain-directionality considerations. The user can conduct identification experimental testing of multivariable systems displaying these challenges while meeting practical plant-friendliness considerations. A series of case studies involving distillation column control are presented to demonstrate the effectiveness of the integrated framework.

The Lord is my shepherd; I shall not want.

He maketh me to lie down in green pastures: he leadeth me beside the still waters.

He restoreth my soul: he leadeth me in the paths of righteousness for his name’s sake.

Psalms 23:1-3

ACKNOWLEDGMENTS

My graduate study at the Control Systems Engineering Lab (CSEL) has been very pleasant and enjoyable thanks to my advisor, Professor Daniel E. Rivera, who was always willing to give me advice on research and life. I arrived at the CSEL with little knowledge of system identification, but Dr. Rivera trained me and strengthened my background in system identification and process control, allowing me to accomplish the research in this dissertation. He always promoted new ideas, helped me fix problems, and was full of humor and insight. I would like to thank Professor Daniel E. Rivera for all he has done for me over the past five years.

I owe many thanks to Professor Hans D. Mittelmann in the Dept. of Mathematics and Statistics; his optimization expertise has proven a powerful resource for generating constrained multisine input signals. For my committee members, I would like to thank Drs. Mittelmann, Spanias, Lin, and Heys for their time and efforts spent reviewing my dissertation. For never-ending concern and encouragement, I would also like to thank Professor William E. Schiesser, my M.S. advisor at Lehigh University. His youthful life and scholastic attitude have reflected on my life since I met him in Bethlehem.

On a personal note, it was difficult to adjust myself to the desert weather here at Arizona State University. I missed snow, rain, and greenery; however, it was interesting to see giant palm trees, beautiful hummingbirds, and plentiful cactus on and around the ASU's Tempe campus. It was also a pleasure working with other CSEL members, including Wenlin Wang, Jay Schwartz, and Mike Pew. We shared ideas, jokes, and Matlab tips, and it was enjoyable running the snack bar inside the CSEL office. I would also like to thank Renate Mittelmann and Brint MacMillan for their computer expertise.

I cannot thank my wife, Youngmi, enough for her love and continuous support throughout my seven years as a graduate student at both ASU and Lehigh. I thank my sons Peter and Paul's patience for I have not had much time with them during my graduate studies. I would like to thank my mother and brother in South Korea for their encouragement and heartfelt prayers to God for me and my family.

Support for this dissertation research was provided by the ACS-PRF (Grant No. 37610-AC9), the Honeywell Foundation, and the Department of Chemical and Materials Engineering.

TABLE OF CONTENTS

Page

Page

Page

Page

LIST OF TABLES

Table Page

LIST OF FIGURES

Figure Page

Figure Page

Figure Page

CHAPTER 1

INTRODUCTION

1. Demands for System Identification and Control

In nature, we refer to dynamics as the subject that is concerned with variation in physiochemical properties with respect to spatiotemporal variables. As we observe the dynamics of a subject, a model presents a mirror of the real system that can simulate its dynamical behavior. A mathematical model can be defined as follows (Fasol and Jörgl, 1980): "the relationships between the physical variables in the system to be modeled are mapped onto mathematical forms like algebraic equations, differential equations or a set of differential equations." Systematic modeling is often required to describe a phenomenon of interest with improved understanding for the purposes of simulation, prediction, and control.

System identification is the field that considers how to build the dynamics of a system as a set of mathematical equations based on the observation of input and output data (Ljung, 1999). The types of system identification are usually classified into black, grey, and white-box methods by the level of dependence on physical prior knowledge of a system (Worden *et al.*, 2006). White-box models are completely described by prior knowledge and physical insight, i.e., they are also referred to as first principles models. Grey-box models are obtained when less physical insight is available and fall into two cases: physical models and semi-physical models. The former models occur when prior knowledge is sufficient to develop a model but is insufficient to provide values of the model parameters and these must be estimated from data. The latter

models occur when prior knowledge is only sufficient to provide which nonlinear combinations of measured data will be relevant for the system; these nonlinear structures are then used in a black-box model. Black-box models are obtained in the absence of prior physical knowledge or insight, and they are completely developed from the measured input and output data.

Many systems are often derived using the laws of conservation, i.e., first principles method, such as mass, energy, and momentum balance equations. However, the first principles method would not be very suitable for use in automatic control in many cases. These models may be inadequate when exposed to real process environment involving noise, disturbances, nonlinearities, or time-varying parameters. Therefore, models with higher fidelity can be built based on the observed input and output data, i.e., black-box models, that are obtained by judicious application of a system identification procedure (Ljung, 1999).

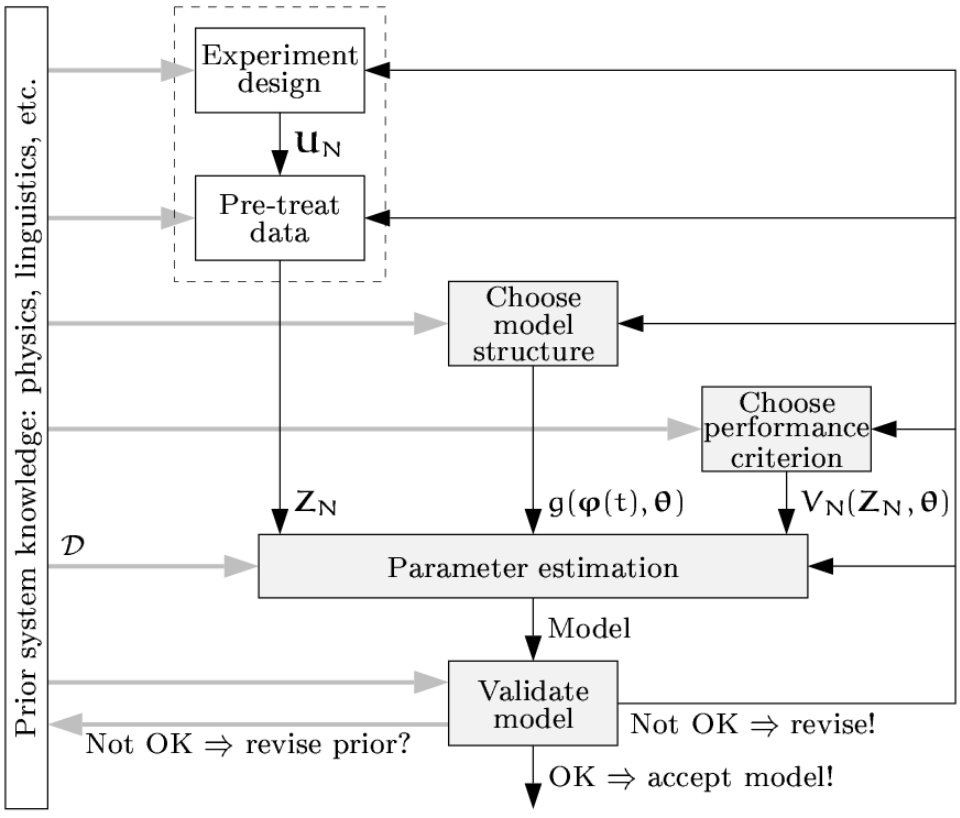

Figure 1. System identification Loop from Lindskog (1996b)

The construction of a mathematical model via system identification methodology requires several basic components: experimental testing to obtain an input/output dataset, model structure selection, parameter estimation, and model validation (Ljung, 1999). A schematic representation of system identification is illustrated in Figure 1 (Lindskog, 1996*b*). The details of the identification components are briefly summarized as follows (Ljung, 1999; Lindskog, 1996*a*; Lindskog, 1996*b*):

- *Experiment Design, Execution, and Data Pre-treatment*

  The first question is concerned with how users can perform an input signal design and implement it to achieve experimental testing of an unknown system to be identified. *A priori* information of a system can guide users to choose design variables for inputs that can meet information-theoretic requirements depending on the dynamics of the system. Common input signals for identification experiments include the double pulse, random binary sequence (RBS), pseudo random binary sequence (PRBS), multi-level pseudo random sequence (MPRS), and multi-sinusoidal sequence. PRS and MPRS signals are discussed in detail in Godfrey (1993) and multisine signal will be extensively examined in this dissertation. Both inputs and outputs to be measured are stored in a dataset with suitable sampling techniques during the experimental testing. If necessary, pre-treatment such as detrending, filtering, or removing outliers can be accomplished for subsequent system identification analysis.

- *Model Structure Selection*

  Physicochemical and mathematical intuition or theoretical assumptions could help users select appropriate model structures. Model structure selection involves making an initial guess and iterating based on validation measures. The general task of choosing a model structure consists of two sub-problems: (1) the type of model set, i.e., the user decides either linear or nonlinear structures among black, grey, and white-box approaches, and (2) the dimension of the model set, i.e., the user considers a number of possible variables for the model.

- *Performance Criterion*

  Some goodness-of-fit measure needs to be specified in order to determine the accuracy of model parameters. Measured and model outputs are never matched perfectly in practice, and errors always exist in the models. The sources of model error can fall into two categories: variance and bias. Variance is an error component that arises from noise influence on the measurement and system. This kind of error is not reproducible even with the same input signals, but variance error can be reduced by using multiple testing cycles. On the other hand, bias is systematic error caused by incorrect choice of model structure, an inaccurate parameter set, insufficient input signal power, or mode of operation (e.g., open versus closed-loop). The bias error makes the model unable to represent the system, even if noise is not present in a system. A primary goal of system identification is to reduce errors between models and true systems. However, a "good enough" criterion is often used to determine the model accuracy for users' purposes.

- *Parameter Estimation*

  In parameter estimation, a numerical estimation algorithm, which is usually some forms of regression, is used to obtain model parameters. This involves minimizing an objective function to find the best parameters within a selected model structure. A variety of numerical algorithms are available depending on the model structures and variable dimensions. As indicated in Figure 1, this task is quite iterative until a model estimate can meet the given performance criterion.

- *Validation*

  In general, model quality is evaluated on the ability of the model to reproduce the dynamics of the system. However, model adequacy is largely determined on the basis of the model adequacy to intended applications, i.e., simulation, prediction, or control system design. This is called a validation step, the last step in system identification. A sensible solution is to evaluate the model with all available kinds

of information, e.g., prior knowledge, experimental data, control performance, and experience with the model (Lindskog, 1996*b*). For an improved comparison between model prediction and measured output, it is desirable to use fresh experiment data that are not previously used for estimation; this is called cross-validation. It is also worthwhile to investigate the cross correlation between the residue and input sequences. This level of cross correlation should be small; otherwise the residual sequence still possesses more model information in the output, indicating that there are still unmodeled dynamics present in the residuals. Moreover, the model can also be evaluated in a closed-loop feedback control system to check whether the setpoint tracking or disturbance rejection response meets desired control requirements.

If the model is not acceptable, some or all of the identification steps may have to be re-evaluated; in the worst case one must start from the very beginning and collect new data.

Today, all advanced process control techniques utilize mathematical models as the basis for configuring a control system to achieve required performance. As a consequence, there is a tremendous need to use system identification to improve the model efficiency and performance in the advanced control applications (Zhu, 2006). Unfortunately, the task of system identification often turns into a major hurdle in the implementation of modern process control systems (Andersen and Kümmel, 1992; Hussain, 1999). To identify an ethylene furnace at Mitsubishi Chemicals characterized by 17 independent variables and a six hour settling time, the guideline of a major control software firm suggested nearly a month (25.5 days) of identification testing (Rivera *et al.*, 2003). In another example, Kothare and Mandler (2003) indicate that a large air separation unit involves 2 months of model testing. Mathur and Conroy (2002) mention a case where the total costs of step testing (taking into account reductions in throughput, off-spec product, and engineering time) were estimated at $270,000. It is therefore no surprise that Hussain (1999) reports that model development represents 75% of the cost of developing advanced process control designs.

The difficulty of system identification increases significantly when considering multivariable sys-

tems. For a single-input, single-output (SISO) system, an identification procedure is relatively straightforward to build a model for the use in control design. However, in a multi-input, multi-output (MIMO) process, identification involves an increased work load for engineers to achieve informative testing experiments and to generate effective models. Multiple input channels normally require longer input signal lengths to reduce the correlation between input channels because the presence of input cross correlation reduces the identifiability of a system from the data. Furthermore, strong ill-conditioning and interaction may exist in multivariable processes that make it harder to estimate accurate gain directionality from the input/output data (Andersen and Kümmel, 1992; Koung and MacGregor, 1993; Varga and Jørgensen, 1994). The precise estimation of gain directionality cannot be easily achieved by the conventional input signal designs. Most dynamic processes have nonlinearities that directly increase the difficulty of the tasks in system identification and control system design. Nonlinearity increases complexity in model structure and parameter estimation, and as a consequence control system design involves more time and effort (Pearson and Ogunnaike, 1997). External factors also impact system identification, e.g., noise and disturbances from measurement, sensors, electric interference, mechanical devices, fluid flow fluctuation, and so forth (Ljung, 1999; Ljung and Glad, 1994).

Multivariable control systems have steadily demanded a comprehensive system identification tool effective for large-scale dynamic systems that can be easily accessible to the chemical process industries. Even the most advanced control scheme such as Model Predictive Control (MPC) might fail without an adequate model — MPC is an optimization-based controller that computes a prediction of model estimate and takes appropriate control actions required to drive the predicted output as close as possible to the desired target value (Ogunnaike and Ray, 1994). Morari and Lee (1999) point out that “what limits the performance and applicability of MPC are not the deficiencies of the control algorithm, but difficulties in modeling, sensing, state estimation, fault detection/diagnosis, etc.” Namely, modeling can be stated as the most critical and time-consuming step in implementing a model-based controller with suitable degrees of control-relevance

and robustness (Andersen and Kümmel, 1992; Hussain, 1999; Zhu, 2006).

Historically, significant efforts have been made towards integrating system identification with control design to improve model adequacy for control system applications; this is called control-relevant identification. Two classifications can be given to this methodology: quantification of the model error and identification of a suitable nominal model (Van den Hof and Schrama, 1995). The former focuses on robust control consideration and the latter on achieving desired levels of control performance. Classical system identification emphasizes an open-loop fit to data via least-squares estimation and cross validation, while control design focuses on regulating the controlled variables of a system. Although control-relevant system identification has received significant attention for the last several decades as a novel approach in the realm of control applications (Gaikwad and Rivera, 1996; Hjalmarsson, 2005; Bayard, 1994; Callafon *et al.*, 1996), it still requires a consistent tool to perform informative experimental testing for multivariable systems.

For effective identification of multivariable systems, a systematic yet informative input design procedure is required for simultaneous input perturbations of potentially short test duration. Perturbing input channels *one at a time* can be applied for the estimation of individual transfer functions in MIMO systems. When applied to large dimensional processes, this single-input, multi-output (SIMO) method increases test duration tremendously, proportional to the number of input channels. Therefore, effective yet economical testing signals are significantly demanded for multivariable model development procedures (Rivera *et al.*, 2003; Zhu, 2006).

Another important practical concern is plant-friendliness, which has been considered in system identification methods that can meet the need for informative experiments and minimize extensive and disruptive identification testing (Braun *et al.*, 2002*b*; Rivera *et al.*, 2003). Although pseudo random binary signals (PRBS) have been broadly used as input signals for identification testing, multisine input signals provide a more flexible and powerful design alternative for generating plant-friendly multivariable input signals (Schroeder, 1970; Guillaume *et al.*, 1991; Braun *et al.*, 2002*b*) based on *a priori* process information. It is

interesting to note that for most practitioners, achieving plant-friendliness in the process output enables users to run identification testing at normal process operating conditions while maintaining product quality. Plant-friendly system identification has, therefore, received increasing attention as a critical consideration that can save money and time in control system commissioning. Ultimately, a plant-friendly identification test will produce data leading to a suitable model within an acceptable time period while keeping the variation in both input and output signals within user-defined constraints (Rivera *et al.,* 2003; Braun *et al.*, 2002*b*). A few items that represent plant-friendly identification requirements are listed here:

- keeping output deviations low to minimize variability in product quality,
- implementing a signal of sufficiently short duration to minimize the amount of off-spec product and reduce engineering time associated with an identification test, and
- keeping move sizes small to satisfy actuator limits and minimize "wear and tear" on process equipment.

At this point, one might ask *"Why do we need to design and implement an identification test monitoring framework encompassing experimental testing to control system design?"* The answer becomes much clearer when one considers the large-scale systems commonly found in the chemical or petroleum refinery industries, which can be summarized as:

- testing duration increases significantly, proportional to the number of manipulated (input) variables in the process,
- strong interaction and gain directionality problems might occur in multivariable processes, increasing difficulty in modeling and making traditional experimental testing less useful,
- the nature of the tasks is iterative among experimental testing, model estimation, and control system implementation; ways to reduce the extent of those iterations are beneficial,

- it is useful to apply refined model knowledge from one experiment design to the next, or from one identification analysis to the next, by relying on the insights and model information gained from the previous identification analysis, and
- the use of periodic signals such as multisines offers the opportunity to monitor model quality on line using appropriate modeling and control system analysis tools after each cycle.

Zhu (2006) recently described an example where the test duration for process identification of the crude unit is dramatically reduced from 30 days to 4.5 days using a suitable test monitoring scenario, producing an adequate model representation for Model Predictive Control (MPC) applications.

In this dissertation, we present a comprehensive system identification framework to produce accurate yet robust model estimates for complex multivariable systems. The resultant models should be suitable for advanced control system designs with appropriate control relevance and robust stability and performance, while reducing time-consuming effort and achieving plant-friendliness during the identification testing procedure. Therefore, the proposed identification test monitoring framework is intended as a means to reduce the bottleneck that dynamic modeling currently presents to advanced control implementation.

2. Identification Test Monitoring Overview

In this dissertation, a plant-friendly multivariable system identification framework is developed that implements a systematic identification test monitoring procedure and control-relevant identification methodology. The general scheme of the identification test monitoring is outlined in Figure 2. The identification test monitoring procedure incorporates the steps of input signal design, control-relevant parameter estimation, and robust loopshaping interactively refining process knowledge during multivariable system identification. A systematic procedure is also demanded so that it can intelligently utilize the identification methods and *a priori* knowledge of a system. The essential role of “identification test monitoring” can be described as

a central unit that controls the flow of arrows in Figure 2, connecting appropriate blocks of identification methods.

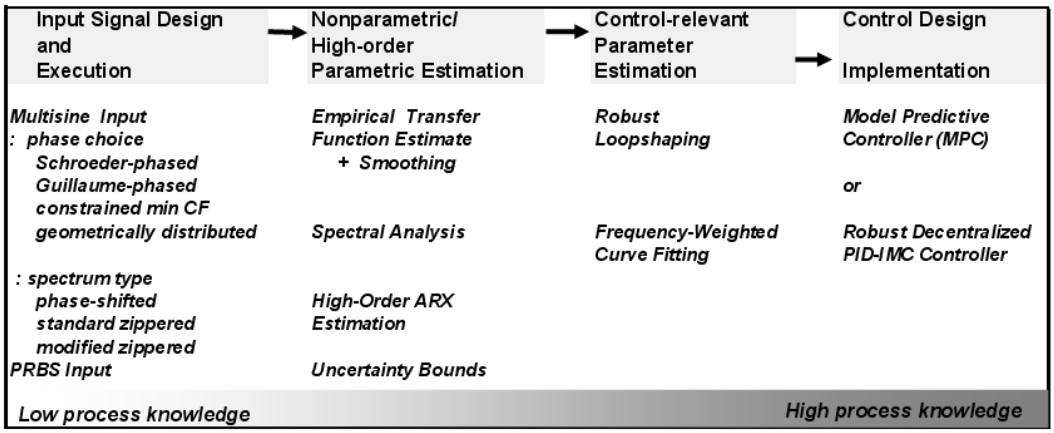

Figure 2. General scheme of the system identification test monitoring procedure developed in this dissertation

The framework is designed for both SISO and MIMO systems; however, the discussion of the effectiveness of the framework will focus on MIMO systems involving strong interaction and gain-directionality issues. The following components are presented as the principal contributions of this dissertation:

1. Design guidelines for multisine and PRBS input signals for multivariable systems, with an emphasis on strongly interactive systems.

2. Plant-friendly identification test formulations based on constrained optimization techniques.

3. Multivariable frequency response and model uncertainty estimation procedures in support of the signals in Item 1.

4. Control-relevant parameter estimation by weighted frequency response curvefitting, in support of the signals in Item 1 and frequency responses in Item 3.

5. Robust loopshaping analysis that determines model adequacy by computing robust stability and performance conditions during identification testing.

These contributions are summarized in the following subsections.

2.1. Design Guidelines for Multisine Input Signals. The use of multisine signals for multivariable systems is developed as test input signals in this dissertation. A multisine input signal is deterministic and periodic in nature, consists of multiple harmonics of sinusoids, and can be represented by the following equation $u_j(k)$ for the *j*-th channel of a multivariable system with *m* inputs

$$\begin{aligned} u_j(k) &= \sum_{i=1}^{m\delta} \hat{\delta}_{ji} \cos(\omega_i kT + \phi_{ji}^{\delta}) + \lambda_j \sum_{i=m\delta+1}^{m(\delta+n_s)} \sqrt{2\alpha_{ji}} \cos(\omega_i kT + \phi_{ji}) \\ &\quad + \sum_{i=m(\delta+n_s)+1}^{m(\delta+n_s+n_a)} \hat{a}_{ji} \cos(\omega_i kT + \phi_{ji}^{a}) \qquad j = 1, \cdots, m \end{aligned} \tag{1.1}$$

T is the sampling time, N_s is the sequence length, m is the number of channels, δ, n_s, n_a are the number of sinusoids per channel ($m(\delta + n_s + n_a) = N_s/2$), $\phi_{ji}^{\delta}, \phi_{ji}, \phi_{ji}^{a}$ are the phase angles, $\lambda_j\sqrt{2\alpha_{ji}}$ represents the Fourier coefficients defined by the user, $\hat{\delta}_{ji}, \hat{a}_{ji}$ are the "snow effect" Fourier coefficients (Guillaume *et al.*, 1991), and $\omega_i = 2\pi i/N_s T$ is the frequency grid. Design parameters such as the sampling time, number of sinusoids, and sequence length are determined based on *a priori* knowledge such as dominant time-constants and speed of response requirements.

Rivera *et al.* (1997) introduce the standard "zippered" power spectrum design where Fourier coefficients for each channel are defined independently over unique frequency grids of interest. The resulting orthogonal multi-frequency signal can be introduced to all channels of the plant to be identified with simultaneous perturbations. In this dissertation, a *modified zippered* power spectrum is specially designed to enhance gain-directionality information in the data. The effective use of modified zippered signals for highly interactive systems is presented.

A phase-shift method is also developed for multisine input signal design. Shorter test duration is usually obtained with these signals since a "zippered" power spectrum design increases the sequence length in proportion to the number of channels. Phase-shifted multisine signals instead share the same frequency

grids using a delay between channels to keep the cross-correlation between signals low enough for model estimation. A comprehensive comparison between shifted and zippered multisine and PRBS input signals is presented in this dissertation. Harmonic suppression is included in the multivariable multisine input signal design procedure to reduce the effects of nonlinear distortion that may exist in nonlinear processes. A harmonically suppressed multisine signal excites the system with limited frequency-dependent dynamics, while the dynamics corresponding to the frequencies of suppressed harmonics are removed in the outputs.

2.2. Plant-Friendly Identification based on Constrained Optimization. It is important in input design to tailor identification testing to be benign to process operating conditions and product quality. These considerations might be in opposition to theoretical requirements associated with consistent estimation (Ljung, 1999). Nonetheless, it is very practical and desirable in the process industries since plant-friendliness refers to preserving the product quality and reducing wear and tear of process equipment. As a result, informative yet plant-friendly system identification formulation is strongly demanded so that extensive or disruptive identification testing is discouraged (Parker *et al.*, 2001; Doyle *et al.*, 1999; Braun *et al.*, 2002*b*).

One measure that has been studied in the context of plant-friendliness is the crest factor (*CF*) (Schroeder, 1970; Guillaume *et al.*, 1991; Godfrey, 1993). The crest factor, defined as the ratio of the ℓ_∞ (or Chebyshev) norm and the ℓ_2-norm of a signal,

$$CF(u) = \frac{\ell_\infty(u)}{\ell_2(u)}, \qquad \ell_p(u) = \left[\frac{1}{N_s}\int_0^{N_s} |x(t)|^p dt\right]^{\frac{1}{p}} \tag{1.2}$$

provides a measure of how well distributed the signal values are over the input span. Lowering crest factor can significantly improve the signal-to-noise ratio of the resulting signal, contributing to plant-friendliness during experimental testing (Rivera *et al.*, 2003). This is illustrated in Figure 3, which shows the difference of the crest factor with time-domain sequences that have the identical power spectral density in the frequency-domain. In particular, minimizing the output crest factor while enforcing input and output con-

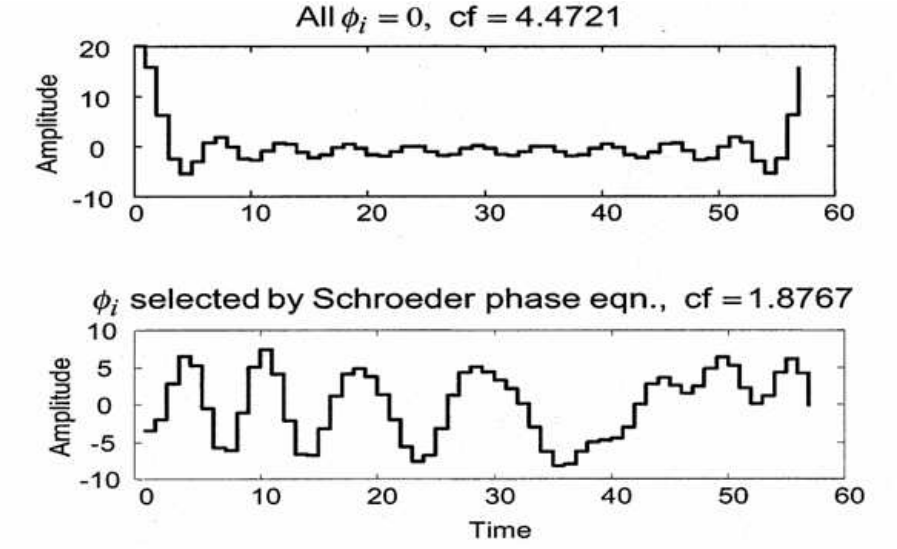

Figure 3. Example of a multisine signal design with equivalent power spectra but different phases, leading to different crest factors, Top: signal with all phases =0 (CF=4.4721) and Bottom: signal with phases per Schroeder equation (CF=1.8767)

straints during identification testing is of great value in the process industries. The nature of the output signal will usually have the most influence on product quality and hence profitability within the enterprise.

The use of powerful constrained optimization techniques is employed in this work to insure that the multisine signals are conducive to "plant-friendliness." A series of optimization problems are proposed which seek to find the optimal phases in the multisine signal (and additionally, the Fourier coefficients in frequency bandwidth not specified by the user, called the "snow effect" (Guillaume *et al.*, 1991)) that directly minimize the crest factor. If the user has some reasonable *a priori* knowledge of model parameters (or, more realistically, develops improved knowledge of the model through identification testing), the crest factor of the output signal anticipated during identification testing can be minimized as well (Braun *et al.*, 2002*b*; Guillaume *et al.*, 1991). In addition, constraints on the inputs and outputs meaningful for engineering practice can be enforced while minimizing the crest factor of input and/or output signals, or for example, move size and high/low limits on the inputs,

$$|\Delta u_j(k)| \leq \Delta u_j^{max} \quad \forall\, k, j \tag{1.3}$$

$$u_j^{min} \leq u_j(k) \leq u_j^{max} \quad \forall\, k, j \tag{1.4}$$

and rate-of-change and high/low limits on the outputs,

$$|\Delta y_i(k)| \leq \Delta y_i^{max} \quad \forall\, k, i \tag{1.5}$$

$$y_i^{min} \leq y_i(k) \leq y_i^{max} \quad \forall\, k, i \tag{1.6}$$

Such constrained multisine input signals prompt interesting challenges with the flexible multisine design interface to constrained optimization problems. The optimization problem is solved using a state-of-the-art Nonlinear Programming (NLP) solver (KNITRO 3.1), which uses an interior-point trust-region method and employs Successive Quadratic Programming (SQP) techniques for the barrier sub-problems.

2.3. Control-Relevant Parameter Estimation. In the last few decades, the topic of control-relevant identification has been studied extensively and accepted as an effective tool for estimating adequate nominal models for controller design (Gaikwad and Rivera, 1996; Hjalmarsson, 2005; Bayard, 1994; Callafon *et al.*, 1996). Identifying a suitable nominal model and quantification of model uncertainty bounds are the basic components of a modern control-relevant identification paradigm (Van den Hof and Schrama, 1995). The latter approach is intended to provide a more suitable model for feedback control applications, possibly at a cost of compromising the open-loop goodness-of-fit.

In this dissertation, a weighted curvefitting procedure is developed for approximating frequency response into Matrix Fraction Description (MFD) models (Bayard, 1994; Callafon *et al.*, 1996; Gaikwad and Rivera, 1996). The weights determine the frequency bandwidth of importance to the control problem, and an adequate model is estimated in this range. Using the frequency responses and input/output data, additive model uncertainty descriptions are derived and are applicable for robust control system design.

2.4. Robust Loopshaping with Uncertainty Estimation. Lastly, an effective decision scheme on model adequacy is required to halt or continue experimental testing for identification. Robust loopshaping

is used as a decision tool that involves a series of transfer functions matrices to compute the robust stability and performance conditions (Morari and Zafiriou, 1988). The robustly bounded conditions are determined numerically, relying on structured singular value analysis (Morari and Zafiriou, 1988).

Instead of a single model representation, a set of models defined by a nominal model estimate and its uncertainty description are considered in robust loopshaping. Based on frequency responses ($\tilde{P}$), uncertainty norm (Δ) bounds are estimated by the use of statistical data analysis methods. A single, control-relevant nominal model ($\hat{P}$) is curvefitted from the frequency responses ($\tilde{P}$). A series of Linear Fractional Transformation (LFT) matrices are formulated based on a parametric model ($\hat{P}$), model error ($E_m = (\tilde{P} - \hat{P})\hat{P}^{-1}$)), uncertainty norm ($\Delta$) bounds, and controller transfer function as well as performance weights. As a result, we can decide whether the model adequacy for control is suitable enough to halt or continue the experiment testing.

The iterative evaluation and refinement of identification signals is systematically achieved by the identification test monitoring procedure, which is counter to the *ad hoc* nature of current industrial practice. The tendency in current practice is to collect and analyze data in one batch in order to determine (after pursuing the complete identification cycle) if the data is adequate. This results in costly re-testing and requires significant user intervention and effort. However, a systematic test monitoring approach with the use of periodic input signals allows the opportunity to improve experimental testing without having to perform a full comprehensive analysis of a set of data.

3. Importance of Identification Test Monitoring to Highly Interactive Systems

Identifying multivariable systems has been a challenging issue in the realm of system identification and control applications. If strong interaction and ill-conditioning exists in a multivariable system, conventional open-loop identification tests might result in a poor model estimate particularly under noisy

conditions (Andersen and Kümmel, 1992; Koung and MacGregor, 1993; Varga and Jørgensen, 1994). Since most chemical industry processes consist of multiple inputs and outputs and are nonlinear, a multivariable system identification tool that can address the challenges of ill-conditioning, interaction, and nonlinearity under noisy conditions for a reasonable test duration is highly desirable. A number of highly interactive processes will be considered as examples and case studies of the integrated framework of identification test monitoring developed in this dissertation.

What is the physical limitation in highly-interactive systems? Different from SISO systems, MIMO systems may exhibit ill conditioning and be highly interactive, which is manifested in models displaying large condition numbers and relative gain array (RGA) values (Morari and Zafiriou, 1988; Andersen and Kümmel, 1992). Highly interactive processes naturally respond in the high-gain direction, which makes it very difficult to obtain information in the low-gain direction using conventional open-loop identification tests (Andersen and Kümmel, 1992; Koung and MacGregor, 1993; Varga and Jørgensen, 1994; Chou *et al.*, 2000). Inaccurate gain directionality in the model estimates imposes significant limitations in closed-loop control performance (Andersen and Kümmel, 1992; Jacobsen, 1994; Chien and Ogunnaike, 1992; Varga and Jørgensen, 1994; Morari and Lee, 1999).

When systems are highly interactive, it is not easy to change a specified output independently; changing one controlled variable causes others to change in the principal direction as well. Moving controlled variables in the high-gain direction is very easy; however, moving them in the low-gain direction is very difficult. An illustrative example of ill-conditioning and gain direction is stated in Chapter 3 of Skogestad and Postlethwaite (1996):

Example 1.1 ***Shopping cart.*** *Consider a shopping cart (supermarket trolley) with fixed wheels which we may want to move in three directions; forwards, sideways and upwards. This is a simple illustrative example where we can easily figure out the principal directions from experience. The strongest direction, corresponding to the largest singular value, will clearly be in the forwards direction. The next direction, corresponding*

to the second singular value, will be sideways. Finally, the most "difficult" or "weak" direction, corresponding to the smallest singular value, will be upwards (lifting up the cart).

For another example, strong ill conditioning and high interaction are also observed in 2×2 high-purity distillation processes (see Figure 4) where the top composition is to be controlled at $y_D = 0.99$ (output y_1), the bottom composition at $x_B = 0.01$ (output y_2), L is the reflux ratio, V is the boilup flow, D is the distillate flow, and B is the bottom product flow. The external flows (D and B) have large mixing effects in trays and a large effect on compositions while the internal flows (L and V) have a small effect on compositions (Skogestad and Morari, 1988*b*). Since an imbalance between ΔL and ΔV causes a change of the external flows, simultaneous changes of $\Delta L = \Delta V$ are preferable for the manipulated variables. Namely, flow changes with $\Delta L = \Delta V$ are related to the low-gain direction and flow changes with $\Delta L = -\Delta V$ are related to the high-gain direction. Such flow behavior requires that input signal designs for identification experiment of a high-purity distillation column only allows changes mainly with $\Delta L = \Delta V$ and (if necessary) very small changes with $\Delta L = -\Delta V$. Therefore, a high-purity distillation column requires a large control action to move the compositions in the low-gain direction (Figure 5b), while it takes a small action in the high-gain direction (Figure 5a). Figure 6 shows an example of an open-loop identification experiment (Butoyi and Zhu, 2002) in the output state-space (y_1 vs. y_2) using a linear high-purity distillation column model. Although the low-gain direction is very desirable to increase product quality (i.e., both the top and bottom products have higher purity), moving outputs in the low gain direction represents a difficult control problem.

A mathematical analysis is available for understanding the high- and low-gain directions from a gain matrix of a process system. For example, singular value decomposition (SVD) of a 2×2 system transforms its gain matrix into three matrices: output direction (U), singular value (Σ), and input direction (V) matrices, as follows:

$$SVD(K) = U \Sigma V^T = \bar{u} \bar{\sigma} \bar{v} + \underline{u} \underline{\sigma} \underline{v}$$

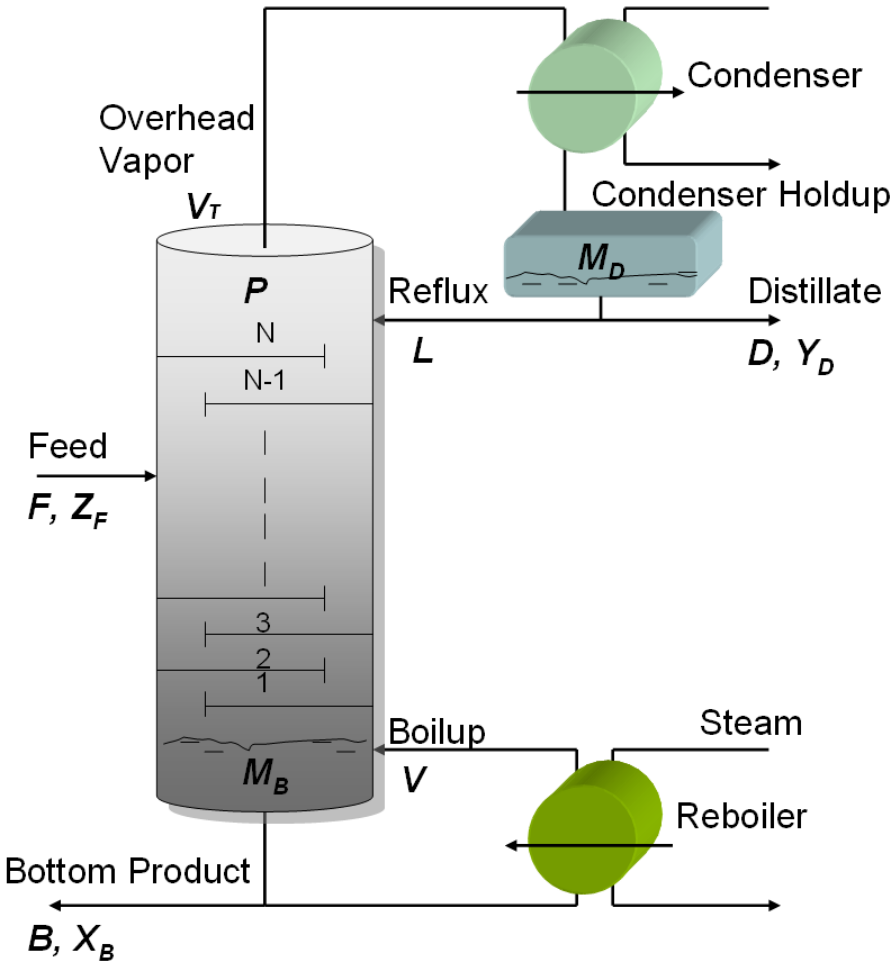

Figure 4. Typical binary distillation column, per Skogestad and Morari (1988)

where $U = [\bar{u}\ \underline{u}], V^T = [\bar{v}\ \underline{v}]$, and $\Sigma = diag(\bar{\sigma},\ \underline{\sigma})$ while $\bar{u}$, $\underline{u}$, $\bar{v}$, and $\underline{v}$ are orthogonal (unitary) vectors and $\bar{\sigma} > \underline{\sigma}$. The high gain-directional input ($\bar{v}$) and output directions ($\bar{u}$) are related to the higher singular value ($\bar{\sigma}$) while the low gain-directional ones ($\underline{v}$ and $\underline{u}$) are related to the lower singular value ($\underline{\sigma}$). Outputs in the low gain-directional direction are very small relative to those of the high gain-directional one in their magnitude comparison when the ratio of high and low singular values is very large, i.e., $\bar{\sigma} \gg \underline{\sigma}$ (such a plant is referred to as ill-conditioned, $\bar{\sigma}/\underline{\sigma} \gg 1$).

Utilizing this SVD analysis, special identification testing signals have been studied to increase the low-gain directional content in output data (Li and Lee, 1996*a*; Koung and MacGregor, 1993). To move the

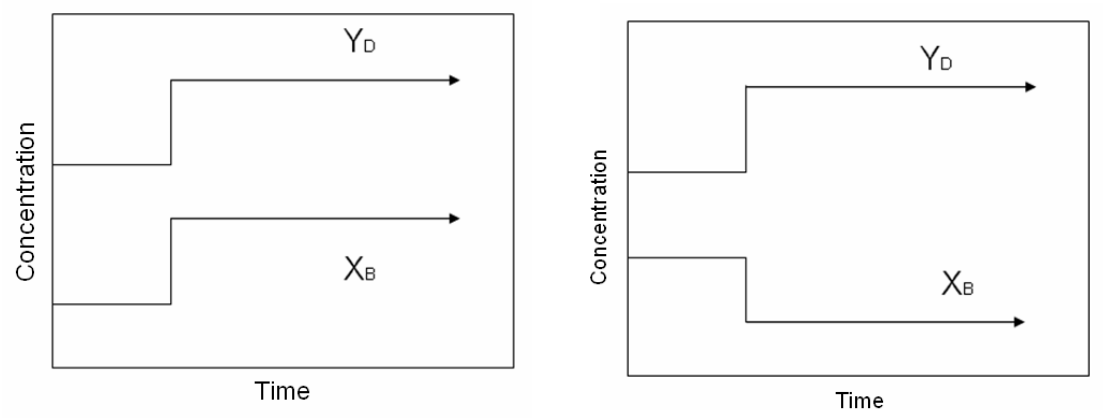

(a) High-gain direction (b) Low-gain direction

Figure 5. Example of the gain-directional changes in high-purity distillation column: the high-gain output direction (a) and the low-gain output direction (b)

outputs in the low-gain direction, Koung and MacGregor (1993) studied an input signal design for improved geometric distribution using open-loop system identification. However, this geometric method has to rotate input signals for exciting the low-gain direction while minimizing the higher singular value so that the system is transformed to be less ill-conditioned. Li and Lee (1996*a*) meanwhile try to obtain precise input and output directions based on the gain matrix generated during model estimation.

Full or partial closed-loop identification has been tried for more precise gain-directional estimation of highly interactive systems in Varga and Jørgensen (1994), Li and Lee (1996*a*), and Jacobsen (1994). The low-gain directional dynamics can be more easily captured if the closed-loop system is involved because the inverse system implied by the control system makes the low-gain directional dynamics more dominant than the high-gain directional dynamics (Li and Lee, 1996*a*; Li and Lee, 1996*b*). Although a dataset from a closed-loop test could provide balanced gain directional information, this requires an *a priori* process model suitable to design a feedback controller. However, such a model is not often available to engineers at the initial stages of identification.

In spite of the myriad of efforts with this problem, the issue of effective input signal design for highly interactive systems remains a challenge. In this dissertation, we propose a modified zippered spec-

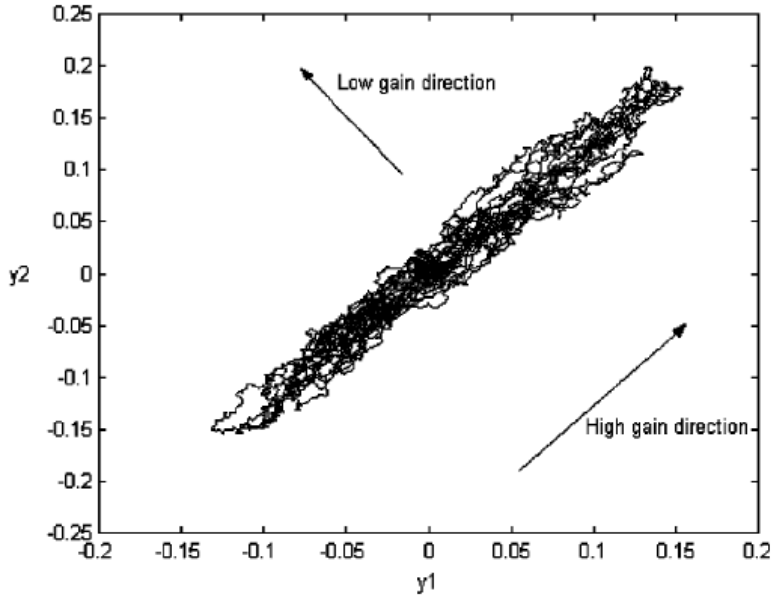

Figure 6. Excitation of output directions in a traditional open-test for a typical highly interactive system, per Zhu and Butoyi (2002)

trum specially designed to estimate accurate gain direction information using the conventional open-loop identification testing. A systematic direction and power adjustment on the correlated multisine harmonics is achieved to improve low-gain directionality from the experimental data, leading to adequate models for control applications (Lee and Rivera, 2006*a*; Lee and Rivera, 2006*b*). A process knowledge refinement procedure is efficiently illustrated by use of the identification test monitoring with emphasis on highly interactive systems.

4. Data-Centric Input Signal Design with MoD-MPC Application

4.1. Model-on-Demand Estimation Methodology. Model-on-Demand (MoD) estimation is a data-centric, nonlinear black-box identification method that enhances the classical local modeling problem (Braun *et al.*, 2001; Stenman *et al.*, 1996). The appeal of MoD estimation is that it enables nonlinear estimation while reducing the structural decisions made by the user and maintaining reliable numerical computations.

In MoD estimation, an adaptive bandwidth selector determines the size of data to be used for the local regression. The data is weighted using a kernel or weighting function. A local regression is performed using a linear or quadratic model to estimate the plant output at each time step; all observations are stored on a database and the models are built 'on demand' as the actual need arises. Local modeling techniques such as the MoD predictor use only small portions of data relevant to the region of interest to determine a model as needed. Such a data region can be divided into smaller regions based on operating conditions for local modeling procedures, as shown in Figure 7.

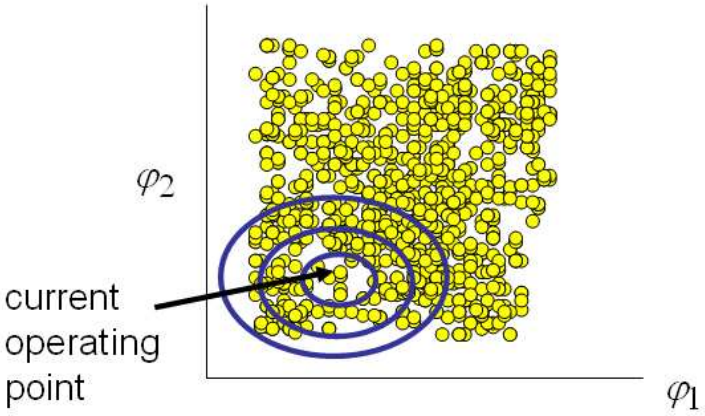

Figure 7. A selection of a data region from the stored database for MoD estimation

4.2. Data-Centric Input Signal Design. The performance of data-centric modeling with MoD estimation is highly dependent upon the availability of quality and informative databases. Consequently, good experimental designs are an imperative. A novel challenge in experimental design for these estimation methods is to achieve uniform coverage of regressors in the database. In Chapter 5 of this dissertation, we will examine the development of data-centric signal designs using multisine inputs that meet this criterion while satisfying plant-friendliness constraints during identification testing.

The idea of uniformly distributed experimental designs for system identification relying on multisine signals has previously been examined by Duym and Schoukens (1995), who rely on minimizing an objective

function quantifying the real and actual discrepancy from a user-defined grid. A more general approach that we present in this dissertation is to rely on the principles of geometric discrepancy theory (Matousek, 1999) as a means for achieving uniformity of the data in a regressor space. This is accomplished by minimizing a discrepancy function made up of trigonometric polynomials arising from Weyl's Theorem that insure the points are equidistant on a state-space. The optimization problem calls for minimizing this discrepancy function on the anticipated outputs of the system subject to the restrictions of an orthogonal "zippered" spectrum (used to enable multi-channel implementation) while simultaneously enforcing plant-friendliness time-domain constraints on upper and lower limits, move sizes, and rates of change in either (or both) input and output signals. The benefits of the data-centric signal design are demonstrated in a nonlinear distillation column per Weischedel and McAvoy (1980) under MoD-MPC application.

5. Publication Summary

A number of conference presentations and journal and proceedings papers have resulted from this research and the collaboration between my advisor D.E. Rivera, his former student M.W. Braun, the mathematician H.D. Mittelmann, and his former student G.V. Pendse. These cover the topics of plant-friendly multivariable multisine input design (with emphasis on highly interactive systems), control-relevant parameter estimation, and identification test monitoring. Plant-friendly multisine input signal designs meaningful for highly interactive systems are considered in the following:

1. D.E. Rivera, H. Lee, M. Braun, and H. Mittelmann, "Identification of multivariable process systems using constrained minimum crest factor multisine inputs," paper 255f, *2002 AIChE Annual Meeting*, Indianapolis, IN, Nov. 3-8, 2002.

2. H. Lee, D.E. Rivera, and H.D. Mittelmann, "Constrained minimum crest factor multisine signals for plant-friendly identification of highly interactive systems," in *13th IFAC Symposium on System Identification (SYSID 2003)*, Rotterdam, The Netherlands, August 27-29, 2003. pp. 947-952.

3. H. Lee, D. E. Rivera, and H.D. Mittelmann, “A Novel Approach to Plant-Friendly Multivariable Identification of Highly Interactive Systems,” paper 436a, *2003 AIChE Annual Meeting*, San Francisco, CA, Nov. 16-21, 2003.

4. D.E. Rivera, H. Lee, H.D. Mittelmann, and M.W. Braun, “Constrained multisine input signals for plant-friendly identification of chemical process systems,” submitted to *Journal of Process Control*.

5. D.E. Rivera, H. Lee, H.D. Mittelmann, and M.W. Braun, “High Purity Distillation: using plant-friendly multisine signals for experimental testing of a strongly interactive process,” submitted to *IEEE Control System Magazine*.

6. H. Lee, D.E. Rivera, and H.D. Mittelmann, “A Novel Multivariable System Identification Experimental Designs for Highly-Interactive Chemical Processes,” in preparation for submission to *Industrial and Engineering Chemistry Research*.

The control-relevant parameter estimation problem for multivariable system identification and control has been described in:

1. H. Lee and D.E. Rivera, “A Control-Relevant, Plant-Friendly System Identification Methodology using Shifted and Zippered Multisine Input Signals,” paper 414r, *2004 AIChE Annual Meeting*, Austin, TX, Nov. 16-21, 2004.

2. H. Lee and D.E. Rivera, “Control-Relevant Curvefitting for Plant-Friendly Multivariable System Identification,” *2005 American Control Conference, Portland,* Oregon, 2005, pp.1431-1436.

3. H. Lee and D.E. Rivera, “An Integrated Methodology for Plant-Friendly Input Signal Design and Control-Relevant Estimation of Highly Interactive Processes”, paper 242k, *2005 AIChE Annual Meeting*, Cincinnati, OH, 2005.

4. H. Lee and D.E. Rivera, “An Integrated Input Signal Design and Control-Relevant Parameter Estimation Approach for Highly Interactive Multivariable Systems,” *2006 American Control Conference*, Minneapolis,

MN, 2006, pp.1665-1670.

5. H. Lee, and D.E. Rivera, “A Control-Relevant Parameter Estimation with Frequency-response Curvefitting for Multivariable Systems,” in preparation for *Computers and Chemical Engineering*.

The plant-friendly identification test monitoring methodology is presented in:

1. Rivera, D., H. Lee, M. Braun, and H. Mittelmann, “Plant-friendly system identification: a challenge for the process industries,” *13th IFAC Symposium on System Identification (SYSID 2003)*, Rotterdam, Netherlands, 2003, pp. 917-922.

2. H. Lee and D.E. Rivera, “Demonstration of Identification Test Monitoring Procedure to a Highly Interactive System using Control-Relevant Identification Methodology,” in preparation for *Industry and Engineering Chemistry Research*.

A MATLAB-based software package named CR-IDENT (Control-Relevant IDENTification) has been developed as part of this research, which provides an implementation of the integrated framework environment and is available in the public domain. It is described in the following:

1. H. Lee and D.E. Rivera, “CR-IDENT: A MATLAB Toolbox for Multivariable Control-Relevant System Identification (Paper ID: 137, Invited Paper),” *the 14th IFAC Symposium on System Identification (SYSID 2006)*, Newcastle, Australia, pp.708-713.

Data-centric input signal for geometrical uniform distribution based on Weyl Theorem, suitable for Model-on-Demand estimation, is described in:

1. D.E. Rivera , H. Lee, H. D. Mittelmann, and G. Pendse, “Optimization-based Design of Plant-Friendly Input Signals for Data-Centric Estimation and Control,” paper 520b, *2005 AIChE Annual Meeting*, Cincinnati, OH, 2005.

2. D.E. Rivera, H. Lee, H.D. Mittelmann, and G. Pendse, "Optimization-Based Design of Plant-Friendly Multisine Signals using Geometric Discrepancy Criteria," *the 14th IFAC Symposium on System Identification (SYSID 2006)*, Newcastle, Australia, pp.1133-1138.

3. H.D. Mittelmann, G. Pendse, D.E. Rivera, and H. Lee, "Optimization-based Design of Plant-Friendly Multisine Signals using Geometric Discrepancy Criteria," *Comp. Math. and Applications* in press.

4. D.E. Rivera, H. Lee, H.D. Mittelmann, and M.W. Braun, "High Purity Distillation: using plant-friendly multisine signals for experimental testing of a strongly interactive process," submitted to *IEEE Control System Magazine*.

5. Lee, Hyunjin and Daniel E. Rivera, Hans D. Mittelmann, and Martin W. Braun, "A Data-Centric Input Signal Design Framework for Model-on-Demand Model Estimation of Nonlinear Systems," in preparation for *Computers and Chemical Engineering*.

6. Dissertation Summary

This dissertation is organized as follows: Chapter 2 discusses a derivation of the design guidelines of multivariable multisine input signals based on *a priori* information of a system. A primary excitation bandwidth is defined, which also consequentially specifies the signal length, sampling time, and number of sinusoids for multisine signals. To improve the low-gain directional content in identifying highly interactive systems, an analysis of the gain-directionality is presented and focused on highly interactive systems. As a result, a "modified zippered" power spectrum design is formulated based on the steady-state gain matrix and its corresponding SVD analysis.

A series of plant-friendly identification test formulations associated with multisine input signals are also presented in Chapter 2, which involves the use of state-of-the-art optimization techniques. At the initial stage, only the input signals are considered for minimizing its crest factor. Once a nominal model is available, the optimizer is able to minimize the crest factors of both inputs and (predicted) outputs. A

linear, highly-interactive distillation column model is used as an example to demonstrate the capability of improving the gain-directional information through the plant-friendly identification test formulations. Subsequently, in Chapter 2 a nonlinear, highly interactive system per Weischedel and McAvoy (1980) is examined using various multisine signal designs for use in both linear and nonlinear system identification. The quality of the model estimates from a series of multisine signals is evaluated by performing closed-loop setpoint tracking tests with MPC; specifically, these models are estimated from data under noisy conditions.

Chapter 3 describes the control-relevant parameter estimation that consists of a weighted frequency response curvefitting procedure, producing a suitable nominal model for control system designs. A linear parametric model is approximated into frequency-response data using weighted least squares minimization. A full-polynomial matrix fraction description (MFD) is applied for this task, and weights are obtained from the feedback controller with input disturbances. The use of MFD model representations is considered since it is superior to the common denominator approach of Bayard (1994) or the diagonal matrix approach of Gaikwad and Rivera (1997). The Shell heavy-oil fractionator problem is utilized to test this control-relevant parameter estimation method using data from the zippered power spectrum multisine inputs.

In Chapter 4, a robust loopshaping procedure is presented that relies on a structured singular value analysis on a set of models. Robust loopshaping is a numerical procedure that generates a series of linear fractional transformation structures and searches robustness conditions with user-specified performance weights. This procedure involves generating a set of models associated with the uncertainty descriptions. The problem naturally iterates between control-relevant parameter estimation and robust loopshaping until the model estimate can meet desired robust stability and performance requirements. An illustrative case with Jacobsen-Skogestad highly interactive distillation column demonstrates the effectiveness of the identification test monitoring.

Chapter 5 describes a novel data-centric input signal design, motivated by the plant-friendly, constrained optimization-based input signal formulations of Chapter 2. A geometrical objective problem based

on Weyl's theorem using multisine input signal is derived for achieving the uniformity distribution in outputs, suitable for data-centric modeling estimation algorithm such as Model-on-Demand estimation. The benefits of the design procedure are presented for a Model-on-Demand MPC application to the Weischedel-McAvoy distillation column.

Finally, Chapter 6 summarizes the contributions of this dissertation. It describes how the proposed identification test monitoring framework can impact current practice in model development for process control applications. A research summary and future research directions are presented that could further improve the effectiveness and applicability of identification test monitoring to the process industries.

CHAPTER 2

PLANT-FRIENDLY MULTISINE INPUT SIGNAL DESIGNS

1. Introduction

The first consideration in a comprehensive identification framework for multivariable systems is designing effective input signals. In the framework developed in this dissertation, multisine inputs are mainly used as signals for the experimental testing of system identification. A set of design guidelines for multisine inputs are derived that specify the power spectral densities of the signals based on *a priori* dynamic characteristics of a SISO or MIMO system. In particular, a power spectrum design with directional adjustment is developed that excites the weak gain directions of highly interactive systems.

As a practical requirement during experimental testing, plant-friendliness considerations are incorporated in the multisine input signal design procedure by formulating it as a constrained optimization problem. Time-domain constraints are imposed on both input and output signals. The optimization problems are solved by state-of-the-art constrained nonlinear programming algorithms. A constrained problem formulation meaningful for the data-centric input design approach is introduced in Chapter 7.

A proof-of-concept demonstration of plant-friendly identification testing is presented using the nonlinear high-purity distillation column per Weischedel and McAvoy (1980) that is widely considered as a challenging problem for identification and control. This nonlinear distillation process shows strong ill-conditioning and interaction that requires special attention for effective experimental testing in identifica-

tion. A variety of multisine input signals are generated meeting plant-friendliness requirements and resulting in informative datasets, ultimately leading to suitable model estimates for multivariable control.

This chapter is organized as follows: Section 2 describes the preliminaries of input signals for identification experimental testing. Section 3 presents the design guidelines of multisine input signals for SISO and MIMO systems. Section 4 gives special attention to identification input signal requirements for highly interactive systems, and Section 5 describes the modified zippered spectrum signals with directional and power adjustments that are specially designed for highly interactive systems. In addition, a phase-shifted technique is applied to multisine signals in Section 6. Section 7 discusses harmonic suppression on multisine sinusoids that can be used to reduce nonlinear distortions for approximating nonlinear systems into linear representations. Plant-friendliness is considered with multisine input designs by using constrained optimization problem formulations in Section 8. A case study with the 2×2 nonlinear, binary distillation column with high interaction and ill conditioning per Weischedel and McAvoy (1980) is examined in Section 9. Section 10 presents the summary and conclusions.

2. Preliminaries for Identification Input Signal

Model building in system identification practice relies on the observed input and output signals. The accuracy of model estimates is dependent of how well a dataset is generated for system identification purposes. The input signal should be able to drive the system so that its dynamic behavior can be sufficiently reflected in the output. The design of input signals is, therefore, a fundamental step in the system identification procedure to make the dataset be as informative as possible.

To generate an effective input signal, the use of *a priori* process information is an important consideration for selecting input design variables. Such design variables establish a primary excitation bandwidth that should be targeted on the system dynamics. Two theoretical requirements are considered for an informative input signal: persistent excitation and signal-to-noise ratio (Ljung, 1999).

Persistent Excitation (PE): A quasi-stationary signal $u(k)$ with spectrum $\Phi_u(\omega)$ has *persistent excitation of order n*, if, for all moving filters of the form

$$M_n(q) = m_1 q^{-1} + m_2 q^{-2} + ... + m_n q^{-n} \tag{2.1}$$

the relation

$$|M_n(e^{i\omega})|^2 \Phi_u(\omega) \equiv 0 \tag{2.2}$$

implies that $|M_n(e^{i\omega})|^2 \equiv 0$, where q is the shift operator. The above equation can be interpreted as follows:

1. The input $u(k)$ has persistent excitation of order n if $\Phi_u(\omega)$ is different from zero at n points in the interval $-\pi < \omega \leq \pi$

2. A signal $u(k)$ with degree n of persistent excitation cannot be suppressed completely by an $(n-1)$ order moving average filter

If $u(k)$ is a persistent exciting signal of order n, then a maximum of n parameters can be estimated and the covariance matrix ${R_u}^n$ of $u(k)$ is nonsingular (Ljung, 1999; Stoica and Moses, 1997; Söderström and Stoica, 1989).

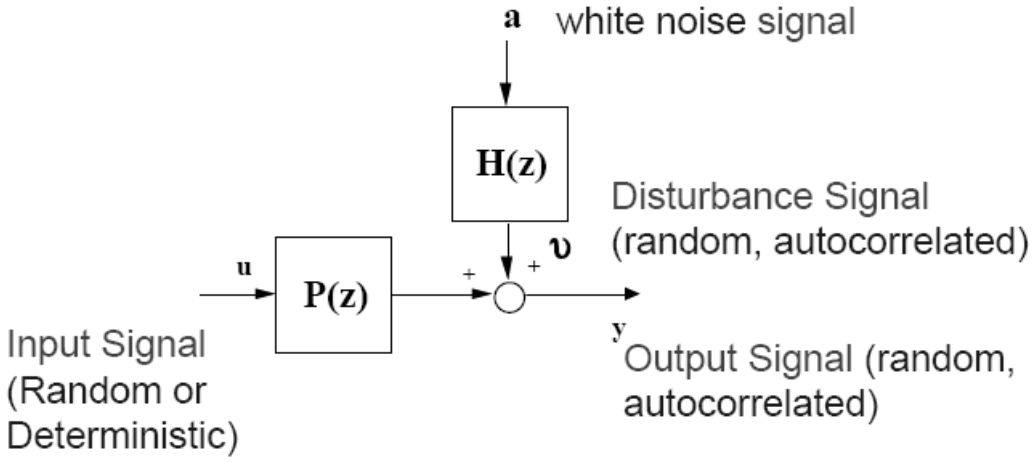

Figure 8. Model structure for system identification

The other consideration is related to the error criterion. As mentioned in Chapter 1, two principal sources of error, bias and variance, exist in system identification (see Figure 8). The mean square error is given as a sum of the bias and variance contributions to the model error

$$Error = Bias^2 + Variance$$

Asymptotically (as the number of observations $N \to \infty$), the least squares estimation problems can be written as:

$$\lim_{N\to\infty} \sum_{i=1}^{N} e_F^2(t) \;=\; \frac{1}{2\pi} \int_{-\pi}^{\pi} \Phi_{e_F}(\omega) d\omega \tag{2.3}$$

and Φ_{e_F}, the power spectrum of the prediction error, is defined as

$$\Phi_{e_F} = |p_e^{-1}|^2 (|p-\tilde{p}|^2 \Phi_u + 2Re((p-\tilde{p})H^*(e^{i\omega})\Phi_{ua}) + |H(e^{i\omega})|^2 \sigma_a^2) \tag{2.4}$$

where p is a true plant, $\tilde{p}$ is a model estimate, H is a noise model, and $v(t) = H(z)a(t)$ is the disturbance. Since the input power spectrum directly weights the term $|p-\tilde{p}|^2$, the error between the true system and the estimated model is reduced at those frequencies at which the input power spectrum is persistently excited. The variance is given as a ratio of the disturbance and input power spectra such that

$$Var(\tilde{p}) \;\propto\; \frac{n}{N} \; \frac{\Phi_v(\omega)}{\Phi_u(\omega)} \tag{2.5}$$

where n is the number of model parameters and N is the number of data points. Using a small number of model parameters, increasing the length of the data set, and increasing the power of the input signal all contribute to variance reduction in system identification. Particularly, the Signal-to-Noise Ratio (SNR) is defined as the ratio of signal power spectrum $\Phi_u(\omega)$ and noise power spectrum $\Phi_v(\omega)$

$$SNR \;=\; \frac{\Phi_u(\omega)}{\Phi_v(\omega)} \tag{2.6}$$

This is a measure of the amount of degradation of a signal by additive noise. For effective estimation a suitable level of SNR should be selected via a trade-off between the bias and variance aspects. Although

a higher SNR is desirable, a normal operating condition dictates a span of input magnitudes which in turn gives a power level to input signal as low as possible according to "plant-friendliness" in identification experiment practice. The design procedure presented in this chapter addresses all of these considerations.

3. Multisine Input Signal Design for SISO and MIMO Systems

The design guidelines developed in this dissertation for multisine input signals start with *a priori* knowledge of a system to be identified. The parameters $\{\alpha,\ \beta,\ \tau_{dom}^{H}$, and $\tau_{dom}^{L}\}$ rely on the availability of *a priori* information to specify a meaningful frequency bandwidth for excitation. The parameters α and β adjust the desired range of high and low frequencies for input signal excitation depending on user specification of the dominant time constants. β is normally equal to 3, 4 , or 5, which specifies a low frequency range corresponding to 95%, 98%, and 99% settling time of the open-loop plant. α indicates a high frequency range and is defined on the basis of how much faster the intended closed-loop speed of response will be relative to the open-loop response. *A priori* knowledge of the dominant time constants, τ_{dom}^{H} and τ_{dom}^{L}, provides the information of a frequency range to place a primary power spectrum of the input signal associated with α and β. Therefore, a bandwidth of the primary power spectrum should fall within the range specified by the inequality of (2.7) (Braun *et al.*, 2002*b*; Rivera *et al.*, 2002).

$$\frac{1}{\beta\,\tau_{dom}^{H}} \;=\; \omega_{*} \leq \;\; \omega \;\; \leq \omega^{*} \;=\; \frac{\alpha}{\tau_{dom}^{L}} \tag{2.7}$$

Equation (2.7) forms the basis guidelines for multisine input signals that decide signal design parameters such as the number of sinusoid harmonics, signal length, and sampling time (Lee *et al.*, 2003). Other considerations, however, must be recognized for the identification of highly interactive systems; a modified "zippered" spectrum is developed as a means for achieving precise gain-direction estimation. Phase-shifting is also considered as an economical testing experiment in multisine input design, which is traditionally

utilized for PRBS input signals (see Section 6). Finally, harmonic suppression is often necessary for the identifying nonlinear systems.

3.1. Single-Channel Input Signal Design. A multisine input signal for the single-input, single-output (SISO) case is represented by the following equation (Schroeder, 1970; Bayard, 1993*b*)

$$u(k) = \lambda \sum_{i=1}^{N_s/2} \sqrt{2\alpha_i}\, cos(\omega_i kT + \phi_i) \tag{2.8}$$

where $\omega_i = 2\pi i/N_s T$. The power spectrum in a multisine input can be directly specified by the user through the selection of the scaling factor λ, the Fourier coefficients α_i, the number of harmonics n_s, the signal length N_s, and the sampling time T. Since n_s is the number of persistent excitation within the primary bandwidth, the order of model estimate should be less than n_s such that

$$\text{Model Order: } n \;\leq\; n_s \tag{2.9}$$

where $n_a + n_b = n$. The primary frequency bandwidth of the input signal is bounded by the design variables as follows

$$\omega_* \geq \frac{2\pi}{N_s T} \tag{2.10}$$

$$\omega^* \;\leq\; \frac{2\pi n_s}{N_s T} \;\leq\; \frac{\pi}{T} \tag{2.11}$$

where π/T is the Nyquist frequency. As a result, a multisine input signal is designed to cover this frequency bandwidth via specifying n_s, N_s, and T, as illustrated in Figure 9.

The multisine input signal is easy to implement in a real-time setting; as a deterministic signal, one cycle can be designed to include all the frequency content needed for consistent estimation of the plant dynamics. This is illustrated in Figure 9. The power spectrum of the multisine input signal is shaped by a series of the relative magnitudes of the harmonics in Equation (2.12), which is transformed into the Fourier coefficients. A signal with a flat power spectrum from ω_* to ω^* with a number of harmonics of n_s is

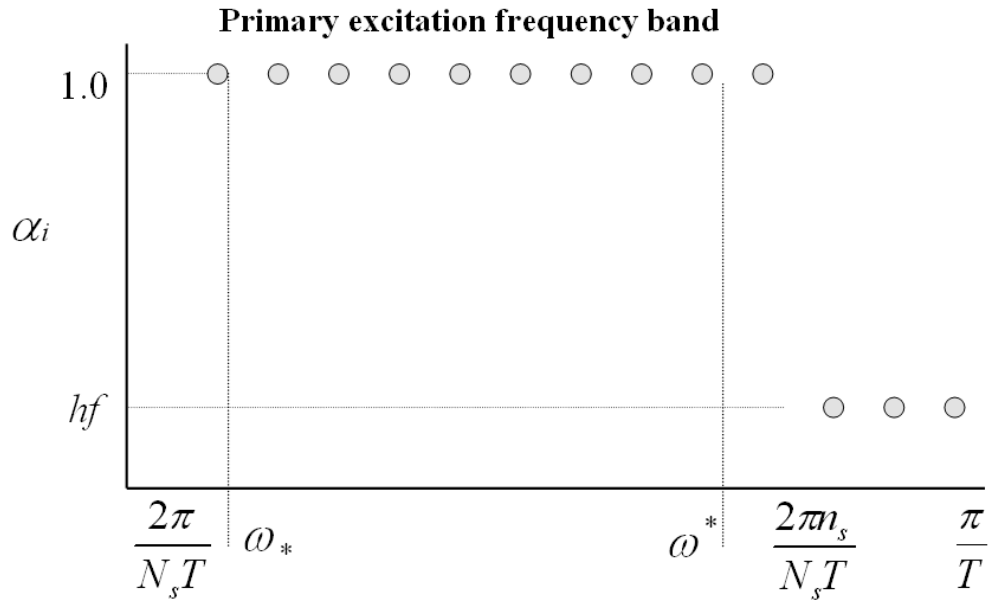

Figure 9. Relative magnitudes of Fourier coefficients for low-pass signal, SISO case

designed as

$$\alpha(i) = \begin{cases} 1, & i = 1,...,n_s \\ hf, & i = n_s+1,...,N_s/2 \end{cases} \tag{2.12}$$

where hf is the high frequency coefficient magnitude over ω^*, which is often less than "1" to reduce high frequency activity in input signal, and is similar to a low-pass filter.

In addition, a notch input power spectrum design can be specified; this makes the input signal more precisely focused on the important (mid) frequencies based on *a priori* knowledge of the given process (Braun *et al.*, 2002*b*; Rivera *et al.*, 2002; Ortiz-Mojica, 2000). The structure of the relative magnitude for a notch power spectrum becomes

$$\alpha(i) = \begin{cases} lf, & i = 1,...,\delta \\ 1, & i = \delta+1,...,n_s \\ hf, & i = n_s+1,...,N_s/2 \end{cases} \tag{2.13}$$

where δ is the low frequency interval number - a positive integer- whose corresponding Fourier coefficients are lowered to lf, the low frequency relative magnitude. This flexible specification of δ and lf makes it possible to manipulate the signal power spectrum over the low frequencies shown in Figure 10. For example, when $\delta > 0$, the number of δ points is located below ω_* with the relative spectral magnitude lf. The corresponding input power spectrum for a notch design (Figure 10) can be defined as

$$\Phi_u(i) = \begin{cases} \frac{\lambda^2 lf}{2} N_s, & i = 1, \ldots, \delta \\ \frac{\lambda^2}{2} N_s, & i = \delta + 1, \ldots, n_s \\ \frac{\lambda^2 hf}{2} N_s, & i = n_s + 1, \ldots, N_s/2 \end{cases} \tag{2.14}$$

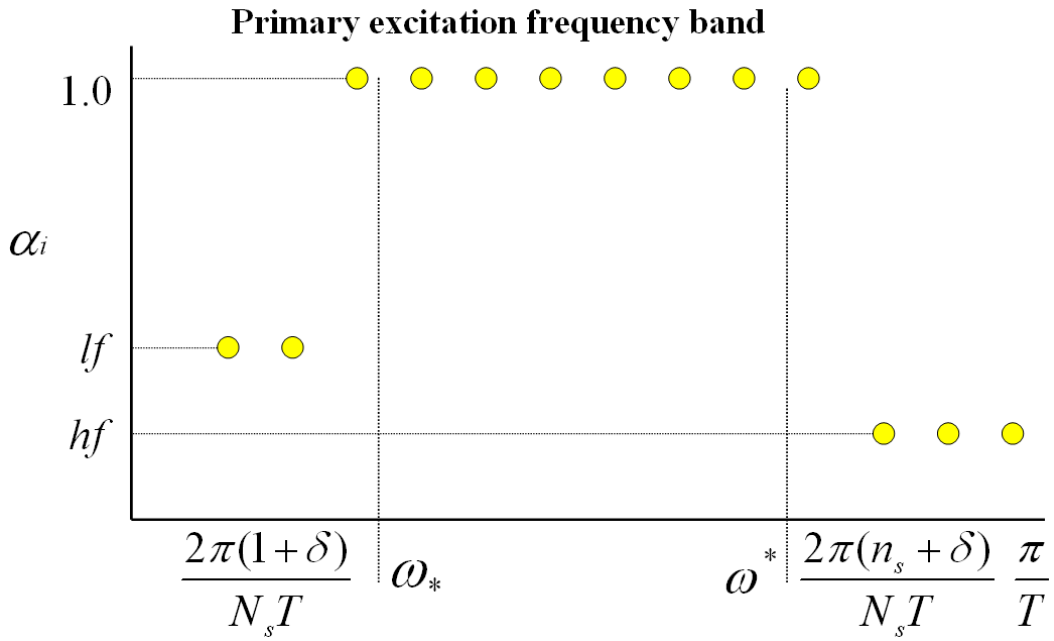

Figure 10. Relative magnitudes of Fourier coefficients for a SISO notch spectrum case with $\delta = 2$

3.2. Multi-Channel Input Signal Design using A Zippered Power Spectrum. For the MIMO case, no cross correlation should exist between the input channel for the identifiability of a system. In this dissertation, two approaches are considered for designing multi-channel multisine inputs: a phase-shifted method in the time-domain and a zippered power spectrum in the frequency-domain. The former

approach is a commonly used technique for multivariable PRBS inputs with spectral correlations (Briggs and Godfrey, 1966; Rivera and Jun, 2000). The latter uses independent frequency grids for each input channel which insures independence in the frequency domain, allowing no cross correlation between channels. The design of a zippered power spectrum is discussed in this section.

A multisine input $u_j(k)$ for the *j*-th channel of a multivariable system with *m* inputs can be defined as

$$\begin{aligned} u_j(k) &= \sum_{i=1}^{m\delta} \hat{\delta}_{ji} \cos(\omega_i kT + \phi_{ji}^{\delta}) + \lambda_j \sum_{i=m\delta+1}^{m(\delta+n_s)} \sqrt{2\alpha_{ji}} \cos(\omega_i kT + \phi_{ji}) \\ &\quad + \sum_{i=m(\delta+n_s)+1}^{m(\delta+n_s+n_a)} \hat{a}_{ji} \cos(\omega_i kT + \phi_{ji}^{a}), \qquad j = 1, \cdots, m \end{aligned} \tag{2.15}$$

where T is sampling time, N_s is the sequence length, m is the number of channels, δ, n_s, n_a are the number of sinusoids per channel ($m(\delta + n_s + n_a) = N_s/2$), $\phi_{ji}^{\delta}, \phi_{ji}, \phi_{ji}^{a}$ are the phase angles, $\lambda_j\sqrt{2\alpha_{ji}}$ represents the Fourier coefficients defined by the user, $\hat{\delta}_{ji}, \hat{a}_{ji}$ are the "snow effect" Fourier coefficients that contribute to a decrease in the crest factor (Guillaume *et al.*, 1991)., and $\omega_i = 2\pi i/N_s T$ is the frequency grid.

3.2.1. *Standard Zippered Spectrum.* In the standard "zippered" design procedure described by Rivera *et al.* (1997), Fourier coefficients for each channel are defined independently over unique frequency grids of interest. The resulting orthogonal multi-frequency signal can be simultaneously introduced to all channels of a plant. Figure 11 shows a zippered input power spectrum for a three-channel MIMO case. To achieve a zippered spectrum we define the Fourier coefficients α_{ji} for $u_j(k)$ as

$$\alpha_{ji} = \begin{cases} \neq 0, & i = m\delta + j, m(\delta+1) + j, ..., m(\delta + n_s - 1) + j \\ = 0, & \text{for all other } i \text{ from } m\delta \text{ to } m(\delta + n_s) \end{cases} \tag{2.16}$$

Equivalent expressions to Equation (2.16) can be developed for the "snow effect" coefficients, $\hat{\delta}_{ji}$ and $\hat{a}_{ji}$ that defined as

$$\delta_{ji} = \begin{cases} \neq 0, & i = j, m + j, ..., m(\delta - 1) + j \\ = 0, & \text{for all other } i \text{ from 1 to } m\delta \end{cases} \tag{2.17}$$

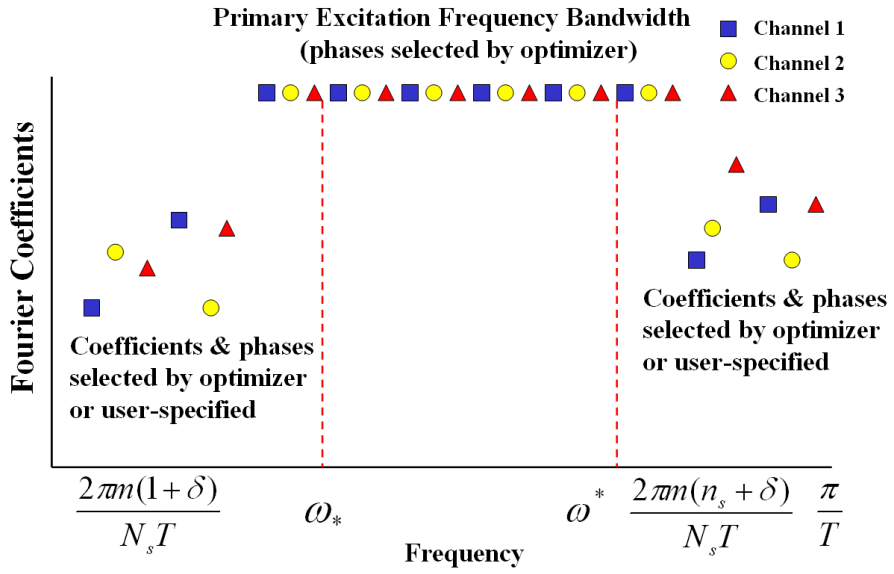

Figure 11. Conceptual design of a standard "zippered" spectrum for a three-channel signal.

$$\hat{a}_{ji} = \begin{cases} \neq 0, & i = m(\delta + n_s) + j, m(\delta + n_s + 1) + j, \ldots, m(\delta + n_s + n_a - 1) + j \\ = 0, & \text{for all other } i \text{ from } m(\delta + n_s) \text{ to } m(\delta + n_s + n_a) \end{cases} \tag{2.18}$$

3.2.2. *Multisine Input Signal Design Guideline Derivation.* The frequency bandwidth is interpreted into a series of inequalities for the number of sinusoids (n_s), sampling time (T), and length of signal (N_s). In addition to the single-channel input signal design, this guideline of multisine signal satisfies orthogonal requirements by "zippered" power spectrum for multi-channel input signals. Subtracting Equation (2.11) from (2.10) yields a frequency range for the primary excitation

$$\omega^* - \omega_* \leq \frac{2\pi}{N_s T}(n_s - 1) \tag{2.19}$$

For multi-channel signals, the primary frequency band is expanded by multiplying the number of channels m in Equation (2.19)

$$\omega^* - \omega_* \leq \frac{2\pi}{N_s T}(n_s - 1) \times m \tag{2.20}$$

in which multiplication by m means that the required bandwidth must accommodate m-input channels. If the sampling time is fixed, signal length must be flexible to make more frequency grids so that the primary

harmonics can be located within the frequency bandwidth.

In multivariable systems, the dominant time constants τ_{dom}^{L} and τ_{dom}^{H} can be found by

$$\tau_{dom}^{H} = \max(\tau_1, \tau_2, ..., \tau_m), \quad \tau_{dom}^{L} = \min(\tau_1, \tau_2, ..., \tau_m) \tag{2.21}$$

These consequently define ω_* and ω^*, as shown in (2.7). Incorporating this with the multisine signal design parameters and frequency bandwidth, the following is obtained for multiple channels:

$$\frac{2\pi m}{N_s T} \leq \omega_* \leq \omega \leq \omega^* \leq \frac{2\pi n_s m}{N_s T} \leq \frac{\pi}{T} \tag{2.22}$$

As previously defined, δ is the low frequency interval and is applied to achieve a notch power spectrum; δ is inserted into the lower and upper frequency bounds,

$$\frac{2\pi m(1+\delta)}{N_s T} \leq \omega_* \tag{2.23}$$

$$\omega^* \leq \frac{2\pi m(n_s+\delta)}{N_s T} \leq \frac{\pi}{T} \tag{2.24}$$

and the primary frequency bandwidth of a multi-channel, notch spectrum design becomes

$$\omega^* - \omega_* \leq \frac{2\pi m}{N_s T}(n_s - 1) \tag{2.25}$$

In the latter two terms of Equation (2.24), π and T cancel, and the inequality of the two terms becomes

$$\frac{2m(n_s+\delta)}{N_s} \leq 1 \tag{2.26}$$

Arranging the resultant inequalities with respect to N_s, the length of signal is determined from the following inequalities:

$$N_s \geq \max\{2m(n_s+\delta), \frac{2\pi m(1+\delta)}{\omega_* T}\} \tag{2.27}$$

and

$$N_s \leq \frac{2\pi m(n_s+\delta)}{\omega^* T} \tag{2.28}$$

Finally, a bounded equation is formed as the lower and upper limits of N_s in terms of $m, n_s, \delta, T, \omega_*$, and ω^*.

$$\max\left(2m(n_s+\delta),\ \frac{2\pi m(1+\delta)}{\omega_* T}\right) \leq N_s \leq \frac{2\pi m(n_s+\delta)}{\omega^* T} \tag{2.29}$$

We can now specify n_s. If $\frac{2\pi m(1+\delta)}{\omega_* T}$ represents a lower bound for N_s, it can be inserted into Equation (2.25). As a result, the number of sinusoids (n_s) is found in terms of ω_*, ω^*, and δ.

$$\omega^* - \omega_* \leq \omega_* \frac{n_s - 1}{1+\delta} \tag{2.30}$$

$$\frac{\omega^*}{\omega_*} - 1 \leq \frac{n_s - 1}{1+\delta} \tag{2.31}$$

Thus, the minimum number of sinusoids is determined by:

$$(n_s+\delta) \geq (1+\delta)\frac{\omega^*}{\omega_*} \tag{2.32}$$

In addition, $n_s + \delta$ should be less than $N_s/2m$ from Equation (2.26); as a result, a bounded form of n_s becomes

$$(1+\delta)\ \frac{\omega^*}{\omega_*} \leq n_s + \delta \leq N_s/2m \tag{2.33}$$

In case $\delta = 0$ with no restriction in the low frequencies, Equation (2.33) simply reduces into

$$\frac{\omega^*}{\omega_*} \leq n_s \leq N_s/2m \tag{2.34}$$

As a result, the number of sinusoids is dependent on values specified for ω_*, ω^*, N_s, and δ.

The sampling time T is specified by another set of inequalities. If $2m(n_s+\delta)$ is a low bound for N_s, it can be inserted into Equation (2.25) and then the sampling time is found in terms of ω_*, ω^*, n_s, and δ

$$\omega^* - \omega_* \leq \frac{2\pi m}{N_s T}(n_s - 1) \tag{2.35}$$

$$\omega^* - \omega_* \leq \frac{\pi}{T}\frac{n_s - 1}{n_s + \delta} \tag{2.36}$$

and finally the sampling time is bounded by $\frac{\pi}{\omega^*}$ from Equation (2.24)

$$T \leq \min\{\frac{\pi}{\omega^* - \omega_*}\left(\frac{n_s - 1}{n_s + \delta}\right),\quad \frac{\pi}{\omega^*}\} \tag{2.37}$$

The guideline (2.37) specifies an upper bound on T; however, in practice T is often selected to be much lower than this bound based on the requirement of the eventual control system.

3.3. Iterative Implementation of the Multisine Design Guidelines. The guidelines for multi-channel multisine signals are summarized into specifications of n_s, T, and N_s, which must be implemented sequentially. The user initially specifies α, β, τ_H, τ_L, m and δ, which define ω^* and ω_*. The primary frequency bandwidth is related to the design variables in Equation (2.15) through the relationship

$$\frac{2\pi m(1+\delta)}{N_s T} \leq \omega_* \ \leq \ \omega \ \leq \ \omega^* \ \leq \ \frac{2\pi m(n_s+\delta)}{N_s T} \ \leq \ \frac{\pi}{T} \tag{2.38}$$

which in turn translates into the following inequalities for number of sinusoids, sampling time and sequence length (n_s, T, and N_s, respectively)

$$n_s + \delta \geq (1+\delta)\frac{\omega^*}{\omega_*} \tag{2.39}$$

$$T \leq \min\left(\frac{\pi}{\omega^*}, \ \frac{\pi}{\omega^* - \omega_*}\frac{n_s - 1}{n_s + \delta}\right) \tag{2.40}$$

$$\max\left(2m(n_s+\delta), \ \frac{2\pi m(1+\delta)}{\omega_* T}\right) \ \leq N_s \ \leq \frac{2\pi m(n_s+\delta)}{\omega^* T} \tag{2.41}$$

A n_s value is first obtained, and then the user determines a sampling time T and a length of signal N_s, while satisfying the following inequalities simultaneously

$$(1+\delta)\frac{\omega^*}{\omega_*} \leq n_s + \delta \leq \frac{N_s}{2m} \tag{2.42}$$

$$T \leq \min\left(\frac{\pi}{\omega^*}, \ \frac{\pi}{\omega^* - \omega_*}\frac{n_s - 1}{n_s + \delta}\right) \tag{2.43}$$

$$\max\left(2m(n_s+\delta), \ \frac{2\pi m(1+\delta)}{\omega_* T}\right) \ \leq N_s \ \leq \frac{2\pi m(n_s+\delta)}{\omega^* T} \tag{2.44}$$

Through Equations (2.42) to (2.44), the selected parameters, n_s, T, and N_s, must satisfy the inequality of Equation (2.22). If not, a new value of n_s is obtained by adjusting n_s according to T and N_s:

$$\frac{\omega^* - \omega_*}{2\pi m} N_s T + 1 + \delta \ \leq \ n_s + \delta \ \leq \ \frac{N_s}{2m} \tag{2.45}$$

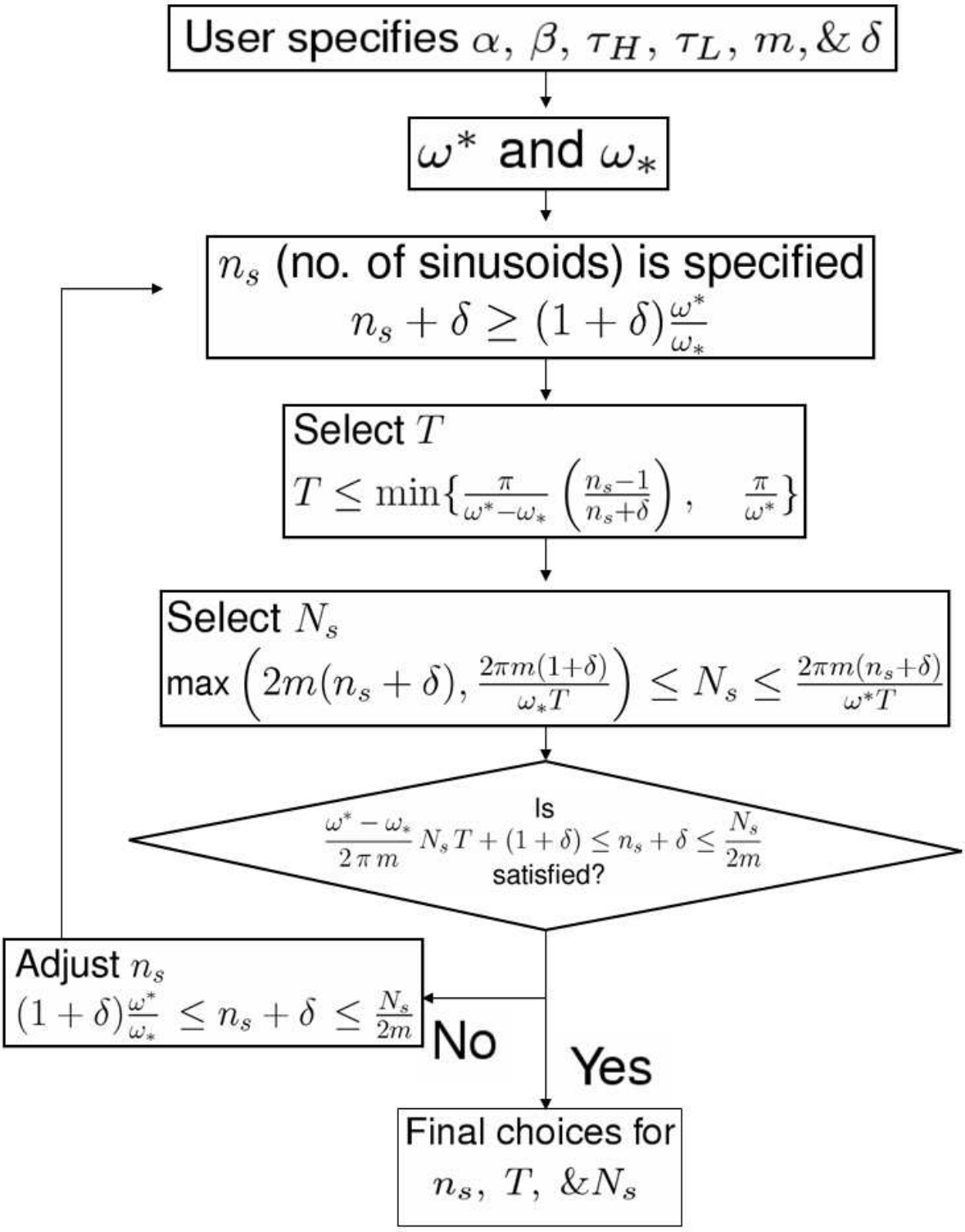

Figure 12. Iterative Algorithm for Selecting Multisine Signal Design Parameters

Adjustment of n_s is accomplished by iterating Equations (2.42) to (2.44) until a new n_s value can meet with the determined T and N_s. If this adjustment fails, T and N_s should be modified. This iterative procedure is illustrated in Figure 12.

4. Input Signal Considerations for Highly Interactive Systems

The challenges of identification problems in multivariable systems have been discussed in Chapter 1. A meaningful multivariable system identification design procedure must address issues associated with highly interactive systems. The flexibility offered by the design in the previous sections can be utilized for identifying highly interactive systems. This involves applying a specialized input power spectrum that will excite the low-gain directional dynamics, in order to make these comparable in magnitude to the high-gain directional dynamics. In this section, a fundamental analysis is presented to understand the general nature of highly interactive systems.

Jacobsen (1994) and Jacobsen and Skogestad (1994) introduce $[1 \quad 1]$ direction to describe the low-gain input direction of a binary high-purity distillation column. The low-gain direction meant by $[1 \quad 1]$ occurs at a 2×2 high-purity distillation column where the top and bottom products are operated at 99% and 1%, respectively. Particularly, $[1 \quad 1]$ direction is based on a material balance described by two inflows. If an input sequence is aligned to $[1 \quad 1]$ direction, its outputs will be lying in the low-gain direction. Thereafter, $[1 \quad 1]$ direction is interpreted into correlated input signals as a means for exciting the low-gain direction in highly interactive systems, specifically for high-purity distillation columns.

Through numerous efforts, the gain-directional information has been of interest as a key to leading reliable model-based controller applications for strongly interactive, ill-conditioned multivariable systems under noisy conditions. Stec and Zhu (2001) have proposed the use of sequential cycles of high-magnitude correlated and low-magnitude uncorrelated input signals in order to capture the low-gain direction information in the data, resulting in wider spread in the output state-space. Herein, a fundamental analysis from the

time-domain reveals how Stec and Zhu's experiment increases the low-gain direction information. In this work, the philosophy of Stec and Zhu (2001) in the time-domain has been adapted to define the "modified" zippered power spectrum, which is meaningful to highly interactive systems.

4.1. An Illustration of Stec and Zhu (2001) Analysis. A highly-interactive, linear high-purity distillation column per Morari and Zafiriou (1988) is presented as an example of the concept that modified multisine input designs can improve the gain-directional information in multivariable systems. A time-domain analysis using multisine signals is investigated to study how the 2×2 system outputs can acquire more low-gain directional information through simple algebraic equations including the steady-state gain. The transfer function matrix of this system is represented as

$$P(s) = \frac{1}{75s+1} \begin{bmatrix} 87.8 & -86.4 \\ 108.2 & -109.6 \end{bmatrix} \tag{2.46}$$

and its steady-state gain is

$$K = P(0) = \begin{bmatrix} 87.8 & -86.4 \\ 108.2 & -109.6 \end{bmatrix} \tag{2.47}$$

Using SVD analysis, output direction, singular value, and input direction vectors per Equation (2.47) are obtained as follows

$$SVD(K) = U\,S\,V^T = \begin{bmatrix} -0.6246 & -0.7809 \\ -0.7809 & 0.6246 \end{bmatrix} \begin{bmatrix} 197.2087 & 0 \\ 0 & 1.3914 \end{bmatrix} \begin{bmatrix} -0.7066 & -0.7077 \\ 0.7077 & -0.7066 \end{bmatrix}^T \tag{2.48}$$

It is assumed that the model information is known as *a priori* such that $\tau_{dom}^L = \tau_{dom}^H = 75$ min, $\delta = 0$, $\alpha_s = 7.5$, $\beta_s = 3.33$, and the primary bandwidth is defined as $\omega_* = 0.0167$, and $\omega^* = 0.40$. Thereafter, a set of feasible design parameters are $T = 15$ min, $n_s = 26$, and $N_s = 210$ by utilizing Equations (2.42)-(2.45) and the procedure in Figure 12. Since the degree of persistent excitation by (uncorrelated) harmonics is 26

per input channel, this 2×2 system can be estimated into an n-th order model such that

$$\text{Model Order } n \leq \frac{n_s}{2} = 13 \tag{2.49}$$

The properties of a standard zippered spectrum signal applied to the system per (2.46) are illustrated in Figures 13 and 14; time sequence (a), input state-space (b), and output state-space (c) plots are presented. This experiment shows significant contrasts between the input and output state-space plots for such a highly interactive system. In particular, the orthogonal power spectrum inputs are evenly distributed in input state-space (see Figure 13b); however, its output state-space is extremely dominant in the high-gain direction which is shown in Figure 13c. The identical (correlated) signal case has opposite directions between input and output state-space; the low-gain direction is highly dominant in the output state-space, as shown in Figure 14c. One could then expect that the combination of these inputs would lead to both high- and low-gain gain information in one set of data. Figure 15a shows that the sequential combination of orthogonal and correlated multisine input signals is applied for balanced gain-directional information. This is similar to the results reported by Stec and Zhu (2001) and Zhu (2001).

4.2. A Time-Domain Analysis of the Gain Direction. The gain directions in the outputs of a 2×2 highly-interactive process are decomposed into the same and opposite directions for simplicity; they can be assumed to be the high-gain ($[1 \quad 1]$) and low-gain ($[1 \quad -1]$) directions, respectively, in the high-purity distillation columns (Weischedel and McAvoy, 1980; Morari and Zafiriou, 1988; Skogestad and Morari, 1988*a*). Using further algebraic simplification, the two output directions can be noted as

$$y_1 \times y_2 < 0, \text{ low-gain direction} \tag{2.50}$$

$$y_1 \times y_2 > 0, \text{ high-gain direction} \tag{2.51}$$

We know for the high-gain direction, and two outputs can easily move in the same direction; however, for the low-gain direction, it is very hard to move the outputs in the opposite direction (Skogestad and

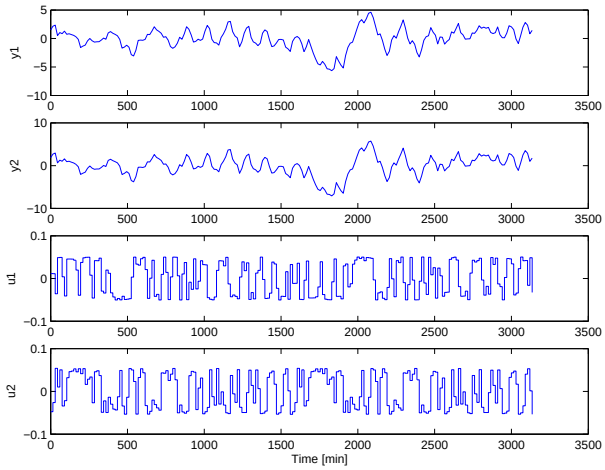

(a)

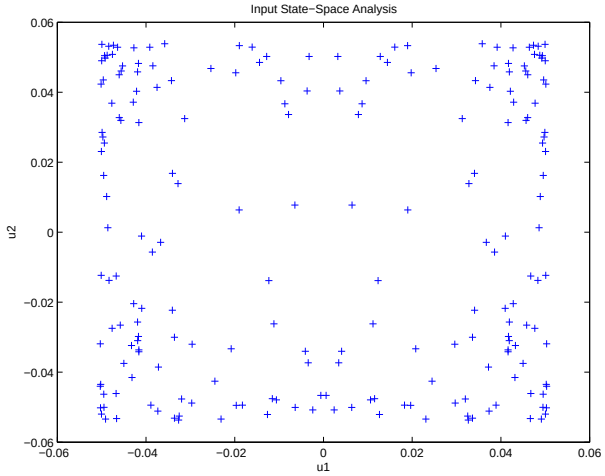

(b)

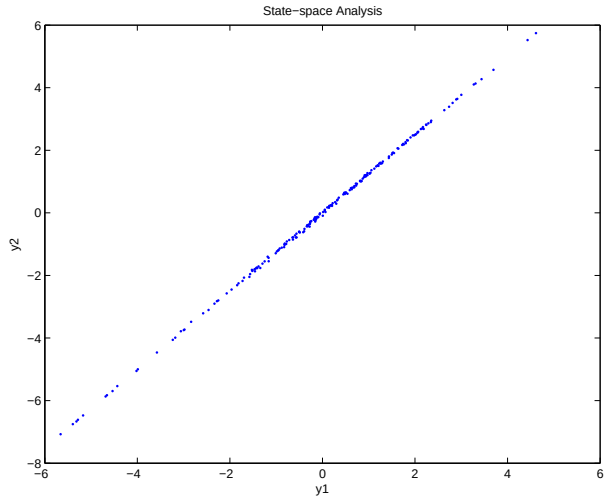

(c)

Figure 13. Open-loop identification test with the plant for Model0 using orthogonal signals: time sequences (a), input state-space (b), and output state-space (c)

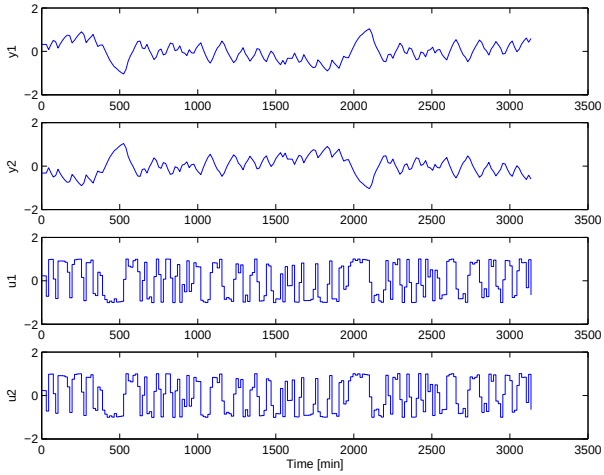

(a)

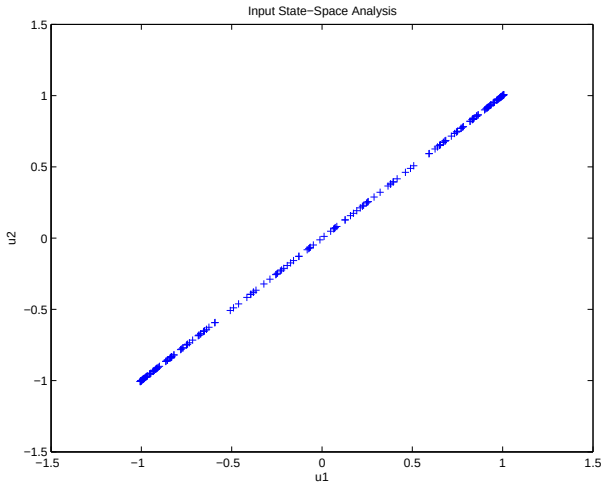

(b)

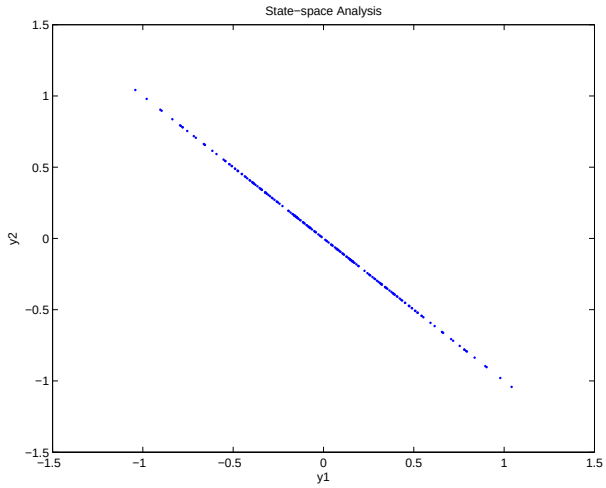

(c)

Figure 14. Open-loop identification test with the plant for the Model0 using correlated (identical) signals : time sequences (a), input state-space (b), and output state-space (c)

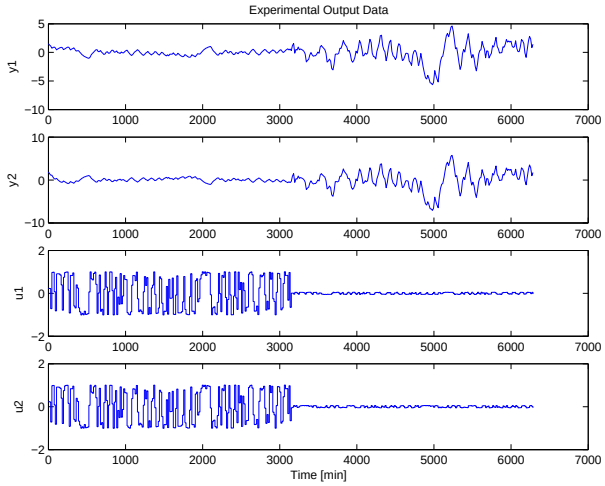

(a)

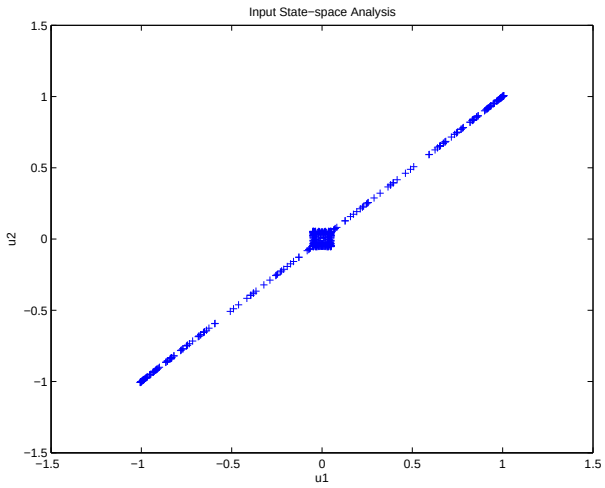

(b)

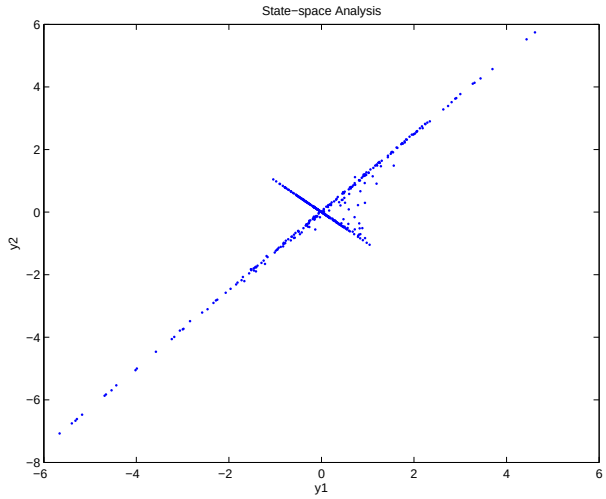

(c)

Figure 15. Analysis inspired by Stec and Zhu (2001) analysis with the plant for Model0 using multisine signals: time-domain input and output signals (a), input state-space plot (b), and output state-space plot (c)

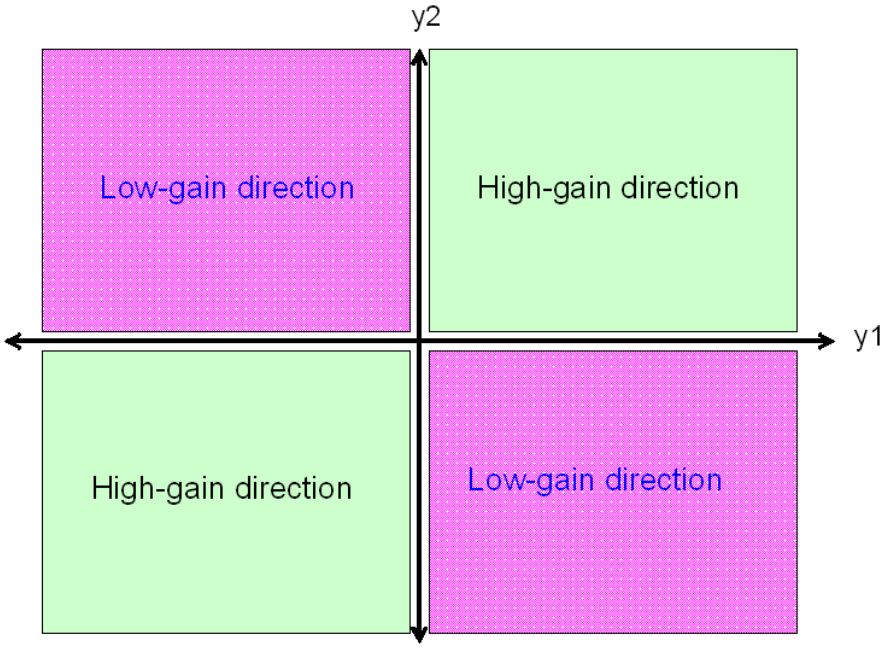

Figure 16. Area of gain directions in the output state-space

Postlethwaite, 1996) (see Figure 16). This description for the output directions is also concerned with a control objective in the distillation column. For high purity distillation performance, it is desirable to move the controlled variables in opposite directions to achieve higher purity in top and bottom products, which reflects the low gain direction.

The individual outputs are represented at steady-state gain per Equation (2.47)

$$y_1(t) = 87.8u_1(t) - 86.4u_2(t) \tag{2.52}$$

$$y_2(t) = 108.2u_1(t) - 109.6u_2(t) \tag{2.53}$$

A multiplication of y_1 and y_2 should be less than "0" for the low-gain direction; therefore, the condition with the two inputs is subject to

$$y_1(t) \times y_2(t) = 0.94999\, u_1(t)^2 + 0.94694\, u_2(t)^2 - 1.89714\, u_1(t)u_2(t) < 0 \tag{2.54}$$

With Equation (2.54), we can make two assumptions for the input signals based on $[1\ \ 1]$ input direction: (1) the two inputs are identical, and (2) the two inputs are very close, satisfying the low-gain direction condition

with a small perturbation. If the two inputs are identical, u_2 is replaced by u_1 as $u_1(t) = u_2(t)$

$$-0.00021\, u_1(t)^2 < 0 \tag{2.55}$$

As a result, Equation (2.55) is always less than 0 when the two inputs are identical as the outputs move in the opposite direction all the time. This explains Figure (14) (c) in which all the output points are in the low-gain direction. The slope between the outputs has only one angle

$$\frac{y_1(t)}{y_2(t)} = \frac{1.4u_1(t)}{-1.4u_1(t)} = -1 \tag{2.56}$$

so that the plot in the output state-space is formed as a thin back-slash line.

If a system is nonlinear and/or higher-order, varied angles or a wider spread in the output state-space would be more desirable in order to identify more precise models. This can be achieved by adding a small perturbation parameter to the second identical input signals instead of being identical, generating $[1 \quad 1+\varepsilon]$ (or $[1+\varepsilon \quad 1]$) inputs

$$u_2(t) = u_1(t) + \varepsilon(t), \qquad |\varepsilon(t)| \ll |u(t)| \tag{2.57}$$

and then the condition becomes

$$-2.1\times 10^{-4}u_1(t)^2 - 0.0033\varepsilon(t)u_1(t) + 0.94694\varepsilon(t)^2 < 0 \tag{2.58}$$

which is now solved with respect to $\varepsilon(t)$ with varying values of $u_1(t)$ at each t:

$$-0.01333u_1(t) < \varepsilon(t) < 0.0167u_1(t) \tag{2.59}$$

Thus, the open-loop test produces more varied low-gain directional distribution by utilizing the perturbation parameter, $\varepsilon(t)$. Figures 17 (a) and 18 (a) illustrate this comparison, while Figures 17 (b) and 18 (b) display the power spectra for these input signals. $\varepsilon(t)$ gives small perturbations to $u_1(t)$ so that the input direction of $[u_1(t)\ u_2(t)]$ is always close to $[1 \quad 1]$ direction.

These two illustrations confirm the analysis of Stec and Zhu (2001) that increasing the low-gain direction contents can be accomplished using correlated inputs in the conventional open-loop test. The

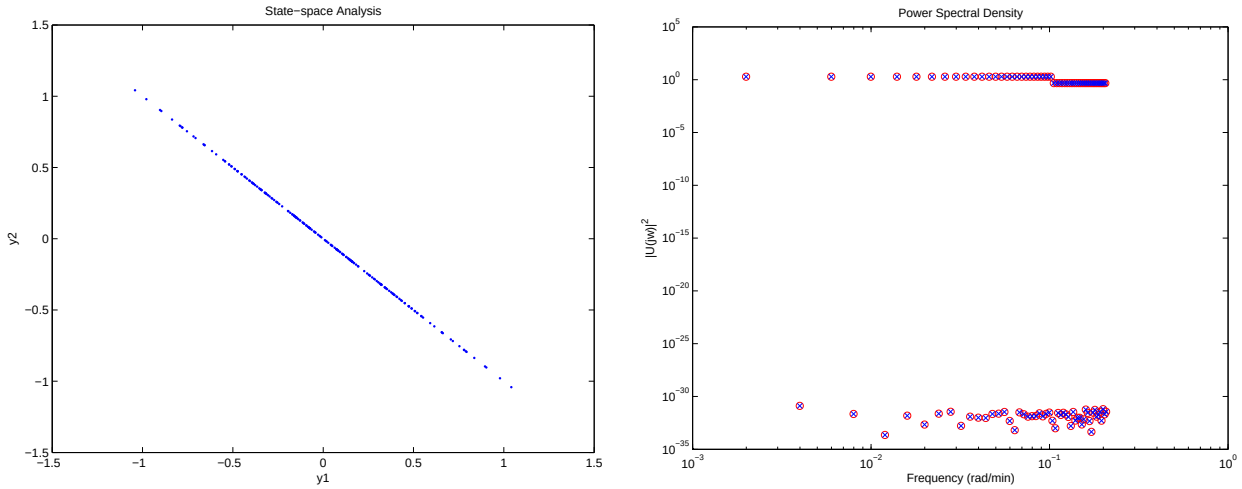

(a) (b)

Figure 17. Low-gain direction analysis using the identical signals per 2.46: output state-space plot(a) and input signals power spectrum (b)

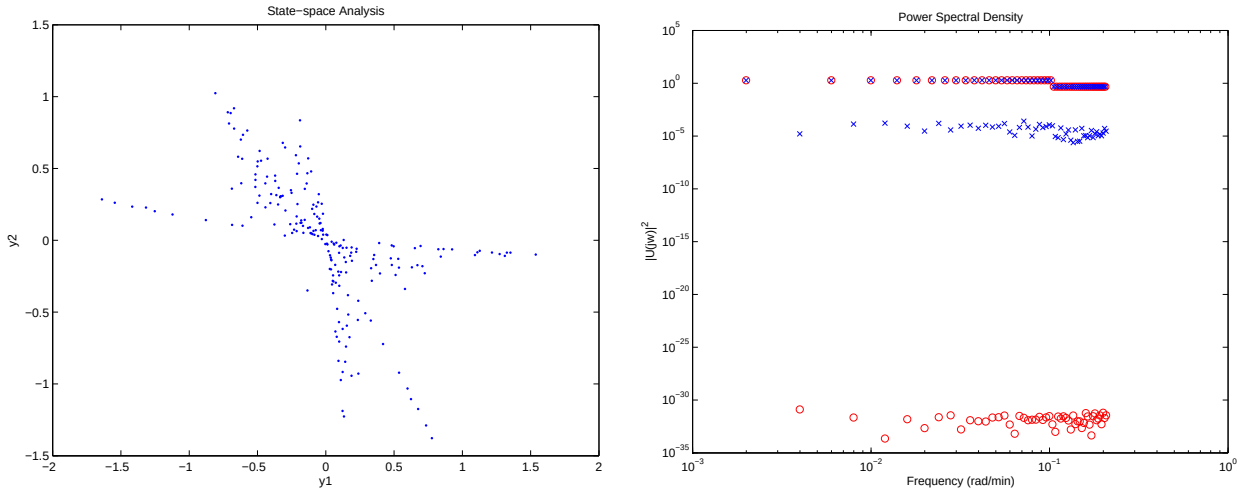

(a) (b)

Figure 18. Low-gain direction analysis using the time-domain modification per 2.46: output state-space plot(a) and input signals power spectrum (b)

correlated input signals are useful for exciting the low-gain directional dynamics in a highly interactive system where the low-gain direction lies on $[1 \;\; 1]$ direction. The small perturbation for $[1 \quad 1+\alpha]$ inputs makes the outputs spread widely in the output state-space. The experimental concept by Stec and Zhu (2001), performed in the time-domain, is adapted to define a *modified zippered* power spectrum from a frequency-domain perspective in the following section (Lee *et al.*, 2003).

5. Directional Multisine Inputs for Highly Interactive Systems using a Modified Zippered Spectrum

Focusing on the identification problems of a highly interactive system, a specialized power spectrum is designed to enhance the gain directional estimation during open-loop identification procedure. The philosophy by Stec and Zhu (2001) illustrated in the previous section is adapted to define a *modified zippered* power spectrum for enhancing the low-gain direction and achieving a varied distribution. This experimental input signal test leads further into the use of a combination of correlated and orthogonal harmonics in one cycle of the multisine input signal. A multisine input signal via a modified zippered power spectrum is designed, containing both correlated and uncorrelated harmonics (Lee *et al.*, 2003). With the modified input power spectrum, orthogonal multisine harmonics are to correspond in the high-gain direction and correlated harmonics are to correspond in the low-gain direction.

5.1. A Modified Zippered Power Spectrum. A general scheme of the modified zippered spectrum is illustrated in Figure 19. The modified zippered power spectrum design includes a channel for correlated harmonics that is part of the overall frequency grid such that

$$m\, n_s^{standard} = (\underbrace{m}_{uncorrelated} + \underbrace{1}_{correlated})\, n_s' \tag{2.60}$$

Other multisine design parameters remain the same with the standard zippered spectrum design per Equations (2.43) and (2.44). The actual degree of persistent excitations for each input channel in a modified

zippered spectrum is

$$n_s{}^{modified} = \left(\frac{n_s{}^{standard}\, m}{m+1}\right) + \left(n_s{}^{correlated}\right) \approx \frac{2mn_s^{standard}}{m+1} \tag{2.61}$$

An n-th order model can be approximated based on the number of uncorrelated harmonics according to

$$n \leq \frac{mn_s}{m+1} \tag{2.62}$$

where $n_s{}^{correlated} \approx \frac{n_s{}^{standard}\, m}{m+1}$.

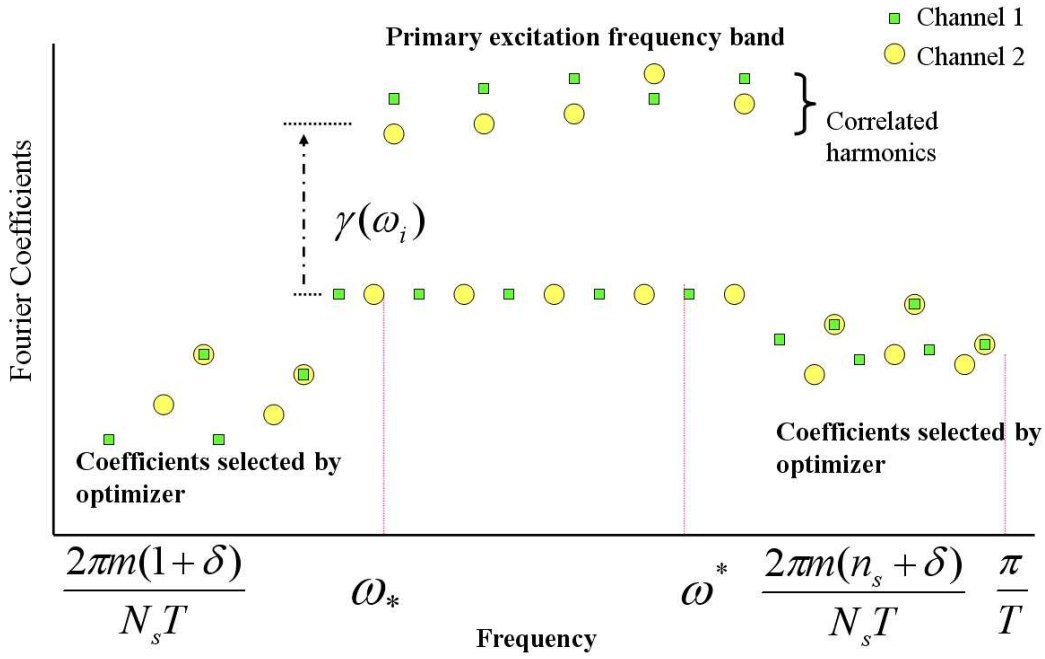

Figure 19. Conceptual design of a modified zippered power spectrum for 2-channel signal

To achieve the above modified zippered input power spectrum (Figure 19), we define the Fourier coefficients α_{ji} as:

$$\alpha_{ji} = \begin{cases} \neq 0, & i = (m+1)\delta + j, (m+1)(\delta+1) + j, \ldots, (m+1)(\delta + n_s' - 1) + j \text{ (uncorrelated)} \\ \neq 0, & i = (m+1)(\delta+1), (m+1)(\delta+2), \ldots, (m+1)(\delta+n_s') \text{ (correlated)} \\ = 0, & \text{for all other } i \text{ up to } (m+1)(\delta+n_s') \end{cases} \tag{2.63}$$

For efficient gain-directional estimation, the phases and Fourier coefficients of the correlated harmonics need to be adjusted according to a user-selected gain direction. The user-selected direction will be based on *a priori* knowledge. Stec and Zhu (2001) arbitrarily choose a larger magnitude for the correlated input signal without fundamental discussion on the ratio between the correlated and uncorrelated signals. In this dissertation, we further derive a systematic design procedure for these correlated harmonics, resulting in a meaningful modified zippered spectrum for a highly interactive system (Lee and Rivera, 2005; Lee and Rivera, 2006*a*).

5.2. Directional Design Approach for Multisine Input Signals. In highly interactive systems, the output gains between the high and low gain directions are distinctive in relation to the singular values. Koung and MacGregor (1993; 1994) take advantage of knowledge of the condition number to increase the information contents of the low gain direction, comparable to that of the high gain direction. In a similar manner, the correlated multisine harmonics in a modified zippered spectrum are formulated to be collinear in a user-specified direction, usually the low gain direction, with a corresponding amplitude adjustment in the frequency domain.

In general, a $n \times m$ gain matrix (K) is represented in a Singular Value Decomposition (SVD) as follows:

$$SVD(K) = U \Sigma V^H$$

$$U = [u_1, u_2, \ldots u_n] \qquad V^H = [v_1, v_2, \ldots v_m]$$

where Σ contains a diagonal nonnegative definite matrix Σ_1 of singular values arranged in descending order as in

$$\Sigma = \begin{pmatrix} \Sigma_1 \\ 0 \end{pmatrix}, \qquad n \geq m \tag{2.64}$$

$$\Sigma = (\Sigma_1 \quad 0), \qquad n \leq m \tag{2.65}$$

and

$$\Sigma_1 = diag\{\sigma_1, \sigma_2, ..., \sigma_k\}, \qquad k = \min\{m, n\} \tag{2.66}$$

where $\bar{\sigma} = \sigma_1 \geq \sigma_2 \geq ... \geq \sigma_k = \underline{\sigma}$ (Morari and Zafiriou, 1988). The output (U) and input (V^H) directional vectors are unitary and orthogonal, i.e., $[v_k] \times [v_j] = 0$ for $k \neq j$. If an input signal sequence $[x]$ is collinear to the j_{th} input directional vector in V^H such that $[x] = \alpha[v_j]^T$, $\alpha > 0$, then, $[v_j] \times [x]$ becomes

$$[v_j] \times [x] = [v_j] \times \alpha[v_j]^T = \alpha(\sum_{i=1}^{m} v_{ij} v_{ij}) = \alpha \tag{2.67}$$

This enables both direction and power amplitude adjustments of the correlated harmonics in a modified zippered multisine signal.

5.2.1. *Directional Adjustment for Correlated Multisine Harmonics.* A multisine input signal in the time-domain is transformed into the frequency-domain, consisting of a series of power amplitudes and phases. A multisine equation given as

$$x(k) = \sum_{i=1}^{n_s} \alpha_i \cos(\omega_i kT + \phi_i) \tag{2.68}$$

can be transformed into at a specific frequency ω_i

$$X(\omega_i) = \tilde{\alpha}_i e^{-j\tilde{\phi}_i} \tag{2.69}$$

where $X(\omega_i) = FFT([x])$, $\tilde{\alpha}_i = \sqrt{2\alpha_i} N_s$, $\tilde{\phi}_i = \omega_i T + \phi_i$. A multisine signal for multiple channels can be written in vector form as:

$$X(\omega_i) = \begin{bmatrix} \tilde{\alpha}_{1i} e^{j\tilde{\phi}_{1i}} \\ \tilde{\alpha}_{2i} e^{j\tilde{\phi}_{2i}} \\ \vdots \\ \tilde{\alpha}_{mi} e^{j\tilde{\phi}_{mi}} \end{bmatrix} \tag{2.70}$$

If the above multisine input per (2.70) represents the correlated harmonics in a modified zippered spectrum, the amplitude and phases are identical ($\phi_{1i} = \phi_{2i} = ...$ and $\alpha_{1i} = \alpha_{2i} = ...$) and $X(\omega_i) = X_c(\omega_i)$, such that:

$$X_c(\omega_i) = \begin{bmatrix} \tilde{\alpha}_i e^{j\tilde{\phi}_i} \\ \tilde{\alpha}_i e^{j\tilde{\phi}_i} \\ \vdots \\ \tilde{\alpha}_i e^{j\tilde{\phi}_i} \end{bmatrix} \tag{2.71}$$

To achieve the directional signal design, $\tilde{\alpha}_i$ and $\tilde{\phi}_i$ of the correlated harmonics should be adjusted to emphasize a selected input direction vector $[v_j]$. An input direction vector is transformed into spherical coordinates, and the amplitudes and phases of the selected direction vector are obtained as

$$v_j{}^T = \begin{bmatrix} v_{j1} \\ \vdots \\ v_{jm} \end{bmatrix} = \begin{bmatrix} \alpha_{j1}\, e^{j\phi_{j1}} \\ \vdots \\ \alpha_{jm}\, e^{j\phi_{jm}} \end{bmatrix} \tag{2.72}$$

For the first channel, the phases $\tilde{\phi}_i$ may be selected only by satisfying a plant-friendly criterion such as the crest factor of a signal. As a result, the adjusted correlated $X_c'(\omega_i)$ is formulated such that

$$X_c'(\omega_i) = v_j^* \otimes X_c(\omega_i) = \begin{bmatrix} \alpha_{j1}\tilde{\alpha}_i e^{j(\tilde{\phi}_i + 0)} \\ \vdots \\ \alpha_{jm}\tilde{\alpha}_i e^{j(\tilde{\phi}_i + \Delta\phi_{jm})} \end{bmatrix}, \; \Delta\phi_{ji} = \begin{bmatrix} -\phi_{j1} + \phi_{j1} = 0 \\ \vdots \\ -\phi_{jm} + \phi_{j1} \end{bmatrix} \tag{2.73}$$

where $v_j^* = conj(v_j)$ and $\otimes$ is the *Shur* product. $\Delta\phi_{ji}$ indicates that the correlated harmonics are rotated by

$e^{j\phi_{j1}}$. The directional adjustment is verified by a simple test

$$\begin{aligned} v_j^* \times X_c'(\omega_i) &= \begin{bmatrix} \alpha_{j1}\, e^{j\phi_{j1}} \\ \vdots \\ \alpha_{jm}\, e^{j\phi_{jm}} \end{bmatrix}^T \times \begin{bmatrix} \alpha_{j1}\, \tilde{\alpha}_i\, e^{j(\tilde{\phi}_i - \phi_{j1} + \phi_{j1})} \\ \vdots \\ \alpha_{jm}\, \tilde{\alpha}_i\, e^{j(\tilde{\phi}_i - \phi_{jm} + \phi_{jm})} \end{bmatrix} \\ &= \left[\alpha_{j1}^2 e^{j(\phi_{j1}-\phi_{j1})} + \cdots + \alpha_{jm}^2 e^{j(\phi_{jm}-\phi_{jm})}\right] \times \tilde{\alpha}_i e^{j\tilde{\phi}_i} e^{j\phi_{j1}} \\ &= 1 \times \tilde{\alpha}_i e^{j\tilde{\phi}_i} e^{j\phi_{j1}} \end{aligned} \tag{2.74}$$

where $\alpha_{ji}^2 + \cdots + \alpha_{jm}^2 = 1$. Therefore, $v_j^* \times X_c'(\omega_i) \neq 0$, $\tilde{\alpha}_i > 0$. Directional selection using X_c' is now available for selecting the low gain input direction (v_m) (or any other gain direction of the user's interest). Nevertheless, power adjustment is still required because the minimum singular value makes the output span in the low gain output direction too small in comparison with the span in the high gain output direction.

5.2.2. *Power Adjustment for Correlated Multisine Harmonics.* If the input signal $[x_1 \cdots x_m]^T$ is designed to be collinear to one input directional vector $[v_j]$, its corresponding output direction $[u_j]$ is manifested through the system only over correlated harmonics' frequency grids ω_i such that

$$\begin{aligned} Y(\omega_i) &= \begin{bmatrix} u_{1j}\sigma_j(v_{1j}u_1 + v_{2j}u_2 + \ldots + v_{mj}u_m) \\ u_{2j}\sigma_j(v_{1j}u_1 + v_{2j}u_2 + \ldots + v_{mj}u_m) \\ \vdots \\ u_{nj}\sigma_j(v_{1j}u_1 + v_{2j}u_2 + \ldots + v_{mj}u_m) \end{bmatrix}(\omega_i) \\ &= \begin{bmatrix} u_{1j} \\ \vdots \\ u_{mj} \end{bmatrix} \sigma_j \begin{bmatrix} v_{1j} \cdots v_{mj} \end{bmatrix} \begin{bmatrix} x_1 \\ \vdots \\ x_m \end{bmatrix}(\omega_i) \end{aligned} \tag{2.75}$$

Having designed how to adjust the input signal for any system input direction, we focus on the low or weak gain direction whose information contents we wish to increase in the output. If the input signal sequence is also collinear or close to the high gain direction (or not collinear to the low gain direction), the high gain

direction (e.g., $j = 1$) is naturally dominant in the response because of the maximum singular value (Morari and Zafiriou, 1988). At the correlated harmonics, the coefficients are set to $\gamma\alpha_{ji}$, where γ is a user-specified scaling factor. For simplicity with a two-input channel problem, we consider the first three frequencies in the grid (ω_1 denotes the uncorrelated excitation frequency for channel 1, ω_2 denotes the uncorrelated excitation frequency for channel 2, and ω_3 denotes the frequency for the correlated harmonic shared by both channels 1 and 2). The scaling factor γ is chosen such that the output signal power at ω_3 lies within an interval defined by the output power of the uncorrelated harmonics; that is, for both output channels $j = 1,2$ the following inequality should apply.

$$\min_j\{\Phi_{y_j}(\omega_1),\ \Phi_{y_j}(\omega_2)\} \ \leq\ \Phi_{y_j}(\omega_3) \ \leq\ \max_j\{\Phi_{y_j}(\omega_1),\ \Phi_{y_j}(\omega_2)\} \tag{2.76}$$

As a result, the correlated multisine harmonics with both direction and power adjustments for achieving a selected gain direction is obtained by the following

$$X_c'(\omega_i) \ =\ \gamma(\omega_i) \begin{bmatrix} \alpha_{j1}(\omega_i)\ \tilde{\alpha}(\omega_i)\ \exp^{j(\tilde{\phi}_i + \Delta\phi_{j1,i})} \\ \vdots \\ \alpha_{jm}(\omega_i)\ \tilde{\alpha}(\omega_i)\ \exp^{j(\tilde{\phi}_i + \Delta\phi_{jm,i})} \end{bmatrix} \tag{2.77}$$

5.2.3. *A Proof-of-Concept Test with a* 2×2 *Highly Interactive System.* The linear highly interactive system per Equation (2.46) is used to illustrate zippered power spectra in this section (Lee *et al.*, 2003). As presented before, a set of feasible design parameters utilizing Equations (2.42)-(2.44) and the procedure in Figure 12 is $T = 15$ min, $n_s = 26$, and $N_s = 210$. The gain matrix of the system is applied to design a modified zippered spectrum by calculating a ratio for correlated harmonics.

$$K \ =\ \begin{bmatrix} 87.8 & -86.4 \\ 108.2 & -109.6 \end{bmatrix}$$

$$SVD(K) \ =\ U\,S\,V^T \ =\ \begin{bmatrix} -0.6246 & -0.7809 \\ -0.7809 & 0.6246 \end{bmatrix} \begin{bmatrix} 197.2087 & 0 \\ 0 & 1.3914 \end{bmatrix} \begin{bmatrix} -0.7066 & -0.7077 \\ 0.7077 & -0.7066 \end{bmatrix}^T$$

Using the low-gain direction input vector according to (2.46), the minimum and maximum ratios for correlated harmonics are obtained such that

$$56.68 \quad \leq \gamma \leq \quad 88.60 \tag{2.78}$$

If the exact low gain direction $[-0.707 \ -0.708]^T$ is replaced with $[1 \quad 1]^T$, the guideline results in

$$62.21 \quad \leq \gamma \leq \quad 77.78 \tag{2.79}$$

The difference between (2.78) and (2.79) is a result of the input directional sensitivity corresponding to the large condition number. This is shown through a simple comparison of the outputs of $K\underline{v}$ and $K[1 \quad 1]^T$ as

$$y \ = \ K\,\underline{v} \ = \ \begin{bmatrix} -1.0866 \\ \\ 0.8691 \end{bmatrix} \tag{2.80}$$

and

$$y \ = \ K\,[1 \quad 1]^T \ = \ \begin{bmatrix} -1.40 \\ \\ 1.40 \end{bmatrix} \tag{2.81}$$

The output of $y = K\underline{v}$ is lying exactly on the low-gain output direction ($[\underline{u}]$), and $y = K[1 \quad 1]^T$ is close enough to $[\underline{u}]$. Therefore, γ based on $[1 \quad 1]$ direction can be used to move the dynamical system in the low-gain direction. If the low-gain input direction is $\underline{v}$, the correlated harmonics for the directional and power adjustment need to satisfy

$$[u] \ \equiv \ \gamma\,[\underline{v}], \qquad \gamma > 0 \tag{2.82}$$

while this cancels other input directions. For the Model0 system, the value $\gamma = 64.5$ is used for the correlated harmonics in a modified zippered spectrum per the plant (2.46).

Figures 20 and 21 show the input and output power spectral densities, respectively, of both standard and modified zippered signals for the example case per 2.46. $\gamma = 64.5$ per Equation (2.79) is applied to

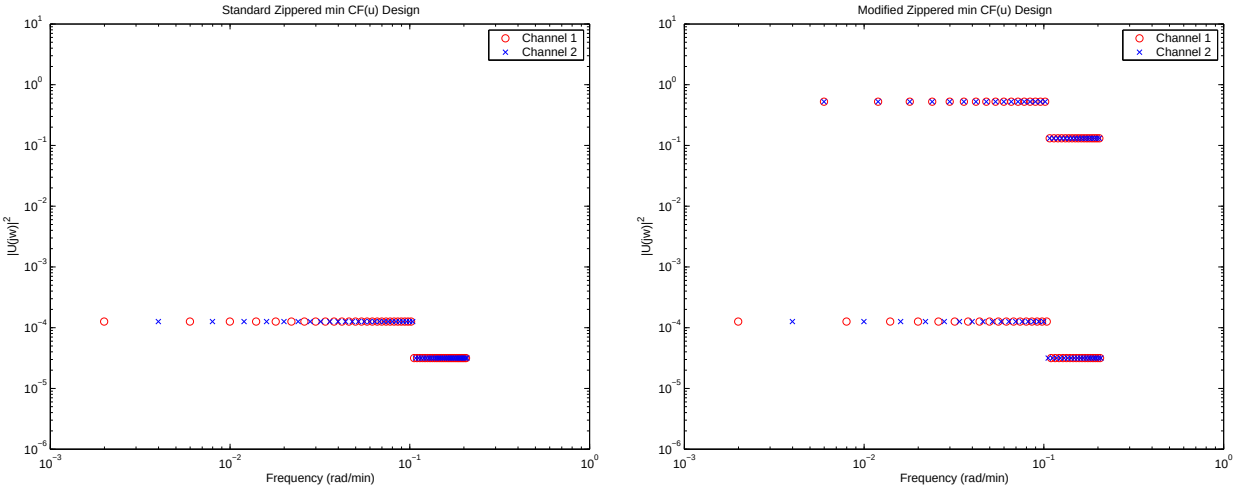

(a) (b)

Figure 20. Input power spectra for the standard zippered (a) and modified zippered (b) signal design ($\gamma = 64.5$); plant model per (2.46).

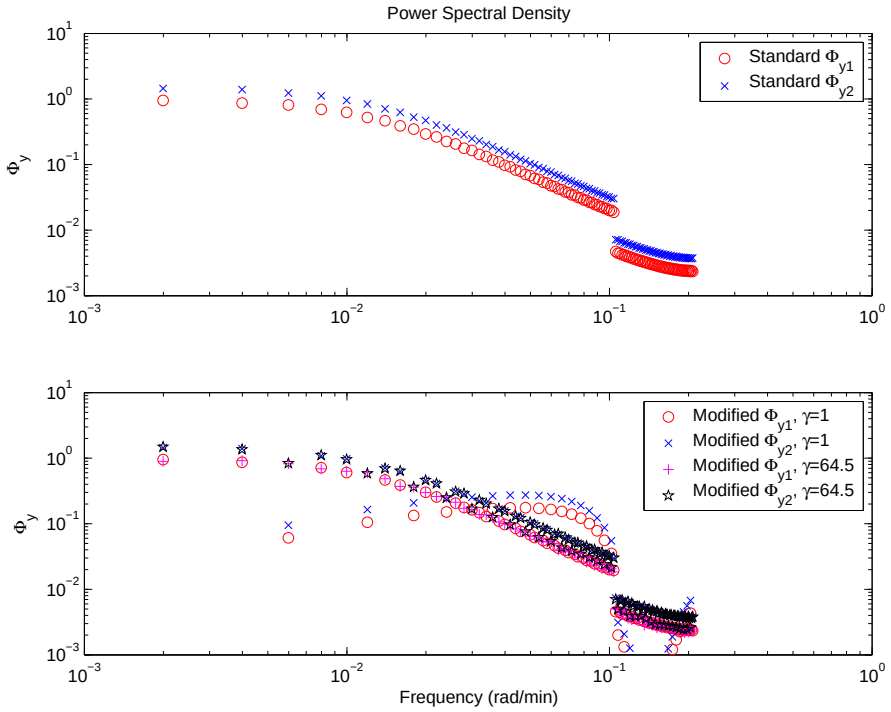

Figure 21. Output power spectra for the standard zippered (top) and modified zippered (bottom) signals ($\gamma = 1$ and $\gamma = 64.5$ cases considered), plant model per (2.46).

generate a modified zippered spectrum (Figure 20b). Figure 21 highlights the effect of the γ ratio in the correlated harmonics. For $\gamma = 1$, the input power in the correlated harmonics does not sufficiently stimulate the low-gain dynamics content in comparison to the standard zippered case. However, for $\gamma = 64.5$ within the range (2.79), the correlated input signal power is now high enough so that the output power in the correlated harmonics is comparable to that of the high gain direction, as seen from the standard zippered signal output spectra (Figure 21).

6. Phase-Shifted Multisine Input Signals

In multivariable system identification, shifting a single-channel signal in the time-domain is a common technique for implementing multi-channel input signals, e.g., PRBS, PRS, etc (Godfrey, 1993), while the base and shifted signals have the identical power spectral density. Multisine signals by the *zippered* power spectrum possess orthogonality in each input channel that allows greater flexibility at the cost of extended sequence length. However, shifting does not change the length since all channels share the same frequency grids. Shifting and zippering techniques have their own merits, respectively. We will explore the properties of the shifting and zippering features in multisine signals and compare these with PRBS signals.

A time-domain shift method is applied to multisine signals with a modification from the guideline previously described for PRBS inputs in Rivera and Jun (2000). The determination of a shift parameter in the time-domain is modified in order to minimize the cross correlation between the signals while their cross input power spectra are nonzero. In this section, we briefly discuss a guidelines for PRBS inputs, its modification for shifted multisine inputs, and a comparison between PRBS and multisine inputs for the Shell Heavy-Oil Fractionator case.

6.1. Design Guideline of PRBS Inputs. The PRBS is a two-level, periodic, deterministic signal generated by using shift register modulo 2 addition (Godfrey, 1993). The PRBS sequence is characterized

by two parameters, the number of registers (n_r) and switching time or the clock period (T_{sw}), which is the minimum time between changes in the level of the signal. The signal repeats itself after $N_s T_{sw}$ units of time, where $N_s = 2^{n_r} - 1$. The excitation bandwidth is obtained by applying *a priori* knowledge of a system such that

$$\frac{1}{\beta_s \tau_{dom}^H} \leq \omega \leq \frac{\alpha_s}{\tau_{dom}^L} \tag{2.83}$$

The above equation serves as a basis for specifying design variables in a PRBS. Following the analysis in Gaikwad and Rivera (1996), one can obtain expressions for specifying T_{sw} and n_r based on the parameters from (2.83)

$$T_{sw} \leq \frac{2.8\tau_{dom}^L}{\alpha_s} \tag{2.84}$$

and a shift parameter for multiple channels is

$$D \geq \frac{5\tau_{dom}^H}{T_{sw}} \tag{2.85}$$

The sequence length is then determined by

$$N_s^{(1)} = \frac{2\pi\beta_s\tau_{dom}^H}{T_{sw}} \tag{2.86}$$

$$N_s^{(2)} = m \times D \tag{2.87}$$

$$N_s = 2^{n_r} - 1 \geq \max(N_s^{(1)}, N_s^{(2)}) \tag{2.88}$$

where n_r and N_s must be integer values; T_{sw} and D must be integer multiples of the sampling time T and T_{sw}, respectively.

Simultaneous multiple input testing offers some advantages including the potential for decreasing the overall duration of experimental testing (Rivera and Jun, 2000). To generate a multi-input PRBS signal, the shift parameter per (2.85) is utilized for keeping cross-correlation sufficiently low between channels. The identical number of registers and switching time are used in each channel; however, the registers must be initialized such that the input appears shifted relative to the previous input by a delay D. Inputs numbered

from 2 to m (the number of channels) will be delayed by $[D, 2D, 3D, ..., (m-1)D]$ with respect to the base input channel.

For the Shell Heavy-Oil Fractionator problem per 2.103, the signal design parameters for PRBS using these guidelines are $\tau_{dom}^{H} = 74min$, $\tau_{dom}^{L} = 48min$, $\alpha = 2$, and $\beta = 3$. Accordingly, a primary bandwidth is defined as $\omega^{*} = 0.04167$ and $\omega_{*} = 0.0045$. The choices for a PRBS input signal are $N_s = 496$, $T = 4\,min$ and $T_{sw} = 64\,min$. We assume that there are three channels ($m = 3$) and a shift parameter is selected as $D = 166 \times T$(=664 min). The base PRBS signal and the correspondingly shifted signals are shown in Figure 22.

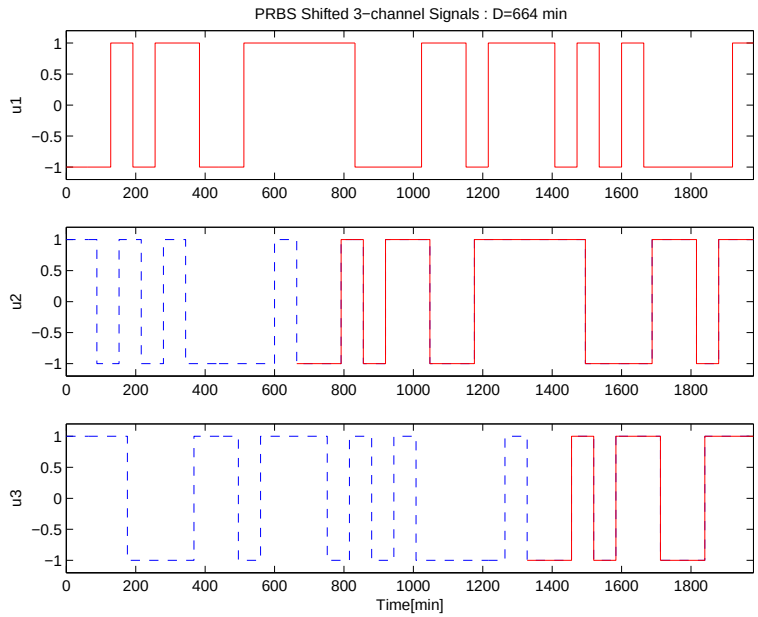

Figure 22. Base and shifted PRBS signals for 3-channel inputs for Shell Heavy-Oil Fractionator Problem Example per (2.103) : $\tau_{dom}^{H} = 74min$, $\tau_{dom}^{L} = 48min$, $\alpha = 2$, $\beta = 3$, $N_s = 496$, $T = 4\,min$, $T_{sw} = 64\,min$, and $D = 166 \times T\,(= 664min)$

6.2. Determination of a Shift Parameter for Multisine Inputs. We first present an example for two-channel input signals: first, a base channel input is defined by the general multisine equation and the

second input is a shifted signal with respect to the base input. The first channel input is given as follows

$$u_1(k) \;=\; \lambda \sum_{i=1}^{n_s} \sqrt{2\alpha_i} cos(\omega_i kT + \phi_i) \tag{2.89}$$

and this signal is shifted by a delay D for the second channel

$$u_2(k) \quad = \quad \lambda \sum_{i=1}^{n_s} \sqrt{2\alpha_i} cos(\omega_i (k+D)T + \phi_i) \tag{2.90}$$

$$= \quad \lambda \sum_{i=1}^{n_s} \sqrt{2\alpha_i} cos(\omega_i kT + \omega_i DT + \phi_i) \tag{2.91}$$

where D is a shift parameter similar to the one defined for the PRBS input guideline. In multisine input, D is added into the sequence index k for a delay in time-domain sequence. As a result, shifted multisine input signals are obtained by

$$u_j(k) \;=\; \lambda \sum_{i=1}^{n_s} \sqrt{2\alpha_i} cos(\omega_i (k+D_j)T + \phi_i) \tag{2.92}$$

The shift parameter needs to be as large as possible to keep cross-correlation low enough for model estimation such as

$$D_j \;=\; \frac{N_s}{m} \times (j-1), \quad j = 2, ..., m \tag{2.93}$$

The shifted channels, therefore, have a delay $D = \frac{N_s}{m}$ which considers the settling time requirement, similar to the PRBS shift parameter per Equation (2.85). D per Equation (2.93) needs to satisfy the following inequality

$$D = \frac{N_s}{m} \;\geq\; \frac{\beta \tau_{dom}^H}{T} \;=\; \frac{1}{\omega_* T} \tag{2.94}$$

where $\beta = 5$ to define the settling time of the process and T is the sampling time for a multisine input signal. As a result, N_s for a base channel is defined by

$$N_s \geq \frac{m}{\omega_* T} \tag{2.95}$$

which indicates that the base channel input length should be increased long enough for shifted inputs. As a result, we have the following inequality for N_s

$$\max\{2(n_s+\delta), \frac{2\pi(1+\delta)}{\omega_* T}, \frac{m}{\omega_* T}\} \leq \; N_s \; \leq \frac{2\pi(n_s+\delta)}{\omega^* T} \tag{2.96}$$

in which it must satisfy

$$\frac{m}{\omega_* T} \leq N_s \leq \frac{2\pi(n_s+\delta)}{\omega^* T} \tag{2.97}$$

namely, n_s should be

$$n_s+\delta \geq \frac{m}{2\pi}\frac{\omega^*}{\omega_*} \tag{2.98}$$

The conclusion of the shift parameter results in an additional inequality for n_s.

To generate shifted multisine signals for m-input channels, a modified guideline for a base input channel is presented as follows:

$$n_s+\delta \geq \max\{(1+\delta)\frac{\omega^*}{\omega_*}, \frac{m}{2\pi}\frac{\omega^*}{\omega_*}\} \tag{2.99}$$

$$T \leq \min\{\frac{\pi}{\omega^*}, \frac{\pi}{\omega^*-\omega_*}(\frac{n_s-1}{n_s+\delta})\} \tag{2.100}$$

$$\max\{2(n_s+\delta), \frac{2\pi(1+\delta)}{\omega_* T}\} \leq N_s \leq \frac{2\pi(n_s+\delta)}{\omega^* T} \tag{2.101}$$

When $\delta = 0$ and if $m > 2\pi(\approx 7)$, n_s is determined by $\frac{m}{2\pi}\frac{\omega^*}{\omega_*}$; unless, n_s is determined by $\frac{\omega^*}{\omega_*}$ per (2.99). N_s is then given by

$$N_s \leq \frac{m}{\omega_* T} = m\frac{\beta_s \tau_{dom}^H}{T} = m \times D \tag{2.102}$$

6.3. Comparison between Shifted and Zippered Signals. For the Shell Heavy-Oil Fractionator problem, the signal design parameters are obtained from *a priori* knowledge of the system: $\tau_{dom}^H = 74$ and $\tau_{dom}^L = 48$ min. The Shell Heavy-Oil Fractionator (Prett and García, 1988) is given as

$$y(t) = \begin{bmatrix} \frac{1.77}{60\,s+1}\exp^{-28s} & \frac{5.88}{50\,s+1}\exp^{-27s} \\ \frac{5.72}{60\,s+1}\exp^{-14s} & \frac{6.90}{40\,s+1}\exp^{-15s} \end{bmatrix} u(t) \tag{2.103}$$

where the sampling time, $T = 4$ min, the physical outputs and inputs are

$$y(t) = \begin{bmatrix} \text{Top End. Product} \\ \text{Side End. Product} \end{bmatrix} \qquad u(t) = \begin{bmatrix} \text{Side Draw} \\ \text{BR Duty} \end{bmatrix} \tag{2.104}$$

A series of PRBS and multisine signals are generated using the same information, and the design parameters of the signals are listed in Table 1. All the cases meet the frequency bandwidth requirements of ω_* and ω^*. Interestingly, the shifted multisine signal has a shorter signal length than the PRBS case by 29.43%. As expected, the zippered multisine signal is the longest duration signal, which is two times longer than the shifted multisine signal.

Signal	α	β	ω_*	ω^*	T (min)	N_s	1_{cycle} (min)	D	CF(x)
PRBS (shifted)	2	3	0.0045	0.0417	4	496	1984.00	248	1.000 1.000
Multisine (shifted)	2	3	0.0045	0.0417	4	350	1400.00	175	1.421 1.421
Multisine (zippered)	2	3	0.0045	0.0417	4	698	2792.00	0	1.218 1.244

Table 1. Design parameters of PRBS signal ($T_{sw} = 64min$) and shifted and zippered multisine signals using Guillaume-phasing ($hf = 0$) for Shell Heavy-Oil Fractionator Problem per 2.103

The comparison of input power spectra, time series signal, correlation analysis, and cross input power spectra is given in Figures 23- 26. First, a comparison of the input power spectra is shown in Figure 23. The shifted signals power spectra show that they are correlated in the sense of frequency-domain; they are not applicable for ETFE but suitable for spectral analysis or high-order ARX to generate multivariable frequency responses. Figure 24 presents the time-domain sequences of input and output signals of PRBS and multisine signals.

Time-domain correlation analysis is given in Figure 25, and variance and standard error bounds are computed as follows

$$Var[\gamma_{xx}(k)] \cong \pm \frac{1}{N}, \quad k > 0 \quad \text{with 95\% confidence.} \tag{2.105}$$

The standard error bound is given by:

$$S.E[\gamma_{xx}(k)] \cong \pm \frac{3}{\sqrt{N}}, \quad k > 0 \quad \text{with 99\% confidence.} \tag{2.106}$$

For cross-correlation analysis, the variance and standard error bounds are:

$$Var[\gamma_{xe}(k)] \cong \pm \frac{3}{N-k}, \quad k > 0 \quad \text{with 99\% confidence, and} \tag{2.107}$$

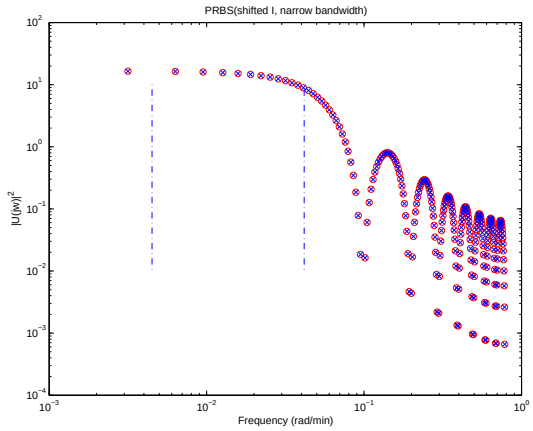

(a)

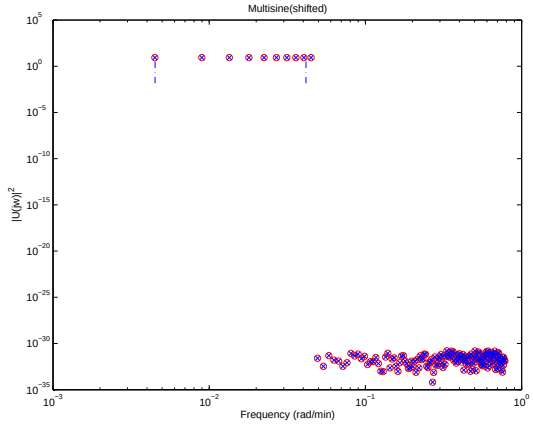

(b)

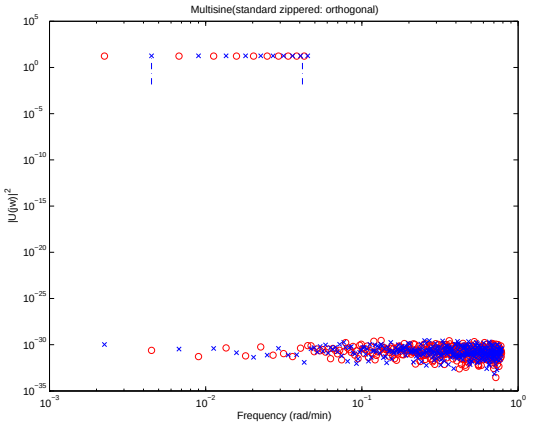

(c)

Figure 23. Shell Heavy-Oil Fractionator Problem Example per (2.103): Input power spectra of PRBS(a), shifted Multisine (b), and zippered Multisine (c) signals

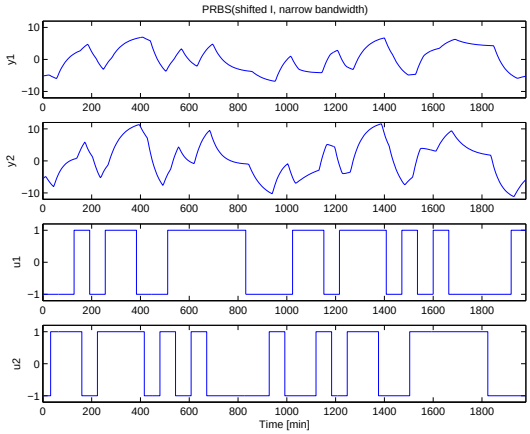

(a)

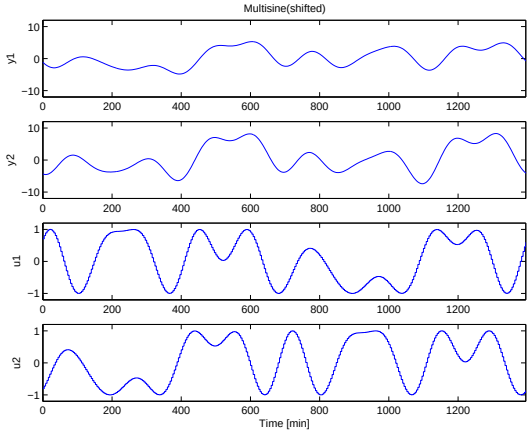

(b)

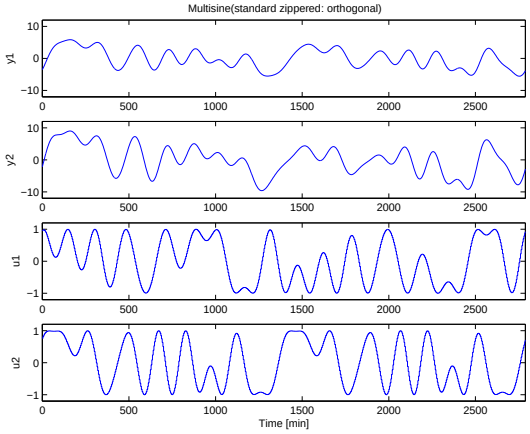

(c)

Figure 24. Shell Heavy-Oil Fractionator Problem Example per (2.103): Time sequences of input and output signals of PRBS(a), shifted Multisine (b), and zippered Multisine (c) signals

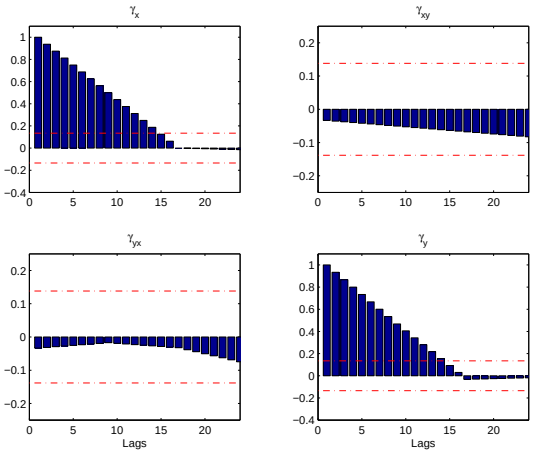

(a)

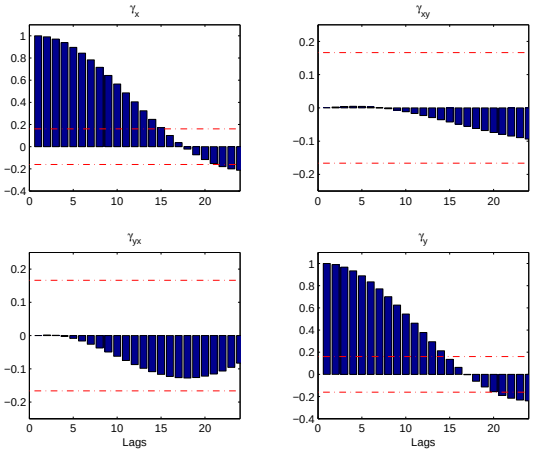

(b)

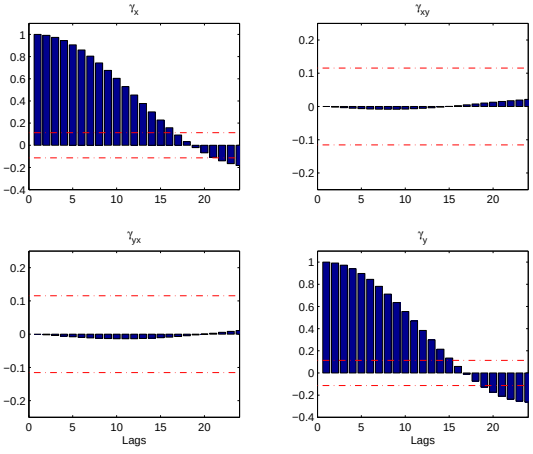

(c)

Figure 25. Shell Heavy-Oil Fractionator Problem Example per (2.103): Correlation analysis of input signals with lag=15, PRBS(a), shifted Multisine (b), and zippered Multisine (c) signals

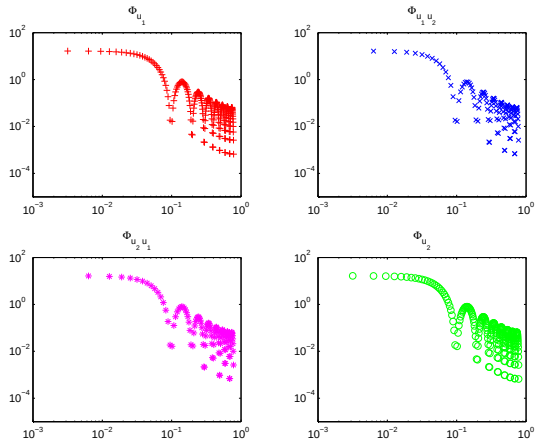

(a)

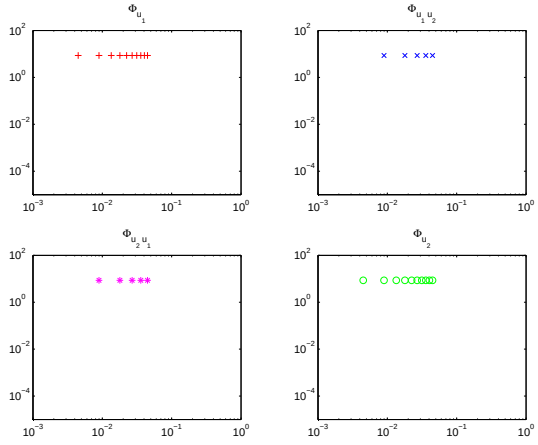

(b)

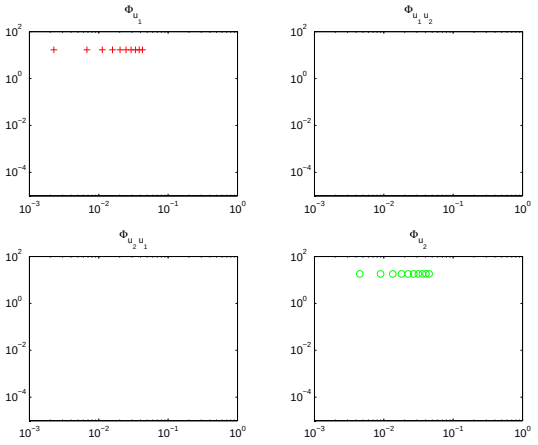

(c)

Figure 26. Shell Heavy-Oil Fractionator Problem Example per (2.103): Cross power spectra of input signals of PRBS(a), shifted Multisine (b), and zippered Multisine (c) signals

$$S.E[\gamma_{xe}(k)] \cong \pm \frac{3}{\sqrt{N-k}}, \quad k > 0 \quad \text{with 99\% confidence.} \tag{2.108}$$

The cross-correlation of the shifted signals indicates that they do not violate the standard error criteria — this means that the shifted multisine signals have sufficiently low cross-correlation between the base input channel. The zippered multisine signal will not violate this standard error criteria in the correlation since their inputs are independent. However, the power spectral analysis shows that the shifted signals have considerable cross spectral power equivalent to auto-correlated spectral power (Figure 26).

We have shown in this section that based on *a priori* knowledge of a system, feasible design parameters are obtained for shifted PRBS and multisine inputs. The shifted PRBS signal technique that is commonly used for multiple input designs is extended for multisine inputs with a necessary modification in its design guideline. Through the example case study, a time-domain shifting technique is easily implemented in both multisine and PRBS signals. Multisine signals for multivariable system identification can therefore be used in either shifted or zippered form depending on the system characteristics.

7. Harmonic Suppression in Multisine Inputs for Nonlinear Systems

Harmonic suppression in a signal can be used to smooth nonlinear distortions in the estimation of a nonlinear system to linear transfer functions (Barker and Al-Hilal, 1985). Suppression of multiples of prime numbers, $h = 2, 3, 5,$ etc., are applied to power spectrum design. For example, if even-order harmonics (multiples of 2) are suppressed in the input signal, the effect of even-order nonlinearities in the system is reduced in the outputs, while odd harmonics reflect the linear part of the process (Barker, 1993). Braun *et al.* (2002*b*) present improved Empirical Transfer Function Estimate (ETFE) for a nonlinear system using harmonic-suppressed multisine input signals in comparison to non-suppressed signal cases.

Suppressing harmonics is easily performed to define an input power spectrum in multisine signals. The conceptual design of harmonic suppression is illustrated in the standard zippered spectrum in Figure 27a

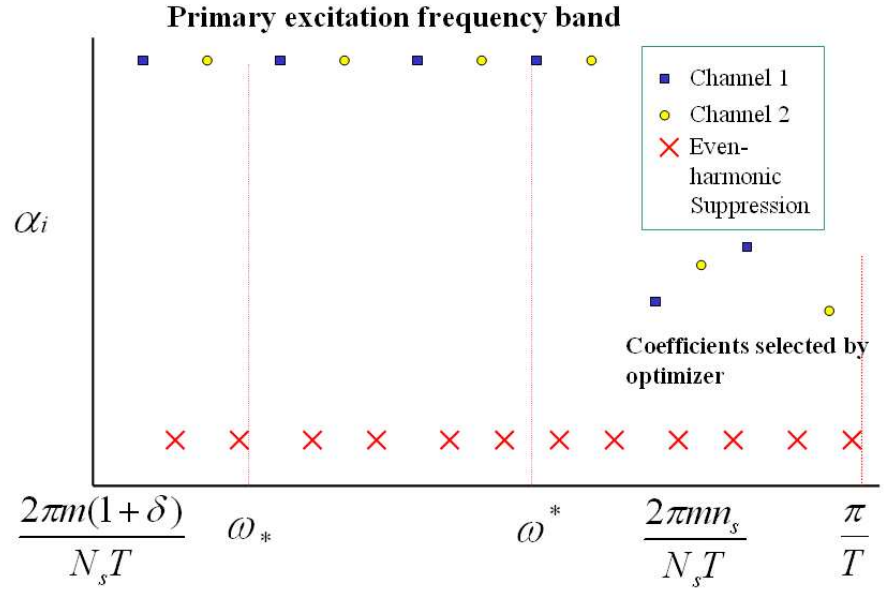

(a)

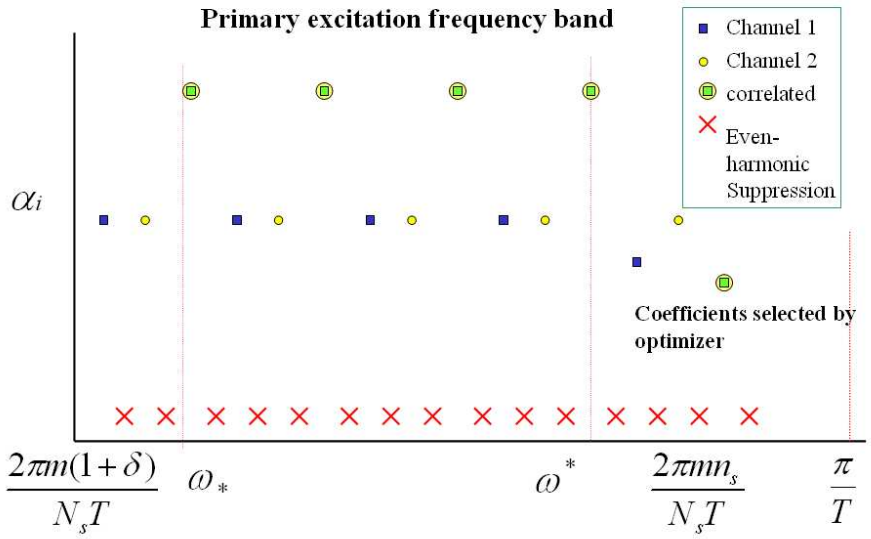

(b)

Figure 27. Conceptual design of even-order harmonic suppression for a standard zippered spectrum (a) and a modified zippered spectrum (b)

and in the modified zippered spectrum in Figure 27b with even-order ($h = 2$) harmonic suppression. The low-frequency interval parameter allows the design guideline to make enough frequency grids satisfying the primary excitation bandwidth requirement for harmonic suppression. For example, with even-harmonic suppression, $\delta = 1$ for the low-frequency interval to ensure at least one degree of excitation below ω_*. The interval number δ accordingly increases the signal length in proportion to $N_s(1+\delta)$. Therefore, harmonic suppression causes a longer identification test duration while all other design parameters remain the same in the non-suppression case.

8. Plant-Friendly Identification by Constrained Optimization Formulations

The fundamental purpose of plant-friendly system identification is to design informative experiments that are not disruptive in the process. A plant-friendly test will produce data leading to a suitable model within an acceptable time period while keeping the variation in both input and output signals within user-defined constraints. As previously stated in the Introduction, a series of plant-friendly constraints (and their impact on process operations) include:

- keeping output deviations low to minimize variability in product quality,
- implementing a signal of sufficiently short duration to minimize the amount of off-spec product and reduce engineering time associated with an identification test, and
- keeping move sizes small to satisfy actuator limits and minimize “wear and tear” on process equipment.

This is accomplished by employing constrained optimization techniques while multisine design values are based on *a priori* knowledge of a system. In this section, a series of plant-friendly experiment formulations employing constrained optimization using multisine input signals are proposed, meaningful for multivariable systems. The concept of the plant-friendly identification is illustrated first in the linear, high-purity

distillation column per Equation (2.46) and then in a nonlinear example per the Weischedel-McAvoy column (1980).

8.1. Preliminaries of Plant-friendly Multisine Input Signal. No single criterion comprehensively defines plant-friendliness, although varied metrics have been proposed (Doyle *et al.*, 1999; Parker *et al.*, 2001; Narasimhan *et al.*, 2003). Doyle *et al.* (1999) use a friendliness index that is defined as a ratio of the number of changes of input value from previous value to the total sequence length,

$$f = 100 \times \left(1 - \frac{n_T}{N-1}\right) \tag{2.109}$$

where N is the sequence length and n_T constitutes the number of transitions (i.e., situations where $u(k) \neq u(k-1)$).

One measure that has been studied extensively in the context of plant-friendliness is the crest factor (CF) (Schroeder, 1970; Guillaume *et al.*, 1991; Godfrey, 1993). The crest factor, defined as the ratio of the ℓ_∞ (or Chebyshev) norm and the ℓ_2-norm of a signal,

$$CF(u) = \frac{\ell_\infty(u)}{\ell_2(u)}, \qquad \ell_p(x) = \left[\frac{1}{N_s}\int_0^{N_s} |x(t)|^p dt\right]^{\frac{1}{p}} \tag{2.110}$$

provides a measure of how well distributed the signal values are over the input span. An alternative measure of signal distribution to crest factor is the Performance Index for Perturbation Signals (PIPS; Godfrey *et al.* (1999)).

$$PIPS(\%) = 200\frac{\sqrt{x_{rms}^2 - x_{mean}^2}}{x_{max} - x_{min}} \tag{2.111}$$

The PIPS measure ranges between 0 and 100% (compared to ∞ versus 1 for crest factor), which gives it an intuitive, practical appeal. Although we do not optimize this PIPS measure directly, it is evaluated along with crest factor. In this dissertation, we focus on minimizing the crest factor by presenting a series of optimization problems to accomplish the plant-friendliness in identification testing.

A low crest factor indicates that most of the elements in the input sequence are distributed near the minimum and maximum values of the sequence. Lowering crest factor can significantly improve the Signal-to-Noise Ratio (SNR) of the resulting signal, thus contributing to plant-friendliness during experimental testing. If two signals with equivalent power spectral densities are to be evaluated for identification purposes, the one with lower crest factor is preferred because it will deliver the same power over a lower overall span with a larger SNR. Minimizing output crest factor while enforcing input and output constraints during identification testing is of particularly great value in the process industries since the nature of the output signal will usually have the most influence on product quality and hence profitability within the enterprise.

In Section 2 we presented a set of design guidelines for multivariable input signals based on *a priori* knowledge of a system that provides a primary bandwidth, sequence length, number of sinusoids, and sampling time. An optimization problem is then solved which seeks to find the optimal phases (ϕ_i) in the multisine signal (and additionally, the Fourier coefficients (α_i) in frequency bands not specified by the user) that directly minimize the crest factor. If the user has some reasonable *a priori* knowledge of model parameters (or, more realistically, develops improved knowledge of the model through identification testing), the crest factor of the output signal anticipated during identification testing can be minimized as well. The optimization problem is solved in the presence of explicit time-domain constraints on upper/lower limits, move sizes, and rate of change in either (or both) input and output signals. This constrained time-domain formulation is appealing to process control engineers, as they tend to think more in terms of maintaining high/low limits, move size constraints, and test duration during identification testing and less in terms of norm criteria that are typically used in the classical optimal experimental design formulations.

The optimization problem of minimizing the crest factor of a signal under time domain constraints represents a challenging computational task, but it is critical to the success of the proposed technique. For one, it is always nonlinear, either in the objective function, the constraints or in both. It is non-convex in general from the statement of the objective function. In addition, it is non-smooth as a consequence of

the ℓ_∞ norm in the objective function. Combined with its size in terms of both variables and constraints, this problem requires the use of state-of-the-art optimization techniques. Ultimately, a desirable goal is to develop these solution techniques so they can be executed in quasi-"real-time" and thus increase their usefulness for the practicing engineer.

8.2. Computational Framework for Minimum Crest-factor Multisine Signal. Early work in the design of low crest factor multisines for system identification includes the work of Schroeder (1970), who derives a closed-form formula to select the phases in the multisine equation.

$$\phi_i = 2\pi \sum_{j=1}^{i} j\alpha_j \tag{2.112}$$

The formula gives a reasonable result when the user-defined spectrum is flat and wideband, but under other conditions (band-limited, in the presence of harmonic suppression, etc.) the results can be largely undesirable.

The deficiencies of Schroeder-phasing justify the need for more rigorous approaches, such as those involving optimization. As noted in the Introduction, the optimization problem associated with minimizing crest factor in a multisine input is not straightforward because the ℓ_∞ norm is non-differentiable. A significant contribution in this regard is the work by Guillaume *et al.* (1991). This method seeks to approximate the minimization of the Chebyshev norm by sequentially minimizing the ℓ_p norm for $p = 4, 8, 16, \ldots$. It is based on Pólya's algorithm which states:

$$\lim_{p\to\infty} \mathbf{p}_p = \mathbf{p}_\infty \tag{2.113}$$

where $\mathbf{p} = [\phi_2 \;\; \phi_3 \;\ldots\; \phi_{n_s}]$ is the real-valued phase vector and $\mathbf{p}_\infty$ is the min-max solution. Note that the ℓ_2-norm remains invariant with respect to the phases ϕ_i. Under certain assumptions, Guillaume and co-workers show that the continuous ℓ_p norm can be equivalently represented in discrete form

$$L_p(u(k)) = \frac{1}{N_s} \sum_{k=1}^{N_s} |u(k)|^p = [\ell_p(u)]^p \tag{2.114}$$

The discrete-time representation of the ℓ_p norm per (2.114) is incorporated into a Gauss-Newton optimization algorithm with Levenberg-Marquardt Hessian approximation. This is accomplished by defining a cost function

$$\min_{\mathbf{p}} \frac{1}{N_s} e^T e \tag{2.115}$$

where

$$e = [u_s(1)^{p/2} \;\; u_s(2)^{p/2} \;\; \ldots \;\; u_s(N_s)^{p/2}]^T \qquad \mathbf{p} = [\phi_2 \;\; \phi_3 \;\; \ldots \;\; \phi_{n_s}]^T \tag{2.116}$$

and p is an even number. The elements of the Jacobian ($\mathbf{J}$) can be represented by

$$J_{ki} = -(p/2)u_s(k)^{(p/2-1)}\sqrt{(2\alpha_i)}\sin(\omega_i kT + \phi_i), \tag{2.117}$$

which form part of the iterative phase update equation

$$\mathbf{p}^{(i)} = \mathbf{p}^{(i-1)} - [\mathbf{J}^{(i-1)T}\mathbf{J}^{(i-1)} + \Lambda^{(i-1)}]^{-1}\mathbf{J}^{(i-1)T}e^{(i-1)} \tag{2.118}$$

An FFT-based algorithm is used to compute $\mathbf{J}^{(i-1)T}\mathbf{J}^{(i-1)}$ and $\mathbf{J}^{(i-1)T}e^{i-1}$. The sequential optimization process in Guillaume *et al.* (1991) is initialized with the phases produced by the Schroeder-phase algorithm. Although a global solution cannot be guaranteed with this approach, most local minima are avoided, and Guillaume *et al.* (1991) report that it performs better than other crest factor minimization techniques.

While the Guillaume *et al.* (1991) algorithm is useful, its applicability to process control problems has some important limitations. The user must accept whatever time-domain realization is produced by the algorithm and is not able to specify time-domain constraints that may be demanded by plant-friendliness considerations. Herein lies the main motivation for the constrained problem formulations developed in this dissertation.

A solution approach to the constrained minimum crest factor multisine problem can take a variety of forms. The first approach is similar to the one used by Guillaume and co-workers and is based on Pólya's algorithm. First, the problem is formulated in the modeling language AMPL (Braun *et al.*, 2002*b*). This has

obvious advantages over a formulation in any high-level programming language including the possibility to utilize a number of available solvers written in various languages. However, a more important benefit results from the fact that AMPL has built-in automatic derivatives — means exact and efficient differentiation up to second derivatives.

Braun *et al.* (2002*b*) minimize a properly scaled (to avoid underflow or overflow) p-norm instead of the Chebyshev norm. Different from Guillaume *et al.* (1991), Braun *et al.* (2002*b*) use an elaborate technique to increase p. While Guillaume and co-workers doubled p repeatedly to quickly reach large values, Rivera *et al.* (2002) increased it in various slower ways, such as adding small, even numbers or adding a slowly increasing number of those with a comparison to the Guillaume technique. This had two advantages. For one, the subsequent problems were close to the previous ones aiding the convergence of the optimizer and, more importantly, did not allow the iteration settle early in a neighborhood of a solution point but allowed it to descend more gradually instead.

While in principle an active-set method of sequential quadratic programming type (generally still considered state-of-the art for general nonlinear programming) could be used, we have turned to interior-point methods in this dissertation. The reason is that these methods are more effective for large problem sizes, particularly those that arise in multivariable cases. Therefore, one effective approach using the interior-point method is minimizing the crest factor (i.e., min CF(x)) as a constraint in the following way:

$$\min t \tag{2.119}$$

subject to

$$-t||x||_2 \leq x_i \leq t||x||_2, \quad i = 1,\ldots,N_s \tag{2.120}$$

where x_i represent the elements of either u,y, or both. This min CF(x) approach is examined for all the multivariable problem formulations with constraints in this dissertation.

A series of novel interior-point approaches have been recently proposed and have partly been made

available by their authors (Waechter and Biegler, 2000; Byrd *et al.*, 1999; Byrd *et al.*, 2000). A successful class of interior-point approaches is that of primal-dual methods. This is certainly true for linear and quadratic programming. For general nonlinear programming it has been shown in Waechter and Biegler (2000) that typical, line search based interior-point methods may fail to converge to feasible points even for well-posed problems. One of the few methods that does not suffer from this is the trust region based method KNITRO developed by Nocedal and co-workers, which was recently made available for research purposes (Byrd *et al.*, 1999). This method possesses the robustness and stability needed for our purposes and at the same time is very efficient for smaller and larger problems. One reason for its efficiency is the use of projected conjugate gradients in its default (non-direct) mode, while robustness is a consequence of the fact that as a trust region method it has steepest descent as the worst-case direction vector.

8.3. Numerical Optimization Problem Formulations. The details of multisine signals have been presented in Section 2-5, and the equation is restated here: a multisine signal $u_j(k)$ corresponding to the j-th channel of a system with m total inputs is given as

$$\begin{aligned} u_j(k) &= \sum_{i=1}^{m\delta} \hat{\delta}_{ji} \cos(\omega_i kT + \phi_{ji}^{\delta}) + \lambda_j \sum_{i=m\delta+1}^{m(\delta+n_s)} \sqrt{2\alpha_{ji}} \cos(\omega_i kT + \phi_{ji}) \\ &\quad + \sum_{i=m(\delta+n_s)+1}^{m(\delta+n_s+n_a)} \hat{a}_{ji} \cos(\omega_i kT + \phi_{ji}^{a}) \qquad j = 1, \cdots, m \end{aligned} \tag{2.121}$$

To achieve a zippered spectrum we define the Fourier coefficients α_{ji} as

$$\alpha_{ji} = \begin{cases} \neq 0, & i = m\delta + j, m(\delta+1) + j, ..., m(\delta+n_s-1) + j \\ = 0, & \text{for all other } i \text{ up to } m(\delta+n_s) \end{cases} \tag{2.122}$$

Given a multisine signal structure per (2.121) for a channel j and a desired power spectral density (standard or modified, defined by the Fourier coefficients α_{ji} for n_s spectral lines), one optimization problem which can be solved is to minimize the maximum crest factor over all the input channels

$$\min_{\{\phi_{ji}^{a}\},\{\phi_{ji}^{\delta}\},\{\phi_{ji}\},\{\hat{a}_{ji}\},\{\hat{\delta}_{ji}\}} \max_{j} \text{CF}(u_j) \quad j = 1, \cdots, m \tag{2.123}$$

subject to maximum move size constraints on the input sequence $\{u_j(k)\}$

$$|\Delta u_j(k)| \leq \Delta u_j^{max} \quad \forall\, k, j \tag{2.124}$$

and high/low limits on $\{u_j(k)\}$

$$u_j^{min} \leq u_j(k) \leq u_j^{max} \quad \forall\, k, j \tag{2.125}$$

It was previously noted that minimizing output crest factor is of great value in the process industries since the nature of the output signal often has the most influence on product quality and hence profitability. If a dynamic model is available *a priori*, optimization problems minimizing the maximum crest factor over all output channels can be formulated as

$$\min_{\{\phi_{ji}^a\},\{\phi_{ji}^b\},\{\phi_{ji}\},\{\hat{a}_{ji}\},\{\hat{b}_{ji}\}} \max_z \text{ CF}(y_z) \tag{2.126}$$

$$j = 1, \cdots, m \qquad z = 1, \cdots, N_{outs}$$

subject to (in addition to the input signal constraints (2.124) and (2.125)) constraints on both changes and upper/lower values of the output signal:

$$|\Delta y_z(k)| \leq \Delta y_z^{max} \quad \forall\, k, z \tag{2.127}$$

$$y_z^{min} \leq y_z(k) \leq y_z^{max} \quad \forall\, k, z \tag{2.128}$$

Alternatively, it is possible to minimize the maximum crest factor of both input and output signals,

$$\min_{\{\phi_{ji}^a\},\{\phi_{ji}^b\},\{\phi_{ji}\},\{\hat{a}_{ji}\},\{\hat{b}_{ji}\}} \max_{j,z} \{ \text{ CF}(u_j),\ \text{CF}(y_z)\} \tag{2.129}$$

$$j = 1, \cdots, m \qquad z = 1, \cdots, N_{outs}$$

subject to (2.124) - (2.125) and (2.127) - (2.128).

While the problem formulations presented in the above are open-loop, their extension to closed-loop identification problems is rather straightforward. For multisine signal design in a closed-loop setting, the

control law must be included as a constraint in the problem formulation similar to the model equations that are part of the constrained output crest factor problem. For instance, for closed-loop identification under feedback-only control, it would be necessary to specify the manipulated variable vector $u(k)$ as:

$$u(k) = C(z)(r(k) - y(k)) + u_d(t) \tag{2.130}$$

$$y(k) = P(z)C(z)(I + P(z)C(z))^{-1}(r(k) - y(k)) + v(t) \tag{2.131}$$

where $C(z)$ is the classical feedback controller, $y(k)$ is the vector of outputs, $r(k)$ is the vector of reference setpoints, $u_d(k)$ is a vector of external manipulated variable changes, and $v(t)$ is the noise in the output measurement. A large class of linear control designs (including unconstrained Model Predictive Control) can be written according to (2.130) and (2.131). Incorporating (2.130) and (2.131) in the multisine design problem corresponds to a set of additional linear equality constraints in the optimization problem, and the search problem now consists of finding the phases of multisine signals that are introduced at external injection points $r(k)$ or $u_d(k)$. One benefit of this approach is that as a result of the action of the control system, it is not necessary to modify the multisine signal spectrum to address the needs of highly interactive systems. However, since the character of the control law and its tuning influence the quality of the results, these become an additional set of design variables that the user now needs to consider in solving the problem.

8.4. Example Study of A Linear Distillation Process. The linear highly interactive system per Equation (2.46)

$$P(s) = \frac{1}{75s+1}\begin{bmatrix} 87.8 & -86.4 \\ 108.2 & -109.6 \end{bmatrix}$$

is examined within a plant-friendly identification framework. A series of open-loop and closed-loop multisine input signal designs (involving a decentralized PI controller with steady-state decoupler) are evaluated, arising prior knowledge of the model. Model estimates obtained from noisy data are validated in a closed-loop set-point tracking performance evaluation.

Now, the following optimization problem formulations based on the system per Equation (2.46) are considered, as noted below:

1. Minimize the maximum crest factor of u using a standard zippered spectrum (Rivera *et al.*, 1997).

2. Minimize the maximum crest factor of u using a modified zippered spectrum.

3. Minimize the maximum crest factor of y using a modified zippered spectrum subject to constraints on $\Delta u, y,$ and Δy.

4. Minimize the maximum crest factor of both u and y using a modified zippered spectrum subject to constraints on $\Delta u, y,$ and Δy.

In all cases involving output crest factor, the model per Equation (2.46) is assumed to be known *a priori*.

For the plant per Equation (2.46), the same design information and parameters are used as mentioned earlier: $\tau_{dom}^{L} = \tau_{dom}^{H} = 75$ min and select $\delta = 0$, $\alpha_s = 7.5$, and $\beta_s = 3.33$. Based on the guideline derived in Section 2, we specify $T = 15$ min, $n_s = n_a = 26$, and $N_s = 210$. The ratio of correlated to uncorrelated harmonic Fourier coefficients is $\gamma = 64.5$ from Equation (2.79). The "snow" effect is not examined in this signal, but all harmonics in the secondary band of excitation possess Fourier coefficient values that are 10% of those of the primary. Figure 28 shows the power spectral densities for both standard and modified zippered signals examined for the linear distillation column. The levels of power densities for uncorrelated harmonics in both standard and modified zippered spectra are scaled to be identical to each other in Figure 28.

8.4.1. *Open-Loop Identification Experiment.* Statistics for all four signals are summarized in Table 2; output state-space plots are shown in Figure 29, while the time-sequences for one cycle are shown in Figures 30 and 31. Evaluating the open-loop experiment data, the standard zippered spectrum $\{\min \mathrm{CF}(u)\}$ signal has information primarily in the high-gain direction, which is reflected via a thinly spread concentration of points in the state-space plot and large output spans (0.6819 to -0.7003 for y_1 and 0.8553 to -0.8712

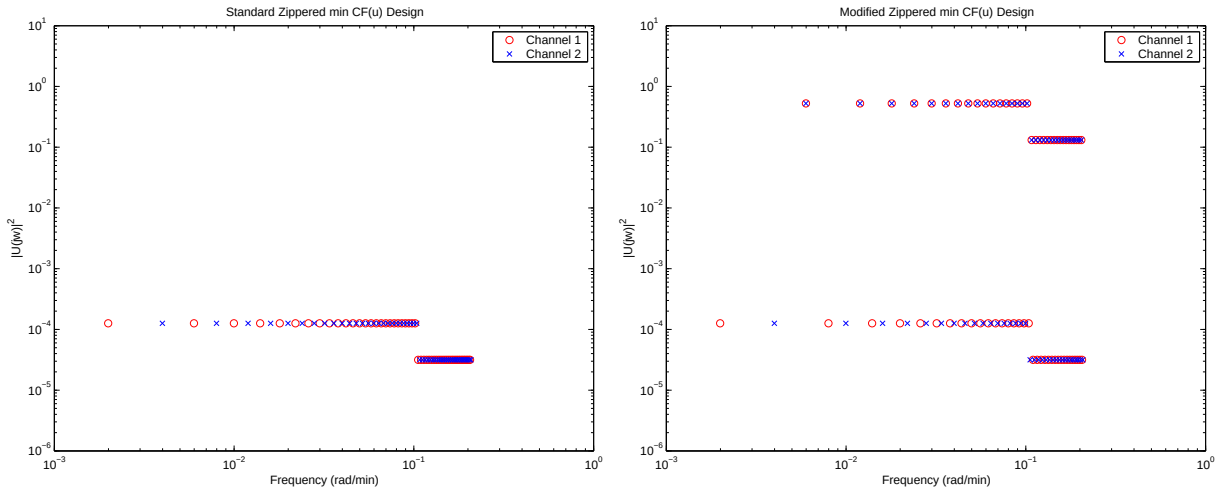

(a) (b)

Figure 28. Power spectrum for the standard zippered (a) and modified zippered ($\gamma = 64.5$) (b) signal designs presented for the plant per Equation (2.46)

for y_2) despite low input magnitude changes (Figure 30 (left)). On the contrary, the modified zippered spectrum $\{\min \mathrm{CF}(u)\}$ signal (Figure 30 (right)) produces a much better directional distribution of the data in the state-space, and despite a much larger input span, results in only modest increases in the output span (30% and 20% greater for y_1 and y_2, respectively) compared to the standard zippered spectrum signal. Minimizing the output crest factor and enforcing input and output constraints on the optimization with a modified zippered spectrum $\{\min \mathrm{CF}(y)\}$ (Figure 31, (left)) lowers the output spans to desirable levels (0.378893 to -0.378896 for y_1 and 0.448301 to -0.448300 for y_2) and generates a bounded rectangular distribution in the state-space plot. Crest factors for both channels of u, however, have increased substantially. The signal corresponding to the $\{\min \max (\mathrm{CF}(u), \mathrm{CF}(y))\}$ problem with constraints (Figure 31, (right)) provides a reasonable balance between input and output crest factors and appears to promote plant friendliness. Compared to the $\{\min \mathrm{CF}(y)\}$ case, input spans (and correspondingly, crest factor) are reduced dramatically (by over 50%), while the output span increases by a small amount (approximately 12% higher for each output).

From these example results we can summarize that while the correlated harmonics in the modified

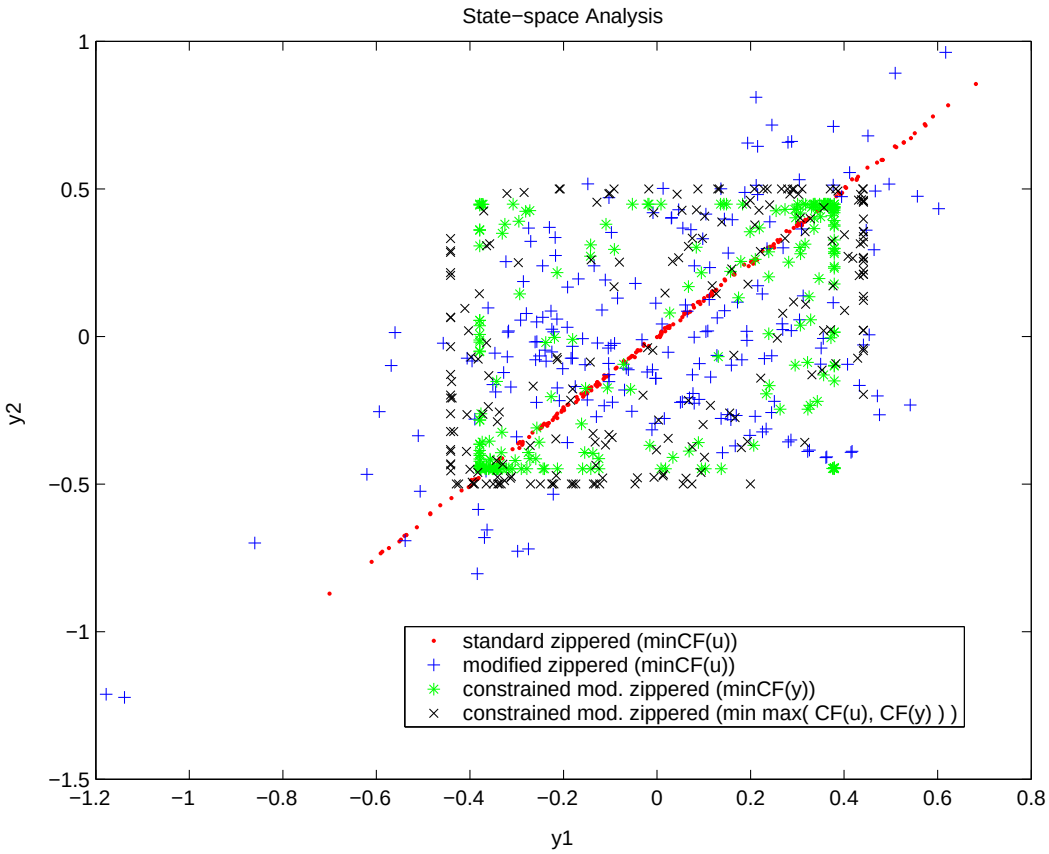

Figure 29. State-space plots from simulations of standard "zippered" spectrum min CF(u) ($\bullet$, red), modified "zippered" spectrum min CF(u) ($+$, blue), modified "zippered" spectrum min CF(y) ($*$, green), and modified "zippered" spectrum min max(CF(u), CF(y)) ($\times$, black), for the plant per Equation (2.46)

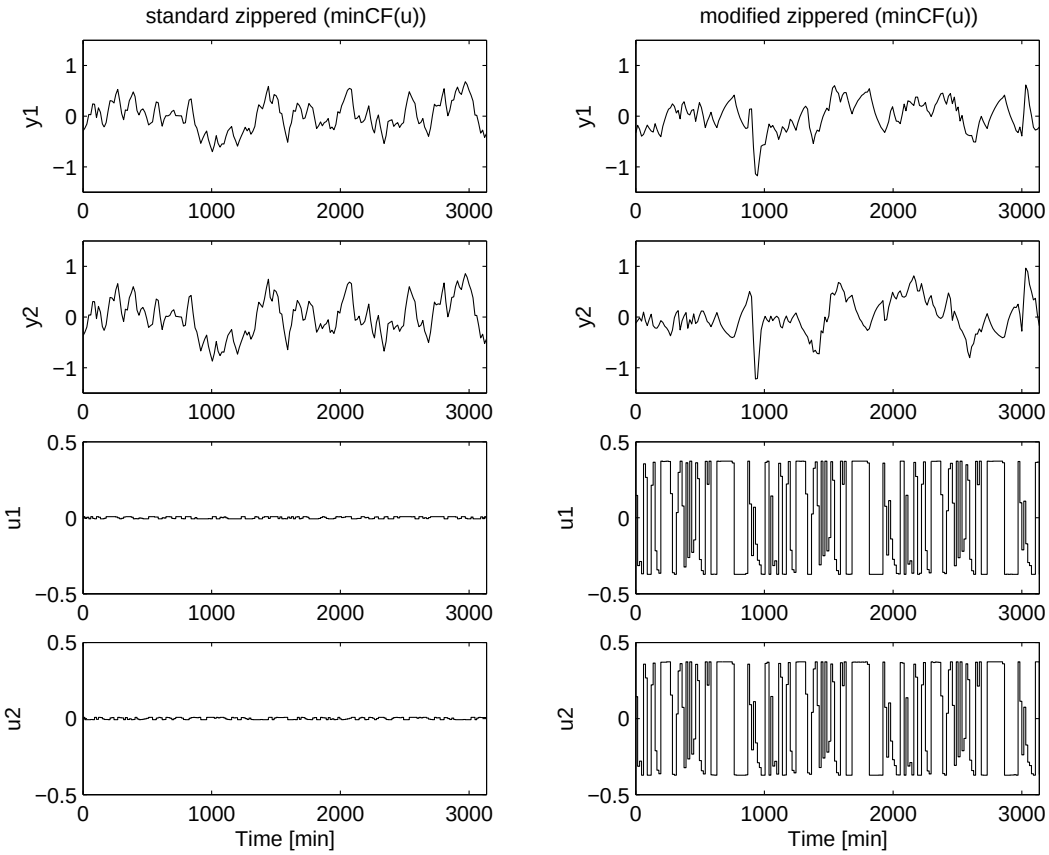

Figure 30. { min CF(*u*) } multisine signals using standard (left) and modified (right) "zippered" spectra, for the plant per Equation (2.46).

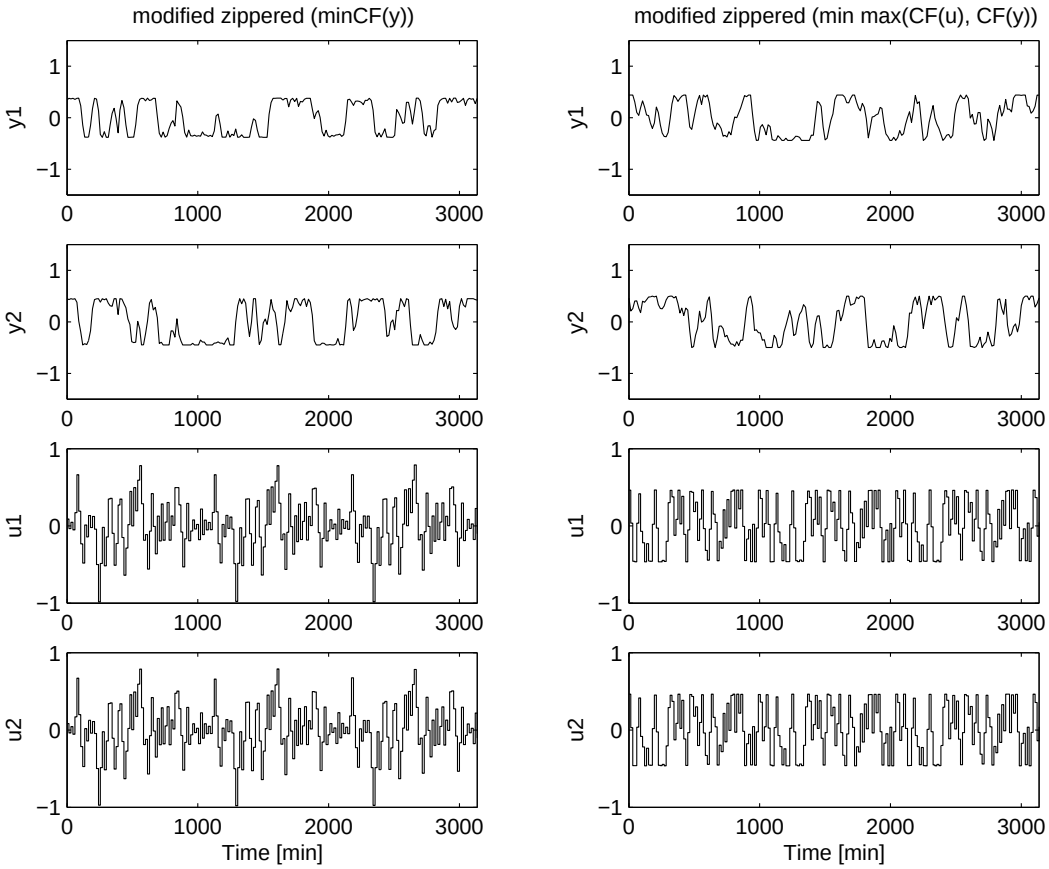

Figure 31. Constrained multisine signals using modified zippered spectrum design { min CF(*y*) } (left) and { min max(CF(*u*), CF(*y*)) } (right), for the plant per Equation (2.46)

Type	Signal (x)	CF(x)	PIPS(%)	max Δx	max x	min x
min CF(u) design; standard zippered spectrum	u_1	1.132425	88.306039	0.014106	0.007079	-0.007079
	u_2	1.136376	87.999046	0.014201	0.007100	-0.007100
	y_1	2.383208	42.520481	0.318468	0.681899	-0.700354
	y_2	2.372958	42.530317	0.397652	0.855283	-0.871213
min CF(u) design; modified zippered spectrum	u_1	1.130450	88.460763	0.745004	0.372522	-0.372526
	u_2	1.130632	88.446404	0.745163	0.372585	-0.372583
	y_1	3.924442	33.358140	0.763222	0.619802	-1.174440
	y_2	3.459978	32.254284	0.863657	0.966114	-1.219642
min CF(y) design; modified zippered, $\lvert\Delta u, y, \Delta y\rvert \leq 0.5$	u_1	3.018388	36.782253	0.499983	0.789886	-0.985599
	u_2	3.004964	36.887273	0.499986	0.789231	-0.981237
	y_1	1.221784	81.847791	0.499897	0.378893	-0.378896
	y_2	1.221781	81.847838	0.499989	0.448301	-0.448300
min max (CF(u) CF(y)) design; modified zippered, $\lvert\Delta u, y, \Delta y\rvert \leq 0.5$	u_1	1.423676	70.240749	0.499997	0.464209	-0.464209
	u_2	1.423675	70.240777	0.499995	0.464217	-0.464217
	y_1	1.423637	70.242767	0.407867	0.441263	-0.441262
	y_2	1.363417	73.346052	0.499934	0.499980	-0.499967

Table 2. Summary of open-loop case study results for the plant per Equation (2.46)

zippered spectrum significantly increase the input span, the output span does not increase proportionately, and in the case of the constrained $\{\min \text{CF}(y)\}$ and $\{\min \max (\text{CF}(u), \text{CF}(y))\}$ problems, the output span is actually lower than the standard spectrum signal, even though the modified spectrum has a much higher level of average power (Figure 28). In Figure 32, we can see the output power spectra of the standard and modified zippered signals through the model per Equation (2.46). The higher correlated input power increases the output power spectrum of the low-gain direction comparable to that of the high-gain direction by orthogonal harmonics.

8.4.2. *Decentralized PI Controller Design.* The control-relevant model quality of the signals is evaluated through model estimation and closed-loop validation. First, a model is estimated from one cycle of noisy data using a multivariable ARX $[na = 1, nb = 1, nk = 1]$ structure. This ARX model is used to design a decentralized PI controller with a steady-state decoupler, which is then applied to the true system. The PI controllers are tuned using the Prett-García tuning rules (Prett and García, 1988),

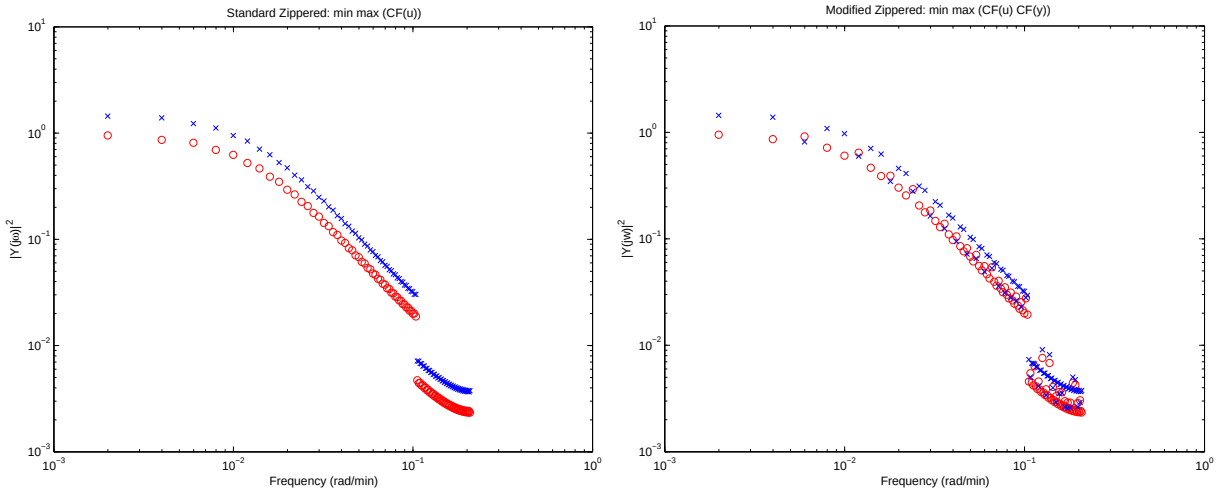

(a) (b)

Figure 32. Output power spectra of the linear distillation system for the plant per Equation (2.46): the standard zippered spectrum {min max CF(u)} (a) and modified zippered spectrum {min max CF(y)} (b)

$$C_{PI}(z) = D_{ss} \times \begin{bmatrix} Kc_{11}\frac{z-exp(-T/\tau_{11})}{z-1} & 0 \\ 0 & Kc_{22}\frac{z-exp(-T/\tau_{22})}{z-1} \end{bmatrix} \tag{2.132}$$

where

$$D_{ss} = K^{-1} \times diag(k_{11}, k_{22}), \quad K = P(0) = \begin{bmatrix} k_{11} & k_{12} \\ k_{21} & k_{22} \end{bmatrix}$$

$$Kc_{11} = \frac{1-exp(-T/\lambda)}{k_{11}}, \; Kc_{22} = \frac{1-exp(-T/\lambda)}{k_{22}}$$

$\lambda = 25$ and $\tau_1 = \tau_2 = 75$ are used for the PI controller.

8.4.3. *Closed-Loop Identification Experiment.* Multisine signals are introduced as reference set-points to a closed-loop system with a decentralized PI controller with a decoupler, designed from an *a priori* model. A closed-loop identification test can be conducted while keeping constraints on input (control action; u) and output (y). A combination of crest factor minimization on u and y is available; however, multiple crest factor minimizations increase the difficulty of optimization convergence. Figure 33 presents an example of

$\{\min \max \mathrm{CF}(u,\, y)\}$ in a closed-loop system structure with the constraint $|\Delta u,\, u,\, \Delta y,\, y| \leq 0.5$ allowing snow effect on the reference at high frequencies (see Figure 33 and Table 3). The case of crest factor minimization and the constraint on y in closed-loop system forces the outputs to track the reference inputs while ignoring impulse-like peaks.

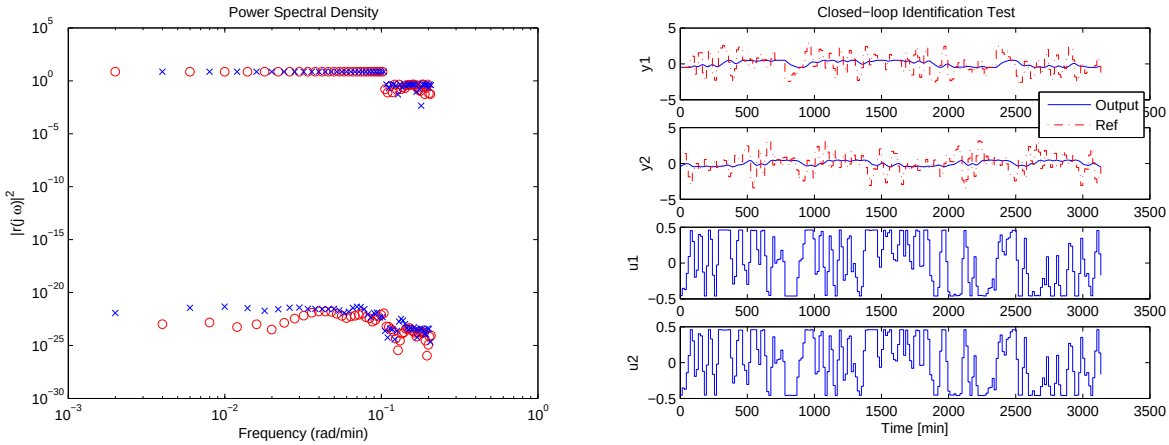

(a) (b)

Figure 33. Closed-loop Identification Test: min max CF(u,y) with a standard zippered reference signal for the plant per Equation (2.46), reference signal power spectrum with snow effect (a) and time sequences (b)

Type	Signal (x)	CF(x)	PIPS(%)	maxΔx	max x	min x
Closed-Loop Identification Test: min max $\mathrm{CF}(u, y)$, $\lvert\Delta u, u, \Delta y, y\rvert \leq 0.5$	u_1	1.3454	74.3226	0.499985	0.460493	-0.4604
	u_2	1.3454	74.3226	0.499990	0.459601	-0.4596
	y_1	1.2878	77.6490	0.258807	0.499997	-0.4999
	y_2	1.3454	74.3225	0.294655	0.459027	-0.4590
	r_1	2.1151	47.2786	2.924074	2.889548	-2.8895
	r_2	2.4847	41.8645	3.633208	3.149447	-3.4135

Table 3. Summary of closed-loop identification test for the plant per Equation (2.46)

8.4.4. *Model Evaluation by Closed-Loop System Performance.* 2nd-order ARX models are estimated from data generated based on the experiment designs. Under noise-free conditions, all the controllers based on the multisine signals result in an equivalent closed-loop performance, as seen in Figure 34. With the addition of significant noise during identification testing (SNR $= -10\,dB$ per channel), the difference in the closed-loop results becomes significant. As noted in Figure 35, the control system based on the

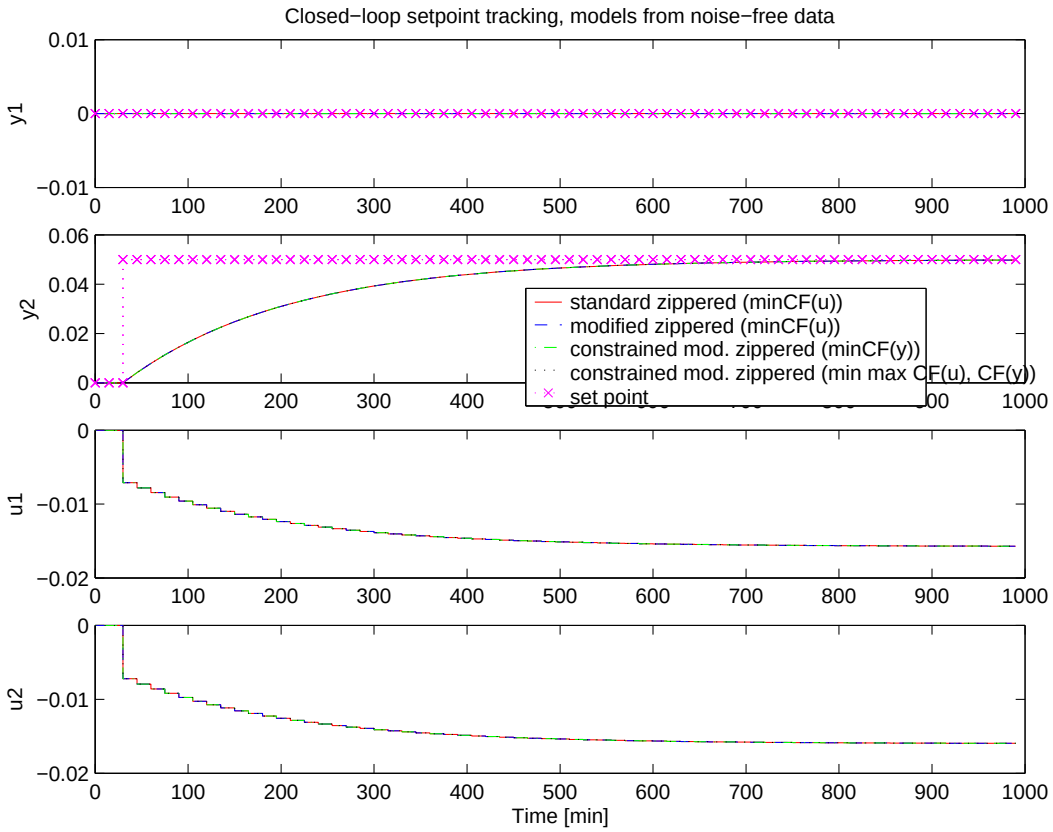

Figure 34. Closed-loop simulation of controllers designed from models estimated from the standard zippered spectrum (min CF(u), — red), modified zippered spectrum (min CF(u), –, blue), constrained modified zippered spectrum (min CF(y), -·, green), and constrained modified zippered spectrum (min max (CF(u), CF(y)), · · ·, black) signals under noise-free condition, for the plant per Equation (2.46)

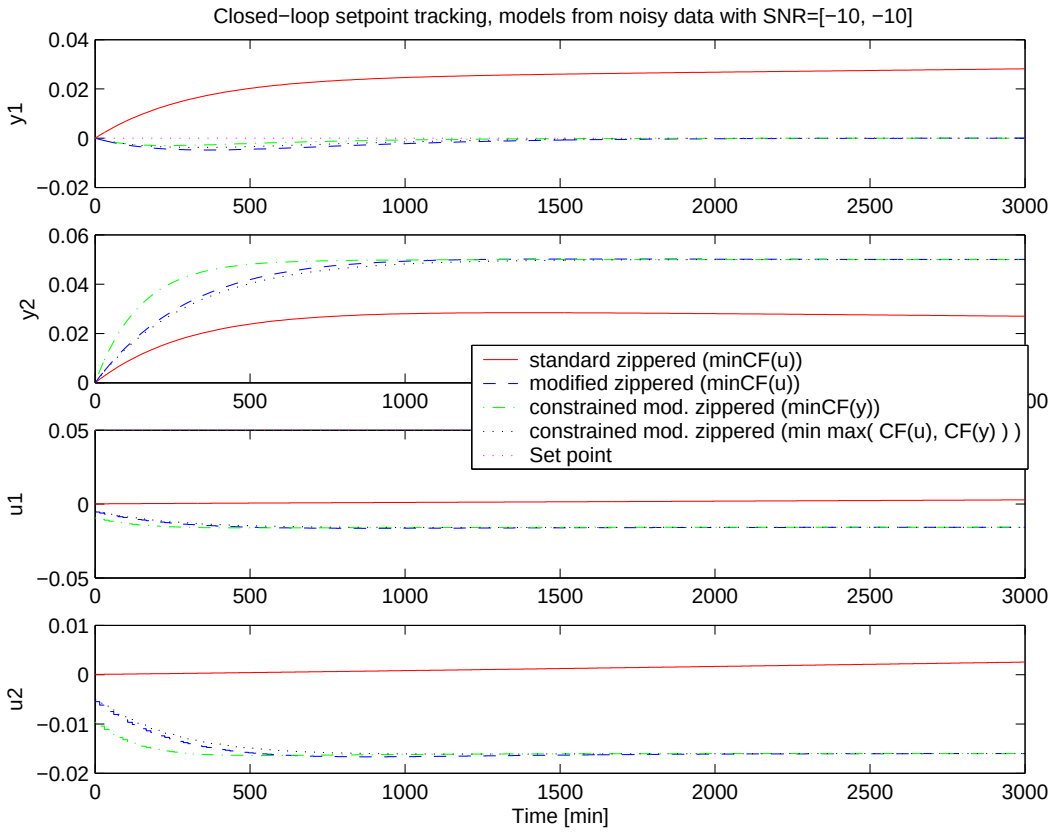

Figure 35. Closed-loop simulation of controllers designed from models estimated from the standard zippered spectrum (min CF(u), — red), modified zippered spectrum (min CF(u), –, blue), constrained modified zippered spectrum (min CF(y), -·, green), and constrained modified zippered spectrum (min max (CF(u), CF(y)), · · ·, black) signals under noisy conditions, for the plant per Equation (2.46)

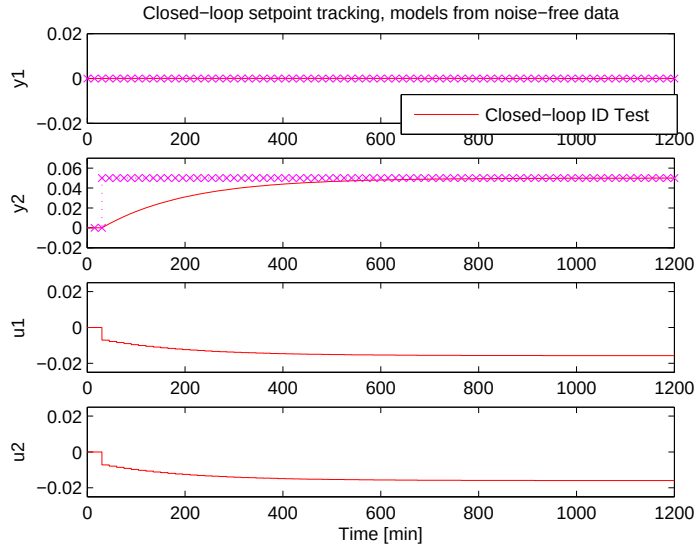

(a)

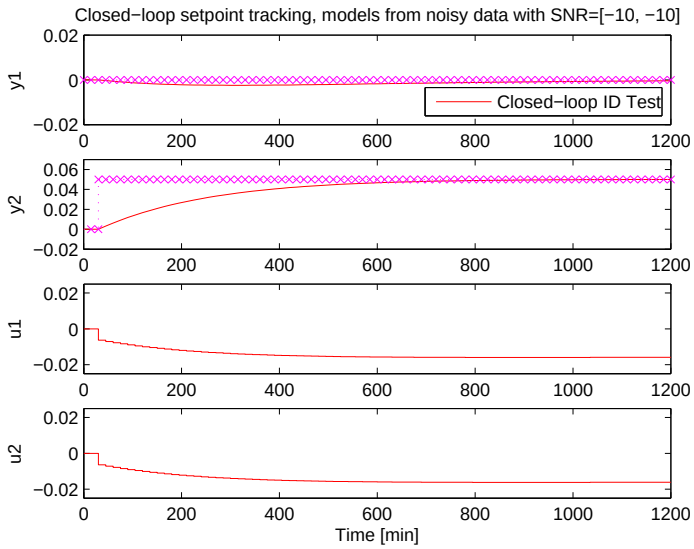

(b)

Figure 36. Closed-loop simulation of controllers designed from models estimated from the closed-loop ID test (min max (CF(*u*), CF(*y*)) signals under noise-free (a) and noisy (b) conditions (SNR=[-10 -10]dB), for the plant per Equation (2.46)

model generated from the standard zippered spectrum data is not able to track the set points properly, while all the models arising from the modified zippered spectrum signals yield stable results with no offset in the controlled variables. In addition, the closed-loop identification test data are evaluated into 2nd-order ARX models under both noise-free and noisy conditions. Their performance in the setpoint tracking test is shown in Figure 36; under noisy conditions, the model displays good performance since the closed-loop identification test data has balanced gain directionality.

9. Case Study of A Nonlinear High-Purity Distillation Process

The nonlinear, high-purity distillation column per Weischedel and McAvoy (1980) is examined in this section featuring multisine input signal designs with plant-friendly identification experiment designs. The detailed operating conditions of the distillation column are described in Table 4. This distillation column

Mixture	Methanol-Ethanol
Product Split	0.01–0.99
Number of Trays	27
Top Temperature	$608.0^{\circ}R$
Bottom Temperature	$642.24^{\circ}R$
Vapor Flow from Reboiler	3.856 mol/min
Reflux Flow Rate	3.384 mol/min
Feed Flow Rate	1.50 mol/min
Feed Composition	0.5

Table 4. Operating conditions for the nonlinear high-purity distillation column per Weischedel-McAvoy (1980)

has been a challenging identification problem for many years in the chemical process field for the accurate estimation of the gain directionality and for its nonlinearity. The use of a modified zippered spectrum improves the low-gain directional contents in the outputs, resulting in robust model estimates under noisy conditions. Various constrained optimization-based plant-friendly identification formulations are examined in this distillation process while addressing its nonlinearity, interaction, and ill-conditioning.

The system under study is a methanol-ethanol column consisting of 27 trays (column "C" per Weischedel and McAvoy (1980)). The dynamic model consists of overall and component mass balances for each tray, resulting in 56 differential equations; the rest of the model consists of algebraic equations obtained from pseudo steady-state energy balances, the Francis-Weir formula for liquid flow from each tray, vapor-liquid equilibrium relations, and other physical property data. The objective of the control system is to independently control the compositions of the distillate and bottom products, which are specified at high purities; 99% and 1% methanol concentration in the top distillate and bottom streams, respectively, (Chien and Ogunnaike, 1992). The controller relies on temperature measurements instead of compositions since these are more reliable and easier to implement on-line. An LV-configuration for the column is considered, with tray temperatures 21 and 7 as controlled variables and the reflux flow L and the vapor boilup flow V serving as manipulated variables.

A series of plant-friendly identification experiments are performed on this system using conventional open-loop and closed-loop tests. Model estimates obtained from the data under noisy conditions are evaluated for setpoint tracking performance with Model Predictive Control (MPC). The cases noted below are considered in this Case Study:

- Unconstrained open-loop identification experiment using a standard zippered spectrum,
- Constrained open-loop identification experiment using a modified zippered spectrum with an ARX model estimate,
- Constrained open-loop identification experiment using an even-harmonic suppressed, modified zippered spectrum with an ARX model estimate for the output,
- Constrained open-loop identification experiment using a modified zippered spectrum with a NARX model estimate for the output, and
- Constrained closed-loop identification experiment using a phase-shifted spectrum with an ARX model

estimate for the output.

9.1. Identification Testing Experiments. Signal parameters are determined for shifted, standard zippered, and modified zippered multisine inputs, based on *a priori* knowledge of the system dynamics. Using the open-loop step responses presented in Chien and Ogunnaike (1992) and Sriniwas *et al.* (1995) (Figure 37), a dominant time constant range for this system can be estimated as $\tau_{dom}^{L} = 5$ and $\tau_{dom}^{H} = 20$ min. Coupled with user choices of $\delta = 0$, $\alpha = 2$, and $\beta = 3$, these lead to acceptable choices for a series of

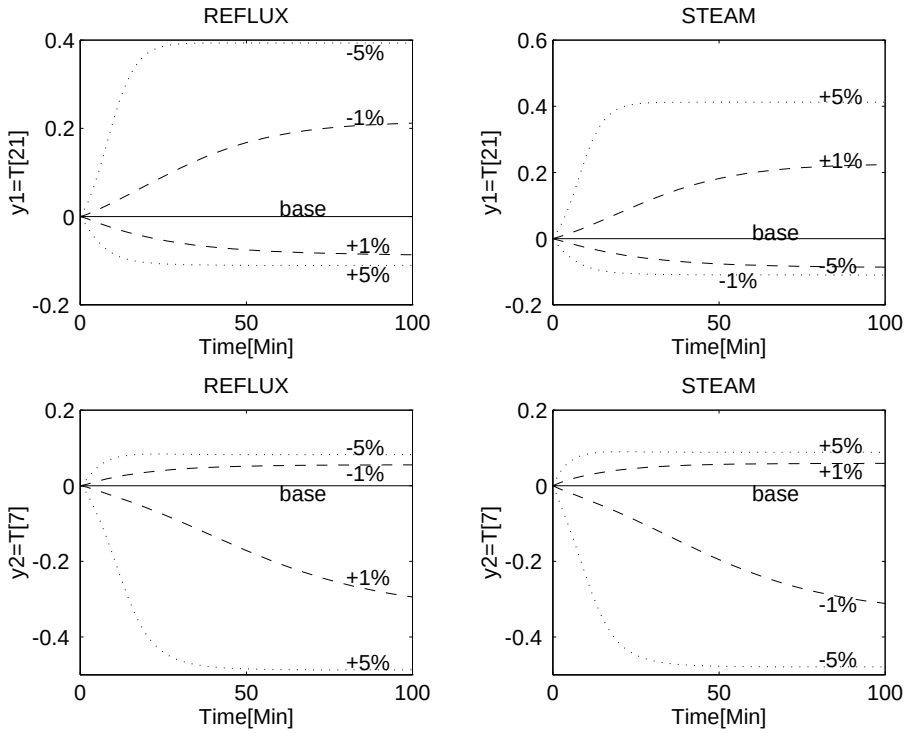

Figure 37. Response of the output y_1 and y_2 for step changes in u_1 and u_2 per the Weischedel-McAvoy distillation column (from Sriniwas *et al.* (1995))

identification testing signals, possibly augmented with model predictions implemented in optimizers that conform to the guidelines derived in Sections 2-5. The “snow” effect is also applied for the frequencies beyond a primary bandwidth, searching for optimal Fourier coefficients by the optimizer (see Figure 38). This approach minimizes the crest factor and satisfies the plant-friendly constraints (Guillaume *et al.*, 1991;

Braun *et al.*, 2002*b*).

Case	Loop	Desgin	Objective	Model	Ns(1 Cycle)	Test Time(3cycles)
A	OL	Standard Zippered	min CF (u)	n/a	378 (12.6 hrs)	37.8 hrs
B^*	OL	Modified Zippered	min CF (y)	ARX	378 (12.6 hrs)	37.8 hrs
C^*	OL	Mod. Zip. with h=2 supp.	min CF(y)	ARX	754 (25.2 hrs)	75.4 hrs
D^*	OL	Modified Zippered	min CF (y)	NARX	378 (12.6 hrs)	37.8 hrs
E^*	OL	Modified Zippered	min CF (u & y)	NARX	378 (12.6 hrs)	37.8 hrs
F^*	CL	Shifted	min CF (u & y)	PI-ARX	190 (6.33 hrs)	19.0 hrs

Table 5. High-purity distillation column per Weischedel and McAvoy: signal design parameters for shifted and zippered multisine inputs with $\delta = 0$, $\alpha = 2$, $\beta = 3$ and $\tau_{dom}^{L} = 5$ and $\tau_{dom}^{H} = 20$ min, * indicates the cases subject to constraints on $\Delta u, y,$ and Δy, (e.g., $|\,\Delta u\,| \leq 0.01,\ |\,\Delta y\,| \leq 0.008,$ and $|\,y\,| \leq 0.0085$), OL stands for open-loop testing and CL for closed-loop testing

In addition to the open-loop identification experiments, a closed-loop identification test is considered. The closed-loop identification test utilizes shifted multisine inputs as reference signals that are fed through the setpoints in the feedback control systems. Because of the presence of the controller, this test is of shorter duration than the open-loop tests. As in the open-loop signal cases, the optimizers are actively applied to constrain u and y, searching for optimal Fourier coefficients and phases of multisine reference signals.

9.1.1. *Effects of Zippered vs. Modified Zippered Spectra: Cases A & B.* The identification experiment initially starts with a standard zippered spectrum signal if there is no *a priori* information regarding directionality to design a modified zippered spectrum. Once initial model estimates are obtained, a γ can be estimated and refined until the modified zippered spectrum signals can satisfy the condition of gain-directional output power spectra for a balanced distribution, leading to models that can meet control-purposes. For example, a gain matrix based on a 2nd-order ARX model is obtained using a set of input signals of standard and (preliminary) modified zippered spectra

$$K = \tilde{P}(0) = \begin{bmatrix} -35.18 & 37.60 \\ -26.09 & 28.55 \end{bmatrix} \tag{2.133}$$

which makes it possible to generate a more meaningful ratio for a modified zippered power spectrum. Gain-directional vectors based on SVD analysis are obtained using the gain matrix per (2.133):

$$\textbf{SVD}\,(K) \;=\; U\,S\,V^T \;=\; \begin{bmatrix} -0.7996 & -0.6006 \\ -0.6006 & 0.7996 \end{bmatrix} \begin{bmatrix} 64.3976 & \\ & 0.3634 \end{bmatrix} \begin{bmatrix} 0.6801 & 0.7331 \\ -0.7331 & 0.6801 \end{bmatrix}^T$$

A range of γ for a modified zippered spectrum obtained using $\underline{v} = [0.7331\ 0.6801] \approx [1\ \ 1]^T$ direction based on the estimated gain matrix (2.133) is:

$$\gamma := \{11.08 \;\leq\; \gamma_i \;\leq\; 15.03\} \tag{2.134}$$

The standard and modified ($\gamma = 15$) input power spectra ((a) and (b), respectively in Figure 38) are generated such that they have the similar power spectral density level for the orthogonal (uncorrelated) harmonics within a primary bandwidth. The optimizer selects variable Fourier coefficients by the snow effects in the high frequency area, as shown in Figure 38.

A series of case studies are evaluated and summarized in Table 8. In Case A, applying the snow effects with $\{\min \text{CF}(u)\}$ produces a very lower crest factor input, close to $CF = 1.0$, so a PRBS-like multisine input is obtained (Figure 39a). From Case A, a 4th-order ARX model is estimated and applied to the optimizer for minimizing the output crest factor and/or enforcing the constraints. Using a modified zippered signal in Case B, the objective $\{\min \text{CF}(y)\}$ forces the optimizer to minimize the crest factor of outputs with additional freedom of variable coefficients in the high frequency area, whereas the correlated harmonics with the higher ratio is to promote the gain directionality in the data (Figure 38b). In geometrical comparison, the input state-space of the standard zippered signals has a rectangle-like spread (Figure 40a) due to the lower CF value, while its output state-space produces a very narrow spread in the high-gain ($[1\ \ 1]$) direction (Figure 40b). The input state-space of the modified zippered signals shows a narrow distribution close to $[1\ \ 1]$ input direction (Figure 40a) with larger magnitudes, while its output state-space shows a rectangular-type distribution (Figure 40b) which is achieved by the constrained optimization.

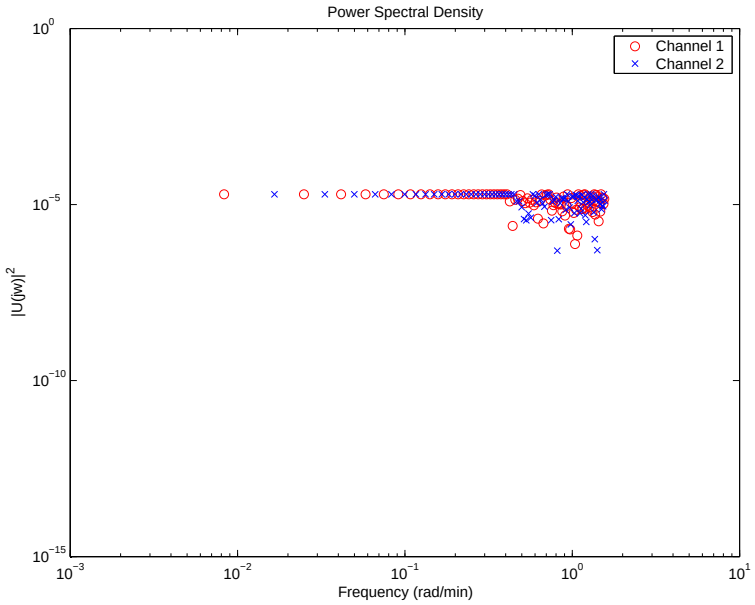

(a)

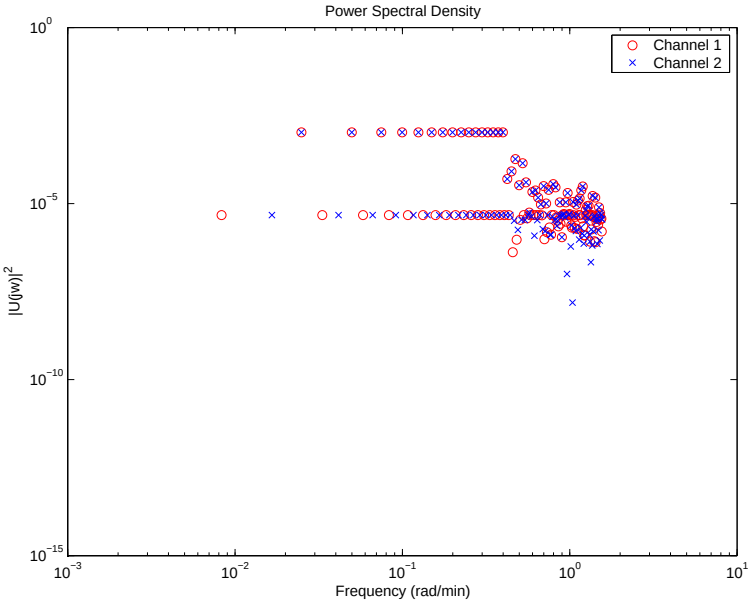

(b)

Figure 38. Input power spectra using the standard zippered spectrum design (a) and the modified zippered spectrum ($\gamma = 15$) design (b)

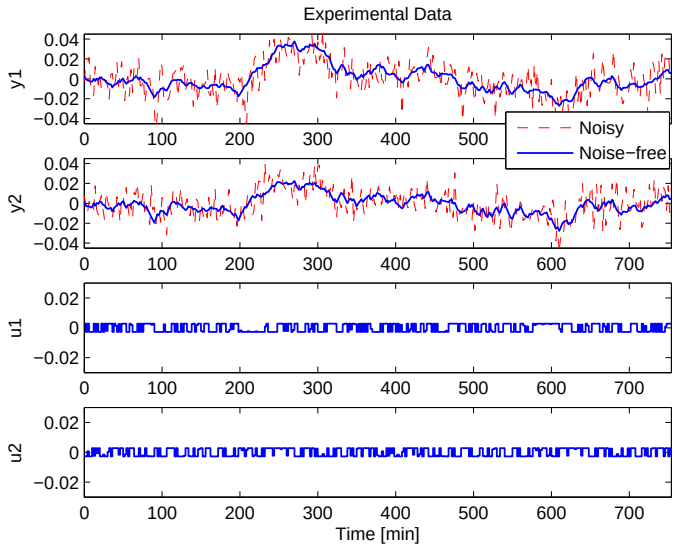

(a)

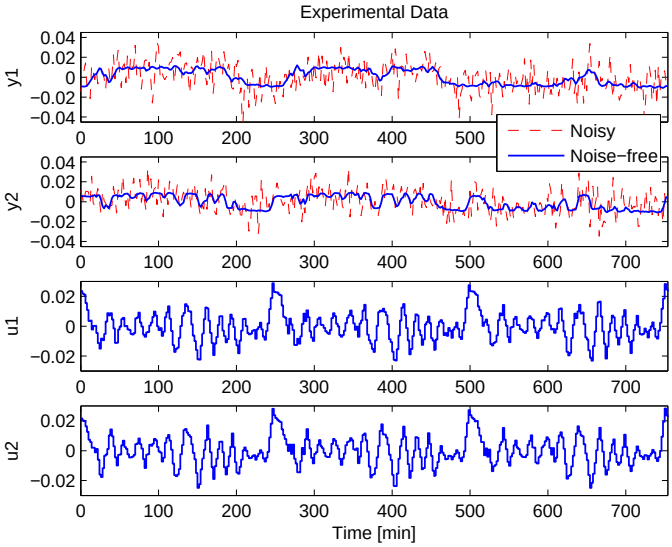

(b)

Figure 39. Open-loop identification test by the standard zippered spectrum min $CF(u)$ signal (a) and the modified zippered spectrum min $CF(y)$ signal ($\gamma = 15$) (b) with $|\Delta u| \leq 0.01$, $|\Delta y| \leq 0.008$, $|y| \leq 0.0085$ using the predictions of a 2nd-order linear ARX model to the optimizer

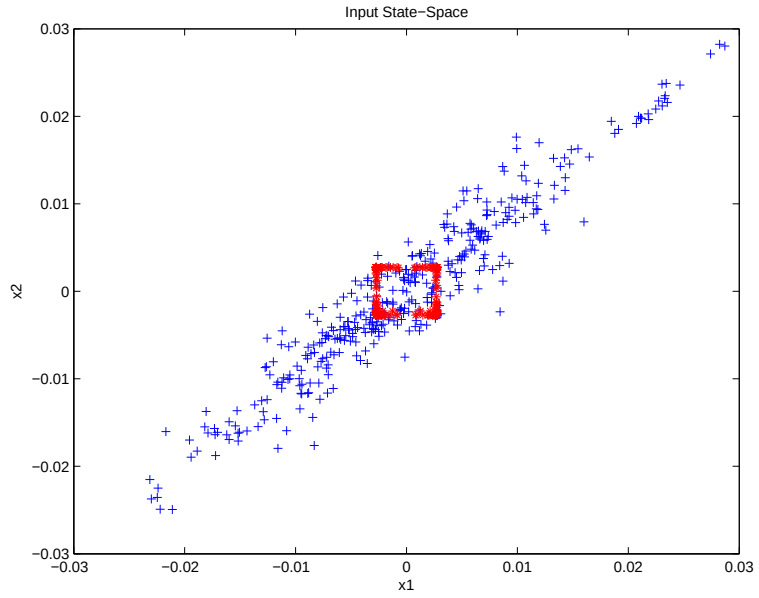

(a)

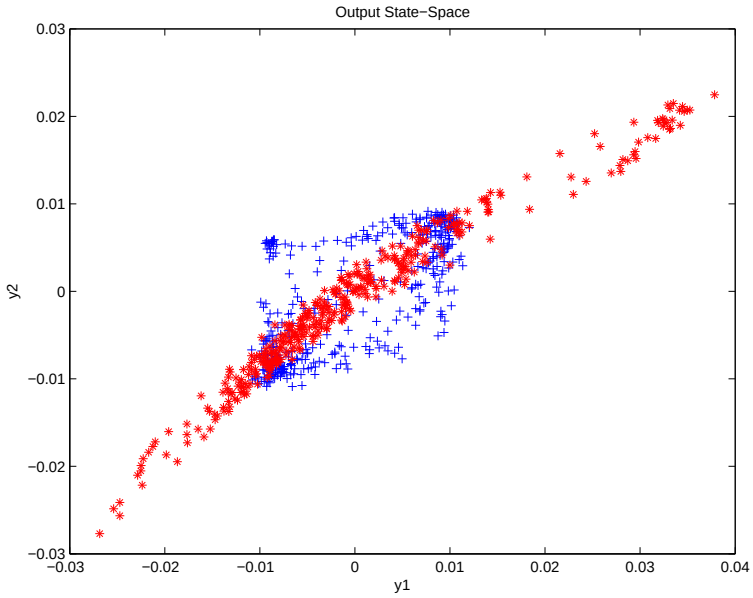

(b)

Figure 40. Input (a) and Output (b) state-space analysis: the standard zippered spectrum (*(red), min $CF(u)$) without constraints and the modified zippered spectrum (+(blue), min $CF(y)$, $\gamma = 15$) with $|\Delta u| \leq 0.01$, $|\Delta y| \leq 0.008$, $|y| \leq 0.0085$

The modified zippered spectrum signals have a ten times larger input magnitude span, in $[1 \;\; 1]$ direction, than the standard (see Figure 40a). In the high-gain $[1 \;\; -1]$ input direction, the two signals have almost the same input spans because the two spectra have similar levels of uncorrelated Fourier coefficients. On the contrary, the outputs of the standard zippered spectrum are approximately three times larger than the modified case due to the larger singular value (Figure 40b). The higher coefficients of correlated harmonics significantly increase the input magnitude span; however, the output signals do not have a corresponding increase.

9.1.2. *Harmonic Suppression for Reducing Nonlinearities: Case C.* The test of $\{\min \mathrm{CF}(y)\}$ based on ARX model predictions (Case B) suffers distortion as the nonlinearity exists in the process. However, this indicates not only the mismatch in outputs but also off-specs from the designed constraints on $|\, y \,|$ and $|\, \Delta y \,|$ that counted for the plant-friendliness. To reduce the extent of these nonlinear distortions, even harmonic suppression is applied to the modified zippered spectrum with a change of N_s from 378 to 754 but with other parameters remaining as the same; all multiples of $h = 2$ harmonics are suppressed in the input power spectrum (Figure 41 (a)). This use of harmonic suppression reduces off-spec derivations in output signals but still experiences nonlinear distortions (Figure 40 (b)). Although more harmonics can be suppressed, such approaches will extend the sequence length significantly over non-suppression cases. This motivates the use of nonlinear modeling in this problem to improve results without extended test duration.

9.1.3. *Nonlinear ARX Model Estimation: Cases D & E.* Although Hammerstein and Weiner models are often utilized for a nonlinear identification method, the asymmetric nonlinearity, input saturation, and strong interaction of this distillation column make these estimations have poor predictions (Eskinat *et al.*, 1991; Pearson, 1999). Sriniwas *et al.* (1995) apply a NARX model structure to estimate the high-purity distillation system, which includes a series of quadratic or higher-order terms using inputs and outputs in addition to the full ARX model terms; as a result, it produces much more accurate predictions. For example, y_i of 2×2 full-MIMO case can be represented in terms of the NARX model structure such that

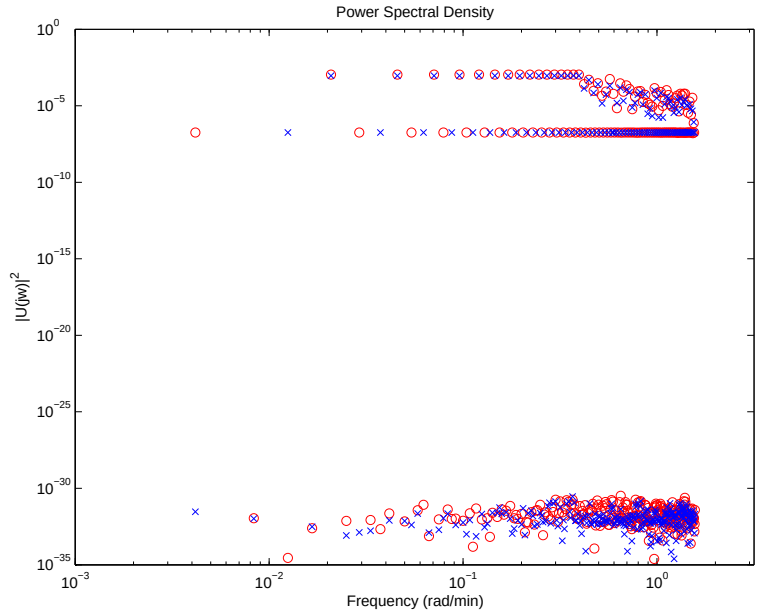

(a)

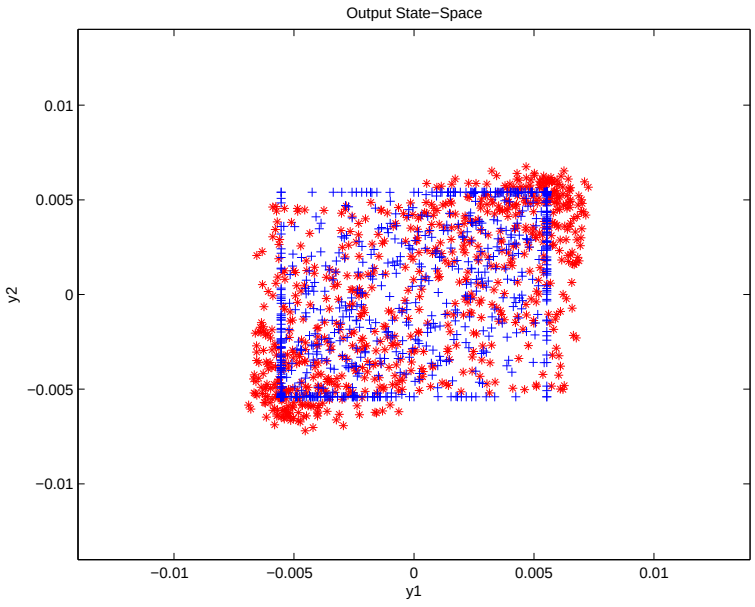

(b)

Figure 41. Even-harmonic suppression: input power spectrum via a modified zippered spectrum $\gamma = 15$, min $CF(y)$ (a) and its output state-space between the plant (*, red) and designed data (+, blue) using a 2nd-order ARX model prediction with $|\ \Delta u\ | \leq 0.01$, $|\ \Delta y\ | \leq 0.008$, $|\ y\ | \leq 0.0085$

$$
\begin{aligned}
y_i(k) \;=\; & \theta^{(0)} + \sum_{i=1}^{n'_{y_1}} \theta_i^{(1)} y_1(k-i) + \sum_{i=1}^{n'_{y_2}} \theta_i^{(2)} y_2(k-i) + \sum_{i=\rho_1}^{\rho_1+n'_{u_1}} \theta_i^{(3)} u_1(k-i) \\
& + \sum_{i=\rho_2}^{\rho_2+n'_{u_2}} \theta_i^{(4)} u_2(k-i) + \sum_{i=1}^{n_{y_1}} \sum_{j=1}^{i} \theta_{(i,j)}^{(5)} y_1(k-i) y_1(k-j) \\
& + \sum_{i=1}^{n_{y_2}} \sum_{j=1}^{i} \theta_{(i,j)}^{(6)} y_2(k-i) y_2(k-j) + \sum_{i=\rho_1}^{\rho_1+n_{u_1}} \sum_{j=\rho_1}^{i} \theta_{(i,j)}^{(7)} u_1(k-i) u_1(k-j) \\
& + \sum_{i=\rho_2}^{\rho_2+n_{u_2}} \sum_{j=\rho_2}^{i} \theta_{(i,j)}^{(8)} u_2(k-i) u_2(k-j) + \sum_{i=1}^{n_{y_1}} \sum_{j=\rho_1}^{\rho_1+n_{u_1}} \theta_{(i,j)}^{(9)} y_1(k-i) u_1(k-j) + \ldots
\end{aligned}
\tag{2.135}
$$

where k is the present sampling time, $y(k)$ is the present value of the output, $u(k)$ is the present value of the input, ρ is the time delay in the input, n'_y and n'_u are the number of output and input lags for mononomial terms, and n_y and n_u are the number of output and input lags for quadratic terms, respectively. For cross-validation, an evaluation criterion is employed from Sriniwas *et al.* (1995):

$$
I_{eval} = \frac{\sum_{k=1}^{N} [y(k) - \hat{y}(k)]^2}{\sum_{k=1}^{N} [y(k) - \bar{y}]^2} \times 100\% \tag{2.136}
$$

where $\bar{y}$ is the average of the output and $\hat{y}$ is the estimated output. Using the orders of the NARX parameters in Table 6, the accuracy of the nonlinear model predictions (Figure 42b) is significantly improved, reducing the mismatch between the model and process data in output state-space in comparison to ARX predictions (Figure 42a). Taking advantage of this improved accuracy, $\{\min \text{CF}\ (u\ \&\ y)\}$ is evaluated in Case E.

Channel	n'_{y_1}	n'_{y_2}	n'_{u_1}	n'_{u_2}	n_{y_1}	n_{y_2}	n_{u_1}	n_{u_2}	ρ_1	ρ_2
$y_1, N(\theta) = 55$	4	4	4	4	2	2	1	1	1	1
$y_2, N(\theta) = 55$	4	4	4	4	2	2	1	1	1	1

Table 6. Order selection of NARX model estimation per the Weischedel and McAvoy distillation column

9.1.4. *Closed-Loop Identification Experiment: Case F.* For achieving a shorter signal length, the use of shifted multisine signals as reference inputs in closed-loop testing is considered. The shifted signals can be used as an external input signal as long as they can meet the cross-correlation criteria (Ljung, 1999).

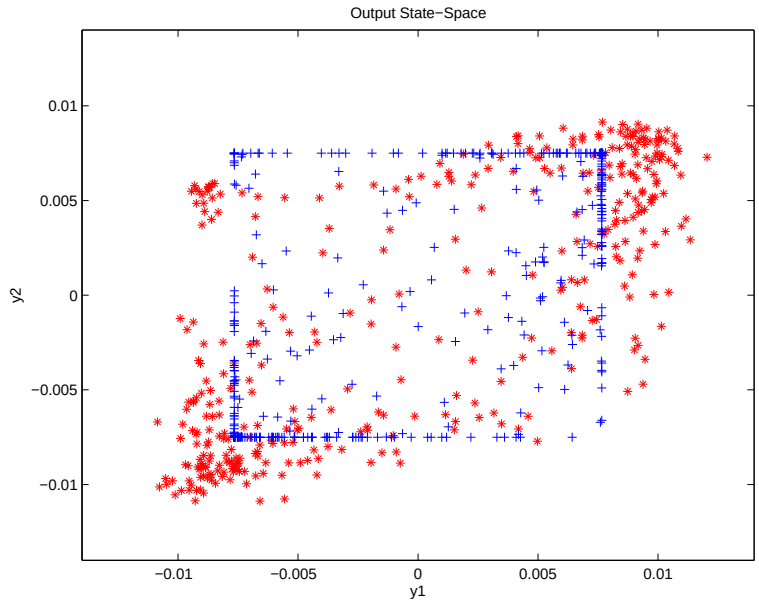

(a)

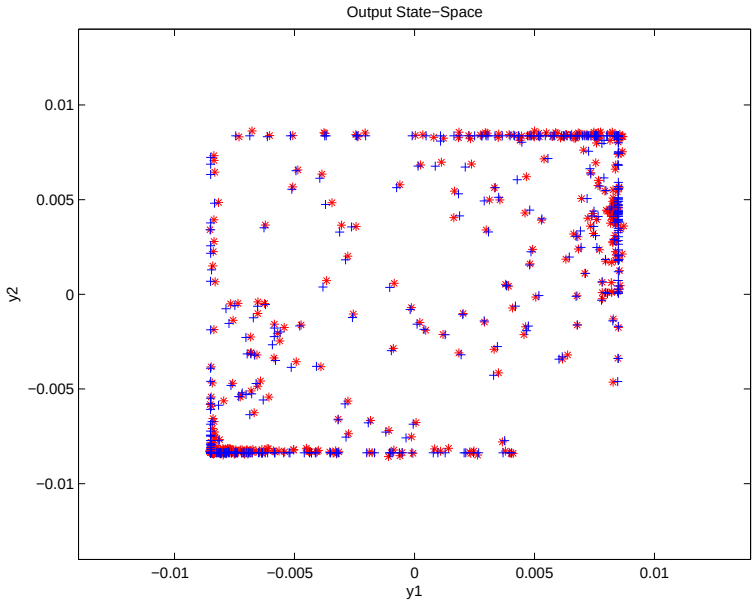

(b)

Figure 42. Open-loop identification experiments: ARX (a) and NARX (b) model output predictions of min CF(y) signals

Using the same model information, the design guideline leads to $n_s = 25$, $T = 2$ minutes, and $N_s = 190$. A shift parameter $D = N_s/m = 95$ is used for shifting the base input into the second channel to lower cross-correlation. Table 7 shows the design parameters for shifted and zippered multisine inputs based on the Weischedel and McAvoy distillation column.

Signal	α_s	β_s	ω_*	ω^*	T (min)	N_s	1_{cycle} (min)	D
Multisine (zippered)	2	3	0.0167	0.400	2	378	756.0	
Multisine (shifted)	2	3	0.0167	0.400	2	190	380.0	95

Table 7. High-purity distillation column per Weischedel and McAvoy: signal design parameters for shifted and zippered multisine inputs

A control law is implemented in the closed-loop formulation associated with model estimates; both the controller and model estimate are utilized by the optimizer for plant-friendly testing designs. The PI controller based on a log-arithmetic model per Chien and Ogunnaike (Chien and Ogunnaike, 1992) is used.

$$C_{PI}(s) = \begin{bmatrix} Kc_{11}\left(1+\frac{1}{\tau_{11}s}\right) & 0 \\ 0 & Kc_{22}\left(1+\frac{1}{\tau_{22}s}\right) \end{bmatrix} \tag{2.137}$$

where $Kc_{11} = -2.69, Kc_{22} = 2.26, \tau_{11} = \tau_{22} = 5$mins and $\tau_{cl} = 2.5$ mins.

The objective $\{\min \text{CF}(u\&y)\}$ with constraints is evaluated for plant-friendly closed-loop testing (Figure 43 (a)). Since the predictions are computed based on a linear ARX model, the designed signals suffer nonlinear distortion in both u and y. The overall agreement between the plant and designed signals is, however, much greater than that of the open-loop testing through the ARX model (Figure 43 (b)). The PI controller rejects sharp disturbance-like changes in u so that only minimal mismatches occur in u and y. Tighter bounds on $|\Delta u|$ and $|\Delta y|$, therefore, are of further interest for reducing sharp moves in u and y as well as nonlinear distortions. The uncertainty in the outputs increases in proportion to the magnitudes of Δu; as a result, a small move of u is desirable to estimate accurate linearized models for nonlinear systems. The shifted multisine reference signals are shorter, but the output result shows a balanced distribution in state-space (Figure 43 (b)). The feedback signals introduce sufficient correlation and G^{-1} dynamics into u

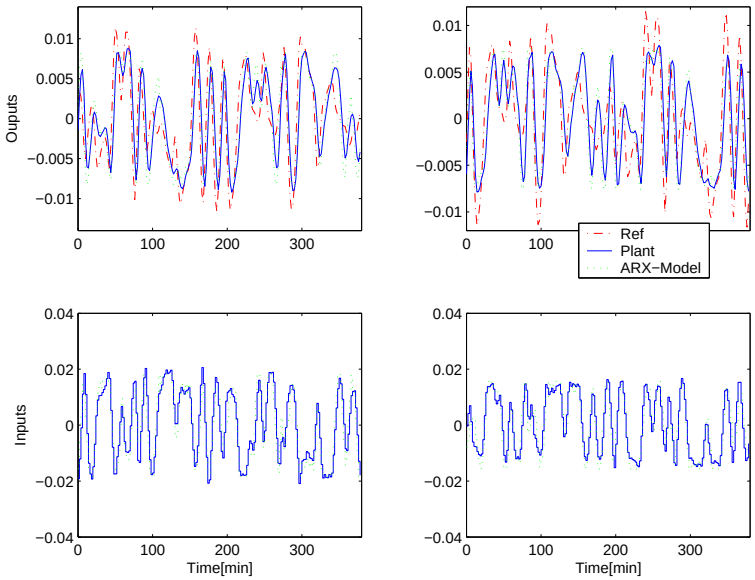

(a)

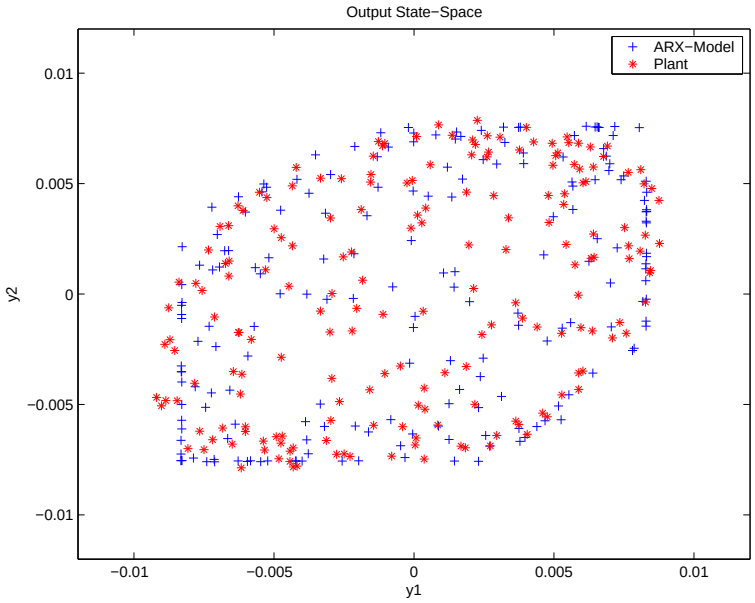

(b)

Figure 43. Closed-loop test using shifted signals for reference points, $\{\min \mathrm{CF}(u,y)\}$ using a 2nd-order ARX model prediction with $|\Delta u| \leq 0.01$, $|\Delta y| \leq 0.008$, and $|y| \leq 0.0085$: time-domain sequences (a) and output state-space (b)

so that the low-gain direction can be easily excited (Li and Lee, 1996*b*).

9.2. Identification Test Results and Evaluation. While the Fourier coefficients in the primary excitation bandwidth are specified by the user, variable coefficients using the snow effect are applied to the high frequency area. This snow effect gives the optimizer greater degrees-of-freedom while minimizing the crest factor and satisfying user-defined constraints. For highly interactive, high-purity distillation columns, a modified zippered spectrum is effectively used in promoting the gain-directionality in the dataset. Harmonic suppression and NARX model estimates are also implemented in the design procedure with the modified zippered spectrum and snow effects. In closed-loop testing, the optimizer chooses the phases of the first channel subject to the crest factor and constraints of u and y for the two (all) channels. The statistics of these identification experiments are evaluated in the nonlinear model simulation, as listed in Table 8.

9.2.1. *Statistical Information.* All the constrained cases are considered with the same constraint bounds. In open-loop tests, the accuracy between the plant and prediction data is evaluated by using the criterion per Equation (2.136), which also indicates how serious the nonlinear distortion is in the plant data. The linear predictions using the ARX model experience the highest mismatch errors with $I_{eval} = [5.96 \;\; 5.11]\%$, while the even-harmonic suppression approach reduces the error criteria to $I_{eval} = [3.50 \;\; 4.63]\%$. On the other hand, the NARX model has a dramatic reduction in the output mismatch, arriving at $I_{eval} = [0.04 \;\; 0.03]\%$. Specifically, the accuracy in the outputs is $[149 \;\; 170]$ times better than the linear ARX model predictions, which is more useful for accomplishing plant-friendly test designs. The same constraints as in the open-loop case are applied to the closed-loop design. Figure 43b demonstrates that the closed-loop output predictions have a good geometrical agreement in state-space, similar to those of the NARX predictions.

9.2.2. *Model Estimation and Performance Evaluation.* The end use of the model obtained from this data (closed-loop control) is the ultimate test for the validation of these designs. The open-loop and closed-

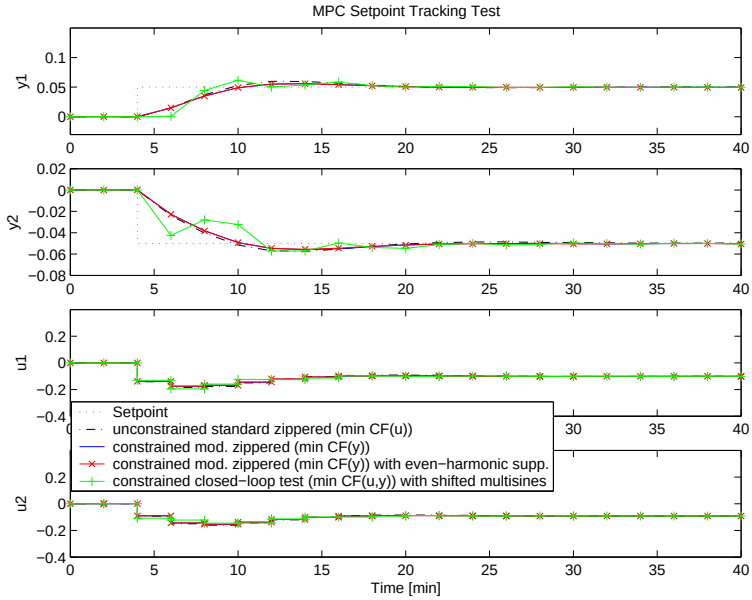

(a)

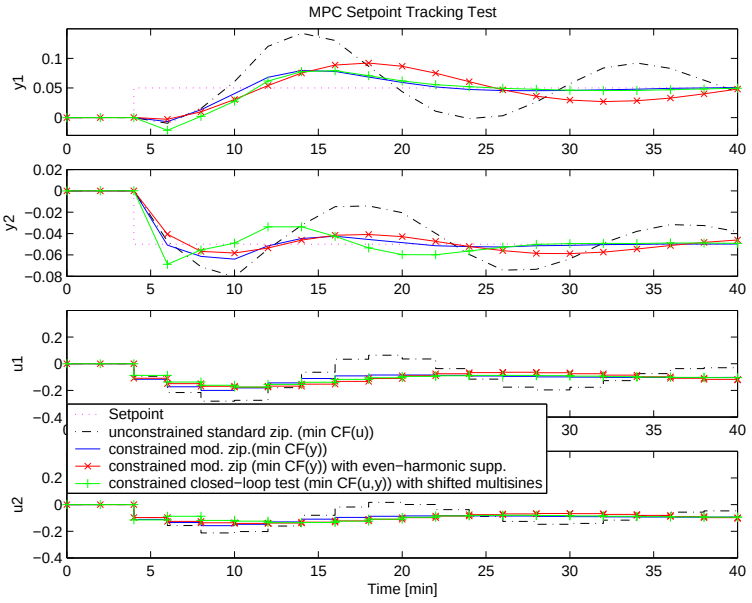

(b)

Figure 44. Closed-loop responses using Model Predictive Control from models estimated from multisine signals under noise-free (a) and noisy conditions (b). Output Signal-to-Noise ratios (presented as [SNR($y1$) SNR($y2$)] dB), SNR = [0.38 -0.53] dB for the min CF(u) signal (Case A), SNR = [-4.34 -3.55] dB for the min CF(y)-ARX signal (Case B), SNR=[-9.18 -8.00]dB for the min CF(y)-ARX harmonically suppressed signal (Case C), and SNR=[-7.93 -6.48]dB for the closed-loop min CF(u & y)-PI-ARX signal (Case F). Tuning parameters for open-loop cases: PH=50, MH=25, Ywt=[1 1], & Uwt=[0.3 0.3] and for closed-loop case: PH=50, MH=25, Ywt=[1.2 1], & Uwt=[0.3 0.35]

Case	Scenario	Signal (x)	CF(x)	PIPS(%)	max Δx	max x	min x	I_{eval}
A	open-loop {min CF (u)} design; standard zippered spectrum	u_1	1.03	96.72	0.0055	0.0027	-0.0027	
		u_2	1.03	96.73	0.0055	0.0027	-0.0027	
		y_1	2.87	40.60	0.0047	0.0378	-0.0271	
		y_2	2.92	37.67	0.0049	0.0225	-0.0277	
B	open-loop {min CF(y)} design; modified zippered spectrum, with ARX model prediction $\mid \Delta u \mid \leq 0.01$, $\mid \Delta y \mid \leq 0.008$ & $\mid y \mid \leq 0.0085$	u_1	2.93	37.78	0.0100	0.0287	-0.0231	
		u_2	2.89	36.80	0.0100	0.0282	-0.0249	
		y_1	1.59	66.48	0.0064	0.0122	-0.0109	5.96%
		y_2	1.62	66.79	0.0074	0.0092	-0.0109	5.11%
C	open-loop {min CF(y)} design; modified zippered spectrum with even harmonic supp. using ARX model prediction $\mid \Delta u \mid \leq 0.01$, $\mid \Delta y \mid \leq 0.008$ & $\mid y \mid \leq 0.0085$	u_1	3.01	33.17	0.0100	0.0215	-0.0215	
		u_2	3.09	32.31	0.0100	0.0206	-0.0206	
		y_1	1.67	60.83	0.0041	0.0073	-0.0070	3.50%
		y_2	1.79	57.68	0.0058	0.0067	-0.0072	4.63%
D	open-loop {min CF(y)} design; modified zippered spectrum using NARX model prediction $\mid \Delta u \mid \leq 0.01$, $\mid \Delta y \mid \leq 0.008$ & $\mid y \mid \leq 0.0085$	u_1	3.74	31.51	0.0100	0.0365	-0.0254	
		u_2	3.25	34.37	0.0100	0.0316	-0.0250	
		y_1	1.30	77.45	0.0051	0.0088	-0.0086	0.04%
		y_2	1.31	77.01	0.0082	0.0087	-0.0086	0.03%
E	open-loop {min CF(u & y)} design; modified zippered spectrum using NARX model prediction $\mid \Delta u \mid \leq 0.01$, $\mid \Delta y \mid \leq 0.008$ & $\mid y \mid \leq 0.0085$	u_1	1.61	62.03	0.0100	0.0159	-0.0159	
		u_2	1.61	62.03	0.0100	0.0158	-0.0158	
		y_1	1.40	74.07	0.0061	0.0094	-0.0087	0.19%
		y_2	1.42	72.18	0.0072	0.0091	-0.0086	0.08%
F	closed-loop constrained {min CF(u & y)} design: shifted reference signals using PI-ARX model prediction $\mid \Delta u \mid \leq 0.01$, $\mid \Delta y \mid \leq 0.008$ & $\mid y \mid \leq 0.0085$	u_1	1.70	59.13	0.0169	0.0206	-0.0209	
		u_2	1.61	64.77	0.0119	0.0167	-0.0152	
		y_1	1.78	57.47	0.0062	0.0088	-0.0092	
		y_2	1.61	62.25	0.0065	0.0079	-0.0079	
		r_1	2.07	48.72	0.0084	0.0115	-0.0116	
		r_2	2.07	48.72	0.0084	0.0115	-0.0116	

Table 8. Nonlinear simulation results summary for open-loop and closed-loop signals designed for identifying the Weischedel-McAvoy distillation column case study.

loop data are used to estimate low-order (e.g., 2nd) linear ARX models whose control adequacy is evaluated by performing a setpoint tracking test using Model Predictive Control (MPC). Although the identification tests are executed for three cycles of data, the last two cycles are utilized for estimation purposes, while the first-cycle data is discarded to eliminate transient behavior. A setpoint change ($r = [0.05 \ \ -0.05]^T$) is given to the feedback control system, which intends to move the outputs in the low-gain direction. For evaluation under noisy environments, all the identification data contain identical noise signals in their output channels by a fixed noise source. As a result, the actual Decibel (dB) levels of signal-to-noise ratio (SNR) vary from case to case, depending on the individual output signals.

All the model estimates have equivalent control performance under noise-free conditions (Figure 44a), and the closed-loop data case has a small under-damping effect in the responses. However, under noisy conditions the models estimated only from the data with a balanced gain-directional distribution have

reasonable performance, with small increases in overshoots, and closely tracking the change in the low-gain direction. The orthogonal spectrum signal case has the highest SNR level (the least noise corruption) while the even harmonic suppression case has the lowest SNR value (the largest noise corruption). The robustness of the data with the poor content in the low-gain direction is, nevertheless, easily disrupted by such light noise corruption; the model from the zippered (orthogonal) input power spectrum case is unable to track the references under noisy conditions (Figure 44b) and will only work under relaxed tuning conditions. All the open-loop cases use the same MPC tuning parameter set, while the closed-loop case uses a different parameter set because it responds quickly to a slight under-damping response without offset (Table 9).

Open-loop Case:	PH=50	MH=25	Ywt=[1 1]	Uwt=[0.3 0.3]
Closed-loop Case:	PH=50	MH=25	Ywt=[1.2 1]	Uwt=[0.3 0.35]

Table 9. MPC tuning parameter sets for setpoint tracking tests

As a result, the models from the modified zippered spectrum and closed-loop tests are better able to resist noise corruption, displaying reasonable closed-loop performance from their end-use models (Figure 44b).

Due to the nonlinearities in this distillation column, the prediction from ARX model estimates suffers significant distortions, which causes off-specs and compromises the plant-friendliness formulations. The nonlinear distortion demands an appropriate nonlinear system identification tool to the Weischedel and McAvoy column. Therefore, both ARX and NARX models are estimated in this case study, and the models are utilized for the optimizer to constrain the output predictions, accomplishing plant-friendliness.

10. Chapter Summary

Multisine signal design guidelines have been derived relying on *a priori* knowledge of a system to determine meaningful parameters for multisine inputs that can perturb the system dynamics. Fourier coefficients and phases of these multisine inputs are specified by the user to meet the theoretical requirements of persistent excitation and signal-to-noise ratio. A zippered spectrum is applied that generates independent

frequency grids for multiple input channels. This spectrum can be modified to include correlated harmonics that improve the gain directional content in data, applicable for highly-interactive systems. A combined direction and power coefficient adjustment procedure is applied to the correlated harmonics to increase the low-gain directional content and make it comparable to that of the high-gain direction. Additionally, harmonic suppression is considered to reduce the nonlinear distortion resulting from these multisine input designs.

A series of plant-friendly identification experiments are formulated as optimization problems with time-domain constraints. The optimizer seeks optimal Fourier coefficients and phases to satisfy these requirements. A modified "zippered" power spectrum in conjunction with constrained optimization has been presented as a means to generate multi-channel multisine inputs that achieve plant-friendliness while addressing the requirements of highly interactive systems. Simulation results show that under noisy conditions the increased information content in the low-gain direction leads to useful models from shorter identification tests in comparison to standard input designs.

The pros and cons of the open-loop and closed-loop identification experimental designs are presented in the high-purity distillation columns by using constrained minimum crest factor multisine inputs. The correlation in the feedback signals also enhances the low-gain directional dynamics, displaying wider distribution in the output state-space in the closed-loop tests. Both the open-loop and closed-loop identification tests show equivalent effectiveness in the model estimates under noisy conditions; the open-loop test uses a modified zippered power spectrum while a shifted multisine input design is appropriate in the closed-loop test. By sharing the same frequency grids for individual input channels, the shifted multisine produces a 50% shorter signal length than the zippered multisine design. Although the open-loop test inputs can be designed from low *a priori* model information, the closed-loop test inputs require more significant process knowledge to design a feedback controller.

Plant-friendly multisine input signal design was applied to the Weischedel-McAvoy in this case

study. This nonlinear distillation column is highly interactive and ill-conditioned, making it extremely difficult to change the controlled variables in the low-gain direction. For the modified zipped spectrum signals, the open-loop identification test data can provide a robust model estimate displaying satisfactory closed-loop performance under noisy conditions. However, such a model suffers nonlinear distortion in model output predictions, violating the designed plant-friendliness specifications. An identification test relying on a modified zippered power spectrum and NARX model structure produces a very accurate model prediction with improved gain-directional contents. Such an accurate NARX model prediction can be extended to design a multisine input signal design for data-centric estimation, which is discussed in Chapter 5 of this dissertation.

CHAPTER 3

CONTROL-RELEVANT PARAMETER ESTIMATION

1. Introduction

Control-relevant identification integrates system identification analysis and control system design procedures into an integrated framework that can provide more adequate models for practical control applications. In many cases, an estimated model from system identification experiment is used as a nominal model for controller design. However, classical system identification and controller design have rather different emphasis on a model's dynamics. Classical system identification emphasizes the open-loop fit to process outputs via least-squares criteria, while controller design focuses on using a model for regulating the controlled variables of a system (Gaikwad and Rivera, 1996). There are two main components to control-relevant identification: model error quantification and control-relevant parameter estimation. In this chapter, we formulate a control-relevant parameter estimation problem (CRPEP) that generates adequate models for control from plant-friendly input/output datasets. Model error quantification for robust control system design will be presented as we demonstrate the identification test monitoring procedure in the next chapter.

The control-relevant system identification methodology is intended to provide more reliable model for feedback control applications at a potential cost of poorer open-loop response fits in the classical sense. To achieve control-relevant estimation, a curvefitting procedure in the frequency-domain is utilized with

control-relevant weights (Bayard, 1994; Callafon *et al.*, 1996; Gaikwad and Rivera, 1996). The systematic determination of a frequency bandwidth of importance is presented in Gaikwad and Rivera (1996) which emphasizes the intended closed-loop performance during the model parameter estimation. This frequency range is a useful criterion to refine or modify the identification input signals; it will be further mentioned later in this dissertation.

A CRPEP starts with frequency responses that may come from a high order ARX estimation, spectral analysis, or nonparametric Empirical Transfer Function Estimates (ETFE). The frequency response is approximated into linear parametric models utilizing control-relevant weights (Bayard, 1994; Gaikwad and Rivera, 1996). The estimated discrete model consists of a fractional representation of numerator and denominator matrix polynomials with input delays (Callafon *et al.*, 1996). During the curvefitting procedure, model-order reduction can be easily performed approximating frequency responses into low-order parametric curves with allowable bias in model estimation.

In this chapter, we present the formulation of a control-relevant parameter estimation procedure that utilizes frequency response curvefitting with MPC-relevant weighting functions into a full polynomial Matrix Fraction Description (MFD) model (Lee and Rivera, 2005). The MFD describes a multivariable system as a fraction of matrices with great flexibility. The following sections discuss the fundamental description and methodology of building frequency response estimation blocks (Callafon *et al.*, 1996), applying the control-relevant pre/post weights (Gaikwad and Rivera, 1997), and solving the minimization of a weighted output error matrix (Bayard, 1994; Gaikwad and Rivera, 1997). The Shell Heavy-Oil Fractionator (Prett and García, 1988) is considered as an example study for control-relevant parameter estimation (Lee and Rivera, 2005). Additionally, the nonlinear high-purity distillation column per Weischedel and McAvoy (1980) is examined as a case study later in this chapter.

2. Frequency Response Estimation

A frequency response is obtained from the input and output data using higher-order ARX estimation, spectral analysis, and ETFE (Ljung, 1999); these estimation methods are summarized below. The output data from s-th cycle of a deterministic, periodic input signal are denoted as

$$y^s(k) = y(k + (s-1)N_s) \tag{3.1}$$

where $k = 0, ..., N_s - 1$ and $s = 1, ..., r$. The ETFE of the $h\ell$-th element of a plant G is obtained from the ratios of output and input DFT sequences (Ljung and Glad, 1994), such that

$$g_{h\ell}(\omega_i) = \frac{\frac{1}{r}\sum_{s=1}^{r} Y_h^s(\omega_i)}{U_\ell(\omega_i)} \tag{3.2}$$

$$i = m(j-1) + \ell + \delta, \quad j = 1, 2, ..., n_s$$

$Y_h^s(\omega_i)$ and $U_\ell(\omega_i)$ represent the DFT sequences of $y_h^s(k)$ and $u_\ell(k)$ at frequency ω_i, respectively. The responses at frequencies with nonzero power can be estimated with arbitrary accuracy as the number of cycles r goes to infinity; ETFE requires persistent input excitation for nonzero $U_\ell(\omega_i)$.

Alternatively, a frequency response estimator can be obtained as follows

$$g_{h\ell}(\omega_i) = \frac{S_{u_\ell y_h}(\omega_i)}{S_{u_\ell u_\ell}(\omega_i)} \qquad i = 1, 2, ..., n_s \tag{3.3}$$

where $S_{u_j y_i}(\omega_i)$ and $S_{u_j u_j}(\omega_i)$ represent cross spectra and auto spectra of the corresponding time sequences, respectively. An advantage of the estimator per (3.3) is that when the sequences $u(k)$ and $v(k)$ in a plant system $y(k) = G(z)u(k) + v(k)$ are statistically independent, $v(k)$ is correlated out. For a higher-order ARX model, a frequency response is approximated as

$$G(\omega_i) \approx (1 + A_1 z^1 + ... + A_{na} z^{na})^{-1} (B_0 + B_1 z^{-1} ... + B_{nb} z^{nb})\, z^{nk} \qquad k \; large \tag{3.4}$$

where $z = e^{-j\omega_i T}$ for a discrete-time model.

3. Matrix Fraction Description Formulation

A frequency domain identification procedure for multivariable systems using MFD models is described in detail in Ljung (1999) and Callafon *et al.* (1996). Here frequency responses are given as

$$\mathscr{G} := \{G(\omega_i)|G(\omega_i) \in \mathrm{C}^{p\times m}, \text{ for } i \in [1,2,...,N]\} \tag{3.5}$$

A model $\tilde{P}$ approximates the frequency response into a linear parametric, real rational transfer function, formed by either a left or right fractional matrix polynomial description.

$$\text{Left MFD} \quad \tilde{P}(\xi^{-1},\theta) = A(\xi^{-1},\theta)^{-1}B(\xi^{-1},\theta) \tag{3.6}$$

$$\text{Right MFD} \quad \tilde{P}(\xi^{-1},\theta) = B(\xi^{-1},\theta)A(\xi^{-1},\theta)^{-1} \tag{3.7}$$

A and B denote parameterized polynomial matrices in the indeterminate ξ^{-1}. $\xi(\omega_i) = j\omega_i$ represents a continuous time model, whereas $\xi(\omega_i) = e^{j\omega_i T}$ represents the shift operator.

A process with m inputs and p outputs is parameterized into $\tilde{P}(\xi,\theta)$ using an MFD of the polynomial matrices per either (3.6) or (3.7). For both the left and right MFD, the polynomial matrix B is defined as a function of ξ^{-1} and θ,

$$B(\xi^{-1},\theta) = \sum_{k=d}^{d+b-1} B_k\xi^{-k}, \ B_k \in R^{p\times m} \tag{3.8}$$

where d denotes the number of leading zero matrix coefficients and b the number of non-zero matrix coefficients in the $B(\xi^{-1},\theta)$. For the left MFD, the A polynomial is parameterized by

$$A(\xi^{-1},\theta) = I_{p\times p} + \xi\sum_{k=1}^{a} A_k\xi^{-k+1}, \ A_k \in \Re^{p\times p} \tag{3.9}$$

and for the right MFD as

$$A(\xi^{-1},\theta) = I_{m\times m} + \xi\sum_{k=1}^{a} A_k\xi^{-k+1}, \ A_k \in \Re^{m\times m} \tag{3.10}$$

where a denotes the number of non-zero coefficients in the polynomial $A(\xi^{-1},\theta)$. The parameter θ consists of the corresponding unknown matrix coefficients in the A and B polynomials. We will utilize the left MFD

parameterization for control-relevant parameter estimation purposes because a left MFD polynomial model can be easily transformed into a state-space form or an ARX model (Ljung, 1999). Now, θ of the left MFD is formulated as:

$$\theta = [B_d \ldots B_{d+b-1}\, A_1 \ldots A_a] \in \Re^{p\times(mb+pa)} \tag{3.11}$$

The structural parameters $d_{i,j}, b_{i,j}$ and $a_{i,j}$ that are specified for each of the elements of the polynomial matrices and A and B separately are given as

$$d := \min\{d_{i,j}\},\ \ b := \max\{b_{i,j}\},\ \ a := \max\{a_{i,j}\} \tag{3.12}$$

Full polynomial matrices are used in this chapter to represent multivariable system frequency response estimation (Callafon *et al.*, 1996; de Callafon, 1998). Non-full polynomial estimation has been studied previously, for instance the common denominator approach by Bayard (1994). Rivera and Gaikwad (1995) extend Bayard's approach using a diagonal polynomial matrix in A that allows each output channel to have different polynomial denominators. Ljung (1999) briefly discusses the properties and identifiability of MFD structures. The stability and error bounds of MFD for closed-loop control design are discussed in de Callafon (1998).

The model order for polynomial estimation via an MFD structure is limited by the McMillan degree based on the resulting estimate $\tilde{P}(\xi,\theta)$ instead of asymptotic higher orders, as in ARX models. A detailed discussion of the exact relation between the McMillan degree, the row degree of the polynomial matrices $A(\xi^{-1},\theta)$ & $B(\xi^{-1},\theta)$, and the observability indices of a model computed by $A(\xi^{-1},\theta)^{-1}B(\xi^{-1},\theta)$ can be referred to Gevers (1986) and Van den Hof (1992). If an order of matrices in MFD is higher than the McMillan degree, the algorithm collapses and iteration will be terminated during estimation because of over-parameterization. Therefore, a low-order MFD model would be a good guess for initial estimation to avoid over-parameterization.

The output error between the process and model is represented as

$$E(\omega_i,\theta) = G(\omega_i) - \tilde{P}(\omega_i) \text{ for } i \in [1,2,...,N] \tag{3.13}$$

where $\tilde{P}$ is given by Left-MFD

$$\tilde{P}(\omega_i) = A(\xi(\omega_i)^{-1},\ \theta)^{-1} B(\xi(\omega_i)^{-1},\ \theta) \tag{3.14}$$

so that $E(\omega_i,\theta)$ is

$$\begin{aligned} E(\omega_i,\theta) &= G(\omega_i) - A(\xi(\omega_i)^{-1},\ \theta)^{-1} B(\xi(\omega_i)^{-1},\ \theta) && (3.15)\\ A(\xi(\omega_i)^{-1},\ \theta) E(\omega_i,\theta) &= A(\xi(\omega_i)^{-1},\ \theta) G(\omega_i) - B(\xi(\omega_i)^{-1},\ \theta) \\ &= G(\omega_i) - \theta\, \Phi(\omega_i) && (3.16)\\ E(\omega_i,\theta) &= A(\xi(\omega_i)^{-1},\ \theta)^{-1} \{G(\omega_i) - \theta\Phi(\omega_i)\} \\ &= A(\xi(\omega_i)^{-1},\ \theta)^{-1} \tilde{E}(\omega_i) && (3.17) \end{aligned}$$

and $\tilde{E}$ is defined by

$$\tilde{E}(\omega_i) = G(\omega_i) - \theta\Phi(\omega_i) \tag{3.18}$$

where

$$\theta = [B_d \ \ldots \ B_{d+b-1}\, A_1 \ \ldots \ A_a] \in R^{p\times(mb+pa)} \tag{3.19}$$

$$\Phi(\omega_i) = \begin{bmatrix} I_{m\times m}\, \xi(\omega_i)^{-d} \\ \vdots \\ I_{m\times m}\, \xi(\omega_i)^{-(d+b-1)} \\ G(\omega_i)\, \xi(\omega_i)^{-1} \\ \vdots \\ G(\omega_i)\, \xi(\omega_i)^{-a} \end{bmatrix} \tag{3.20}$$

If orthogonal multisine signals are utilized for simultaneously exciting all the transfer function elements (Rivera *et al.*, 1997), a permutation matrix, T_m, needs to be introduced in the error function to ensure the zippered power spectrum frequencies during the estimation procedure as

$$\tilde{E}(\omega_i) \;=\; (G(\omega_i) - \theta\Phi(\omega_i))T_m(\omega_i) \tag{3.21}$$

where T_m is defined by

$$T_m(\omega_i) = diag(0,\ \ldots\ \underbrace{1}_{j_{th}}\ \ldots\ 0), \qquad T_m \in \Re^{m\times m} \tag{3.22}$$

If j_{th} input channel has non-zero power at ω_i based on the zippered spectrum, only $T_m^{(j,j)}(\omega_i) = 1$ and all the other elements are zero. This also applies to the frequency grids of harmonically suppressed power spectrum design in consideration of nonlinear systems. Therefore, the permutation matrix is a function of frequency and is applied to the curvefitting estimation when orthogonal multisine input signals are used.

The parameter θ appears linearly in the error equation $\tilde{E}(\omega_i, \theta)$. Minimizing this error function is given by the two-norm formulation,

$$\begin{aligned}
\min J &= \min \frac{1}{2\pi}\int_{-\infty}^{\infty} \|\tilde{E}(\omega_i)\|_2^2 \, d\omega && (3.23)\\
&\approx \min \frac{1}{2\pi}\int_{-\pi}^{\pi} \|\tilde{E}(\omega_i)\|_2^2 \, d\omega && (3.24)\\
&\approx \min \sum_{i=1}^{N} \|\tilde{E}(\omega_i)\|_2^2 \, \Delta\omega_i && (3.25)
\end{aligned}$$

and a model parameter is obtained as

$$\begin{aligned}
\theta &= arg \min_{\theta\in\Re} \sum_{i=1}^{N} \|\tilde{E}(\omega_i, \theta)\|_2^2 && (3.26)\\
&= arg \min_{\theta\in\Re} \|(G - \theta\Phi_\omega)T_m\|_2^2 \Delta\omega && (3.27)
\end{aligned}$$

where $\tilde{E}(\omega_i, \theta)$, G, and P are defined by

$$\tilde{E}(\omega_i, \theta) := [\Re\{\tilde{E}(\omega_1, \theta) \ldots \tilde{E}(\omega_N, \theta)\} \;\; \Im\{\tilde{E}(\omega_1, \theta) \ldots \tilde{E}(\omega_N, \theta)\}] \tag{3.28}$$

$$G := [\Re\{G(\omega_1)T_m(\omega_1)\Delta\omega_1 \ldots G(\omega_N)T_m(\omega_N)\Delta\omega_N\} \;\; \Im\{G(\omega_1)T_m(\omega_1)\Delta\omega_1 \ldots G(\omega_N)T_m(\omega_N)\Delta\omega_N\}] \tag{3.29}$$

$$\Phi_\omega := [\Re\{\Phi(\omega_1)T_m(\omega_1)\Delta\omega_1 \ldots \Phi(\omega_N)T_m(\omega_N)\Delta\omega_N\} \ \Im\{\Phi(\omega_1)T_m(\omega_1)\Delta\omega_1 \ldots \Phi(\omega_N)T_m(\omega_N)\Delta\omega_N\}] \tag{3.30}$$

The output error norm equation is associated with a standard least squares minimization problem. Particularly, a model parameter is estimated from the minimization of $\|E(\omega_i,\theta)\|_2^2$ which is solved using the iterative least squares method, i.e., Sanathanan-Koerner (SK) iteration method (Sanathanan and Koerner, 1963) as

$$\begin{aligned}
\theta_t &= arg \ \min_{\theta\in\Re} \sum_{i=1}^{N} \|E(\omega_i,\theta_{t-1})\|_2^2 \Delta\omega_i && (3.31)\\
&= arg \ \min_{\theta\in\Re} \sum_{i=1}^{N} \|A(\omega_i,\theta_{t-1})^{-1}(G-\theta\Phi_\omega)T_m(\omega_i)\|_2^2 \Delta\omega_i && (3.32)\\
&= arg \ \min_{\theta\in\Re} \|A^{-1}(G-\theta\Phi_\omega)T_m\|_2^2 \Delta\omega && (3.33)
\end{aligned}$$

The SK method, however, is not optimal in the presence of noise and/or incorrect model order, but it provides suitable initial parameter values for a Gauss-Newton optimization. Control-relevant weights are added to the output error formulation in terms of pre/post weights such that

$$\begin{aligned}
\tilde{E}_w(\omega_i,\theta) &= W_2(\omega_i,\theta)E(\omega_i,\theta)W_1(\omega_i,\theta) && (3.34)\\
&= W_2(\omega_i,\theta)A(\omega_i,\theta)^{-1}\tilde{E}(\omega_i,\theta)W_1(\omega_i,\theta) && (3.35)\\
&= \tilde{W}_2(\omega_i,\theta)\tilde{E}(\omega_i,\theta)W_1(\omega_i,\theta) && (3.36)
\end{aligned}$$

where

$$\tilde{W}_2(\omega_i,\theta) = W_2(\omega_i,\theta)A(\omega_i,\theta)^{-1} \tag{3.37}$$

An objective function for control-relevant parameter estimation is therefore given by

$$\begin{aligned}
\min \ J &= \min_{\theta\in\Re} \frac{1}{2\pi}\int_{-\pi}^{\pi} \|\tilde{W}_2\tilde{E}W_1\| \, d\omega && (3.38)\\
&= \min_{\theta\in\Re} \sum_{i=1}^{N} \|\tilde{W}_2\tilde{E}W_1\| \, \Delta\omega_i && (3.39)
\end{aligned}$$

How to obtain the pre/post weights is discussed in the ensuing section.

4. Control-Relevant Weight Functions

In this section, the control-relevant parameter estimation formulation developed in Gaikwad and Rivera (1996; 1997) is presented. To obtain a general expression for the control-relevant parameter problem, it is needed to represent the closed-loop system via an upper linear fractional transformation (LFT) matrix such that

$$e_c = F_u(G,E)v = (G_{22} + G_{21}(I - EG_{11})^{-1}EG_{12})v \tag{3.40}$$

where e_c is a vector of errors which characterize the control system, v is a vector of all signals entering the control system, and G can be written as:

$$G = \begin{bmatrix} G_{11} & G_{12} \\ G_{21} & G_{22} \end{bmatrix} \tag{3.41}$$

which represents the nominal closed-loop system. E is a perturbation matrix that denotes the model estimation error, $P - \tilde{P}$. The LFT structure per (3.40) translates the effect of the model error into an equivalent control error for the closed-loop system. Therefore, the control-relevant parameter estimation formulation is obtained by minimizing e_c,

$$\min_E \ \|e_c\|_i \ = \ \min_E \|F_u(G,E)v\|_i \tag{3.42}$$

where i is the norm determined from the control objective. For the continuous 2-norm objective Parseval's theorem is applied,

$$\|e_c\|_2^2 = \frac{1}{2\pi}\int_{-\infty}^{\infty} e_c^H(-j\omega)e_c(j\omega)d\omega \tag{3.43}$$

while in the case of the discrete 2-norm, the error norm is

$$\|e_c\|_2^2 = \frac{1}{2\pi}\int_{-\pi}^{\pi} e_c^H(-j\omega)e_c(j\omega)d\omega \tag{3.44}$$

A direct solution of the upper LFT per (3.40) for either the continuous or discrete case represents a difficult nonlinear program. If efficient numerical techniques are to be used to accomplish parameter estimation, it

becomes necessary to obtain a problem representation that is *affine* with respect to the estimation error. A general CRPEP of the desired form is possible following some simplification in Gaikwad and Rivera (1997). If the spectral radius (i.e., the maximum eigenvalue) of EG_{11} is less than the unity for all frequencies, that is, $\rho(EG_{11}) < 1 \ \forall \ \omega$ (or $-\pi \leq \omega \leq \pi$ for a discrete-time system), the linear fractional representation can be represented via the series expansion,

$$F_u(G,E) = G_{22} + G_{21}EG_{12} + G_{21}EG_{11}EG_{12} + ... \tag{3.45}$$

Furthermore, if $\rho(EG_{11}) \ll 1$ over a bandwidth (which is dictated by the nature of G_{21} and G_{12}) the following approximation is then valid

$$F_u(G,E) \approx G_{22} + G_{21}EG_{12} \tag{3.46}$$

Note that

$$\|(G_{22} + G_{21}EG_{12})\, v\|_2 \leq \|G_{22}v\|_2 + \|G_{21}EG_{12}v\|_2 \tag{3.47}$$

and an approximate CRPEP of the desired form can be posed as

$$\min_E \ \|G_{21}\, E\, G_{12}\, v\|_2 \tag{3.48}$$

subject to the spectral radius condition

$$\sup_\omega \ \rho(EG_{11}) < 1, \ -\pi \leq \omega \leq \pi \tag{3.49}$$

One way to interpret the result of CRPEP is to evaluate the inequality

$$\|G_{21}EG_{12}v\|_2 \leq \bar{\sigma}(G_{21})\bar{\sigma}(G_{12}v)\bar{\sigma}(E) \tag{3.50}$$

which implies that $\bar{\sigma}(E)$ should be small over a bandwidth of $\bar{\sigma}(G_{21})\bar{\sigma}(G_{12}v)$. These two criteria will be monitored for the model stability and error minimization, respectively.

When the CRPEP considers an *n*-output, *n*-input discrete-time plant $P(z)$, a classical feedback controller is considered as

$$u(t) = C(z)\ (r(t) - y(t)) \tag{3.51}$$

and the general linear interconnection structure is defined with inputs $v = [r \quad d]^T$, $E = P - \tilde{P}$, and $e_c = W_y(r-y)$. W_y is a diagonal, static weight matrix that allows the engineer to selectively scale the controlled variable responses. The resulting closed-loop structure G is

$$G = \begin{bmatrix} \tilde{P}^{-1}\tilde{H} & \tilde{P}^{-1}\tilde{H} & -\tilde{P}^{-1}\tilde{H} \\ -W_y\tilde{S} & W_y\tilde{S} & -W_y\tilde{S} \end{bmatrix} \tag{3.52}$$

where $\tilde{H} = \tilde{P}C(I+\tilde{P}C)^{-1}$ and $\tilde{S} = (I+\tilde{P}C)^{-1}$ are the nominal complementary sensitivity and sensitivity functions, respectively (Morari and Zafiriou, 1988). The sensitivity function $\tilde{S}$ relates the external inputs $d-r$ to the error e while the complementary sensitivity function $\tilde{H}$ relates the external inputs r to the error. As a result, a CRPEP of multivariable systems is represented from Equation (3.48) and (3.49) into

$$\min_E \|G_{21}EG_{12}\|_F^2 \approx \min_E \ \|W_y\tilde{S}E\tilde{P}^{-1}\tilde{H}(r-d)\|_2^2 \tag{3.53}$$

subject to the condition that

$$\sup_\omega \ \rho(E\tilde{P}^{-1}\tilde{H}) < 1, \quad -\pi \le \omega \le \pi \tag{3.54}$$

The solution of Equation (3.53) is meaningful for model reduction and control-relevant parameter estimation. The closed-form expressions for $\tilde{S}$ and $\tilde{H}$ can be obtained using MPC Toolbox in MATLAB.

5. Iterative Parameter Estimation

Incorporating control-relevant weights, the weighted error is represented as

$$\tilde{E}_w(\omega_i,\ \theta) = \tilde{W}_2(\omega_i,\ \theta)\ \tilde{E}(\omega_i,\ \theta)\ W_1(\omega_i,\ \theta) \tag{3.55}$$

where the pre weight is

$$\begin{aligned} \tilde{W}_2(\omega_i,\theta) &= -W_y(\omega_i)\ \tilde{S}(\omega_i,\theta)A(\omega_i,\theta)^{-1} \\ &= -W_y(\omega_i)\ (I+\tilde{P}(\omega_i,\theta)C(\omega_i,\theta))^{-1}A(\omega_i,\theta)^{-1} \end{aligned} \tag{3.56}$$

and the post weight is

$$\begin{aligned} W_1(\omega_i,\theta) &= \tilde{P}^{-1}(\omega_i,\theta)\,\tilde{H}(\omega_i,\theta)(r-d) \\ &= C(\omega_i,\theta)\,(I+\tilde{P}(\omega_i,\theta)C(\omega_i,\theta))^{-1}(r-d) \end{aligned} \tag{3.57}$$

All the matrices in $\tilde{E}_w$ are dependent on frequency and parameters. Thus, an iterative procedure is utilized in this problem as in Sanathanan and Koerner (1963), i.e., SK-iteration. The estimated θ in step t is obtained by taking the weights using θ_{t-1}; $W_2(\omega_i,\theta_{t-1})$ and $W_1(\omega_i,\theta_{t-1})$ are calculated based on the previous model parameters θ_{t-1}. This iterative weighted error equation is denoted by

$$\begin{aligned} \tilde{E}_w(\omega_i,\theta_{t-1},\theta) &= \tilde{W}_2(\omega_i,\,\theta_{t-1})\,\tilde{E}(\omega_i,\,\theta)\,W_1(\omega_i,\,\theta_{t-1}) \\ &= \tilde{W}_2(\omega_i,\,\theta_{t-1})\,[G(\omega_i)\,-\,\theta\Phi(\omega_i)]T_m(\omega_i)\,W_1(\omega_i,\,\theta_{t-1})\Delta\omega_i \end{aligned} \tag{3.58}$$

Now parameter θ is estimated from the minimization of $\tilde{E}_w(\omega_i,\theta_{t-1},\theta)$ which is solved by the iterative minimization procedure

$$\theta_t^{CRPEP} = \arg\,\min_{\theta\in\Re}\sum_{k=1}^{N}\,\|\tilde{W}_2(\omega_i,\,\theta_{t-1})\,\tilde{E}(\omega_i,\,\theta)\,W_1(\omega_i,\,\theta_{t-1})\|_2^2\,\Delta\omega_i \tag{3.59}$$

An SK-iteration problem is solved first and the CRPEP is solved optimally by running the iterative Gauss-Newton optimization.

The computation of minimization steps is much more difficult than a non-weighted error formulation because of the *pre/post* weights on $\tilde{E}_w$. The *Kronecker vector* and *Kronecker product* is applied to the weighted error matrix for column-wise transformation.

Proposition 3.1 *With matrices X, Y, and Z with appropriate dimensions, the matrix product $C = XYZ$ can be obtained by using Kronecker vector and Kronecker product such that*

$$vec(C) = [Z^T \otimes X]\;vec(Y)$$

if Z is a complex matrix, Z^T means Z^H.

Definition 3.1 *Considering matrices $X \in C^{n_1 \times n_2}$ and $Y \in C^{m_1 \times m_2}$, the Kronecker vector $vec(X)$ and Kronecker product $X \otimes Y$ operators are defined by*

$$vec(X) := \begin{bmatrix} x_{1,1} \\ x_{2,1} \\ \vdots \\ x_{n_1,n_2} \end{bmatrix} \in C^{n_1 n_2 \times 1}, \quad X \otimes Y := \begin{bmatrix} x_{1,1}Y & \dots & x_{1,n_2}Y \\ \vdots & \dots & \vdots \\ x_{1,1}Y & \dots & x_{1,n_2}Y \end{bmatrix} \in C^{n_1 n_2 \times 1} \tag{3.60}$$

Considering $\tilde{E}_w$, it can be rewritten as

$$\tilde{E}_w = \tilde{W}_2 \, (G - \theta \, \Phi) \, T_m \, W_1 \tag{3.61}$$

$$= (\tilde{W}_2 G T_m W_1) - (\tilde{W}_2 \theta \, \Phi T_m W_1) \tag{3.62}$$

and we can take advantage of *Kronecker vec* operator for $\tilde{E}_w$ such that

$$vec(\tilde{E}_w) = \underbrace{vec(\tilde{W}_2 \, G \, T_m \, W_1)}_{G_\omega} - \underbrace{[(\Phi T_m W_1)^T \otimes \tilde{W}_2]}_{\Phi_\omega} \, vec(\theta) \tag{3.63}$$

$$= G_\omega - \Phi_\omega \, \bar{\theta} \tag{3.64}$$

where $vec(\theta) = \bar{\theta}$. As the Frobenius-norm is still valid with the *Kronecker* operator, the following is available:

$$||X||_F^2 = ||vec(X)||_F^2 \tag{3.65}$$

For an arbitrary matrix X, the minimization objective function of $\tilde{E}_w$ is obtained as

$$\theta_t^{CRPEP} = \arg \min_{\theta \in \Re} \|vec(\tilde{E}_w(\theta_{t-1}, \, \theta))\|_F^2 = \arg \min_{\theta \in \Re} \|G_\omega - \Phi_\omega \bar{\theta}\|_F^2 \tag{3.66}$$

where G_ω and Φ_ω are formulated as

$$G_\omega := \begin{bmatrix} vec(\Re\{\tilde{W}_2(\omega_1,\ \theta_{t-1})\ G(\omega_1)\ T_m(\omega_1)\ W_1(\omega_1)\Delta\omega_1\}) \\ \vdots \\ vec(\Re\{\tilde{W}_2(\omega_N,\ \theta_{t-1})\ G(\omega_N) T_m(\omega_N)\ W_1(\omega_N)\Delta\omega_N\}) \\ vec(\Im\{\tilde{W}_2(\omega_1,\ \theta_{t-1})\ G(\omega_1) T_m(\omega_1)\ W_1(\omega_1)\Delta\omega_1\}) \\ \vdots \\ vec(\Im\{\tilde{W}_2(\omega_N,\ \theta_{t-1})\ G(\omega_N) T_m(\omega_N)\ W_1(\omega_N)\Delta\omega_N\}) \end{bmatrix} \tag{3.67}$$

$$\Phi_\omega := \begin{bmatrix} \Re\{[\Phi(\omega_1)T_m(\omega_1)W_1(\omega_1,\theta_{t-1})\Delta\omega_1]^T \otimes \tilde{W}_2(\omega_1,\theta_{t-1})\} \\ \vdots \\ \Re\{[\Phi(\omega_N)T_m(\omega_N)W_1(\omega_N,\theta_{t-1})\Delta\omega_N]^T \otimes \tilde{W}_2(\omega_N,\theta_{t-1})\} \\ \Im\{[\Phi(\omega_1)T_m(\omega_1)W_1(\omega_1,\theta_{t-1})\Delta\omega_1]^T \otimes \tilde{W}_2(\omega_1,\theta_{t-1})\} \\ \vdots \\ \Im\{[\Phi(\omega_N)T_m(\omega_N)W_1(\omega_N,\theta_{t-1})\Delta\omega_N]^T \otimes \tilde{W}_2(\omega_N,\theta_{t-1})\} \end{bmatrix} \tag{3.68}$$

The *Kronecker* operators transform the estimation of large-size models into a linear estimation problem seeking a solution of θ.

6. Numerical Solution

To solve the objective function of the weighted output error problem numerically, an iterative least squares minimization is applied in the control-relevant parameter estimation problem. The parameter $\bar{\theta}$ is

obtained such that

$$vec(\tilde{E}_w) = G_\omega - \Phi_\omega \bar{\theta} \tag{3.69}$$

$$F = \|vec(\tilde{E})\|_2^2 = (G_\omega - \Phi_\omega \bar{\theta})^T (G_\omega - \Phi_\omega \bar{\theta}) \tag{3.70}$$

$$\frac{\partial F}{\partial \theta} = -2\,\Phi_\omega^T (G_\omega - \Phi_\omega \bar{\theta}) \tag{3.71}$$

$$= -2\,\Phi_\omega^T G_\omega + 2\Phi_\omega^T \Phi_\omega \bar{\theta} \tag{3.72}$$

and a solution is found when $\frac{\partial F}{\partial \theta} = 0$ such that

$$\bar{\theta} = (\Phi_\omega^T\,\Phi_\omega)^{-1}\,(\Phi_\omega^T\,G_\omega) \tag{3.73}$$

As an iterative minimization procedure, the Hessian-Newton matrix is applied to this problem. Since F is twice differentiable with respect to $\bar{\theta}$,

$$\frac{\partial^2 F}{\partial \theta^2} = 2\,\Phi_\omega^T \Phi_\omega \tag{3.74}$$

and the iterative Newton method is considered

$$\bar{\theta}_{k+1} = \bar{\theta}_k - [H(\theta_k)]^{-1}\ \nabla F(\bar{\theta}_k) \tag{3.75}$$

$$= \bar{\theta}_k - [2\Phi_\omega^T \Phi_\omega]^{-1}\,[-2\Phi_\omega^T\,(G_\omega - \Phi_\omega \bar{\theta}_k)] \tag{3.76}$$

The standard least squares solution provides an initial estimate of the model that can be used to update the control-relevant pre/post weights. A numerical termination criteria can be given for the iteration loop as follows (Rivera and Morari, 1987):

$$\left| \frac{\bar{\theta}_{k+1} - \bar{\theta}_k}{\bar{\theta}_{k+1}} \right| \leq \varepsilon_1 \tag{3.77}$$

$$\left| \frac{\|\tilde{W}_2 \tilde{E} W_1\|_{2,\,(k+1)}^2 - \|\tilde{W}_2 \tilde{E} W_1\|_{2,\,(k)}^2}{\|\tilde{W}_2 \tilde{E} W_1\|_{2,\,(k+1)}^2} \right| \leq \varepsilon_2 \tag{3.78}$$

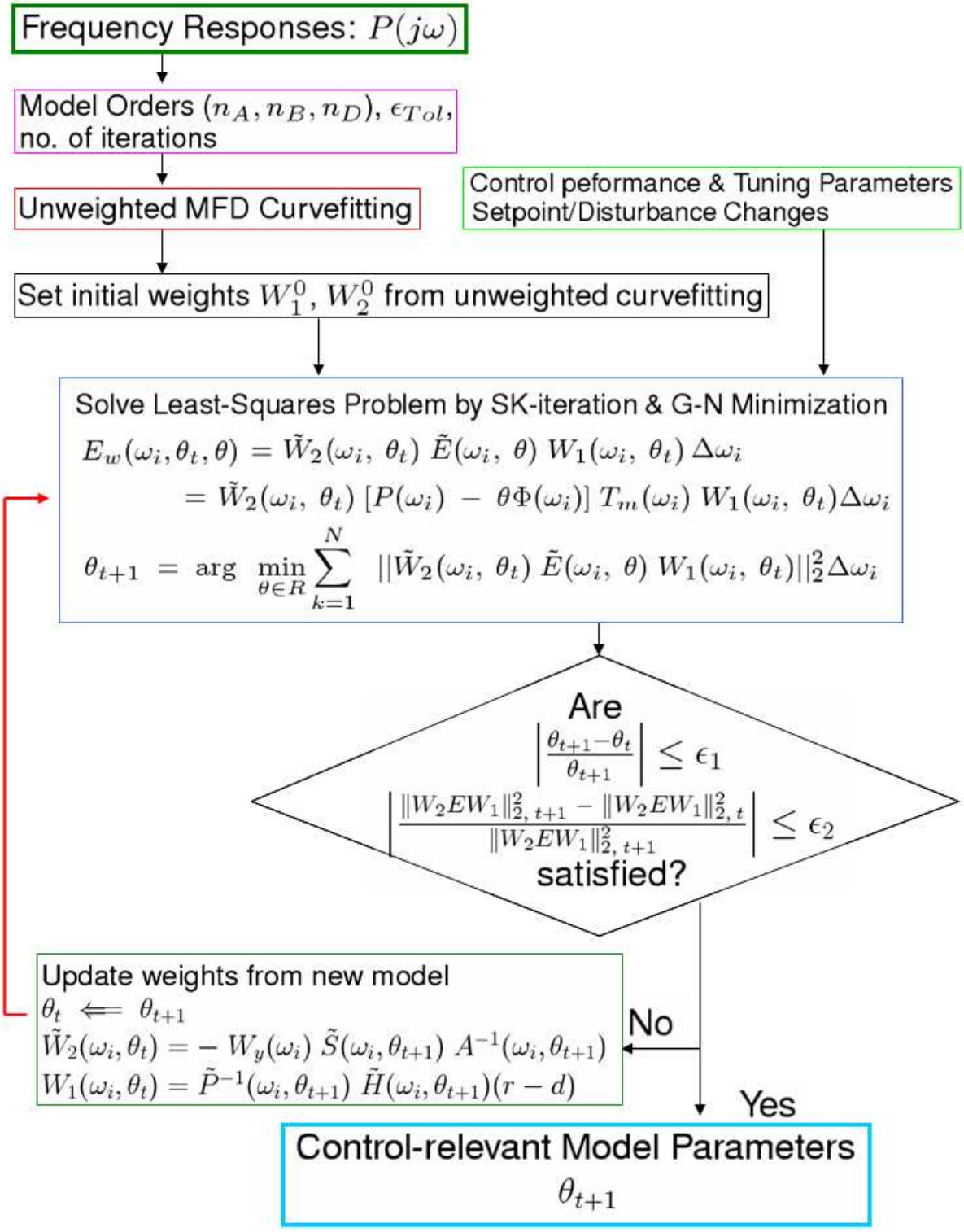

Figure 45. Algorithm for Control-relevant Parameter Estimation

If the two criteria are satisfied simultaneously, we can terminate the iteration loop at step $k+1$ with user specifications of the threshold values ε_1 and ε_2. A summary of this control-relevant parameter estimation is illustrated in Figure 45.

7. Example Study to Shell Heavy-Oil Fractionator Problem

A 2×2 multivariable system is used as an example of control-relevant parameter estimation problem using Model Predictive Control; it is based on the Shell Heavy-Oil Fractionator Process (Rivera and Gaikwad, 1995; Prett and García, 1988). The process is linear and possesses considerable time-delays as the Shell Heavy-Oil Fractionator is given such that

$$y(t) = \begin{bmatrix} \frac{4.05}{50\,s+1}\exp^{-27s} & \frac{1.77}{60\,s+1}\exp^{-28s} \\ \frac{5.39}{50\,s+1}\exp^{-18s} & \frac{5.72}{60\,s+1}\exp^{-14s} \end{bmatrix} u(t) + \begin{bmatrix} \frac{1.44}{40\,s+1}\exp^{-27s} \\ \frac{1.83}{20\,s+1}\exp^{-15s} \end{bmatrix} d(t) \tag{3.79}$$

where the physical outputs and inputs are

$$y(t) = \begin{bmatrix} \text{Top End. Product} \\ \text{Side End. Product} \end{bmatrix} \quad u(t) = \begin{bmatrix} \text{Top Draw} \\ \text{Side Draw} \end{bmatrix} \quad d(t) = [\text{URDuty}] \tag{3.80}$$

For a comparison between the unweighted and weighted curvefittings, the time delay in Equation (3.79) has been increased, leading to a modified plant, as follows

$$y(t) = \begin{bmatrix} \frac{4.05}{50\,s+1}\exp^{-50s} & \frac{1.77}{60\,s+1}\exp^{-60s} \\ \frac{5.39}{50\,s+1}\exp^{-50s} & \frac{5.72}{60\,s+1}\exp^{-60s} \end{bmatrix} u(t) + \begin{bmatrix} \frac{1.44}{40\,s+1}\exp^{-27s} \\ \frac{1.83}{20\,s+1}\exp^{-15s} \end{bmatrix} d(t) \tag{3.81}$$

The increased time delay creates the opportunity for a larger bias between full and reduced model structures, which will give rise to a greater contrast between control-relevant and unweighted model reduction.

7.1. Input Signal Design and Open-Loop Experiment. The input signal design parameters are obtained from *a priori* knowledge of the system: $\tau_{dom}^{H} = 74$ min, $\tau_{dom}^{L} = 48$ min, and feasible multisine design parameters are obtained as $T = 4$ min, $n_s = 10$, $N_s = 698$ (1 cycle= 1400 min), and $hf = 0.0$ with

α=2 and β=3. An open-loop identification experiment is performed using orthogonal multisine input signals without time-domain constraints (Figure 46).

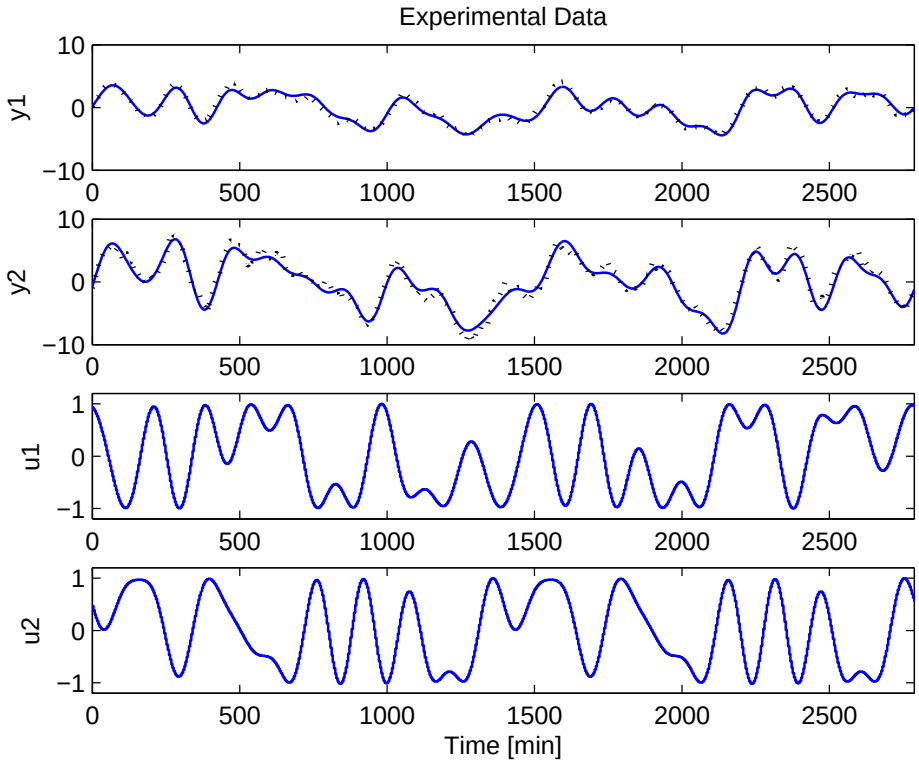

Figure 46. Open-loop experiment with orthogonal multisine input signals for the plant per Equation (3.81) ($\sigma_d^2 = 2.0$ to the disturbance model for noisy conditions)

The dataset of 2 cycles is used for calculating ETFEs and solving the control-relevant parameter estimation problem.

7.2. Solving a Control-Relevant Parameter Estimation Problem. The parameter estimation methodology is now applied to the frequency responses generated from the modified plant per Equation (3.81). Curvefitting with the order of $[na = 1, nb = 1, nd = 1]$ is performed under noise-free conditions and noisy conditions ($\sigma_d^2 = 2.0$) with control-relevant weights. This low-order indicates significant model order reduction while increasing bias error to curvefit models, which is shaped by the control-relevant weights. Using

the modified plant per Equation (3.81), the bias error shift could be observed in the following.

7.2.1. *Noise-Free Conditions.* Comparing ETFEs vs. the estimated model, the shapes of curvefits between non-weighted and weighted cases show a difference in the low frequency area in Figure 47. In general, the weighted curves emphasize the low frequency responses for the closed-loop dynamics so that they have more accurate gains, as shown in open-loop step responses in Figure 48. Due to the long time delays in the plant, we apply a set of relaxed MPC tuning parameters (PH=35, MH=5, Ywt=[1 1], Uwt=[45 90]) to evaluate the setpoint tracking performance. In the tracking test, both the cases show no offset in y_1 and y_2, as shown in Figure 49. Singular values of the weights and model errors are shown in Figure 50a. The spectral radius analysis (Figure 50b) indicates that the spectral radius conditions of both the unweighted and weighted cases are satisfied as $\rho(\tilde{E}_m H) < 1$ in the low frequencies. The spectral analysis condition of the weighted model is shifted, lower than that of the unweighted model in the low frequencies (Figure 50b) but has similar values in the high frequencies.

7.2.2. *Noisy Conditions.* Under noisy conditions ($\sigma_d^2 = 2.0$), we utilize a tuning set for MPC:PH=35, MH=5, Ywt=[1 1], and Uwt=[24 48] for the setpoint tracking test and the weighting functions. The weighted curvefits still emphasize the low frequency dynamics (Figure 51) since they display the most mismatch in the high frequencies. A comparison of open-loop step responses displays no significant difference of gain values among the unweighted and weighted MFD models and the modified Shell plant (Figure 52); they both have gain errors. However, in the setpoint tracking test, the weighted model has no offset in y_1 and y_2 while the unweighted suffers oscillation and slow responses in y_1 and y_2 (Figure 53). Figure 54b shows the spectral radius analysis that the weighted model has much lower values than the unweighted model in the high frequencies. Consequently, the model error of the weighted has lower values in low frequencies (see Figure 54a (bottom)).

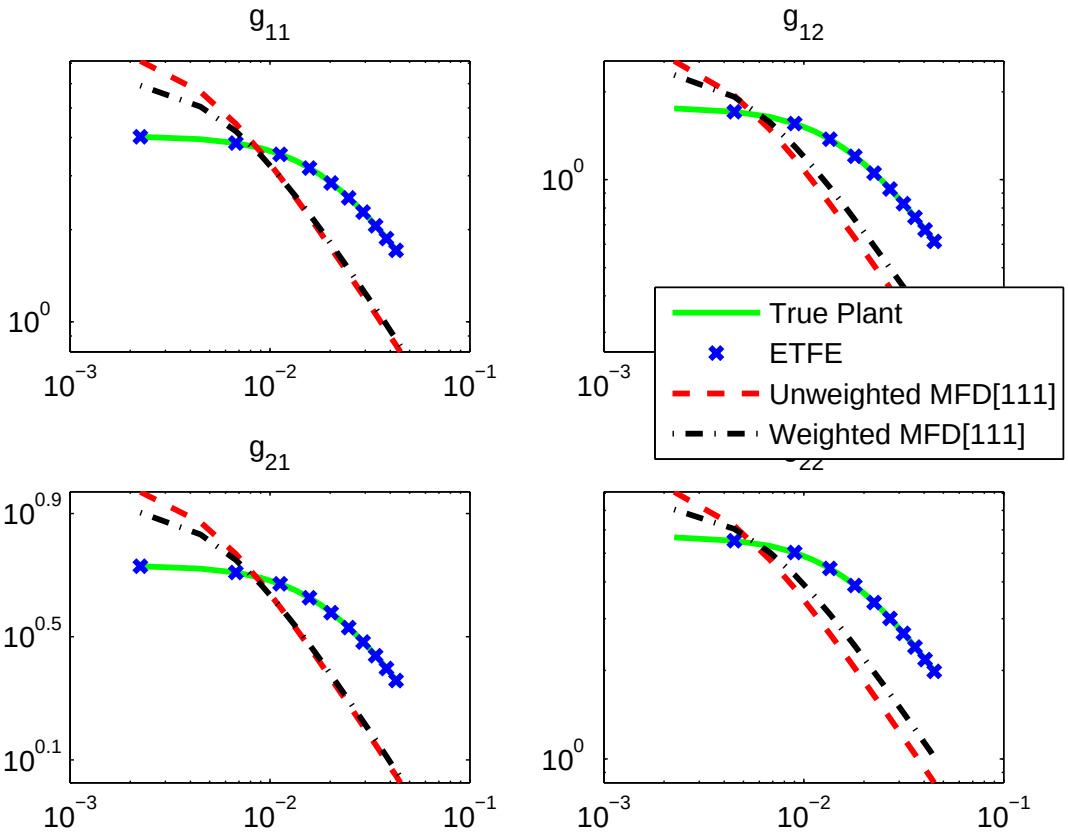

Figure 47. MFD curvefitting for the plant per Equation (3.81) with [na=1, nb=1, nd=1] under noise-free conditions (solid: true plant, x: ETFE values, dashed: unweighted MFD, dash-dotted: weighted MFD)

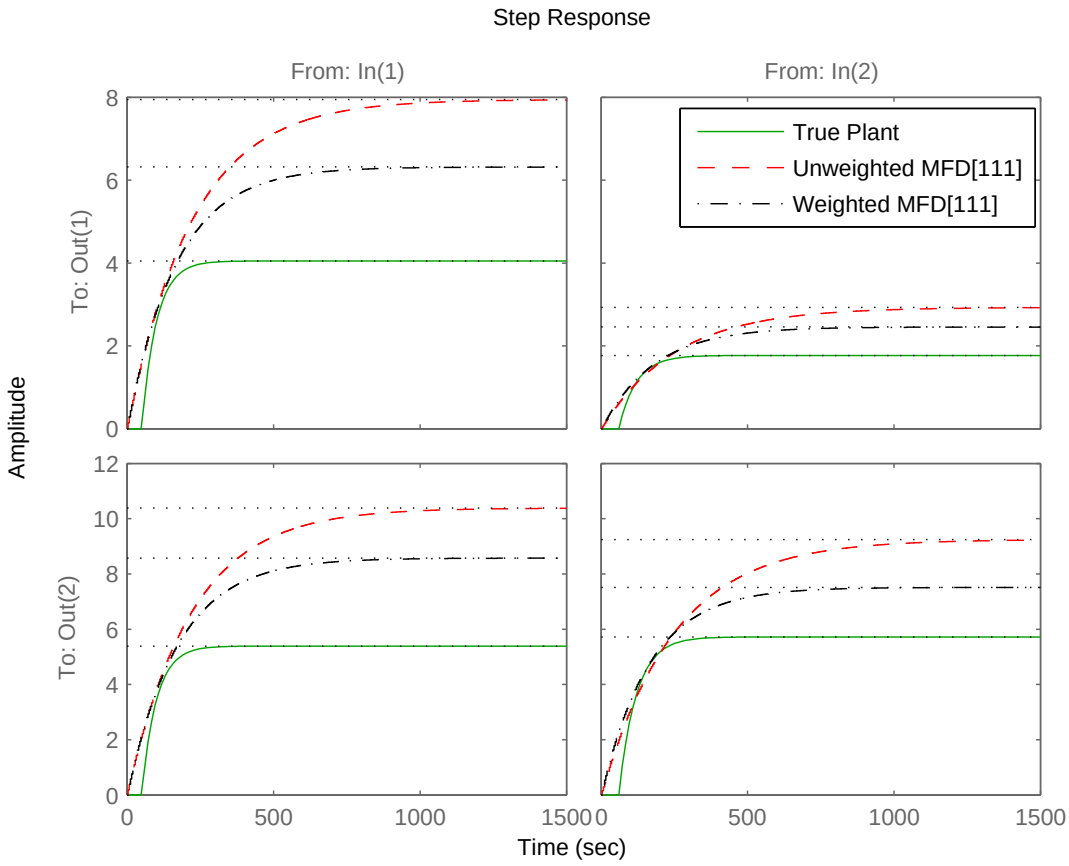

Figure 48. Open-loop step responses of model estimates for the plant per Equation (3.81) with [$n_a = 1$, $n_b = 1$, $n_d = 1$] under noise-free conditions

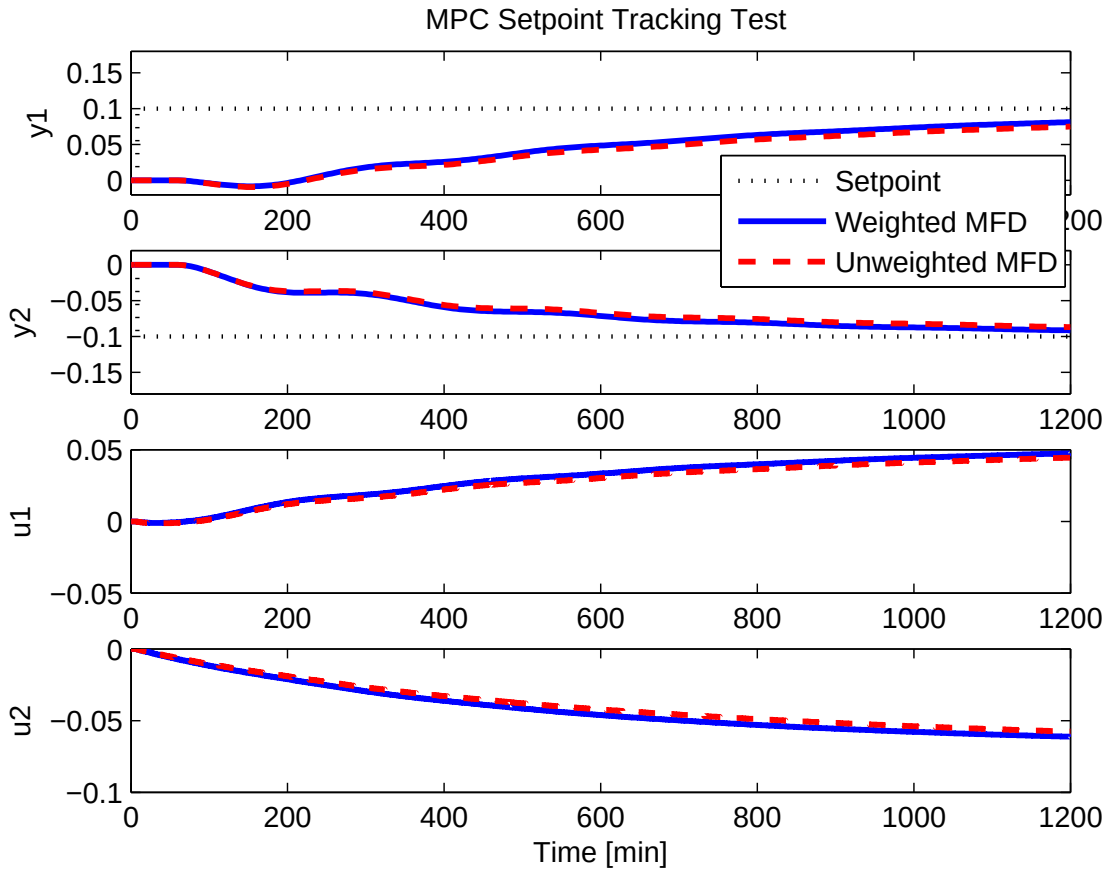

Figure 49. MPC tracking test of MFD estimates for the plant per Equation (3.81) with [$n_a = 1$, $n_b = 1$, $n_d = 1$] and PH=35, MH=5, Ywt=[1 1], Uwt=[45 90] under noise-free conditions

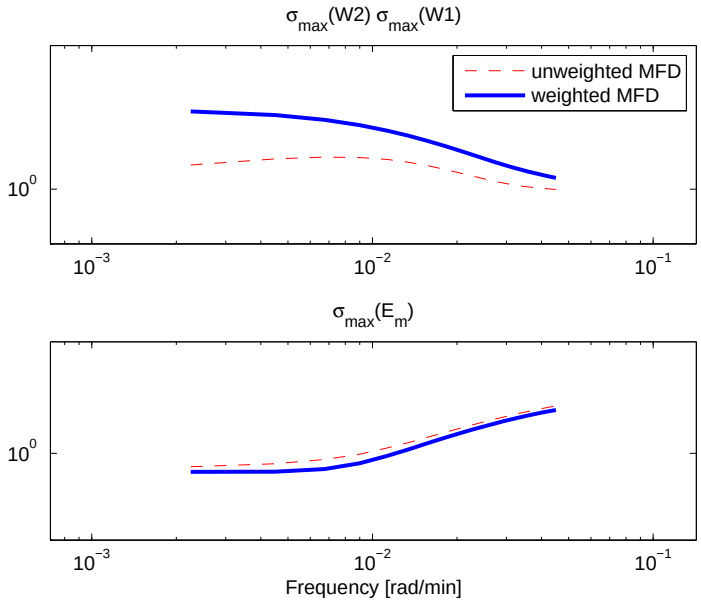

(a)

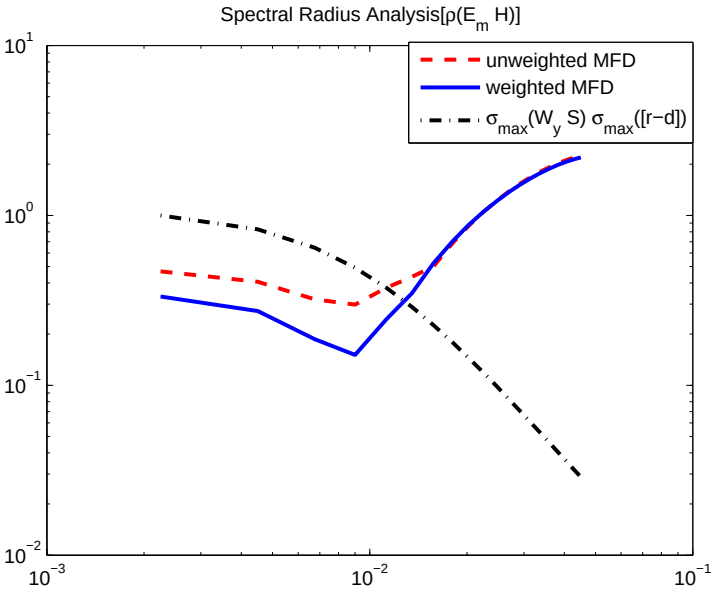

(b)

Figure 50. MFD curvefitting for the plant per Equation (3.81) with $[n_a = 1, n_b = 1, n_d = 1]$ under noise-free conditions, singular value analysis of weights (top) and model error (bottom) (a) and spectral radius analysis (b)

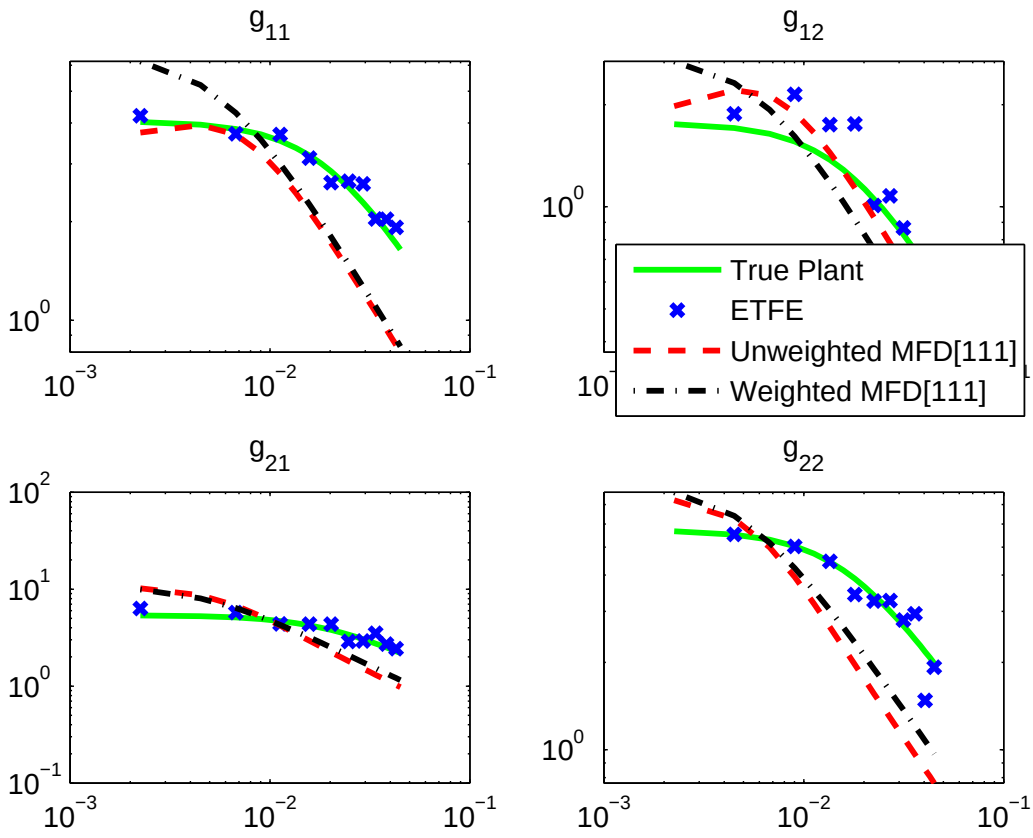

Figure 51. MFD curvefitting for the plant per Equation (3.81) with $[n_a = 1, n_b = 1, n_d = 1]$ under noisy conditions, $\sigma_d^2 = 2.0$ (solid: Shell plant, *: ETFE values, dashed: unweighted MFD, dotted: weighted MFD).

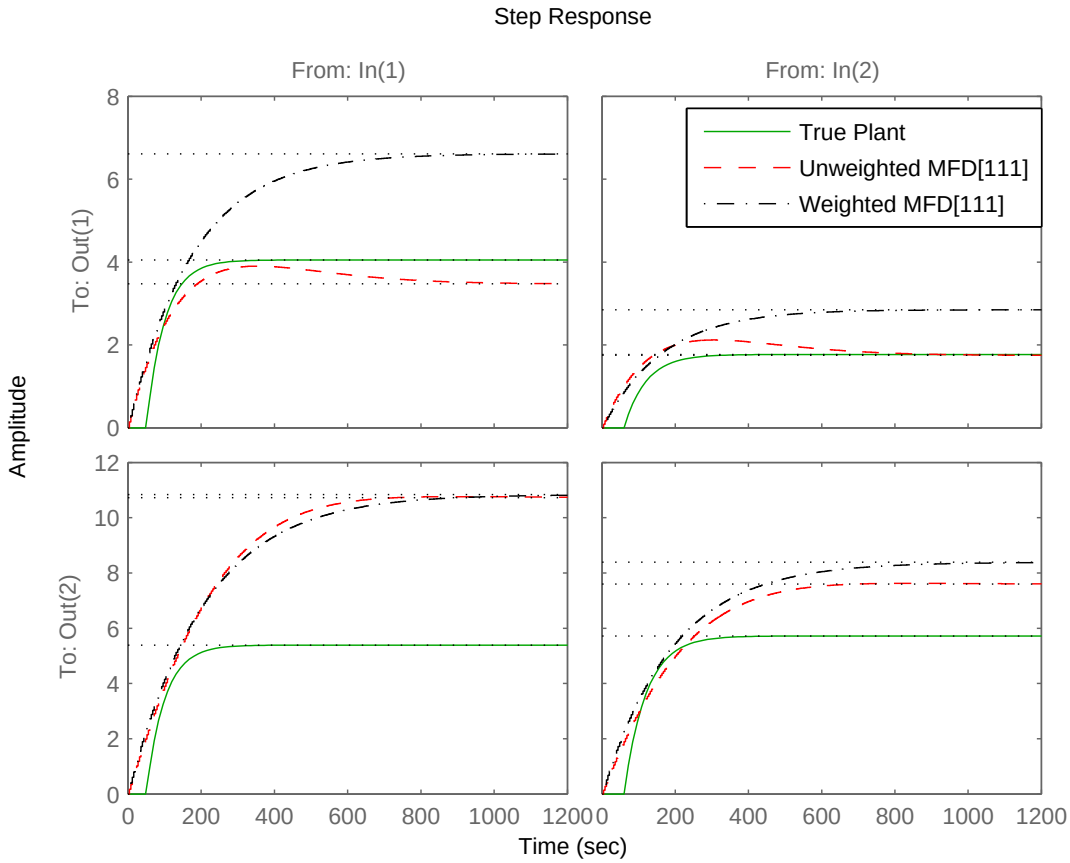

Figure 52. Open-loop step responses of MFD curvefitting for the plant per Equation (3.81) with [$n_a = 1, n_b = 1, n_d = 1$] under noisy conditions, $\sigma_d^2 = 2.0$.

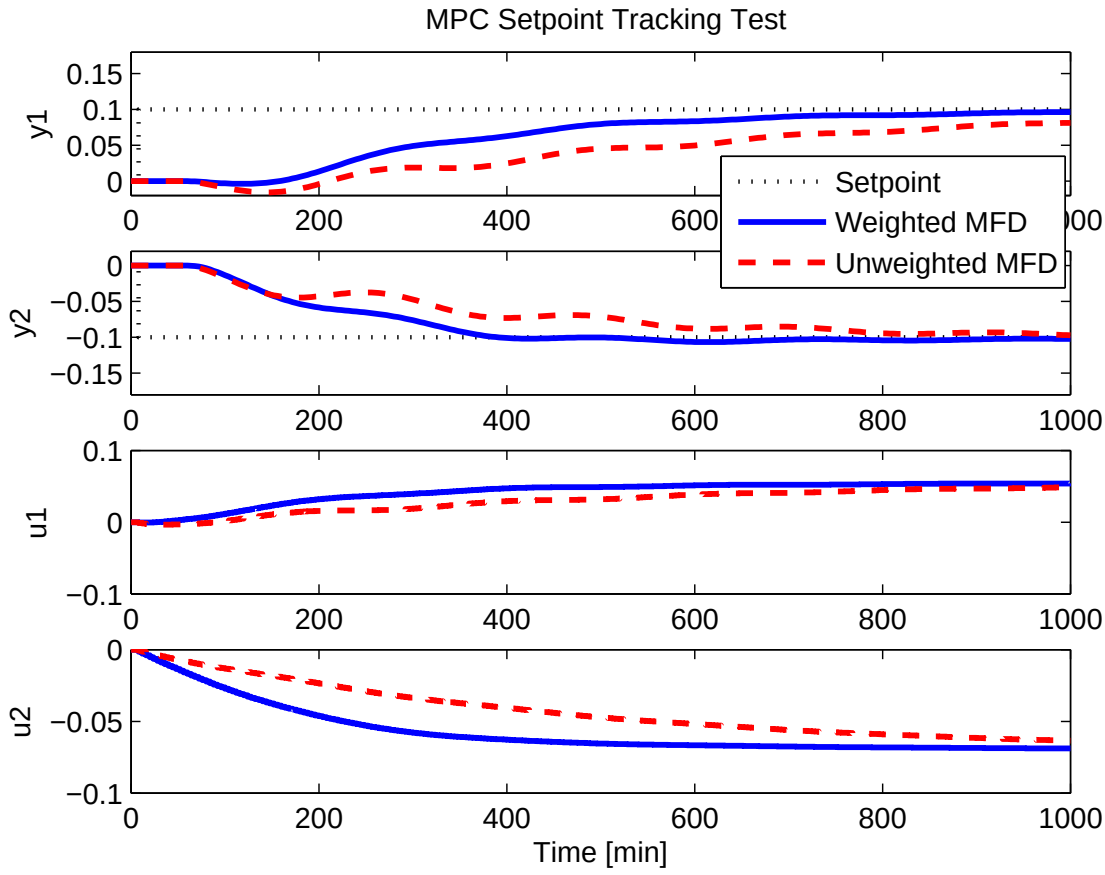

Figure 53. MPC tracking test of MFD estimates for the plant per Equation (3.81) with [$n_a = 1$, $n_b = 1$, $n_d = 1$] under noisy conditions, $\sigma_d^2 = 2.0$, and PH=35, MH=5, Ywt=[1 1],& Uwt=[24 48]

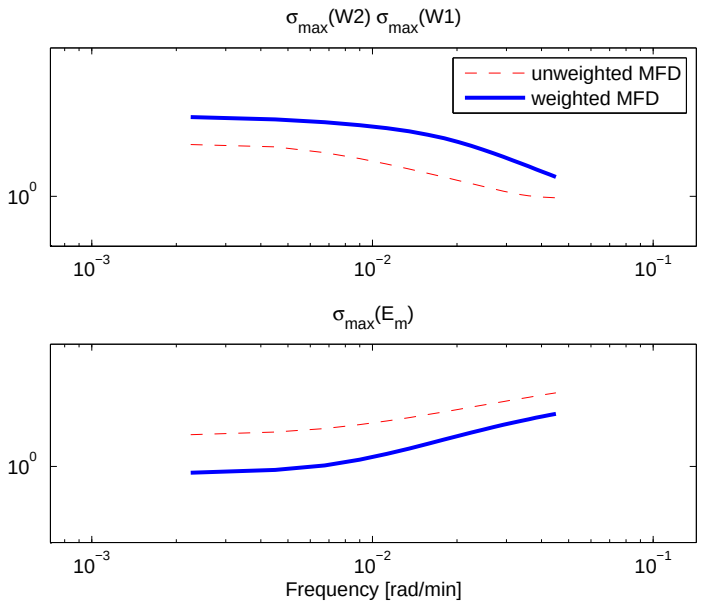

(a)

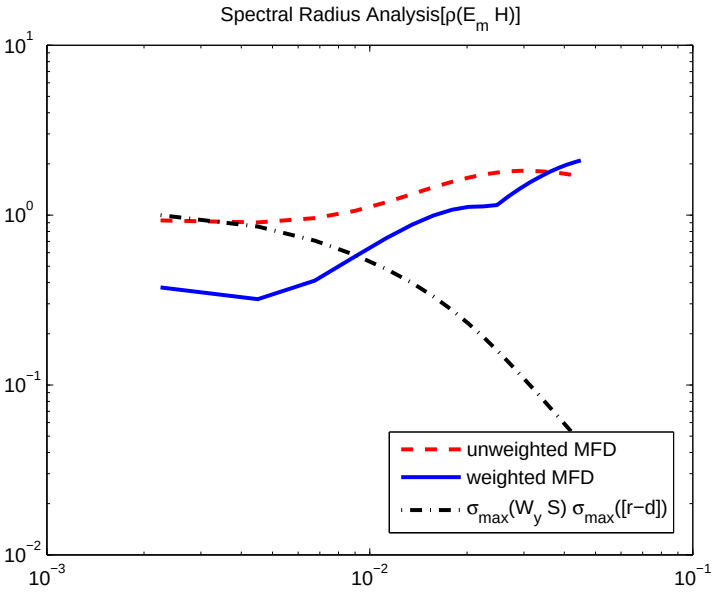

(b)

Figure 54. MFD curvefitting for the plant per Equation (3.81) with $[n_a = 1, n_b = 1, n_d = 1]$ under noisy conditions, $\sigma_d^2 = 2.0$: singular value analysis of weight(top) and model error (bottom) (a) and spectral radius analysis (b)

8. Case Study to Nonlinear High-Purity Distillation Columns

In this section, the control-relevant parameter estimation is considered for the nonlinear multivariable system per Weischedel-McAvoy distillation column (1980). This case contrasts the example problem of the modified Shell heavy-oil fractionator, which is linear and has considerable time-delays. However, the Weischedel-McAvoy problem is nonlinear and highly-interactive, much more sensitive to the gain direction estimation in the identification and control points of view, as discussed in Chapters 1 and 2. ETFEs based on the standard zippered spectrum are only used to test the capability of the curvefitting algorithms on various frequency grids. To reduce the nonlinearity of the system, an even harmonic suppression multisine signal is applied to the Weischedel-McAvoy distillation column at a cost of extended signal length from $N_s = 378$ to $N_s = 754$. The even-harmonic suppressed signals provide less distorted frequency response curves, which facilitate more precise curvefitting models.

8.1. Non-Harmonic Suppression Case. Figures 55 and 56 show the model curvefits with $[n_a = 1,\ n_b = 1,\ n_d = 1]$ order and MPC closed-loop test evaluation, respectively, of the standard zippered signal case under noise-free conditions. Since the unweighted curvefits have equivalent values to the weighted curvefits, the setpoint tracking performance displays almost identical results in spite of a very aggressive MPC tuning set (PH=50, MH=5, Ywt=[1 1], & Uwt=[0.1 0.1]). Therefore, we could assume that the unweighted curvefits possess no considerable bias in model estimates; model-order reduction in this case does not contribute much benefit. Nevertheless, the weighted case shows less oscillation than the unweighted case in the setpoint test with $r = [0.05\ \ -0.05]$ (Figure 56).

Under noisy conditions (SNR=$[1,1]dB$), the weighted model demonstrates closer agreement to the ETFE values in the low frequencies (Figure 57). The setpoint tracking results for the weighted case shows no offset in y_1 and y_2. However, the non-weighted case suffers unstable responses with significantly large offsets in y_1 and y_2 (Figure 58), which is unsatisfactory.

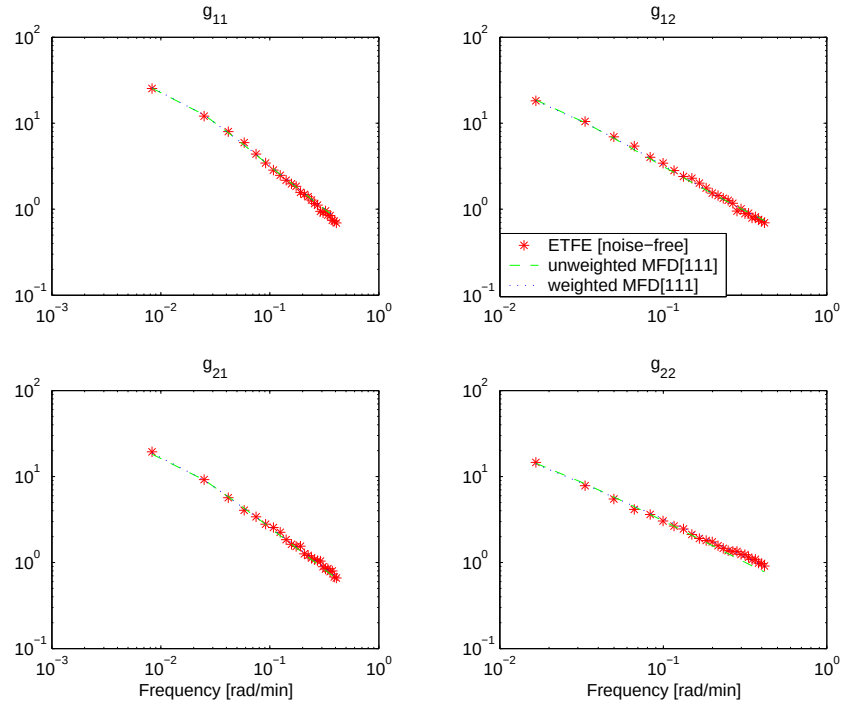

Figure 55. MFD curvefitting [$n_a = 1$, $n_b = 1$, $n_d = 1$] under noise-free conditions for Weischedel-McAvoy distillation column (1980)

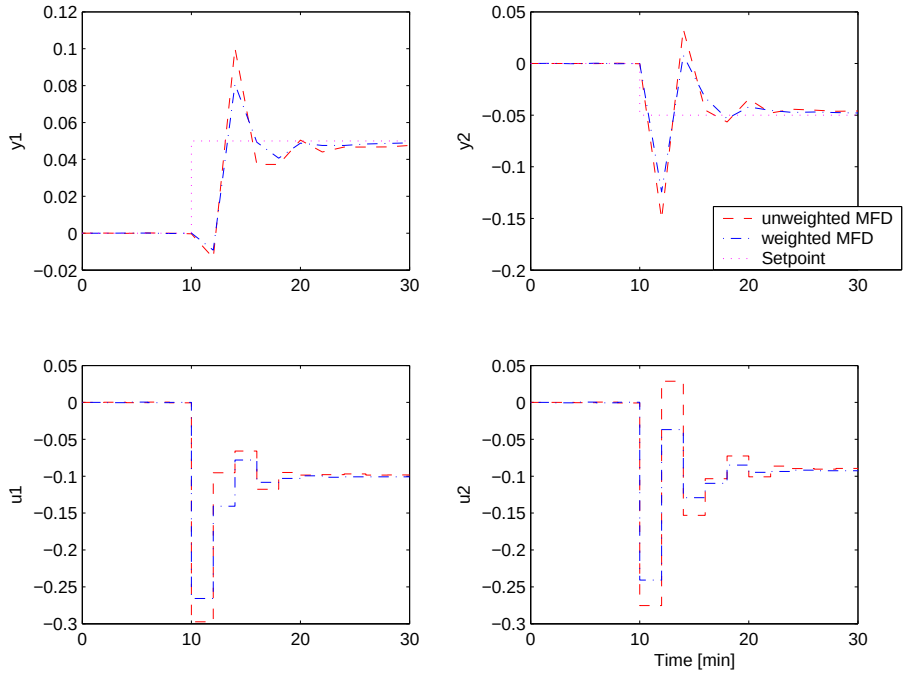

Figure 56. MPC setpoint tracking test of MFD estimates [$n_a = 1$, $n_b = 1$, $n_d = 1$] under noise-free conditions: PH=50, MH=5, Ywt=[1 1], Uwt=[0.1 0.1] for Weischedel-McAvoy distillation column (1980)

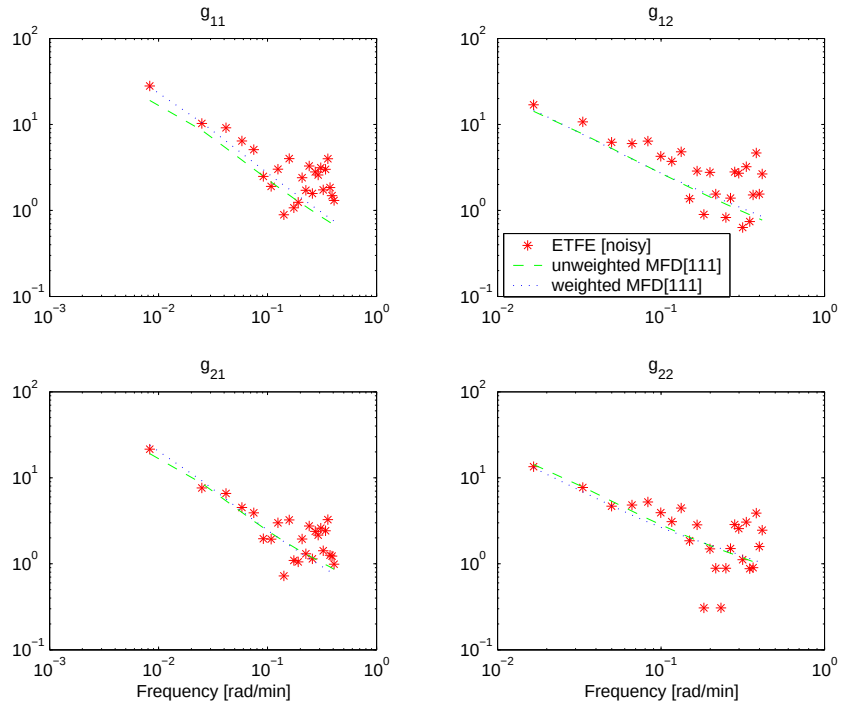

Figure 57. MFD curvefitting $[n_a = 1, n_b = 1, n_d = 1]$ under noisy conditions, SNR=[1, 1]dB for Weischedel-McAvoy distillation column (1980)

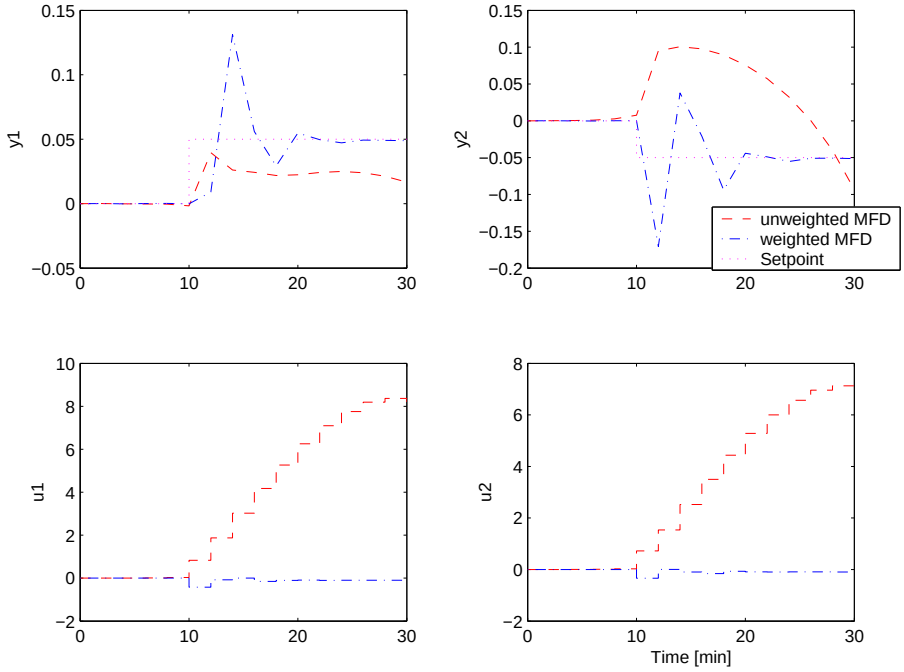

Figure 58. MPC setpoint tracking test of MFD estimates $[n_a = 1, n_b = 1, n_d = 1]$ under noisy conditions, SNR=[1, 1]dB, PH=50, MH=5, Ywt=[1 1], and Uwt=[0.1 0.1] for Weischedel-McAvoy distillation column (1980)

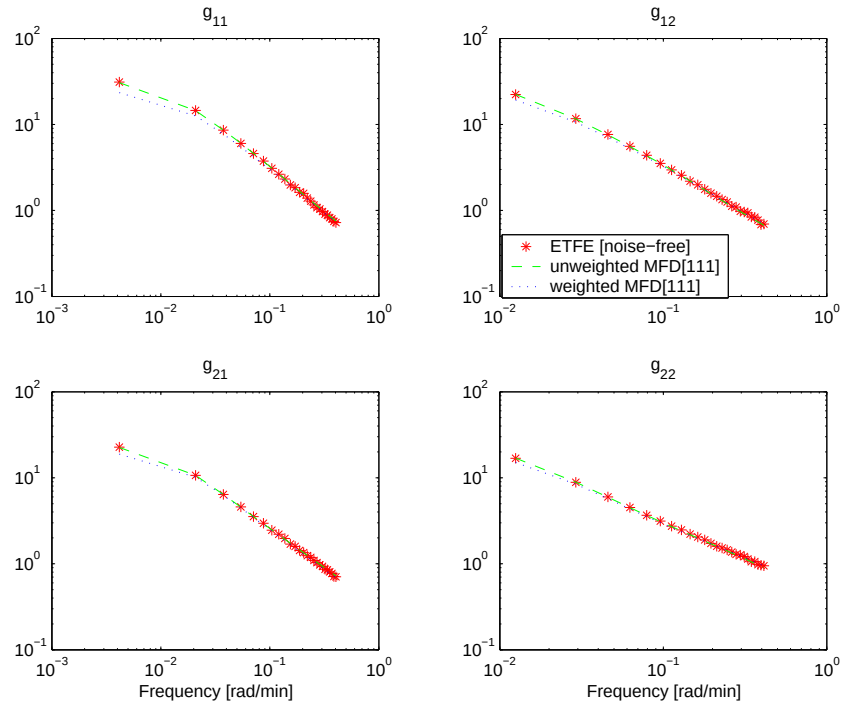

Figure 59. MFD curvefitting $[n_a = 1, n_b = 1, n_d = 1]$ under noise-free conditions using even-harmonics suppressed multisine signals for Weischedel-McAvoy distillation column (1980)

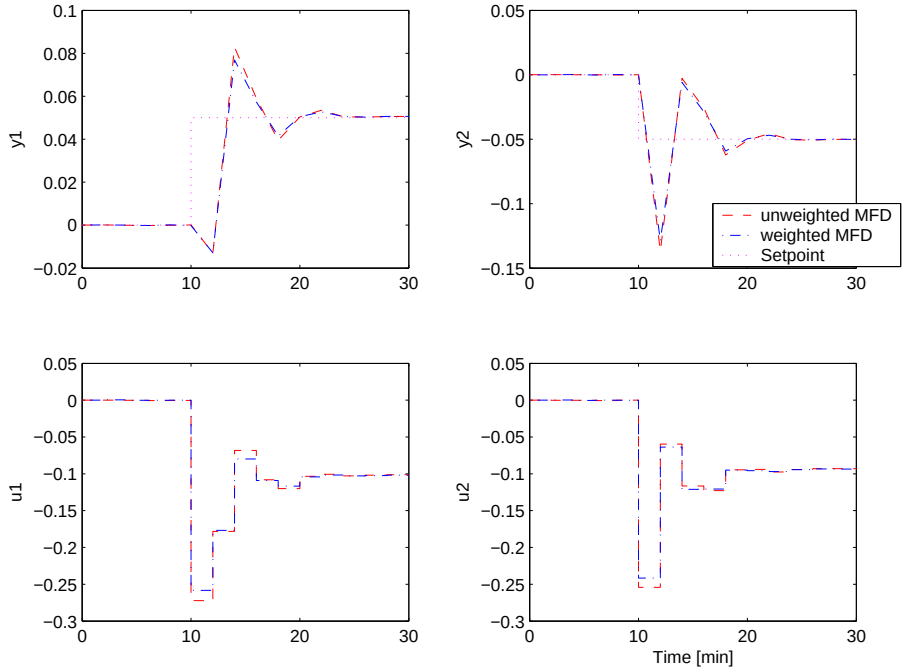

Figure 60. MPC setpoint tracking test of MFD estimates $[n_a = 1, n_b = 1, n_d = 1]$ under noise-free conditions, (PH=50, MH=5, Ywt=[1 1], and Uwt=[0.1 0.1]) using even-harmonics suppressed multisine signals for Weischedel-McAvoy distillation column (1980)

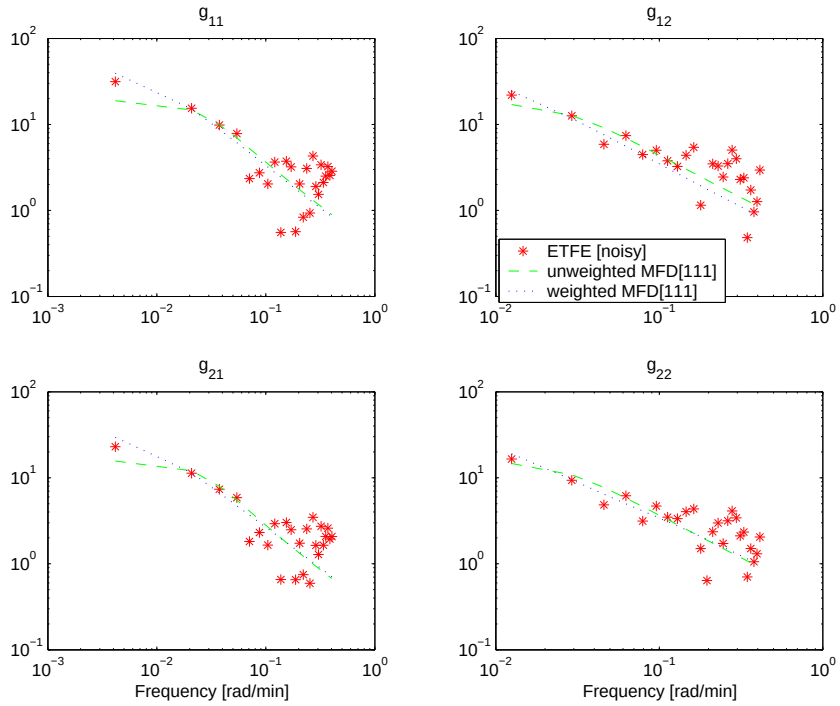

Figure 61. MFD curvefitting $[n_a = 1, n_b = 1, n_d = 1]$ under noisy conditions, SNR=[1,1]dB, using even-harmonics suppressed multisine signals for Weischedel-McAvoy distillation column (1980)

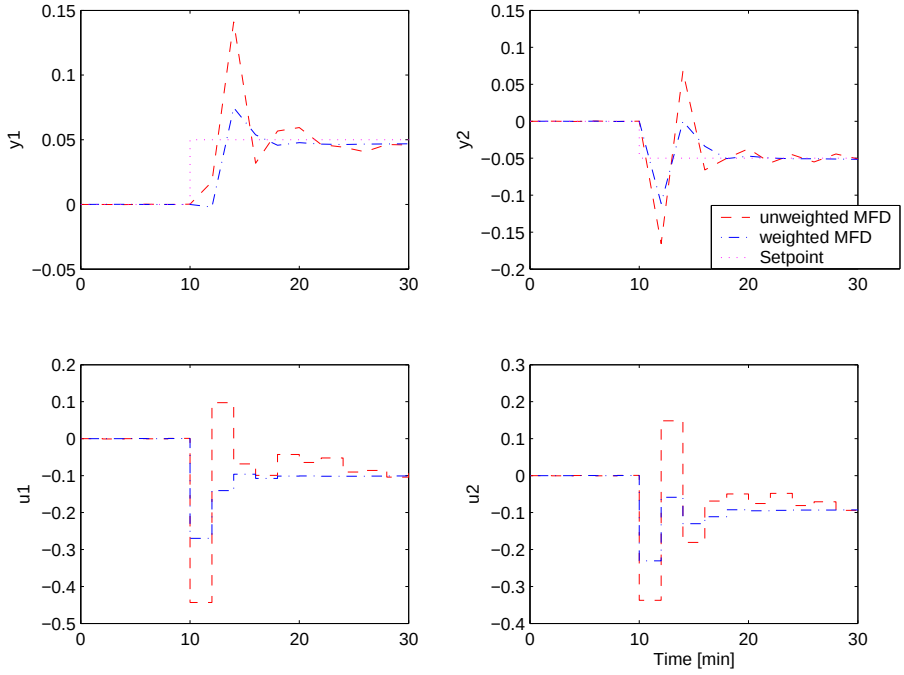

Figure 62. MPC setpoint tracking test of MFD estimates $[n_a = 1, n_b = 1, n_d = 1]$ under noisy conditions, SNR=[1, 1]dB, (PH=50, MH=5, Ywt=[1 1], Uwt=[0.1 0.1]), using even-harmonics suppressed multisine signals for Weischedel-McAvoy distillation column (1980)

8.2. Even-Harmonic Suppression Case. Similar to the non-harmonic suppression case, the model from the curve fits (Figure 59) with even-harmonic suppression has almost equivalent closed-loop performance under noise-free conditions (Figure 60). Possibly due to the suppressed frequency grids, the unweighted case shows slightly improved results, i.e., less overshoot, than the non-suppressed, unweighted case. Under noisy conditions ($SNR = [1,1]dB$), the weighted models emphasize the low frequency response portion with good interpolation to ETFE values, as shown in Figure 61. The weighted case shows no offset in y_1 and y_2 in the setpoint tracking test with MPC (Figure 62) while the unweighted suffers minor offsets in y_1 and y_2 with larger oscillation. The improved results of the unweighted case occur because of the reduced nonlinear effects achieved by applying the suppressed frequency grids in spite of noisy conditions. Specifically, the estimated curves show less distorted responses in the curvefitting than those of the non-suppressed case, as expected.

9. Chapter Summary

Control-relevant parameter estimation incorporates system identification and control system design considerations into an integrated procedure associated with the closed-loop performance requirements. The output error of estimating model parameters is weighted by considerations arising from desired closed-loop dynamics. The weighting functions emphasize a specific frequency bandwidth, which is important for desirable closed-loop performance. The control-relevant parameter estimation problem requires defining a control design procedure that can be used for regulating controlled variables of the system with desired inputs. Classical PID, IMC, or MPC control design can be used to define the control-relevant weights. The weighting matrices are frequency-dependent and naturally incorporate closed-loop transfer function that dictate performance.

In this chapter, a Shell fractionator example is modified to create more practical model bias in the model parameter estimation. In spite of low-order model structure, the weighted curvefitting shows the

frequency-dependent error minimization according to the control-relevant weights. Since the weighting functions emphasize the low-frequency dynamics, most of the bias is shifted into the high frequency area that is less relevant to closed-loop control performance. This is shown using spectral radius analysis that demonstrates that $\rho(\tilde{E}_m H) < 1$ is satisfied in the low frequencies.

The weighted and unweighted curvefitting models, however, show no significant difference under noise-free conditions in the Weischedel and McAvoy distillation column case. Since the nonlinear distillation process has less delay than the modified Shell model, the weighted case is unable to display noticeable improvement, especially under noise-free conditions. Under noisy conditions, the weighted case shows better tracking performance than that of the unweighted case; however, the curvefitting response might depend on the nature of the noise and its variance effect in the frequency response. The curvefitting algorithm is capable of addressing the zippered and harmonic-suppressed frequency grids, demonstrating its flexibility to a variety of input signal designs. In addition, modified zippered spectrum signals with a directional adjustment can produce frequency responses by spectral analysis, which can be further applied to the control-relevant curvefitting procedure in the next chapter.

CHAPTER 4

IDENTIFICATION TEST MONITORING PROCEDURE AND ITS APPLICATIONS

It is a primary goal in this chapter to present a systematic plant-friendly identification test monitoring procedure, producing a set of models with uncertainty descriptions that satisfy desired requirements of control relevance and robust stability and performance. To accomplish such an identification test monitoring framework, this chapter focuses on implementing multivariable model uncertainty estimation and robust loop-shaping during identification testing. A case study problem with high interaction and strong ill-conditioning is considered to evaluate the effective use of an integrated framework for the identification test monitoring procedure.

1. Introduction

A systematic identification test monitoring procedure was proposed as a novel approach to plant-friendly system identification in Rivera *et al.* (2003). Currently, system identification methods are normally applied in the batch-type sense. The interval between a new input signal design and identification analysis is problematic in the classical identification test. However, identification test monitoring procedures can be established that work in "quasi-real" time, where the data resulting from prior cycles of multisine signals are analyzed for refining the current model information (Lee and Rivera, 2006*b*)

In identification test monitoring, initial input signals are designed based on whatever available *a priori* knowledge of the system is present. This may require a low signal-to-noise ratio and wide bandwidth for the input signal. Once model information (e.g., gain(s) and time constant(s)) is obtained from initial data, preliminary signal designs can be updated and subsequent identification tests can be implemented under higher signal-to-noise ratios and narrower bandwidths. The refined input signal design can produce more informative and plant-friendly data that ultimately lead to effective control-relevant models.

Therefore, the essential role of an identification test monitoring procedure is to systematically refine process knowledge during identification testing, generating effective models for advanced control applications. This approach may avoid a completely new experimental testing procedure, taking advantage of all updated process information. The monitoring procedure needs to adjust and choose appropriate input signal designs, experimental testing, and identification methods while insuring plant-friendliness and control-relevance.

One might wonder what kind of analysis can determine model quality and can be implemented in the identification test monitoring framework. Robust performance measures would be a useful criterion to determine model quality. Robust loopshaping techniques (Morari and Zafiriou, 1988) can provide necessary and sufficient robustness conditions on a set of models defined by model uncertainty bounds. However, it may be too conservative to satisfy robustness bounds when variance and bias exist in models because such model error increases uncertainty bounds (Morari and Zafiriou, 1988). One must, therefore, collect a sufficient number of experimental data cycles to lower model uncertainty bounds to suitable levels. A short input sequence length is more favorable to perform multiple testing cycles. Identification test monitoring can provide the means by which to achieve this. Instead of such extended testing cycles, a closed-loop identification testing can be achieved if an effective nominal model and *a priori* controller are available during the identification testing.

This chapter considers the implementation of multivariable model uncertainty estimation and ro-

bust loopshaping procedures during identification testing, integrated into an identification test monitoring framework. Its effectiveness is illustrated with a highly interactive process where the method systematically improves model adequacy suitable for advanced process control applications. All of the analysis components in this framework interactively share acquired model knowledge with one another. As a result, the identification test can be accomplished over a shorter duration and with less effort than the conventional identification fashion. The individual components of the tools can also be used independently; we have developed software, CR-IDENT: a Matlab-based toolbox, for this purpose (Lee and Rivera, 2006*b*). This chapter consists of the following sections; Section 2 presents a conceptual example of an identification test monitoring procedure using a SISO problem. Section 3 formulates the estimation of multivariable uncertainty descriptions based on frequency response. Robustness with unstructured uncertainty is described in Section 4, and Section 5 considers robustness with structured uncertainty using the concept of the structured singular value. Section 6 details a robust loopshaping procedure that takes advantage of estimated uncertainty descriptions and user-specified performance weights. A case study involving the linear high-purity distillation column by Jacobsen and Skogestad (1994) is considered in Section 7 to demonstrate the effectiveness of the identification test monitoring procedure, systematically increasing process knowledge and ultimately leading to a robust control system and, alternatively, a stable closed-loop identification test (Lee and Rivera, 2006*a*; Lee and Rivera, 2006*b*). Section 8 presents the summary and conclusions.

2. A Conceptual Scenario of Identification Test Monitoring Procedure based on a SISO Problem

In shaping of transfer functions, the user specifies the magnitudes of some transfer function(s) as a function of frequency, and then finds a controller which gives the desired shape(s) (Morari and Zafiriou, 1988; Skogestad and Postlethwaite, 1996). Extending to a controller design procedure, “loop shape” can refer to the magnitude of the loop transfer function $L = C\tilde{P}$ as a function of frequency. One can shape this loop transfer function by selecting C such that a large loop gain ($|C\tilde{P}| > 1$) is obtained at low frequencies

below crossover and a small gain ($|C\tilde{P}| < 1$) is obtained at high frequencies above crossover (Skogestad and Postlethwaite, 1996).

2.1. Uncertainty Description and Loopshaping. Data generated from periodic inputs can be used to calculate an Empirical Transfer Function Estimate (ETFE) (Ljung, 1999). According to Bayard (1993*a*), a confidence region in the Nyquist plane for the ETFE $p^*(\omega_i)$ is a perfect circle centered at $p^*(\omega_i)$ of radius ε_i where

$$\varepsilon_i^2 = \frac{\hat{\sigma}^2 |\overline{W}(e^{-j\omega_i T})|^2 F_{1-\kappa}(2,\nu)}{\Phi_u(\omega_i) n_{cycle}} \tag{4.1}$$

$\overline{W}(z)$ is the estimated noise model, $\hat{\sigma}^2$ is the estimated variance from the residual output spectrum, n_{cycle} corresponds to the number of cycles of the periodic input, and $F_{1-\kappa}(2,\nu)$ is the 2-way Fisher statistic computed for a specified statistical confidence of $(1-\kappa)\times 100\%$. Noting that $F_{1-\kappa}(2,\nu)$ is bounded as ν becomes large (e.g., $F_{1-\kappa}(2,\nu) \leq 3$ for $1-\kappa = .95$ and $\nu > 120$), it becomes clear that the uncertainty region increases with the noise-to-signal ratio $\hat{\sigma}^2|\overline{W}|/\Phi_u$ and decreases as the number of input signal cycles n_{cycle} increases. Equation (4.1) provides significant insights regarding signal magnitude and test length in system identification.

The confidence regions defined by (4.1) can be expressed as norm-bounded multiplicative uncertainty

$$\begin{aligned} |(p(e^{j\omega_i T}) - p^*(\omega_i))p^{*-1}(\omega_i)| &\leq \bar{\ell}_m(\omega_i) \\ &= \varepsilon_i/|p^*(\omega_i)| \end{aligned} \tag{4.2}$$

which in turn can be used to assess robust performance as μ analysis measures

$$\mu^* = \sup_{\omega_i} |\eta^*(e^{j\omega_i T})\bar{\ell}_m(\omega_i)| + |\varepsilon^*(e^{j\omega_i T}) w_P(j\omega_i)| \tag{4.3}$$

and w_P weights the sensitivity function $\varepsilon^* = (1+p^*c)^{-1}$; $\eta^* = p^*c(1+p^*c)^{-1}$ is the complementary sensitivity function. η^* and ε^* are the frequency responses of the closed-loop transfer functions based on the

estimated frequency response p^*. Whenever $\mu^* < 1$, the following condition is satisfied for the closed-loop system

$$|\varepsilon^*| \leq 1/|w_P| \quad \forall p \in \bar{\ell}_m \quad 0 \leq \omega_i \leq \pi/T \tag{4.4}$$

The paper by Braatz *et al.* (1991) presents a procedure for determining necessary and sufficient bounds on the nominal closed-loop transfer functions based on process uncertainty and performance specifications. For a SISO system, sufficient bounds on η^* and ε^* are

$$|\eta^*| < \frac{1-|w_P|}{|w_P|+\ell_m}, \qquad |\varepsilon^*| < \frac{1-\bar{\ell}_m}{|w_P|+\ell_m} \tag{4.5}$$

Additional bounds (namely necessary upper and lower bounds on $|\eta^*|$ and $|\varepsilon^*|$) can be found in Braatz *et al.* (1991). Using this analysis, one realizes that the robust loopshaping bounds on η^* and ε^* can be computed in real-time during identification testing by relying on $\bar{\ell}_m$ calculated experimentally and w_p user-specified. The decision to halt or modify an identification test can be made on the basis of how these bounds evolve while increasing a number of cycles of the testing input.

2.2. A SISO Example Problem. Rivera *et al.* (2003) presented a plausible example of identification test monitoring for a SISO system based on a simulated representative scenario. The experimental testing procedure is depicted in Figure 63 with relevant statistics summarized in Table 10. The simulation considers a first-order system according to the transfer function

$$p(s) = \frac{1}{10s+1}$$

The parameters for this system are assumed to be vaguely known *a priori*. We further assume that the plant is facing significant disturbances, but plant operating restrictions dictate that the test be carried out under low Signal-to-Noise Ratios (SNRs).

Multisine input signals relying on the constrained minimum crest factor design procedure per Chapter 2 are used to construct experimental testing schemes. The initial signal (for Stage 1) is designed with

$\alpha_s = 2$, $\beta_s = 3$, $\tau_{dom}^L = 5$ min, and $\tau_{dom}^H = 20$ min. The result is a signal with a wide bandwidth, implemented using a low amplitude span (± 0.75) to avoid undesirable levels of off-spec product. This signal is represented by Stage 1 in Table 10 and Figure 63. Analysis of the Stage 1 data results in a preliminary model that can then serve as a basis for the design of the signal in Stage 2. This preliminary model will most likely display high variance in the parameters as a result of the low signal-to-noise ratio of the data. Nonetheless, the information contained in this model is useful for determining the design parameters of Stage 2. In this simulated scenario the model time constant range is narrowed to between 8 and 12 minutes; the resulting use of the guidelines produces a signal of much shorter duration. Furthermore, the initial estimate of system gain grants the user confidence to increase the input span to ± 1.5, improving the signal-to-noise ratio. The model estimated from the two cycles of data can be used to generate the third and final stage; in this simulated scenario an input design with a control-relevant power spectrum as defined per Rivera *et al.* (1992) and with higher span (± 2.5) is used. Given the improved model knowledge from analysis of the first two cycles, the increased input span does not result in unacceptable swings in the output. This final design takes advantage of improved process knowledge to incorporate control requirements, which ultimately results in a high performance control system.

Type	Signal (x)	CF(x)	PIPS(%)	max $\lvert\Delta x\rvert$	max x	min x	SNR (db)
Stage 1: flat PSD (with snow); $\lvert\Delta u\rvert \leq 0.5$, $\lvert u\rvert \leq 0.75$	u	1.0898	91.7598	0.4999	0.7042	-0.7042	-18.99
	y	2.0623	50.4701	0.2437	0.6174	-0.6705	-10.80
Stage 2: flat PSD (with snow); $\lvert\Delta u\rvert \leq 0.5$, $\lvert u\rvert \leq 1.5$	u	1.2665	78.9565	0.4999	1.4999	-1.4999	-13.67
	y	1.4816	67.4283	0.6497	1.0248	-1.0247	-3.35
Stage 3: control-relevant PSD; $\lvert\Delta u\rvert \leq 0.7$, $\lvert u\rvert \leq 2.5$	u	1.6620	60.1671	0.6999	2.4999	-2.4999	-13.46
	y	1.3619	75.3906	0.3079	1.0850	-1.1457	-4.74

Table 10. Summary of results for the simulated SISO identification test monitoring problem scenario. All statistics for u and y (except SNR) are calculated on the noise-free portion of the signal.

Robust loopshaping can be used to measure achievable control performance limitations from the data in real-time, during identification testing. Considering the signal design per Stage 1, a Type-I weight

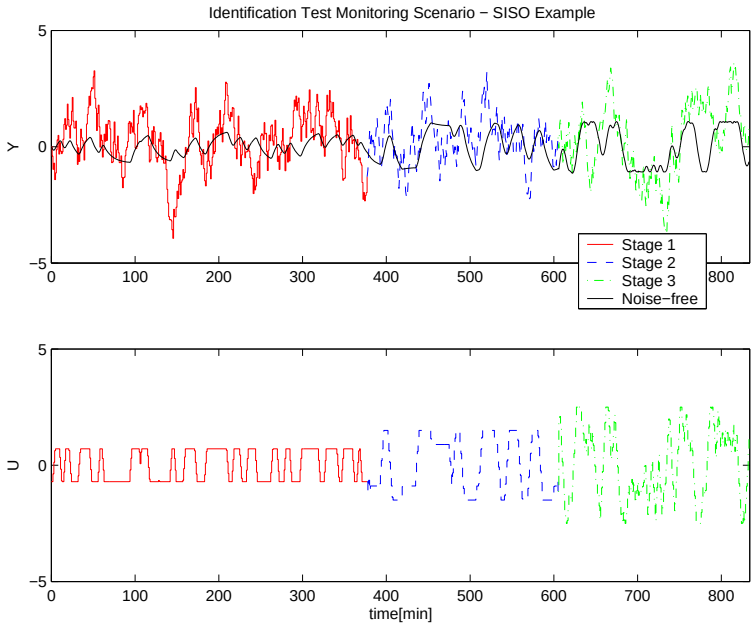

(a)

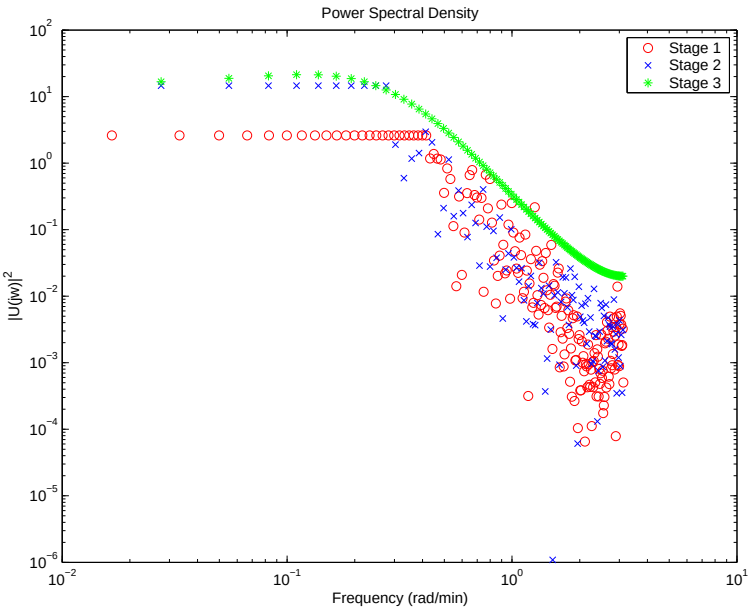

(b)

Figure 63. Simulated identification test monitoring scenario for a single-input, single-output plant: (a) time series and (b) input power spectra. The “snow effect” is enabled only in the high frequency range of Stages 1 and 2.

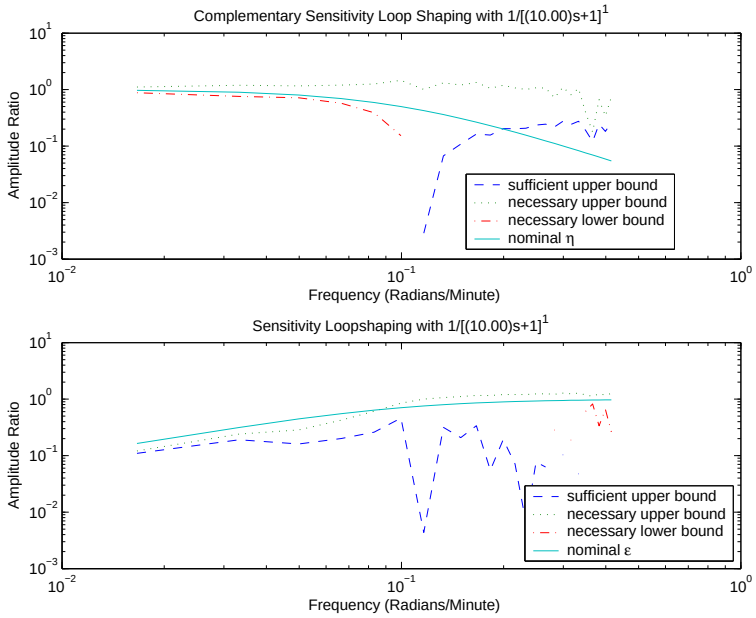

Figure 64. Robust loopshaping example results with Stage 1.

function per Skogestad and Postlethwaite (1996) is chosen:

$$w_P = \frac{s/M_p + \omega_B^*}{s + \omega_B^* A} \tag{4.6}$$

where M_p and ω_B^* represent the upper maximum peak and lower bandwidth bounds in ε, respectively. A (set to zero in this analysis) is a zero-frequency upper bound. Figure 64 presents the results of the various bounds in Braatz *et al.* (1991) for two cycles of the signal per Stage 1 with SNR = 1 and performance specs defined by $M_p = 2$ and $\omega_B^* = 0.1$. Figure 64 shows that a nominal control design with sensitivity and complementary sensitivity operators per

$$\varepsilon(s) = \frac{10s}{10s+1}, \qquad \eta(s) = \frac{1}{10s+1}$$

satisfies robust performance conditions. Having confirmed via loopshaping that the data is sufficiently informative to yield a model leading to acceptable performance requirements, the experimental test can be halted.

3. Multivariable Uncertainty Estimation

In spite of the complexity of model uncertainty in MIMO systems, it is useful to obtain the uncertainty descriptions for robust control design, which provide conditions for robust stability and performance. This demands efficient model uncertainty estimation procedures for multivariable systems from the experimental data. In general, two kinds of descriptions are available for the quantification of model uncertainty in MIMO systems: *unstructured uncertainty* and *structured uncertainty* (Morari and Zafiriou, 1988):

- *Unstructured uncertainty* is expressed in terms of a single perturbation (Δ). Although the unstructured uncertainty bounds are necessary and sufficient, they are generally conservative from a practical point of view. When model uncertainty is lumped into a single norm-bounded perturbation, it may include many more plants than are actually needed.

- *Structured uncertainty* implies that the individual sources of uncertainty are identified and represented directly – there is no need to lump them together. This generally leads to an uncertainty description with multiple perturbations (Δ_i's). By assuming norm bounds on these uncertainties (e.g.,$\bar{\sigma}(\Delta_i) \leq 1$), it is possible to derive necessary and sufficient, non-conservative conditions for robust stability and performance using the Structured Singular Value μ (Morari and Zafiriou, 1988; Skogestad and Postlethwaite, 1996). One disadvantage of this procedure is that the resulting conditions are not in terms of a simple bound on $\bar{\sigma}(\tilde{H})$ or $\bar{\sigma}(\tilde{S})$ but involve $\mu(M)$ where M may be a complicated function of $\tilde{S}$ and $\tilde{H}$.

$\mu(M)$ analysis based on structured uncertainty is an important facet in the development of the identification test monitoring framework. Mathematical expressions for multivariable uncertainty descriptions generated from frequency responses are presented in the next subsections.

3.1. Model Uncertainty Descriptions. For unstructured model uncertainty, we can distinguish multiplicative uncertainty at the plant input (L_I) and the plant output (L_O). The uncertainties L_I and L_O can be loosely interpreted as actuator and sensor uncertainty, respectively. The plant P is related to the model $\tilde{P}$ and its uncertainty description is observed in Figure 65.

$$P = \tilde{P} + L_A \qquad L_A = P - \tilde{P} \tag{4.7}$$

$$P = \tilde{P}(I + L_I) \qquad L_I = \tilde{P}^{-1}(P - \tilde{P}) \tag{4.8}$$

$$P = (I + L_O)\tilde{P} \qquad L_O = (P - \tilde{P})\tilde{P}^{-1} \tag{4.9}$$

In each of the above cases the magnitude of the perturbation L may be measured in terms of a bound on $\bar{\sigma}(L)$

$$\bar{\sigma}(L) \leq \bar{\ell}(\omega_i) \qquad \forall \omega_i \tag{4.10}$$

where

$$\bar{\ell}(\omega_i) = \max_{P \in \Pi} \bar{\sigma}(L) \tag{4.11}$$

and the bound $\bar{\ell}(\omega_i)$ can also be interpreted as a scalar weight on a normalized perturbation $\Delta(s)$

$$L(s) = \bar{\ell}(s)\Delta(s), \quad \bar{\sigma}(\Delta(\omega_i)) \leq 1 \qquad \forall \omega_i \tag{4.12}$$

Particularly, the additive uncertainty takes measuring the distance between P and $\tilde{P}$ in the Nyquist plane into a account. (Figure 66).

To obtain uncertainty bounds available for robust loopshaping, we need to specify the magnitude(s) of either the unstructured or structured uncertainty perturbations as follows

- *Single Perturbation:*

  Similar to the SISO case, MIMO uncertainty can be specified with a single perturbation parameter as

$$\bar{\sigma}(P - \tilde{P}) \leq \bar{\ell}_a(\omega_i) \tag{4.13}$$

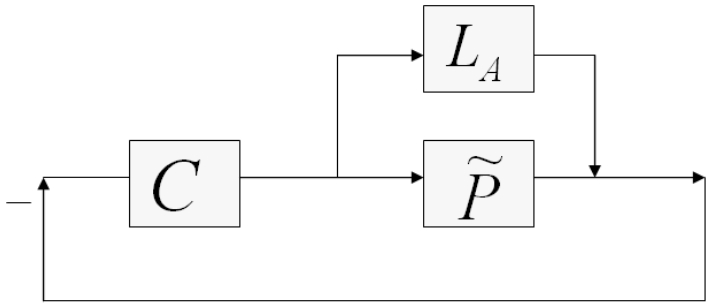

(a) $\bar{\ell}_a = \bar{\sigma}(L_A) \leq \bar{\sigma}(P - \tilde{P})$

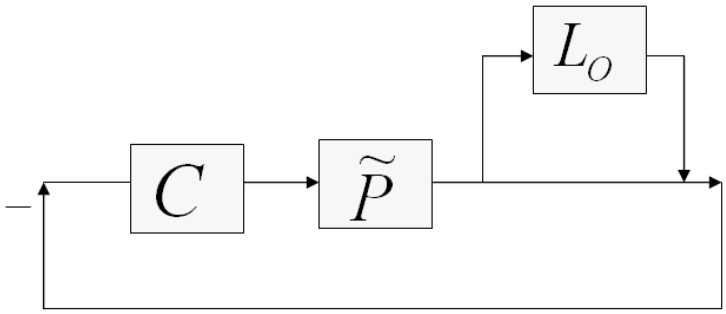

(b) $\bar{\ell}_o = \bar{\sigma}(L_O) \leq \bar{\sigma}((P - \tilde{P})\tilde{P}^{-1})$

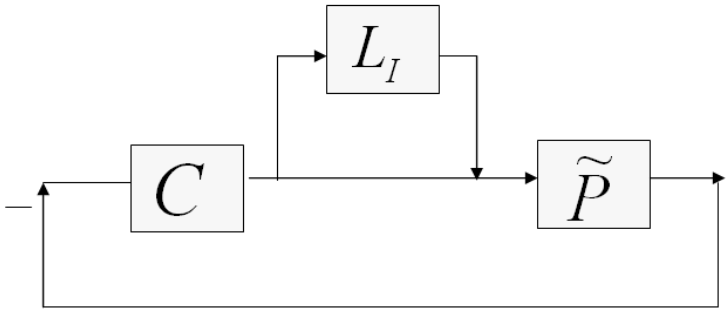

(c) $\bar{\ell}_i = \bar{\sigma}(L_I) \leq \bar{\sigma}(\tilde{P}^{-1}(P - \tilde{P}))$

Figure 65. Uncertainty descriptions involving single perturbations: L_A additive uncertainty (a), L_O output multiplicative uncertainty (b), and L_I input multiplicative uncertainty (c) from Morari and Zafiriou (1988).

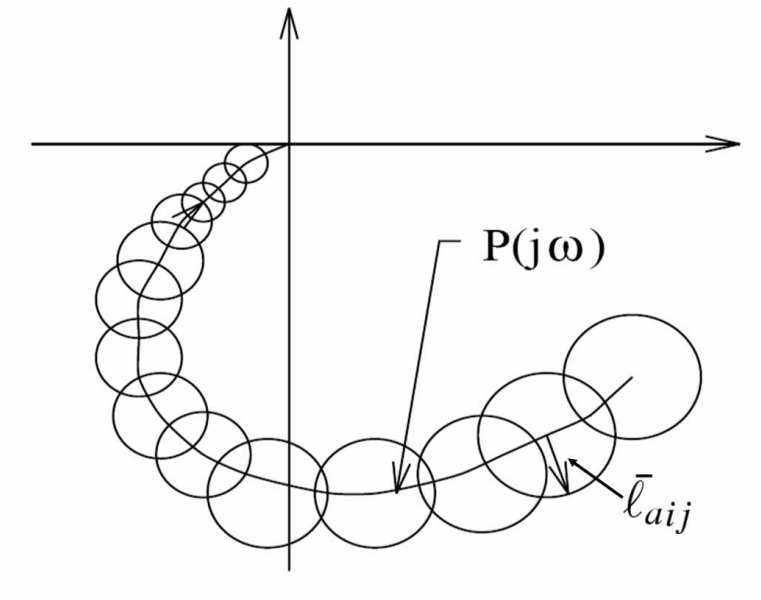

Figure 66. Additive uncertainty norm bound in Nyquist plane, from Zhou and Doyle (1998)

$\bar{\ell}_a(\omega_i)$ represents a norm bound of additive model uncertainty.

- *Individual Perturbation:*

  One can assume that uncertainty in each element p_{ij} in the plant P is independent, but confined to a disk with radius $\bar{\ell}_{ij}$ at $\tilde{p}_{ij}$ in the Nyquist plane

$$|p_{ij} - \tilde{p}_{ij}| \leq \bar{\ell}_{aij}(\omega_i) \tag{4.14}$$

  or equivalently

$$|p_{ij} - \tilde{p}_{ij}| \leq \bar{\ell}_{mij}(\omega_i)|\tilde{p}_{ij}| \tag{4.15}$$

  where $\bar{\ell}_{aij}$ and $\bar{\ell}_{mij}$ are the additive and multiplicative (relative) uncertainty, respectively. The main limitations of these uncertainty descriptions include correlations between the uncertainty elements that cannot be handled. Defining the scalar complex perturbation Δ_{ij}, Equation (4.14) becomes

$$|p_{ij} - \tilde{p}_{ij}| \leq \Delta_{ij}\bar{\ell}_{aij}, \qquad |\Delta_{ij}| \leq 1 \tag{4.16}$$

written equivalently in a matrix form as

$$P-\tilde{P} = \begin{bmatrix} \Delta_{11}\bar{\ell}_{a11} & \Delta_{12}\bar{\ell}_{a12} & \cdots \\ \Delta_{21}\bar{\ell}_{a21} & \cdots & \\ \cdots & & \Delta_{nn}\bar{\ell}_{ann} \end{bmatrix} \tag{4.17}$$

and this is compactly expressed as

$$P-\tilde{P} = L\Delta E \tag{4.18}$$

L, E, and Δ are written as

$$L = \begin{bmatrix} \mathbf{l_1} & & & \\ & \mathbf{l_2} & & \\ & & \ddots & \\ & & & \mathbf{l_n} \end{bmatrix}, \quad \mathbf{l_i} = \begin{bmatrix} \bar{\ell}_{1i} \\ \bar{\ell}_{2i} \\ \vdots \\ \bar{\ell}_{ni} \end{bmatrix} \tag{4.19}$$

$$\Delta = diag\{\Delta_{11},\ \ldots,\Delta_{n1},\ \Delta_{12},\ \ldots,\Delta_{n2},\ldots,\ \Delta_{1n},\ \ldots,\Delta_{nn}\} \tag{4.20}$$

$$E = [I\ I\ \ldots\ I] \tag{4.21}$$

3.2. Uncertainty Estimation from Plant Experiment Data. For convenience in the multivariable system, an additive uncertainty description is considered for subsequent robustness analysis, estimating individual uncertainty elements from the input and output data. From the individual descriptions, the single perturbation of the upper norm bound is approximated such that

$$\ell_a \leq \max_{i,j} \|\ell_{ij}\|_2 \tag{4.22}$$

Additive uncertainty estimation is practically useful and can avoid any additional algebraic matrix manipulation. In this identification framework, a single upper bound norm is utilized based on the additive uncertainty descriptions of individual components. Additive uncertainty estimation for multivariable systems based on ETFE, spectral analysis, and high-order ARX approximation, respectively, are presented in the following section.

3.2.1. *Uncertainty Estimation from ETFE.* Uncertainty estimation from the ETFEs of multivariable systems is presented by Bayard and Hadaegh (1994). P is a given discrete-time plant and $\tilde{P}$, a DFT plant estimator[1], is estimated from the experiment data with multiple cycles of multisine inputs when P is a $p \times m$ system

$$\tilde{P}(\omega_i, n_2, n_1) \triangleq \frac{\bar{Y}(\omega_i, n_2, n_1)}{U(\omega_i, n_1)}; \quad n_1 = 1, ..., m; \quad n_2 = 1, ..., p \tag{4.23}$$

where n_{cycle} is the number of cycles, $n_1 = 1, ..., m$ denotes n_1th input, and $n_2 = 1, ..., p$, the plant response at n_2th sensor, and

$$\bar{Y}(\omega_i, n_2, n_1) \triangleq \frac{1}{n_{cycle}(n_1)} \sum_{\ell=1}^{n_{cycle}(n_1)} Y^{\ell}(\omega_i, n_2, n_1) \tag{4.24}$$

$$Y^{\ell}(\omega_i, n_2, n_1) \triangleq \sum_{k=1}^{N_s} y_s^{\ell}(k, n_2, n_1)\, e^{-j\omega_i kT} \tag{4.25}$$

$$U(\omega_i, n_1) \triangleq \sum_{k=1}^{N_s} U_s^{\ell}(k, n_1)\, e^{-j\omega_i kT} \tag{4.26}$$

$$y_s^{\ell}(k, n_2, n_1) = y_s(k + (\ell - 1)N_s, n_2, n_1), \ \ \ell = 1, ..., n_{cycle} \tag{4.27}$$

A multivariable uncertainty norm bound can be found if

$$\bar{\sigma}(P(\omega_i) - \tilde{P}(\omega_i)) \leq \varepsilon_i \tag{4.28}$$

is satisfied with a least probability $1 - \kappa$ at each grid point i. Using the Frobenious norm bound, ε_i is determined as

$$\bar{\sigma}(P(\omega_i) - \tilde{P}(\omega_i))^2 \leq \|P(\omega_i) - \tilde{P}(\omega_i)\|_F^2 \tag{4.29}$$

$$= \sum_{n_2=1}^{p} \sum_{n_1=1}^{m} |P(\omega_i, n_2, n_1) - \tilde{P}(\omega_i, n_2, n_1)|^2 \tag{4.30}$$

This equation can be overbounded using Fisher statistics to probability $(1 - \gamma)$ such that

$$|P(\omega_i, n_2, n_1) - \tilde{P}(\omega_i, n_2, n_1)|^2 \leq \rho_i^{1-\gamma}(n_2, n_1) \tag{4.31}$$

[1] P stands for a plant; $\tilde{P}$, a non-parametric frequency response; and $\hat{P}$, a parametric model estimate in this chapter

where

$$\rho_i^{1-\gamma}(n_2,n_1) = \frac{2|\,\hat{W}(\omega_i,n_2)\,|^2}{\alpha_i(n_1)n_{cycle}(n_1)N_s}.\,F_{1-\gamma}\,(2,2m(n_1)-2) \tag{4.32}$$

and $F_{1-\gamma}(\nu_1,\nu_2)$ denotes the $\%(1-\gamma)\times 100$ percentile for the Fisher distribution. $\hat{W}$ and α_i are computed from MIMO data as

$$|\hat{W}(\omega_i,n_2)|^2 \triangleq \frac{\sum_{n_2=1}^{p}\sum_{n_1=1}^{n_{cycle}(n_1)}|Y(\omega_i,n_2,n_1)-\bar{Y}\,(\omega_i,n_2,n_1)|^2}{N_s(n_{cycle}-m)} \tag{4.33}$$

$$\alpha_i = \frac{2\Phi_u}{N_s}, \qquad \Phi_u = \frac{U^*U}{N_s} \tag{4.34}$$

As a result, ε_i is estimated from

$$\bar{\sigma}(P(\omega_i)-\tilde{P}(\omega_i)) \leq \sqrt{\sum_{n_2=1}^{r}\sum_{n_1=1}^{q}\rho_i^{1-\gamma}(n_2,n_1)} \triangleq \varepsilon_i \tag{4.35}$$

with probability $(1-\kappa)=(1-\gamma)^{p\times m}$. Bayard and Hadaegh (1994) utilize multisine input signals with multiple testing cycles for averaged frequency response data to estimate the plant uncertainty information.

3.2.2. *Uncertainty Estimation from Spectral Analysis.* An uncertainty description based on spectral analysis is obtained similar to ETFEs. The estimation formulation is basically taken from Jenkins and Watts (1968) and is summarized as follows

$$\bar{\sigma}(P(\omega_i)-\tilde{P}(\omega_i)) \;\cong\; \sqrt{\frac{1}{n_{cycle}}\frac{\Phi_v(\omega_i)}{\Phi_u(\omega_i)}} \tag{4.36}$$

where n_{cycle} is the number of cycles. Using the theoretical construction of uncertainty estimation of ETFEs (Bayard and Hadaegh, 1994), the above equation is modified for spectral analysis with the following assumptions:

- Φ_v is measured in a way similar to computing $\hat{W}(\omega_i)$ in ETFEs from the periodic multisine input signals.
- $\frac{\Phi_v}{\Phi_u}$ is an approximate of $|P_d|^2$.

As a consequence, one can obtain

$$\frac{1}{n_{cycle}}\frac{\Phi_v(\omega_i)}{\Phi_u(\omega_i)} = \frac{1}{n_{cycle}}|P_d(\omega_i)|^2 \tag{4.37}$$

and $|P_d(\omega_i)|^2$ is estimated as

$$|P_d(\omega_i)|^2 = \frac{\sum_{k=1}^{k=n_{cycle}}(\tilde{P}^k(\omega_i) - \tilde{P}(\omega_i))^2}{n_{cycle}\, N_s} \tag{4.38}$$

where $\tilde{P}(\omega_i)$ is estimated using the total cycles and $\tilde{P}^k(\omega_i)$ is obtained using k_{th} cycle of the data. Therefore, the uncertainty description by spectral analysis is measured as

$$\sigma(P(\omega_i) - \tilde{P}(\omega_i)) \;\leq\; \sqrt{\frac{1}{n_{cycle}}\frac{\sum_{k=1}^{k=n_{cycle}}(\tilde{P}^k(\omega_i) - \tilde{P}(\omega_i))^2}{n_{cycle}\, N_s}\, F_{1-\gamma}(2, 2n_{cycle}-2)} \;\triangleq\; \varepsilon_i \tag{4.39}$$

Alternatively, $\tilde{P}(\omega_i)$ can be obtained from

$$\tilde{P}(\omega_i) = \frac{\sum_{k=1}^{k=n_{cycle}}\tilde{P}^k(\omega_i)}{n_{cycle}} \tag{4.40}$$

3.2.3. *Uncertainty Estimation from a High-Order ARX Model.* The formulation by Zhu (1989) is utilized for the uncertainty description of parametric model estimation as

$$\sigma(P(\omega_i) - \tilde{P}(\omega_i)) \;\cong\; \sqrt{\frac{n_a + n_b}{n_{cycle}}\frac{\Phi_v(\omega_i)}{\Phi_u(\omega_i)}} \tag{4.41}$$

where n_a and n_b are orders of numerator and denominator in ARX models, respectively, and n_{cycle} is the number of input cycles. The above is applied to experimental data based on periodic multisine input signals in this dissertation. An equivalent uncertainty description to those of ETFE and spectral analysis is derived with the similarity such that

$$\sigma(P(\omega_i) - \tilde{P}(\omega_i)) \;\triangleq\; \kappa\sqrt{\frac{n_a + n_b}{n_{cycle}}\,\frac{1}{n_{cycle}N_s}\frac{\tilde{\Phi}_v(\omega_i)}{\Phi_u(\omega_i)}} \tag{4.42}$$

$$\tilde{\Phi}_v(\omega_i) = \frac{1}{n_{cycle}}\sum_{k=1}^{k=n_{cycle}}\tilde{\Phi}_v^k(\omega_i) \tag{4.43}$$

where κ is given 3.2905 (99.9%), 2.5758 (99.0%), 2.1701 (97.0%), and 1.96 (95%) for the normal distribution. $\tilde{\Phi}_v^k$ is calculated from $v^k = y^k - \tilde{y}^k$ where y^k is the plant output and $\tilde{y}^k$ is the estimated ARX output

based on k_{th} cycle of the data.

4. Robust Stability and Performance with Unstructured Uncertainty

4.1. Robust Stability. With the single perturbation description *L*, we can determine the meaningful bounds for robust stability conditions (Morari and Zafiriou, 1988). Particularly, “unstructured” uncertainty means that several sources of uncertainty are described as a single perturbation, which is a full-matrix using the same dimension as the plant *P*.

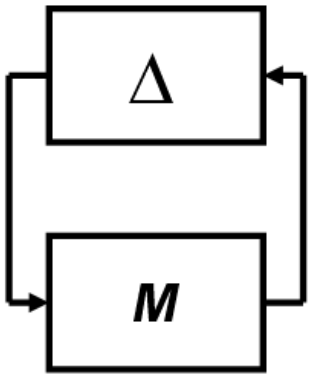

Figure 67. General M - Δ structure for robustness analysis

4.1.1. *General Robust Stability Theorem.* Robust stability of *M*-Δ can be analyzed using the influence of Δ to *M*. Since the detailed discussion of the robust stability is beyond this chapter; however, the following text briefly summarizes the properties of the robust stability and performance from Chapter 11 of Morari and Zafiriou (1988). If the nominal system is stable, then *M* is stable and Δ is a perturbation which can destabilize the system. The following theorem establishes conditions on *M* so that it cannot be destabilized by Δ.

Theorem 4.1 *Assume that M is stable and that the perturbation Δ is of such a kind that the perturbed closed-loop system is stable if and only if the map of the Nyquist D contour under $det(I - M\Delta)$ does not encircle the origin. Then the closed-loop system of the $M-\Delta$ structure is stable for all perturbations $\Delta(\bar{\sigma}(\Delta) \leq 1)$ if and only if one of the following three equivalent conditions is satisfied:*

$$det\ (I - M\Delta(\omega)) \neq 0 \quad \forall\omega, \quad \forall\Delta\ \ni\ \bar{\sigma}(\Delta) \leq 1 \tag{4.44}$$

$$\Leftrightarrow \quad \rho(M\Delta(\omega)) < 1 \ \ \forall\omega,\ \forall\Delta \ni \bar{\sigma}(\Delta) \leq 1 \tag{4.45}$$

$$\Leftrightarrow \quad \bar{\sigma}(M(\omega)) < 1 \ \ \forall\omega \tag{4.46}$$

$$\Leftrightarrow \quad \|M\|_\infty < 1 \tag{4.47}$$

Theorem 4.1 states that if $\bar{\sigma}(M) < 1$, there is no perturbation $\Delta(\bar{\sigma}(\Delta) \leq 1)$ which makes $det(I - M\Delta(s))$ encircle the origin as *s* traverses the *Nyquist D* contour. Note that we assume that the absence of encirclement is necessary and sufficient for robust stability (Morari and Zafiriou, 1988).

4.1.2. *Multiplicative Output Uncertainty.* Let *M* be such that

$$M = -\tilde{P}C(I + \tilde{P}C)^{-1}\bar{\ell}_O \tag{4.48}$$

The closed system is stable for all perturbations $L_o(\bar{\sigma}(L_o) \leq \ell_o)$ if and only if

$$\bar{\sigma}(\tilde{P}C(I + \tilde{P}C)^{-1})\bar{\ell}_o < 1, \qquad \forall\omega \Leftrightarrow \|\tilde{H}\bar{\ell}_o\|_\infty < 1 \tag{4.49}$$

The robust stability condition (4.49) can always be satisfied for open-loop stable systems since $\tilde{H} = 0$ (no feedback) is always possible. However, good disturbance rejection and good command following require $\tilde{H} \approx 1$ (i.e., $\bar{\sigma}(\tilde{H}) \approx 1$). This indicates that the control system must be detuned ($\bar{\sigma}(\tilde{H}) < 1$) at frequencies where $\bar{\ell}_o(\omega) \geq 1$.

$$\bar{\sigma}(\tilde{P}C(I+\tilde{P}C)^{-1}) = \underline{\sigma}^{-1}(I+(\tilde{P}C)^{-1}) \approx \bar{\sigma}(\tilde{P}C) \tag{4.50}$$

Therefore, the robust stability condition becomes

$$\bar{\sigma}(\tilde{P}C) < \bar{\ell}_o^{-1} \qquad \omega \text{ large} \tag{4.51}$$

which implies that the controller gain for high frequencies is limited by uncertainty; the loop gain $\bar{\sigma}(\tilde{P}C)$ must be *shaped* to fall below the uncertainty bound $\bar{\ell}_o^{-1}$.

4.1.3. *Multiplicative Input Uncertainty.* Let M be such that

$$M = -(I+\tilde{P}C)^{-1}C\tilde{P}\bar{\ell}_I \tag{4.52}$$

The closed-loop system is stable for all perturbations $L_I(\bar{\sigma}(L_I) \leq \bar{\ell}_I)$ if and only if

$$\bar{\sigma}(\tilde{H}_I)\bar{\ell}_I < I, \quad \forall\omega \Leftrightarrow \|\tilde{H}_I\bar{\ell}_I\|_\infty < 1 \tag{4.53}$$

where

$$\tilde{H}_I = (I+C\tilde{P})^{-1}C\tilde{P}$$

$\tilde{H}_I$ is the nominal closed-loop transfer function, as seen from the input of the plant. It is desirable for this transfer function to be close to I in order to reject disturbances affecting the inputs to the plant. Robust performance is usually measured at the output of the plant, and a bound can be derived assuming $\tilde{P}$ is square

$$\bar{\sigma}(\tilde{H}_I) = \bar{\sigma}(\tilde{P}^{-1}\tilde{H}\tilde{P}) \leq \bar{\sigma}(\tilde{P}^{-1})\bar{\sigma}(\tilde{H})\bar{\sigma}(\tilde{P}) = \kappa(\tilde{P})\bar{\sigma}(\tilde{H}) \tag{4.54}$$

Then, a bound for robust stability is

$$\bar{\sigma}(\tilde{H})\bar{\ell}_I(\omega) < \frac{1}{\kappa(\tilde{P})} \quad \forall\omega \tag{4.55}$$

where $\kappa(\tilde{P})$ is the condition number of $\tilde{P}$. For $\kappa(\tilde{P})$ larger, the above condition may be arbitrarily conservative even though the uncertainty is tightly described in terms of a norm-bounded input uncertainty.

Note that for high frequencies $C\tilde{P}$ is "small"

$$\bar{\sigma}(C(I+\tilde{P}C)^{-1}\tilde{P}) = \underline{\sigma}^{-1}(I+(C\tilde{P})^{-1}) \approx \bar{\sigma}(C\tilde{P}) \tag{4.56}$$

and therefore, Equation (4.53) becomes

$$\bar{\sigma}(C\tilde{P}) < \bar{\ell}_I^{-1} \qquad \omega \text{ large} \tag{4.57}$$

which implies that the controller gain for high frequencies is limited by uncertainty. The loop gain $\bar{\sigma}(C\tilde{P})$, which is generally not equal to $\bar{\sigma}(\tilde{P}C)$, has to be "shaped" to fall below the uncertainty bound $\bar{\ell}_I^{-1}$ for robust stability.

4.1.4. *Additive Uncertainty.* Let M be such that

$$M = -C(I+\tilde{P}C)^{-1}\bar{\ell}_a \tag{4.58}$$

The closed-loop system is stable for all perturbations $L_a(\bar{\sigma}(L_a) \leq \bar{\ell}_a)$ if and only if

$$\bar{\sigma}(\tilde{P}^{-1}\tilde{H})\bar{\ell}_a < I, \quad \forall\omega \Leftrightarrow \|\tilde{P}^{-1}\tilde{H}\bar{\ell}_I\|_\infty < 1 \tag{4.59}$$

4.2. Robust Performance. Robust performance bounds can be derived from unstructured uncertainty descriptions, as described in Morari and Zafiriou(1988). The H_2 performance specification places bounds such that

$$\bar{\sigma}(W_p\tilde{S}) < 1 \qquad \forall\omega_i,\ \forall P \in \Pi \tag{4.60}$$

and

$$\bar{\sigma}(W_u P^{-1}\tilde{H}) < 1 \qquad \forall\omega_i,\ \forall P \in \Pi \tag{4.61}$$

where W_p is a scalar performance weight on the sensitivity function $\tilde{S}$ and W_u is on $P^{-1}\tilde{H}$. Based on the nominal performance bound, robust performance bounds are derived associated with the unstructured uncertainty descriptions.

4.2.1. *Performance Weight Specifications.* The two performance weights are considered in the LFT system for the robust control system (Zhou and Doyle, 1998): (1) W_p performance weight (Figure 68) on the sensitivity function $\tilde{S}$ such that

$$\|W_p\,\tilde{S}\| \;< 1 \tag{4.62}$$

$$W_p = \frac{s/M_s + \omega_b}{s + \omega_b \varepsilon} \tag{4.63}$$

where M_s is the peak sensitivity, ω_b is the bandwidth, and ε is given as $|\tilde{S}(0)| \le \varepsilon$, and (2) W_u on $\tilde{P}^{-1}\tilde{H} = C\tilde{S}$ (Figure 69) is given as

$$\|W_u\,\tilde{P}^{-1}\tilde{H}\| \;< 1 \tag{4.64}$$

$$W_u = \frac{s + \omega_{bc}/M_u}{\varepsilon_1\, s + \omega_{bc}} \tag{4.65}$$

where M_u is the maximum gain of $C\tilde{S}$, ω_{bc} is the controller bandwidth, and $\varepsilon_1 \ge |C\tilde{S}|$ at high frequencies.

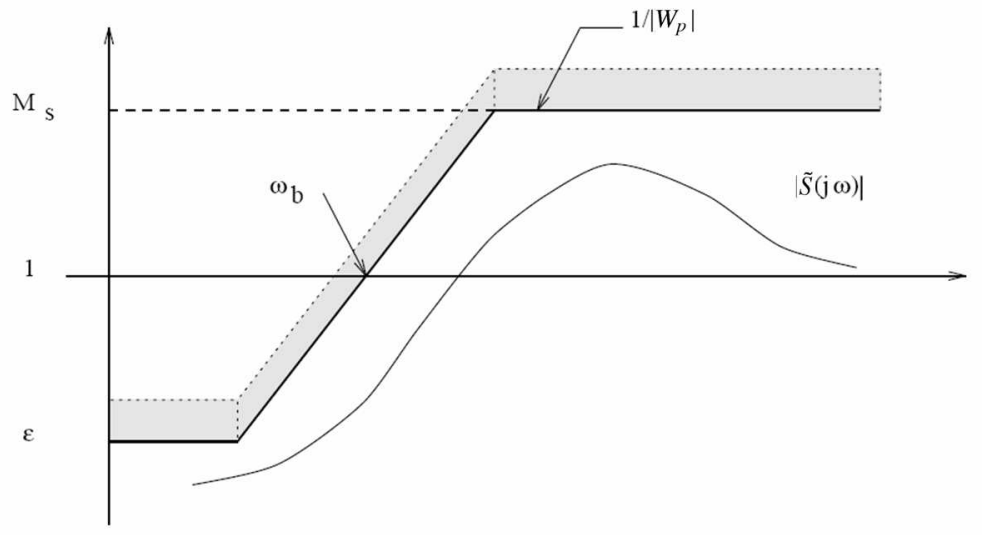

Figure 68. Performance weight W_p on $\tilde{S}$, from Zhou and Doyle (1998)

4.2.2. *Multiplicative Output Uncertainty.* The set of plants is considered for robust performance problem with the multiplicative output uncertainty as

$$\Pi = \{P = (I + \bar{\ell}_o \Delta_o)\tilde{P},\;\; \bar{\sigma}(\Delta_o) \le 1\} \tag{4.66}$$

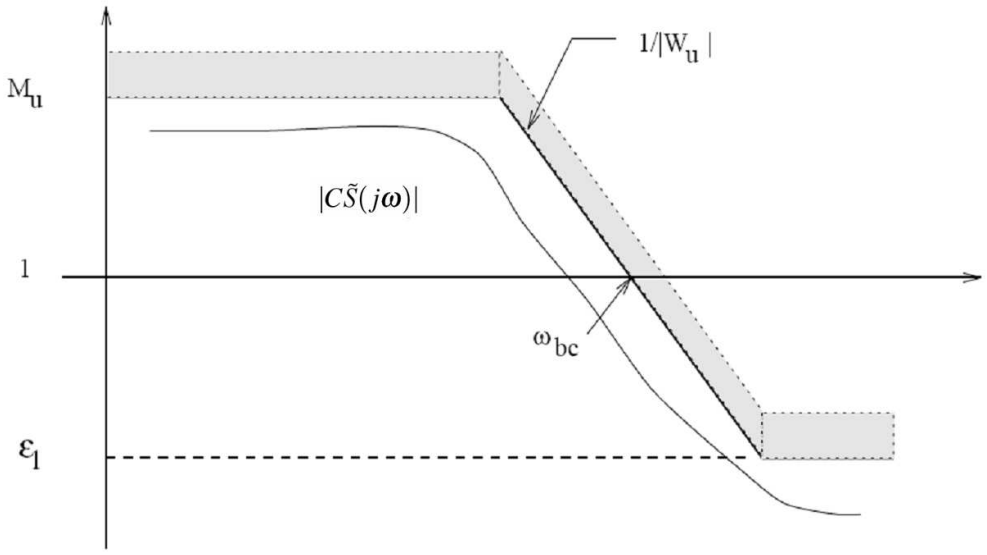

Figure 69. Performance weight W_u on $C\tilde{S}$, from Zhou and Doyle (1998)

and the robust performance bound with W_p and W_u then becomes

$$\bar{\sigma}(W_p\tilde{S}) + \bar{\sigma}(W_u\tilde{P}^{-1}\tilde{H}) + \bar{\sigma}(\bar{\ell}_o\tilde{H}) < 1 \tag{4.67}$$

which is a sufficient condition for robust performance.

4.2.3. *Multiplicative Input Uncertainty.* Alternatively, the set of plants associated with multiplicative input uncertainty is described by

$$\Pi = \{P = \tilde{P}(I + \bar{\ell}_I\Delta_I),\ \ \bar{\sigma}(\Delta_I) \leq 1\} \tag{4.68}$$

and $\bar{\ell}_o\Delta_o$ in Equation (4.66) can be replaced with $\bar{\ell}\tilde{P}\Delta_I\tilde{P}^{-1}$. As a result, the robust performance bound with W_p and W_u becomes

$$\bar{\sigma}(W_p\tilde{S}) + \bar{\sigma}(W_u\tilde{P}^{-1}\tilde{H}) + \kappa(\tilde{P})\bar{\sigma}(\bar{\ell}_I\tilde{H}) < 1 \tag{4.69}$$

where $\kappa(\tilde{P})$ is the condition number of $\tilde{P}$.

4.2.4. *Additive Uncertainty.* Similarly, the set of plants associated with additive uncertainty is described by

$$\Pi = \{P = \tilde{P} + \bar{\ell}_a\Delta_a),\ \ \bar{\sigma}(\Delta_a) \leq 1\} \tag{4.70}$$

The robust performance bound with W_p and W_u becomes

$$\bar{\sigma}(W_p\tilde{S}) + \bar{\sigma}(W_u\tilde{P}^{-1}\tilde{H}) + \bar{\sigma}(\bar{\ell}_a\tilde{P}^{-1}\tilde{H}) < 1 \tag{4.71}$$

5. Robustness with Structured Uncertainty

5.1. Structured Uncertainty Description. The structured uncertainty is described as multiple perturbation (Δ_i) by identifying the sources and locations in the system (Morari and Zafiriou, 1988). Each perturbation Δ_i is assumed to be a norm-bounded transfer matrix on the nominal system

$$\bar{\sigma}(\Delta_i) \leq 1 \quad \forall\omega \tag{4.72}$$

The perturbations (uncertainties) may occur at different locations in feedback system that can be collected and placed into one large block diagonal perturbation matrix, as shown in Figure 67,

$$\Delta \;=\; \text{diag}\{\Delta_1, ..., \Delta_m\} \tag{4.73}$$

while it satisfies

$$\bar{\sigma}(\Delta) \;\leq\; 1 \quad \forall\omega \tag{4.74}$$

5.2. Structured Singular Value ($\mu(M)$). $\mu(M)$ is defined such that $\mu^{-1}(M)$ is equal to the smallest $\bar{\sigma}(\Delta)$ that makes $(I - \Delta M)$ singular. This can be expressed as

$$\mu^{-1}(M) \;=\; \min_{\delta}\{\; \delta \;\mid\; det(I - M\Delta) = 0 \text{ for some } \Delta, \quad \bar{\sigma}(\Delta) < \delta\} \tag{4.75}$$

If no Δ exists such that $det\ (I - M\Delta) = 0$, then $\mu(M) = 0$. Δ is a block-diagonal perturbation matrix with a given structure, as defined in Equation (4.73), and it satisfies

$$\bar{\sigma}(\Delta_i) \;<\; \delta \;\forall i \tag{4.76}$$

Therefore, $\mu(M)$ depends on both the matrix M and the structure of the perturbation Δ.

Theorem 4.2 *Assume that the nominal system M is stable and that the perturbation* Δ *is of such a kind that the perturbed closed-loop system is stable if and only if the map of the Nyquist D contour under* $det(I - M\Delta)$ *does not encircle the origin. Then the closed-loop system in the* $M - \Delta$ *structure is stable for all perturbations* Δ_i *if and only if*

$$\mu(M(\omega)) < 1 \quad \forall\omega \tag{4.77}$$

Theorem 4.2 can be interpreted as a "generalized small gain theorem" which also takes into account the structure of Δ. The structured singular value is used to obtain the tightest possible bound on M such that the robust stability condition is satisfied. More properties of $\mu(M)$ and its computation methodology can be referred to Morari and Zafiriou (1988).

5.3. Robustness Conditions in Transfer Matrices. In Figure 67, M is the interconnection matrix, the nominal transfer function from the output of the perturbation Δ_i to their inputs. With the interest of the uncertainty Δ, M is represented as a Linear Fractional Transformation matrix such that

$$M = N_{11} + N_{12}\Delta(I - N_{22}\Delta)^{-1}N_{21} \tag{4.78}$$

and Δ can also be replaced with the transfer function matrix. In general, M can be denoted as the dependence of N on a particular choice of T

$$M = N_{11} + N_{12}T(I - N_{22}T)^{-1}N_{21} \tag{4.79}$$

In robust loopshaping, the sensitivity (S) and complementary sensitivity (H) functions will be considered as T in the LFT structure.

Using the closed-loop $M - \Delta$ system, the necessary and sufficient conditions based on the structured singular value is derived (Morari and Zafiriou, 1988)

$$\mu_\Delta(M) \leq k(\omega), \quad \forall\omega \tag{4.80}$$

for robust stability and performance. A bound on $\bar{\sigma}(T)$ provides important properties for robust control system, where T denotes a transfer matrix of engineering significance, e.g., the sensitivity $\tilde{S}$, the complementary sensitivity $\tilde{H}$, or the loop gain $\tilde{P}C$. Deriving such bounds on $\bar{\sigma}(T)$ is the goal while we satisfy the condition of (4.80). However, it is important that N be independent of the controller C in an LFT.

6. Robust Loopshaping

It is of practical consideration to derive necessary and sufficient bounds on a controller that can guarantee robust stability and performance. Designing a controller C on P in robust control, the sensitivity S and complementary sensitivity H transfer matrices are to be bounded. This requires several steps to derive N^S - S and N^H - H LFTs from $M-\Delta$ structure. Once the derived LFTs are formulated and solved, c_S and c_H bound the loops of the controller, i.e., either of the following conditions should be satisfied

$$\mu_{\tilde{\Delta}}(N^S) < c_S, \quad \tilde{\Delta} = diag\{\Delta, S\} \tag{4.81}$$

or

$$\mu_{\tilde{\Delta}}(N^H) < c_H, \quad \tilde{\Delta} = diag\{\Delta, H\} \tag{4.82}$$

at any frequency grids, and this approach is called robust loopshaping (Morari and Zafiriou, 1988).

6.1. Linear Fractional Transformation on Transfer Matrices.

6.1.1. *General Derivation.* Several steps are considered to derive LFT structures that are independent of a particular transfer function, as illustrated in Figure 70a-d. This involves step-by-step LFT derivations in the following:

1. Find M-Δ structure:

   Arrange the closed-loop system dynamics depending on the perturbation Δ.

$$F(M,\Delta) = M_{11} + M_{12}\Delta(I - M_{22}\Delta)^{-1}M_{21}$$

2. Write M block as a G-C structure

   From the M-Δ structure, the M is rearranged into another LFT structure as G and C.

$$M = G_{11} + G_{12}C(I - G_{22}C)^{-1}G_{21} \tag{4.83}$$

3. Write C as a J-T structure

   The controller C can be written as an LFT of the transfer matrix of interest (T) such as H.

$$C = J_{11} + J_{12}T(I - J_{22}T)^{-1}J_{21} \tag{4.84}$$

   For example, C - H is found in

$$C = P^{-1}H(I - H)^{-1}$$

4. Write H independent of S

   This can be accomplished by

$$H = I - S$$

Using the above procedure, N^H and N^S are derived from M. In the identification test monitoring procedure, frequency response ($\tilde{P}$) and a parametric model estimate ($\hat{P}$) are considered for generating LFT structures, respectively.

6.1.2. *LFT Formulations on $\tilde{P}$.* With the additive uncertainty description $\Delta_a = L\Delta_a E$ and two performance weights, $M - \Delta$ structure based on the frequency response $\tilde{P}$ is considered first to formulate an LFT for robust loopshaping, as illustrated in Figure 71. The $M - \Delta$ is arranged by input (Δu) and output (Δy) such that

$$\begin{bmatrix} \Delta y_1 \\ \Delta y_2 \\ \Delta y_3 \end{bmatrix} = \begin{bmatrix} -LC(I+\tilde{P}C)^{-1}E & -LC(I+\tilde{P}C)^{-1} & -LC(I+\tilde{P}C)^{-1} \\ -W_uC(I+\tilde{P}C)^{-1}E & -W_uC(I+\tilde{P}C)^{-1}E & -W_uC(I+\tilde{P}C)^{-1} \\ W_pC(I+\tilde{P}C)^{-1}E & W_pC(I+\tilde{P}C)^{-1} & W_pC(I+\tilde{P}C)^{-1} \end{bmatrix} \begin{bmatrix} \Delta u_1 \\ \Delta u_2 \\ \Delta u_3 \end{bmatrix} \tag{4.85}$$

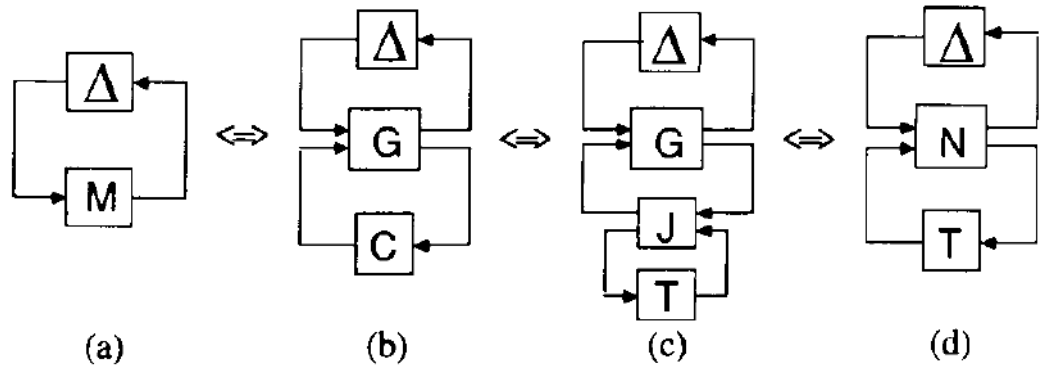

Figure 70. Equivalent representations of $M-\Delta$ structure (Morari and Zafiriou, 1988)

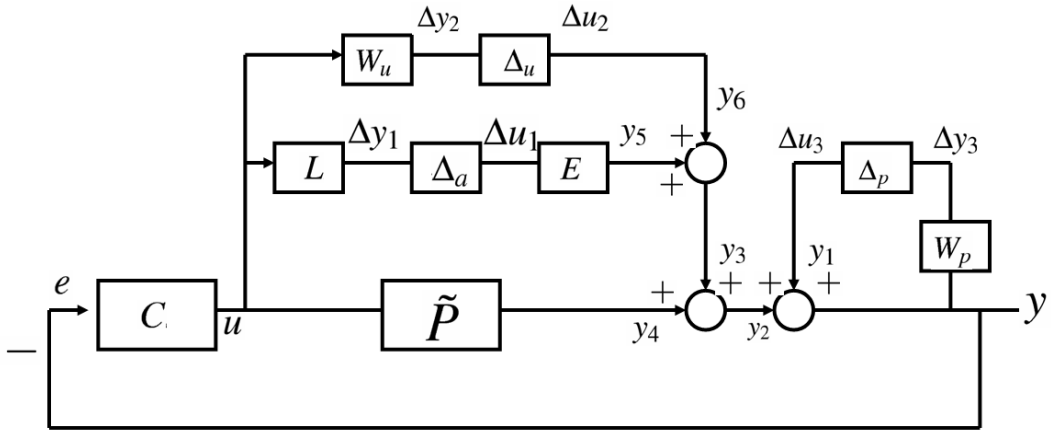

Figure 71. Model estimate ($\tilde{P}$) with additive uncertainty (Δ_a) and performance weights (W_p and W_u)

From the equation, $\Delta y = M\Delta u$ is obtained and rewritten by substituting $\tilde{P}^{-1}\tilde{H} = C(I+\tilde{P}C)^{-1}$ and $\tilde{S} = (I+\tilde{P}C)^{-1}$

$$M = \begin{bmatrix} -L\tilde{P}^{-1}\tilde{H}E & -L\tilde{P}^{-1}\tilde{H} & -L\tilde{P}^{-1}\tilde{H} \\ -W_u\tilde{P}^{-1}\tilde{H}E & -W_u\tilde{P}^{-1}\tilde{H} & -W_u\tilde{P}^{-1}\tilde{H} \\ W_p\tilde{S}E & W_p\tilde{S} & W_p\tilde{S} \end{bmatrix} \tag{4.86}$$

Equation (4.86) is rewritten, independent of $\tilde{S}$ and $\tilde{H} = I - \tilde{S}$ as follows

$$M = \begin{bmatrix} -L\tilde{P}^{-1}\tilde{H}E & -L\tilde{P}^{-1}\tilde{H} & -L\tilde{P}^{-1}\tilde{H} \\ -W_u\tilde{P}^{-1}\tilde{H}E & -W_u\tilde{P}^{-1}\tilde{H} & -W_u\tilde{P}^{-1}\tilde{H} \\ W_p(I-\tilde{H})E & W_p(I-\tilde{H}) & W_p(I-\tilde{H}) \end{bmatrix} \tag{4.87}$$

$$M = \begin{bmatrix} 0 & 0 & 0 \\ 0 & 0 & 0 \\ W_pE & W_p & W_p \end{bmatrix} + \begin{bmatrix} -L\tilde{P}^{-1}\tilde{H}E & -L\tilde{P}^{-1}\tilde{H} & -L\tilde{P}^{-1}\tilde{H} \\ -W_u\tilde{P}^{-1}\tilde{H}E & -W_u\tilde{P}^{-1}\tilde{H} & -W_u\tilde{P}^{-1}\tilde{H} \\ -W_p\tilde{H}E & -W_p\tilde{H} & -W_p\tilde{H} \end{bmatrix} \tag{4.88}$$

$$M = \begin{bmatrix} 0 & 0 & 0 \\ 0 & 0 & 0 \\ W_pE & W_p & W_p \end{bmatrix} + \begin{bmatrix} -L\tilde{P}^{-1} \\ -W_u\tilde{P}^{-1} \\ -W_p \end{bmatrix} \cdot \tilde{H} \cdot [E \;\; I \;\; I] \tag{4.89}$$

Therefore, M is rewritten in terms of $N^{\tilde{H}}$ components

$$N_{11}^{\tilde{H}} = \begin{bmatrix} 0 & 0 & 0 \\ 0 & 0 & 0 \\ W_pE & W_p & W_p \end{bmatrix} \tag{4.90}$$

$$N_{12}^{\tilde{H}} = \begin{bmatrix} -L\tilde{P}^{-1} \\ -W_u\tilde{P}^{-1} \\ -W_p \end{bmatrix} \tag{4.91}$$

$$N_{21}^{\tilde{H}} = [E \;\; I \;\; I] \tag{4.92}$$

$$N_{22}^{\tilde{H}} = 0 \tag{4.93}$$

Similarly, M can be written as an LFT of $\tilde{S}$

$$\begin{aligned} M &= N_{11}^{\tilde{H}} + N_{12}^{\tilde{H}}\tilde{H}N_{21}^{\tilde{H}} \\ &= N_{11}^{\tilde{H}} + N_{12}^{\tilde{H}}(I-\tilde{S})N_{21}^{\tilde{H}} \\ &= N_{11}^{\tilde{H}} + N_{12}^{\tilde{H}}N_{21}^{\tilde{H}} - N_{12}^{\tilde{H}}\tilde{S}N_{21}^{\tilde{H}} \end{aligned} \tag{4.94}$$

From the above it follows that

$$N_{11}^{\tilde{S}} + N_{12}^{\tilde{S}} \tilde{S} N_{21}^{\tilde{S}} = N_{11}^{\tilde{H}} + N_{12}^{\tilde{H}} N_{21}^{\tilde{H}} - N_{12}^{\tilde{H}} \tilde{S} N_{21}^{\tilde{H}} \tag{4.95}$$

$$N^{\tilde{S}} = \begin{bmatrix} N_{11}^{\tilde{H}} + N_{12}^{\tilde{H}} N_{21}^{\tilde{H}} & -N_{12}^{\tilde{H}} \\ N_{21}^{\tilde{H}} & 0 \end{bmatrix} \tag{4.96}$$

Therefore, $N^{\tilde{S}}$ matrix is obtained as

$$N_{11}^{\tilde{S}} = \begin{bmatrix} -L\tilde{P}^{-1}E & -L\tilde{P}^{-1} & -L\tilde{P}^{-1} \\ -W_u\tilde{P}^{-1}E & -W_u\tilde{P}^{-1} & -W_u\tilde{P}^{-1} \\ 0 & 0 & 0 \end{bmatrix} \tag{4.97}$$

$$N_{12}^{\tilde{S}} = -N_{12}^{\tilde{H}} = \begin{bmatrix} L\tilde{P}^{-1} \\ W_u\tilde{P}^{-1} \\ W_p \end{bmatrix} \tag{4.98}$$

$$N_{21}^{\tilde{S}} = N_{21}^{\tilde{H}} = [E \;\; I \;\; I] \tag{4.99}$$

$$N_{22}^{\tilde{S}} = N_{22}^{\tilde{H}} = 0 \tag{4.100}$$

6.1.3. *LFT formulations on $\hat{P}$.* Since $\tilde{P}$ is the nonparametric frequency response from the experimental data, initial robust bounds cannot be used for the parametric model $\hat{P}$. The initial loopshaping bounds on $\tilde{P}$ facilitates the search for preliminary controller tuning set for control-relevant curvefitting. Once a parametric model $\hat{P}$ is obtained, the robust loopshaping on $\hat{P}$ should run again, taking into account the uncertainty (Δ) and model error $(\tilde{P} - \hat{P})$ in LFT structures. This is required to modify the previously derived LFTs on $\tilde{P}$ into LFTs on $\hat{P}$.

The robust loopshaping using $\hat{P}$ that searches the bounds on $\hat{H} = \hat{P}C(I + \hat{P}C)^{-1}$ and $\hat{S} = (I + \hat{P}C)^{-1}$. $\hat{H}$ is considered first, such that

$$\tilde{H} = \tilde{P}\hat{P}^{-1}\hat{H}(I + E_m\hat{H})^{-1} \tag{4.101}$$

where $E_m = (\tilde{P} - \hat{P})\hat{P}^{-1}$. Equation (4.101) is then substituted into M

$$\begin{aligned} M &= N_{11}^{\tilde{H}} + N_{12}^{\tilde{H}}\{\tilde{P}\hat{P}^{-1}\hat{H}(I + E_m\hat{H})^{-1}\}N_{21}^{\tilde{H}} \\ &= N_{11}^{\hat{H}} + N_{12}^{\hat{H}}\hat{H}(I - N_{22}^{\hat{H}}\hat{H})^{-1}N_{21}^{\hat{H}} \end{aligned} \tag{4.102}$$

The above results in the following

$$N_{11}^{\hat{H}} = N_{11}^{\tilde{H}} = \begin{bmatrix} 0 & 0 & 0 \\ 0 & 0 & 0 \\ W_pE & W_p & W_p \end{bmatrix} \tag{4.103}$$

$$N_{12}^{\hat{H}} = N_{11}^{\tilde{H}}\tilde{P}\hat{P}^{-1} = \begin{bmatrix} -L\hat{P}^{-1} \\ -W_u\hat{P}^{-1} \\ -W_p\tilde{P}\hat{P}^{-1} \end{bmatrix} \tag{4.104}$$

$$N_{21}^{\hat{H}} = N_{21}^{\tilde{H}} = [E \;\; I \;\; I] \tag{4.105}$$

$$N_{22}^{\hat{H}} = -E_m = -(\tilde{P} - \hat{P})\hat{P}^{-1} \tag{4.106}$$

Similarly, the LFT of $\hat{S}$ is derived from $\tilde{S}$,

$$\tilde{S} = \hat{S}(I - E_s\hat{S})^{-1}\hat{P}\tilde{P}^{-1} \tag{4.107}$$

where $E_s = (\tilde{P} - \hat{P})\tilde{P}^{-1}$. The LFT of M by $\tilde{S}$ is substituted into the above equation

$$\begin{aligned} M &= N_{11}^{\tilde{S}} + N_{12}^{\tilde{S}}\tilde{S}N_{21}^{\tilde{S}} \\ &= N_{11}^{\tilde{S}} + N_{12}^{\tilde{S}}\hat{S}(I - E_s\hat{S})^{-1}\hat{P}\tilde{P}^{-1}N_{21}^{\tilde{S}} \end{aligned} \tag{4.108}$$

Therefore, $N^{\hat{S}}$ matrix is obtained as

$$N_{11}^{\hat{S}} = N_{11}^{\tilde{S}} = \begin{bmatrix} -L\tilde{P}^{-1}E & -L\tilde{P}^{-1} & -L\tilde{P}^{-1} \\ -W_u\tilde{P}^{-1}E & -W_u\tilde{P}^{-1} & -W_u\tilde{P}^{-1} \\ 0 & 0 & 0 \end{bmatrix} \tag{4.109}$$

$$N_{12}^{\hat{S}} = N_{12}^{\tilde{S}} = \begin{bmatrix} L\tilde{P}^{-1} \\ W_u\tilde{P}^{-1} \\ W_p \end{bmatrix} \tag{4.110}$$

$$N_{21}^{\hat{S}} = \tilde{P}\hat{P}^{-1}N_{21}^{\tilde{S}} = \begin{bmatrix} \tilde{P}\hat{P}^{-1}E & \tilde{P}\hat{P}^{-1} & \tilde{P}\hat{P}^{-1} \end{bmatrix} \tag{4.111}$$

$$N_{22}^{\hat{S}} = E_s \tag{4.112}$$

6.2. Deriving $\bar{\sigma}(T)$ from $\mu(M)$-Analysis. Based on Chapter 11 of Morari and Zafiriou (1988), the following is applied to robust loopshaping in this dissertation. When M is written as an LFT of T

$$M = N_{11} + N_{12}T(I - N_{22}T)^{-1}N_{21}$$

where k is a given constant. Assume $\mu_\Delta(N_{11}) < k$ and $det(I - N_{22}T) \neq 0$. Then

$$\mu_\Delta(M) < k \tag{4.113}$$

if

$$\bar{\sigma}(T) \leq c_T \tag{4.114}$$

where c_T implicitly solves

$$\mu_{\tilde{\Delta}} \begin{pmatrix} N_{11} & N_{12} \\ kc_T N_{21} & kc_T N_{22} \end{pmatrix} = k \tag{4.115}$$

and $\tilde{\Delta} = diag\{\Delta, T\}$.

6.3. Remarks on Loopshaping. It has significant importance to derive a bound on any transfer matrix T that provides a powerful method for generating robustness conditions on the closed-loop system. With a set of models defined by the uncertainty description, a controller can be designed and tuned to satisfy the robustness bounds on C. The controller C is involved in the transfer matrix S and H, which are derived

into N^S and N^H structures from $M-\Delta$. Solving c_S and c_H provides the sufficient and necessary robustness conditions.

As a result, a controller can be designed and iteratively tuned to satisfy the robustness bounds. Control-relevant parameter estimation takes advantage of the robustness bounds to tune the controller. This procedure naturally becomes iterative between the robust loopshaping and control-relevant curvefitting tasks. In the following section, a linear high-purity distillation by Jacobsen and Skogestad (1994) is used as a case study to demonstrate a scenario of the identification test monitoring procedure.

7. Identification Test Monitoring Procedure Case Study

In this case study, the two-input, two-output high purity distillation column problem per Jacobsen and Skogestad (1994) is considered to demonstrate the effectiveness of the proposed identification test monitoring framework. Based on this framework, we apply an experimental testing scenario in order to refine process knowledge suitable for advanced process control applications. As the process is strongly ill-conditioned and highly interactive, it is a nontrivial problem to achieve accurate gain directionality in models using standard identification testing. Therefore, a modified zippered spectrum with direction and power adjustments on correlated harmonics is utilized for identifying highly interactive systems, and its design parameters are refined as plant knowledge increases. The identification test monitoring procedure accomplishes this scenario systematically.

An identification test monitoring scenario using Guillaume-phasing multisine input signals is presented in this case study that generates a series of $\{\min \mathrm{CF}(u)\}$ signals (Guillaume *et al.*, 1991). Relying on limited *a priori* process knowledge at Stage 1, a standard zippered spectrum design is considered with a wide bandwidth. Input signals at Stages 2 and 3 are consequently redesigned based on *a priori* knowledge and updated model information gained during the identification testing. Nominal model performance is considered at Stages 1 and 2; a robust control system is obtained at Stage 3a where a suitable level of uncertainty

bound is available and robustness conditions are satisfied. Alternatively, we can consider a closed-loop identification test at Stage 3b that takes advantage of the weighted curvefit model and a nominally stable MPC controller obtained from Stage 2. White noise with variance $\sigma^2 = 0.001$ is added to each output channel at all stages, enabling evaluation of the effectiveness of identification test monitoring for a highly interactive system under noisy conditions.

7.1. Identification Testing Stage 1. A standard zippered spectrum signal is designed using *a priori* knowledge of time constants $\tau_{dom}^{H} = 194$ and $\tau_{dom}^{L} = 15$, the speed of response factor $\alpha = 2$, and the settling time requirements $\beta = 3$ (Figure 72a). The time sequences of the experimental data are plotted in Figure 72b. Because of its long signal length, three cycles are tested. The last two cycles are considered for identification analysis.

Examining the experiment data from the standard zippered spectrum signal shows that the distillation column is highly interactive (Figure 73). Input sequences are distributed well in all directions; however, output sequences are distributed in the high gain direction so that the outputs are moving in the same direction. This characteristic demands significant attention to design a directional input signal using a modified zippered spectrum to create balanced gain directionality in the output.

Frequency responses ($\tilde{P}$) by means of spectral analysis using a Hamming window with 256 lags are computed for the control-relevant weighted curvefitting and robust loopshaping steps. The frequency responses are shown in Figure 74a. Robust loopshaping is applied to $\tilde{P}$ with a performance weight (W_p) on the sensitivity function with bandwidth $\omega_b = 0.001$ and maximum peak $M_s = 4$ (Figure 68) such that

$$W_p(s) = \frac{0.25s + 0.001}{s + 1.0^{-9}} \tag{4.116}$$

Robustness conditions lead to significantly rough bounds due to the variance in the data and a high uncertainty bound. Only the nominal model is considered in the weighted curvefitting. We tried to use the rough bounds as a preliminary tuning guideline in control-relevant curvefitting to estimate a nominal paramet-

ric model $\hat{P}$ (Figure 74a). The Small Gain condition (Figure 74b) of the weighted model is reshaped by the control-relevant weights based on an MPC tuning set: PH=35, MH=5, Ywt=[1 1], and Uwt=[0.05 0.03]*0.5. In the low frequencies, the Small Gain condition ($\rho(E_m\hat{H})$) is less than the unity but is larger than the unity in the high frequencies (Figure 74b). Robust loop conditions (Figure 76) based on the nominal model and estimated uncertainty bound (Figure 75) evaluated using Equation (4.39) and performance weight (4.116) are not satisfied at this stage because the loop bounds are partly available and very rough. However, robust stability only is satisfied over the bandwidth, as shown in Figure 77. A closed-loop evaluation of the curvefit models is performed in Figure 78 where the unweighted and weighted models have no significant difference in setpoint tracking; they both, however, have slow responses. Estimated singular values from the models show that both have accurate high singular values but inaccurate low singular values to the true plant (see Figure 79). The data does not contain much low gain directional information compared to the high gain direction. The control-relevant model thus cannot improve the low singular value estimate and hence the closed-loop control performance.

In summary, the Stage 1 experiment indicates that the distillation column is highly interactive and strongly ill-conditioned, and the data displays inaccurate low gain directionality information under noisy conditions. It is necessary to proceed to the next experimental stage; we hence design a modified zippered spectrum utilizing information from the weighted model estimated from Stage 1.

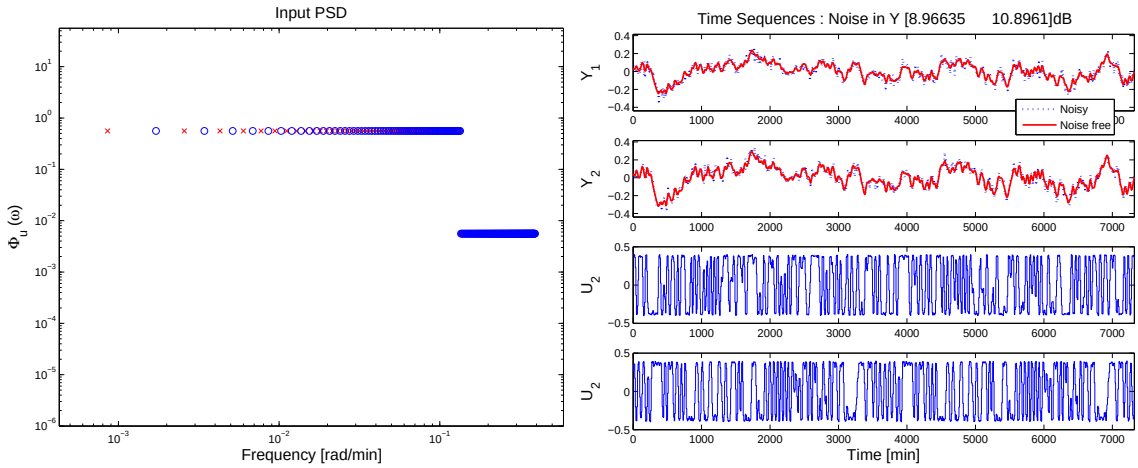

(a) Input PSD (b) Time Sequences

Figure 72. Stage 1 of identification test monitoring for the Jacobsen-Skogestad high purity distillation column: a standard zippered power spectrum design (a) and time series of input and output data (b)

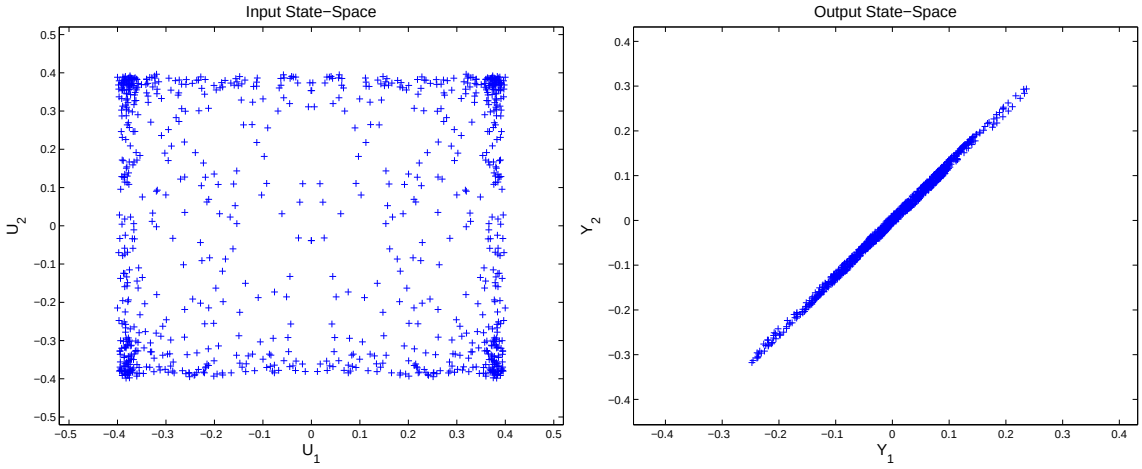

(a) Input State-Space (b) Output State-Space

Figure 73. Stage 1 of identification test monitoring for the Jacobsen-Skogestad high purity distillation column: input (a) and output (b) state-space plots

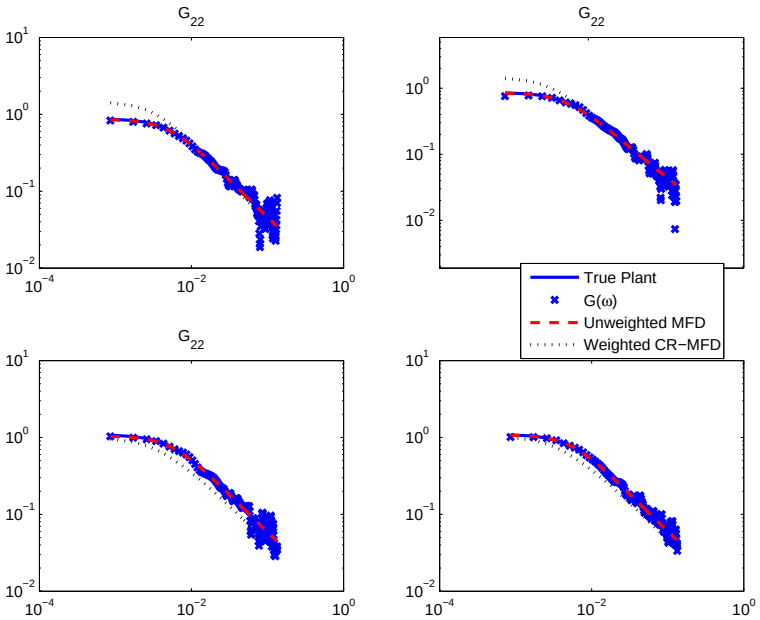

(a) Frequency Responses and Curvefits

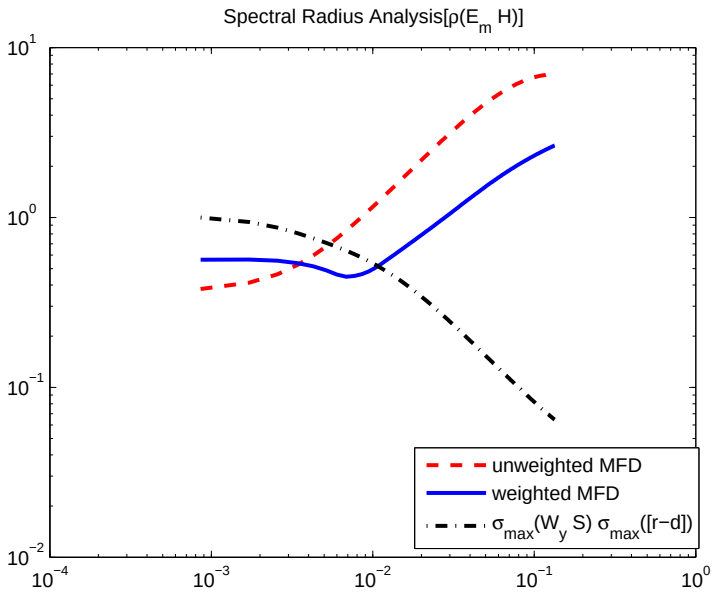

(b) Small Gain Condition $\rho(E_m\hat{H})$

Figure 74. Stage 1 of identification test monitoring for the Jacobsen-Skogestad high purity distillation column: frequency responses and curvefitting with MPC tuning set: PH=35, MH=5, Ywt=[1 1], and Uwt=[0.05 0.03]*0.5 (a) and Small Gain condition for the unweighted and weighted curvefit models (b)

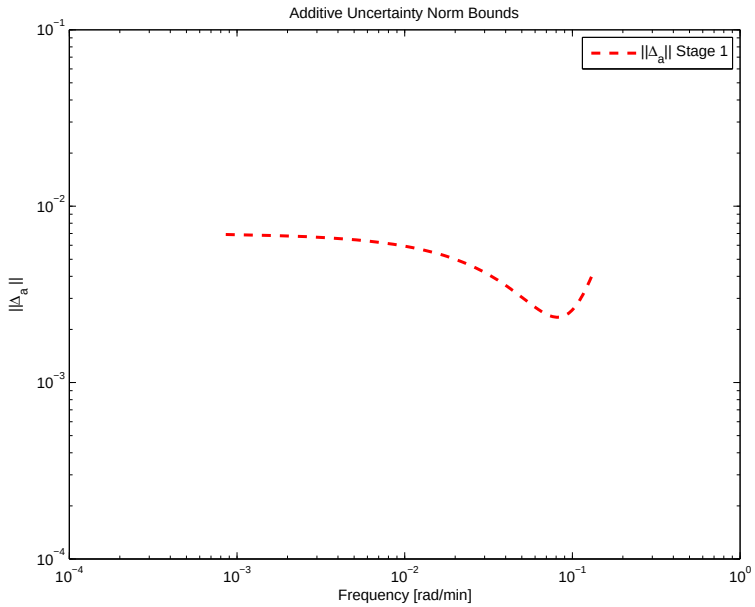

Figure 75. Stage 1 of identification test monitoring for the Jacobsen-Skogestad high purity distillation column: additive model uncertainty norm bound with 2 cycles

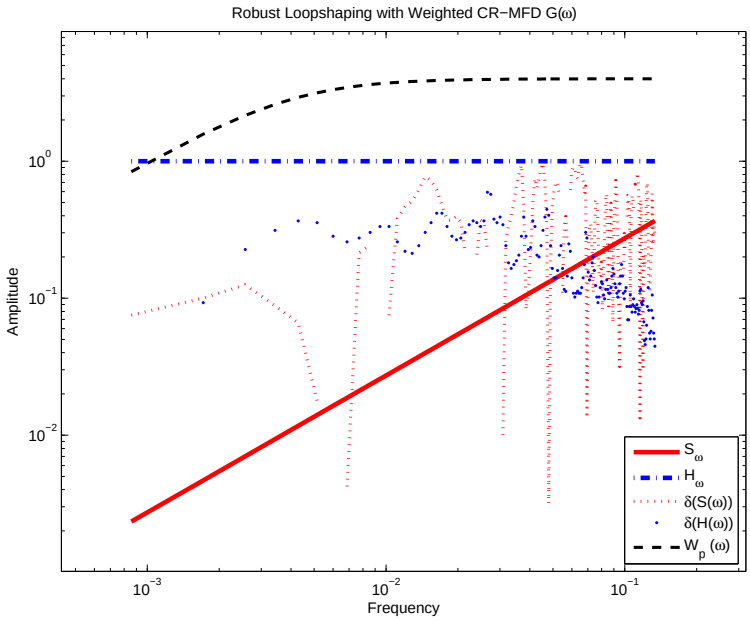

Figure 76. Stage 1 of identification test monitoring for the Jacobsen-Skogestad high purity distillation column: robust loopshaping bounds on $\hat{P}$ with MPC tuning set: PH=35, MH=5, Ywt=[1 1], and Uwt=[0.05 0.03]*0.5

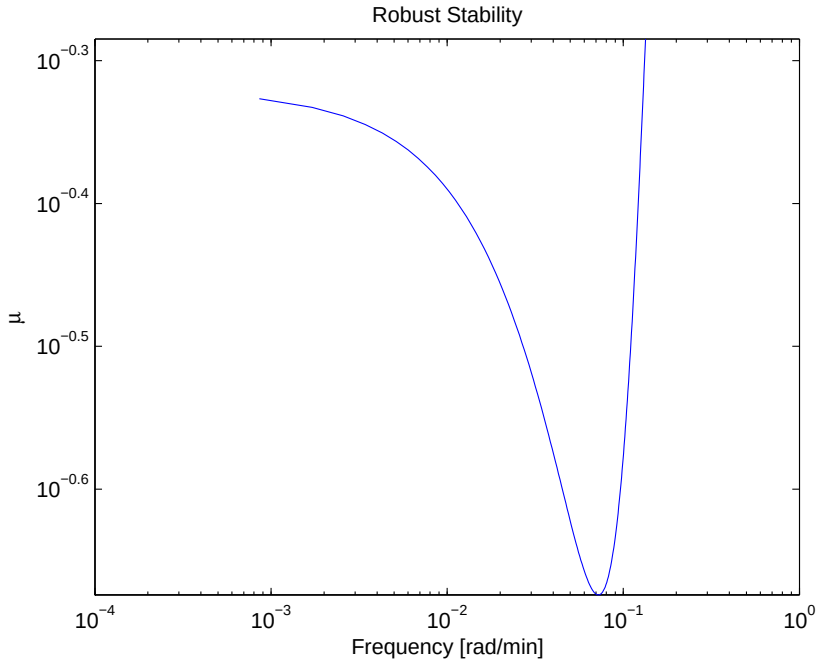

Figure 77. Stage 1 of identification test monitoring for the Jacobsen-Skogestad high purity distillation column: robust stability analysis

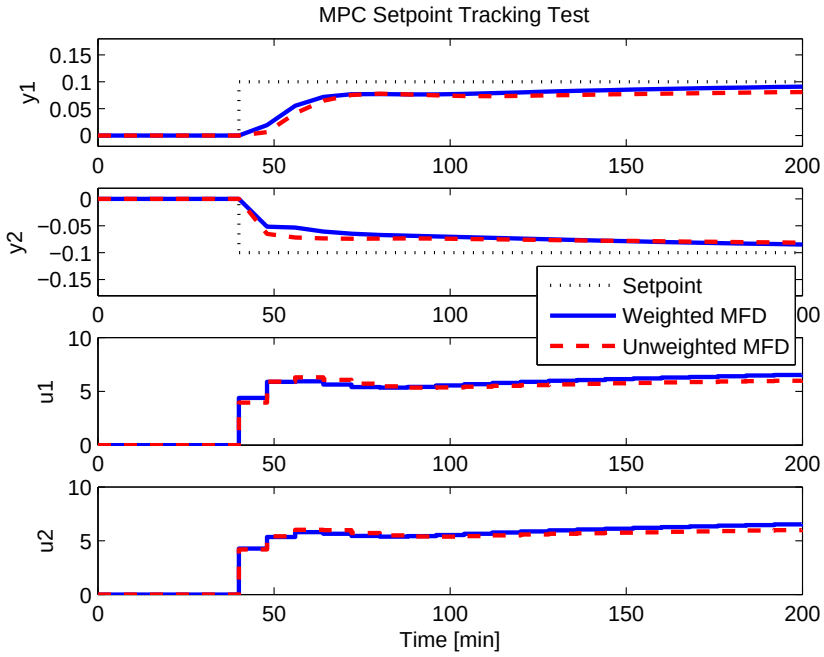

Figure 78. Stage 1 of identification test monitoring for the Jacobsen-Skogestad high purity distillation column: setpoint (r=[0.1 -0.1]) tracking test with MPC, MPC tuning set: PH=35, MH=5, Ywt=[1 1], and Uwt=[0.05 0.03]*0.5

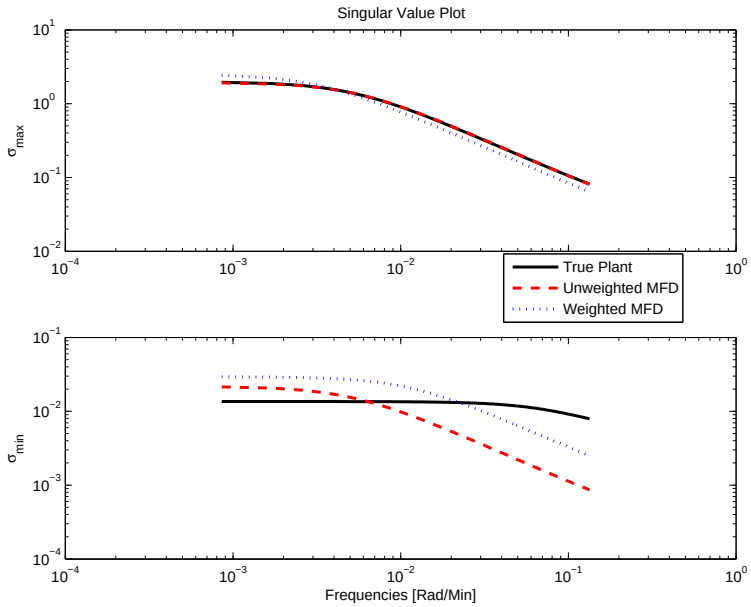

Figure 79. Stage 1 of identification test monitoring for the Jacobsen-Skogestad high purity distillation column: singular values of true plant vs. estimated models in frequency domain, MPC tuning set: PH=35, MH=5, Ywt=[1 1], and Uwt=[0.05 0.03]*0.5

7.2. Identification Testing Stage 2. A directional input signal design using a modified zippered spectrum is required to achieve balanced gain directionality in the output for the high purity distillation column. From the control-relevant weighted model estimated in Stage 1, a steady-state gain is obtained such that

$$K_1 = \begin{bmatrix} 1.4636 & -1.4625 \\ 0.9832 & -1.0328 \end{bmatrix} \tag{4.117}$$

and SVD analysis on K_1 gives

$$U = \begin{bmatrix} -0.8234 & -0.5674 \\ -0.5674 & 0.8234 \end{bmatrix} \Sigma = \begin{bmatrix} 2.5127 & 0 \\ 0 & 0.0293 \end{bmatrix} V^H = \begin{bmatrix} -0.7017 & -0.7125 \\ 0.7125 & -0.7017 \end{bmatrix} \tag{4.118}$$

A γ range using the guideline in Equation (2.76) is obtained using the above information as

$$\gamma_{min} = 29.9906 \leq \gamma \leq \gamma_{max} = 63.1574 \tag{4.119}$$

As a result, $\gamma_{avg} = 46.5740$ and $v_2 = [-0.7125 \quad -0.7017]$ are selected for designing a modified zippered spectrum, as shown in Figure 80a.

At this stage, it is of great interest to rely on increased process knowledge to narrow down the signal bandwidth. This action results in a shorter input signal while retaining a necessary and important bandwidth. The control-relevance for closed-loop control is emphasized by focusing on the frequencies where the closed-loop dynamics are important. As the distillation column is highly interactive, particularly at steady-state, it demands a good estimate of the information in the low frequencies. Although a signal length cannot be reduced dramatically because of these characteristics, we can decide on design parameters $\tau_{dom}^H = 106$, $\tau_{dom}^L = 15$, $\alpha = 2$ and $\beta = 3$, which allow for some bandwidth reduction. As a result, we can design a shorter yet informative input signal for the distillation column, i.e., $n_s = 43$ and $N_s = 500$,

which leads to a cycle length 45.4% shorter than Stage 1. Three cycles are tested for Stage 2, as shown in Figure 80a.

Adjusting the magnitude of uncorrelated harmonics in the designed modified zippered spectrum to that of the Stage 1 input signal, a higher input magnitude of $u = [\pm 12 \ \ \pm 12]$ is applied to Stage 2, improving the signal-to-noise ratio (Figure 80a). The Stage 2 input magnitude is significantly higher than in Stage 1 but produces the similar output magnitude span (Figure 80b). The directionally designed input signal using correlated harmonics (Figure 81a) increases the output span only in the intended (low-gain) output gain direction (Figure 81b). As a result, a wider distribution in the low gain direction of the output state-space is obtained, as shown in Figure 81b.

Frequency responses ($\tilde{P}$) by means of spectral analysis using a Hamming window with 256 lags are computed for control-relevant weighted curvefitting and robust loopshaping steps. Robust loopshaping is applied to $\tilde{P}$ with a sensitivity performance weight, as used in Stage 1 (Equation (4.116)). Robustness bounds on the sensitivity function are only partly computed, as shown in Figure 84, using the weighted model and the uncertainty bound from the data of three cycles (Figure 83). As a consequence, we are only able to estimate a nominal parametric model $\hat{P}$ (Figure 82a), without considering robustness as was also the case in Stage 1. Using control-relevant weights by an MPC tuning set; PH=35, MH=5, Ywt=[1 1], and Uwt=[0.05 0.03]*0.3, the weighted curvefitting significantly reduces the Small Gain condition from that of the unweighted model, possibly producing a much more nominally stable model (Figure 74b). Over frequencies, the Small Gain condition $\rho(E_m\hat{H})$ is less than 10^{-1}. Since the robust bound on $\sigma(\hat{H})$ is not meaningful and $\sigma(\hat{S})$ is partly computed, the iteration procedure between the loopshaping and curvefitting is not considered. Robust stability analysis shows that μ is close (yet greater than) to unity in the low frequencies, while it is less than the unity in the mid and high frequencies (Figure 85).

The closed-loop setpoint tracking tests with the curvefitted models are evaluated in Figure 86 where the weighted and unweighted models display significant differences in setpoint tracking performance. This

result significantly contrasts the result of Stage 1. The weighted model shows fast setpoint tracking responses without offset, while the unweighted model displays offset in both output channels with overshoot. Moreover, the weighted model shows accurate estimated singular values in both high and low singular values of the true plant, while the unweighted model has only accurate high singular values (Figure 87). The Stage 2 data contains low gain directional information comparable to the high gain direction in output magnitudes so that the control-relevant curvefitting procedure can improve the low singular value estimate and closed-loop setpoint tracking performance.

From Stage 1 to Stage 2, we are able to improve the low gain directional information by the use of a modified zippered input signal. However, a robust control system cannot be ascertained from three cycles of test data. Two options are considered for Stage 3, which are discussed in this dissertation. In Stage 3a, an open-loop design relying on the model from Stage 2 is considered. Alternatively, in Stage 3b we can consider a stable closed-loop identification test that takes advantage of the updated process information and the MPC controller evaluated from Stage 2. This stage relies on a phase-shifted multisine input applied to the reference points of the control system.

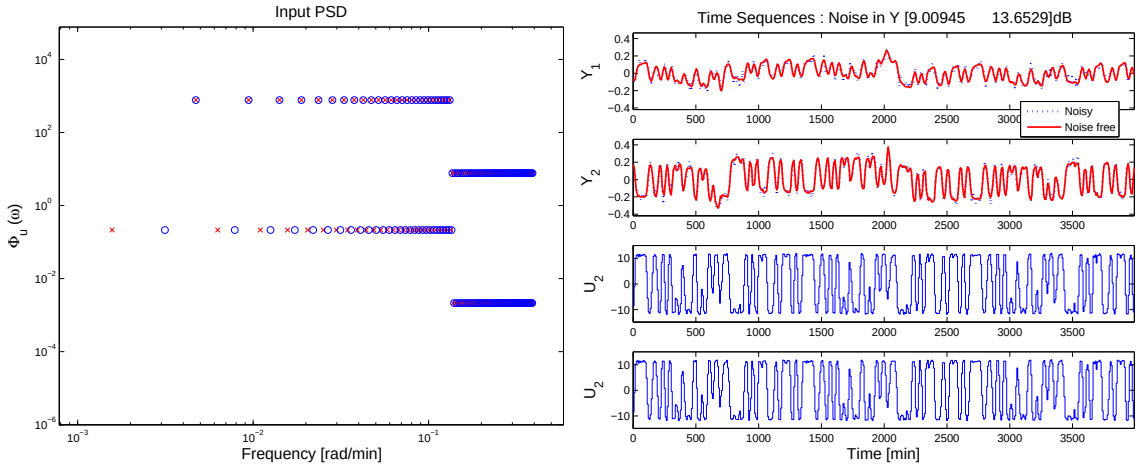

(a) Input PSD (b) Time Sequences

Figure 80. Stage 2 of identification test monitoring for the Jacobsen-Skogestad high purity distillation column: a standard zippered power spectrum design (a) and time series of input and output data (b)

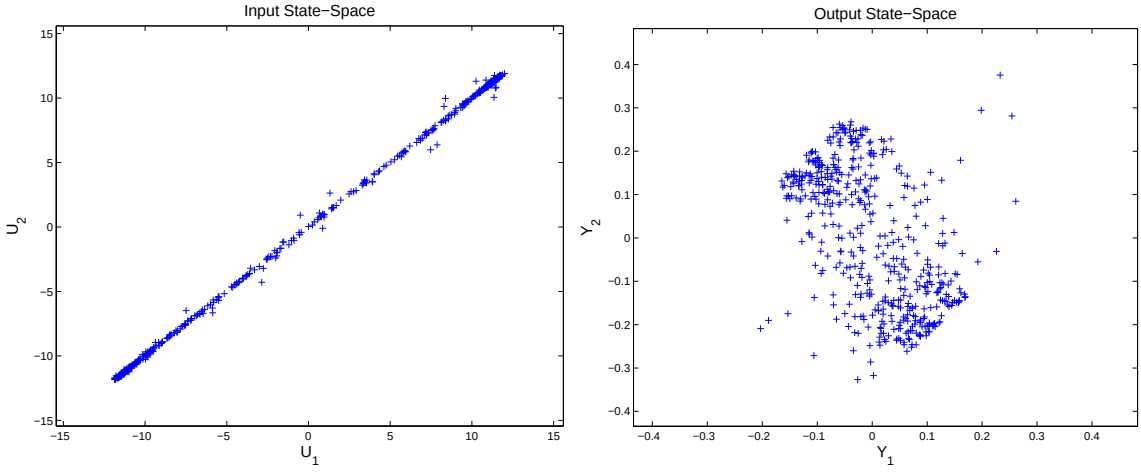

(a) Input State-Space (b) Output State-Space

Figure 81. Stage 2 of identification test monitoring for the Jacobsen-Skogestad high purity distillation column: input (a) and output (b) state-space plots

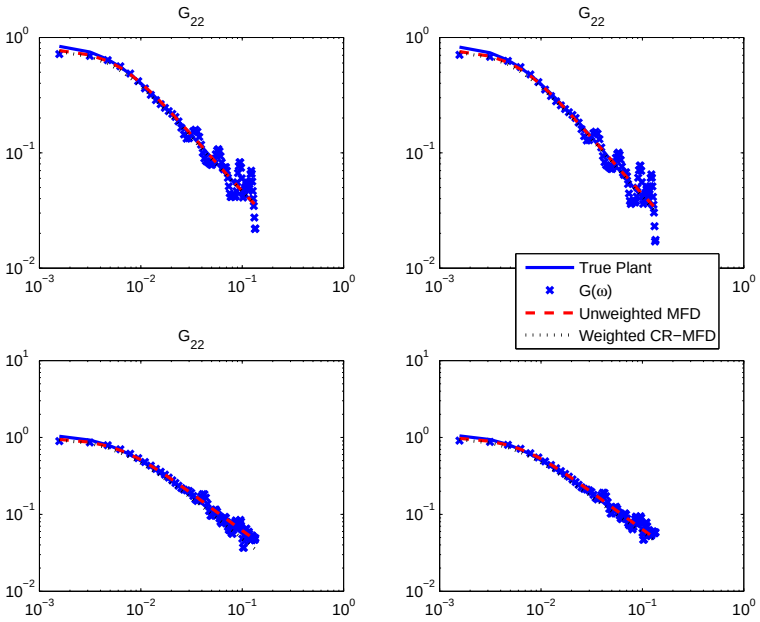

(a) Frequency responses and curvefits

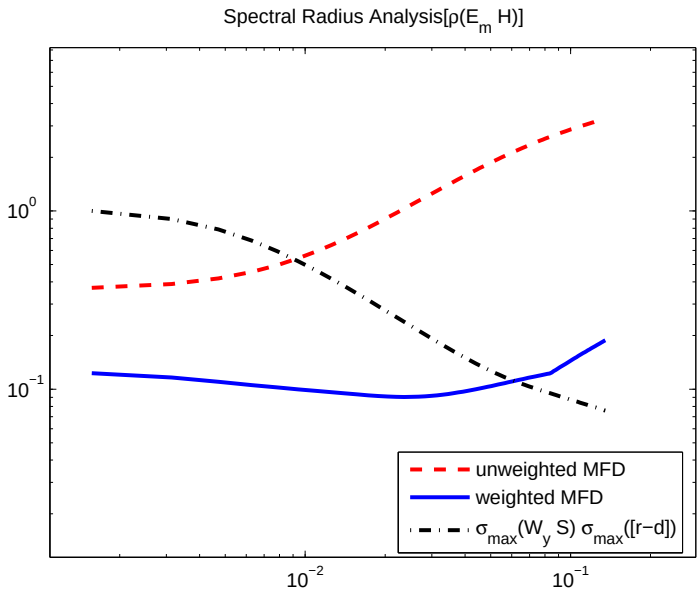

(b) Small Gain condition $\rho(E_m\hat{H})$

Figure 82. Stage 2 of identification test monitoring for the Jacobsen-Skogestad high purity distillation column: frequency responses and curvefitting (a) with MPC tuning set: PH=35, MH=5, Ywt=[1 1], and Uwt=[0.05 0.03]*0.2 and Small Gain condition for the unweighted and weighted curvefit models (b)

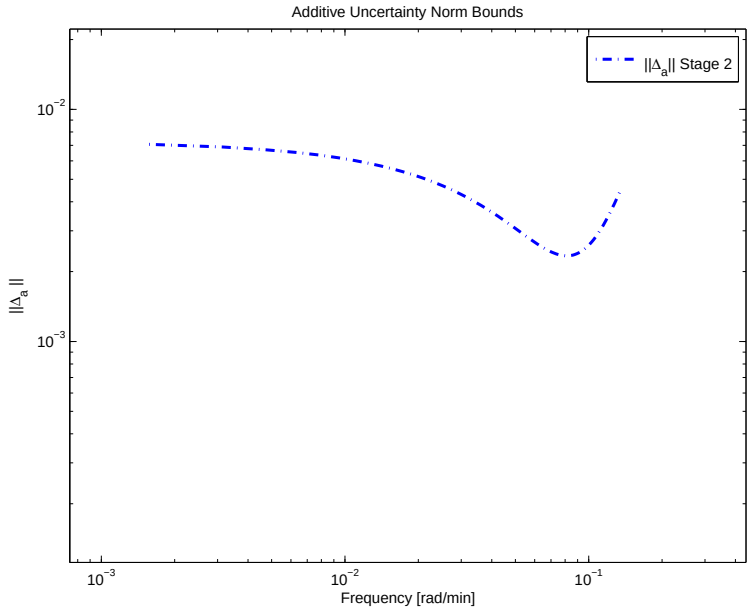

Figure 83. Stage 2 of identification test monitoring for the Jacobsen-Skogestad high purity distillation column: additive model uncertainty norm bound with 2 cycles

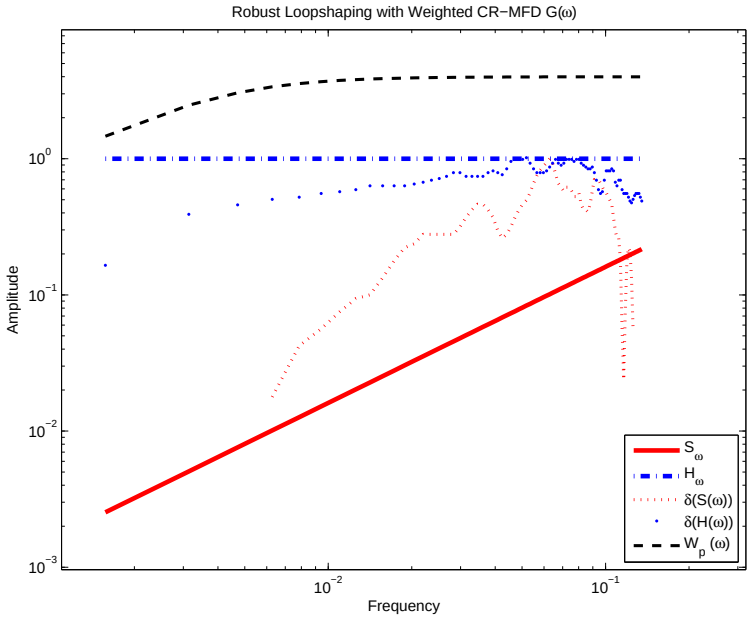

Figure 84. Stage 2 of identification test monitoring for the Jacobsen-Skogestad high purity distillation column: robust loopshaping bounds on $\hat{P}$ with MPC tuning set: PH=35, MH=5, Ywt=[1 1], and Uwt=[0.05 0.03]*0.2

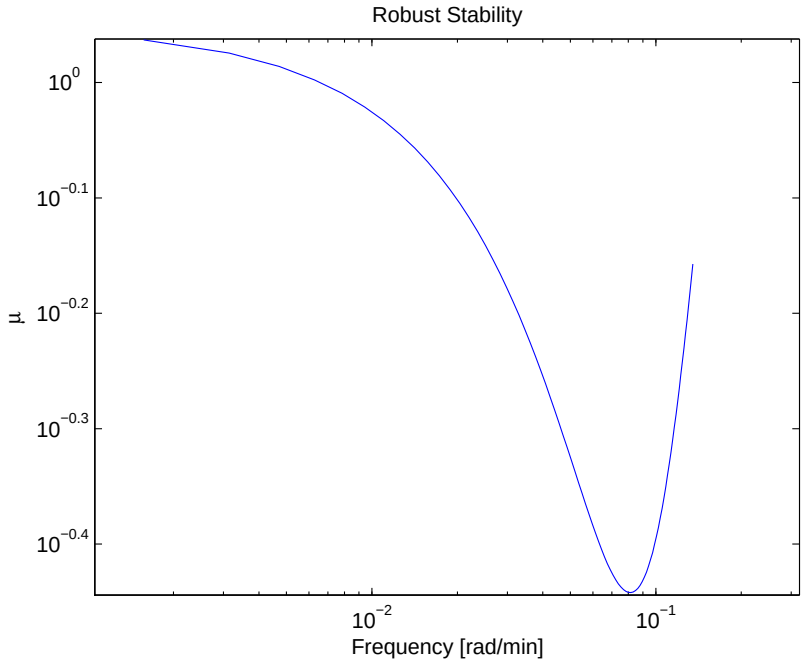

Figure 85. Stage 2 of identification test monitoring for the Jacobsen-Skogestad high purity distillation column: robust stability analysis

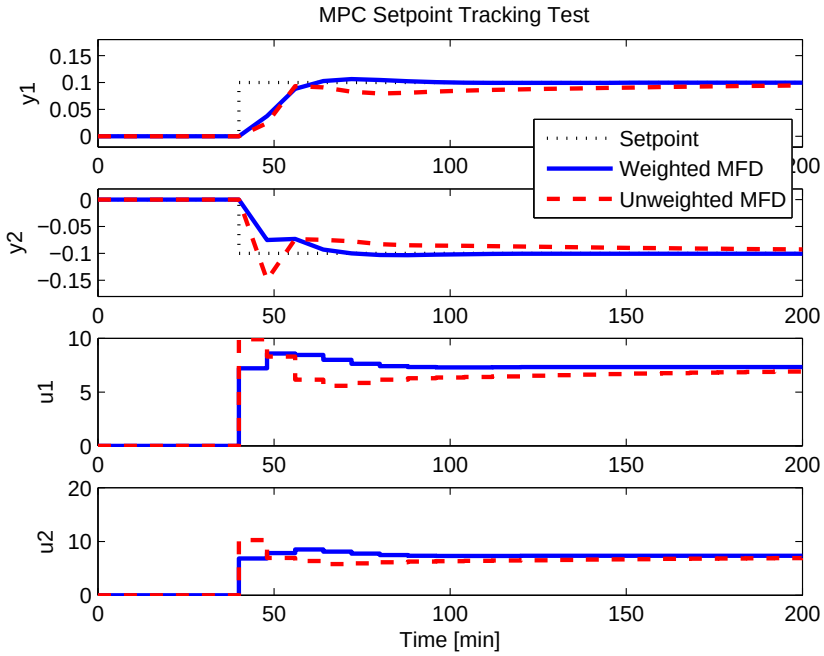

Figure 86. Stage 2 of identification test monitoring for the Jacobsen-Skogestad high purity distillation column: setpoint (r=[0.1 -0.1]) tracking test with MPC, MPC tuning set: PH=35, MH=5, Ywt=[1 1], and Uwt=[0.05 0.03]*0.2

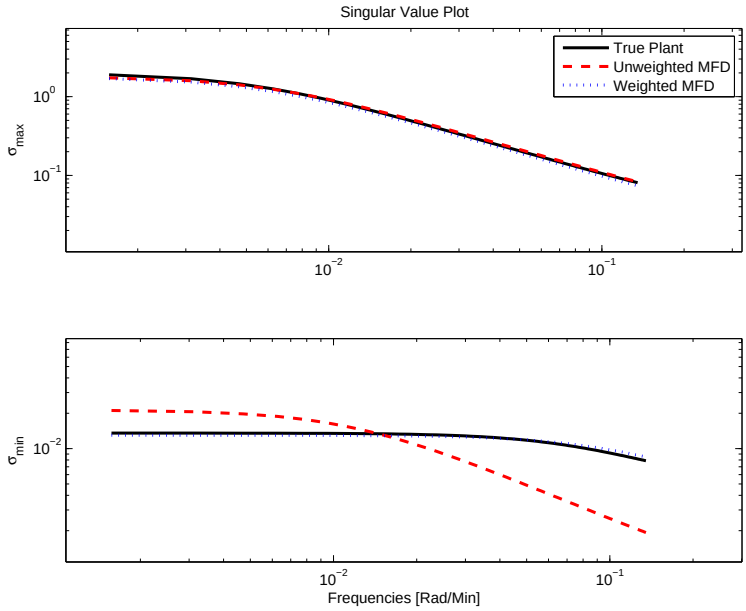

Figure 87. Stage 2 of identification test monitoring for the Jacobsen-Skogestad high purity distillation column: singular values of true plant vs. estimated models in frequency domain, MPC tuning set: PH=35, MH=5, Ywt=[1 1], and Uwt=[0.05 0.03]*0.2

7.3. Identification Testing Stage 3a. A directional input signal design is further refined to achieve balanced gain directionality using the updated model information from Stage 2. From the weighted model of Stage 2, a steady-state gain is obtained such that

$$K_2 = \begin{bmatrix} 0.785 & -0.771 \\ 0.966 & -0.978 \end{bmatrix} \tag{4.120}$$

and SVD analysis on K_2 gives

$$U = \begin{bmatrix} -0.6249 & -0.7807 \\ -0.7807 & 0.6249 \end{bmatrix} \Sigma = \begin{bmatrix} 1.7609 & 0 \\ 0 & 0.0130 \end{bmatrix} V^H = \begin{bmatrix} -0.7072 & -0.7070 \\ 0.7070 & -0.7072 \end{bmatrix} \tag{4.121}$$

A γ range is obtained using the above information as

$$\gamma_{min} = 54.25 \leq \gamma \leq \gamma_{max} = 84.65 \tag{4.122}$$

As a result, $\gamma_{avg} = 69.45$ and $v_2 = [-0.7070 \quad -0.7072]$ are selected for designing a new modified zippered power spectrum, as shown in Figure 88a. The use of the model estimate from Stage 2 allows increased excitation power to the correlated harmonics, which is much more closer to the $[1 \;\; 1]$ input direction. The input magnitude is increased to $u = [\pm 14 \;\; \pm 14]$ for Stage 3a, which is slightly larger than that of Stage 2. The increased magnitude helps in reducing the uncertainty norm bound by applying a higher signal-to-noise ratio, as indicated by the following equation

$$\bar{\ell}_a \;\propto\; \frac{n}{N} \; \frac{\Phi_v}{\Phi_u} \tag{4.123}$$

where n is the number of model parameters and N is the data length.

The nature of the distillation process requires information at the lower frequencies for accurate gain directionality of steady-state, while the closed-loop dynamics requires information at the higher frequencies. Therefore, it is nontrivial to narrow down an input signal bandwidth for this distillation column. Nonetheless, a shorter bandwidth is possibly designed with a precise observation on Figure 82a in which the noise

corrupts the frequency responses higher than $\omega \approx 0.01$. Frequency grids lower than $\omega \approx 0.01$ show quiet frequency responses instead; fewer low frequency grids can possibly be considered. The frequency responses at higher frequency grids required for the closed-loop dynamics can be smoothed by a number of testing cycles. As a result, we can decide on design parameters $\tau_{dom}^{H} = 67$, $\tau_{dom}^{L} = 15$, $\alpha = 2$, and $\beta = 3$ that lead to a much shorter bandwidth for Stage 3a, i.e., a new sequence length $N_s = 316$.

The higher correlated harmonics increase the corresponding output span in the [1 -1] direction (see Figure 89), which ultimately enhances the low gain directionality. Spectral analysis is applied to compute nonparametric frequency responses ($\tilde{P}$) using a Hamming window with 128 lags. An uncertainty description bound is estimated per Equation (4.39) to define a set of models, as shown in Figure 91. As a consequence, robust loopshaping can be applied.

At this stage, robust stability is satisfied over all frequencies, as shown in Figure 92. Robust stability and performance conditions from robust loopshaping can be used to assess control adequacy of the models estimated from the data, and hence can influence the decision to start or stop experimental testing. Stage 3a is tested for 14 cycles to reduce the norm bound of model uncertainty to a suitable level for robust loopshaping analysis. Initially, robust loopshaping on $\tilde{P}$ is performed, providing provides $\bar{\sigma}(\tilde{H})$ and $\bar{\sigma}(\tilde{S})$ as a preliminary tuning guideline to properly tune the MPC controller in control-relevant curvefitting that are selected to satisfy $\sigma(\tilde{H})$ and $\sigma(\tilde{S})$ bounds (Figure 90a). Relying on previously weighted models, we can iteratively tune the weighted curvefitting algorithm until a weighted model meets the loopshaping bounds. When a weighted model satisfies the loopshaping bounds, its Small Gain condition shows sufficient levels of nominal stability, as seen in Figure 90b. The weighted model $(\hat{P})$ is then taken into account again for robust loopshaping including the model error $\tilde{P} - \hat{P}$. The model estimation error and model uncertainty are incorporated into $N^{\hat{H}}$ and $N^{\hat{S}}$ structures for loopshaping. As the bounds of $\sigma(\hat{H})$ and $\sigma(\hat{S})$ are satisfied with the weighted model $\hat{P}$, a finalized model can be obtained that meets both control relevance and robustness requirements with an MPC tuning set of PH=35, MH=5, Ywt=[1 1], and Uwt=[0.05 0.03]*0.13 (Figure 93).

A closed-loop model evaluation of a satisfactory curvefit model using setpoint tracking is shown in Figure 94. With a faster set of MPC tuning parameters, only the weighted model shows fast and over-damped responses without offset; the unweighted model suffers numerical oscillations in y_2 and overshoot in y_1. A synergistic effect of using the directional input signal design and weighted curvefitting clearly results in the accurate estimate of the low singular values (Figure 95). In spite of the large number of testing cycles, the unweighted curvefitted model does not show a reasonable estimate of the low singular values. This is clear evidence that the weighted curvefitting is effectively able to efficiently capture the low gain directional information which is designed to be emphasized by the use of a modified zippered spectrum, as was presented in Chapters 2 and 3.

The performance weight (Equation (4.116)) and tuning parameters can provide flexibility to adjust the robust loop bounds during the iterative procedure between the curvefitting and loopshaping. The success of control-relevant and robust models can be guaranteed when a sufficient number of testing cycles are tested so that the uncertainty norm bound is reduced to a suitable level. A control-relevant model satisfying robustness conditions is obtained after 14 cycles, at which time experimental testing is halted.

At each cycle interval, the identification test monitoring framework evaluates updated robust loop-shaping bounds and whether these are applicable for weighted curvefitting; if so, we can halt identification testing. Figures 97 to 98 show the intermediate identification test monitoring analysis for Stage 3a at 5 and 10 cycles, respectively. Since Stage 2 with three cycle data shows an improved nominal performance, intermediate models at Stage 3a show all nominally stable control performance (Figures 97c to 98c). Their Small Gain conditions are all under the unity (around 10^{-1}) over the bandwidth (Figures 97a to 98a), which is much lower than those of unweighted models. With the increasing number of cycles, the levels of uncertainty bound are lower and have very similar values at 10 and 14 cycles (see Figure 96). The robust loopshaping bounds are changed dynamically along testing cycles. $\bar{\sigma}(H)$ is always lower than the unity in this case; therefore, $\bar{\sigma}(S)$ is only considered for applicable robustness bound in the identification test moni-

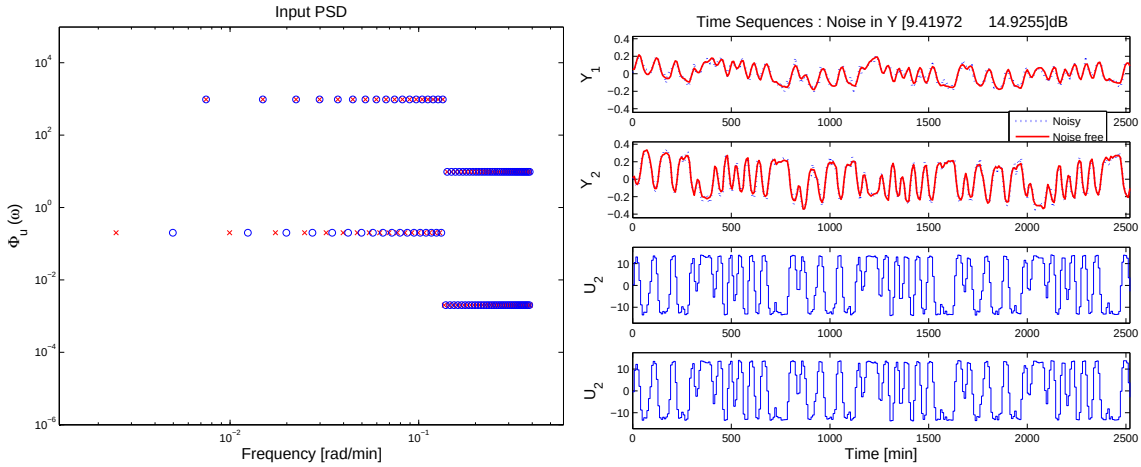

(a) Input PSD (b) Time Sequences

Figure 88. Stage 3a of identification test monitoring for the Jacobsen-Skogestad high purity distillation column: a standard zippered power spectrum design (a) and time series of input and output data (b)

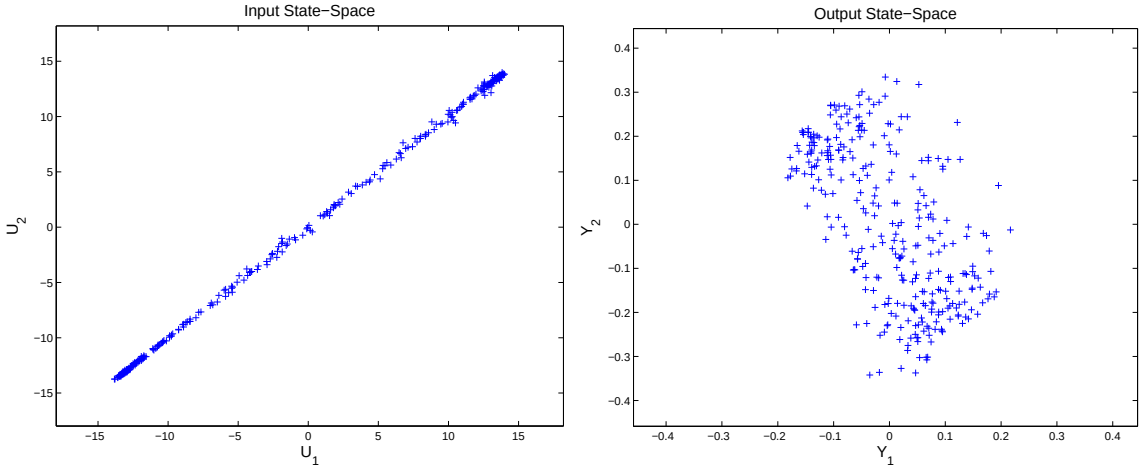

(a) Input State-Space (b) Output State-Space

Figure 89. Stage 3a of identification test monitoring for the Jacobsen-Skogestad high purity distillation column: input (a) and output (b) state-space plots

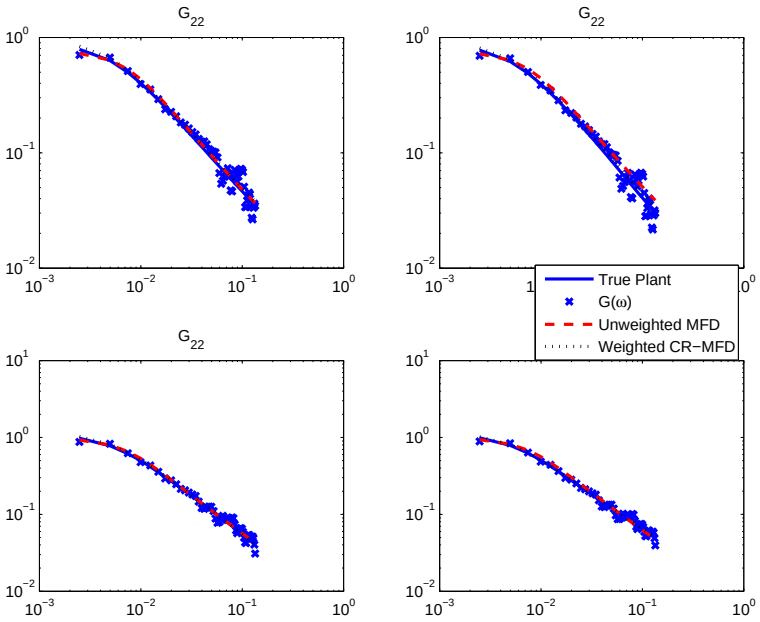

(a) Frequency Responses and Curvefits

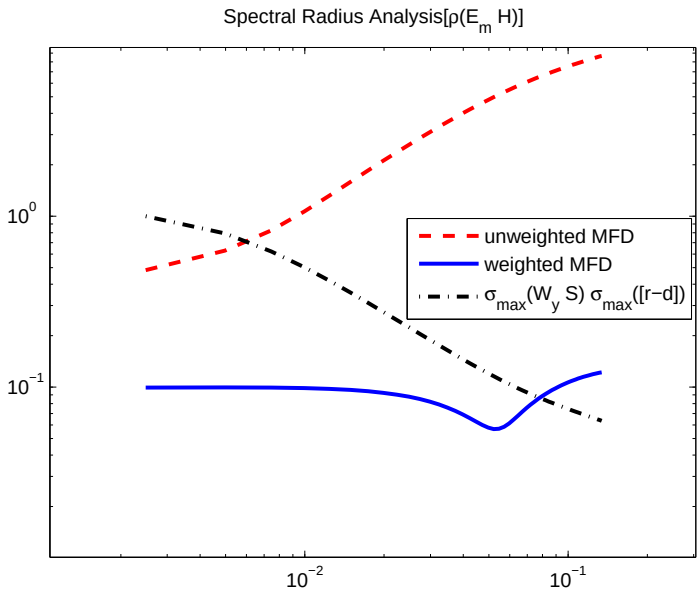

(b) Small Gain Condition $\rho(E_m\hat{H})$

Figure 90. Stage 3a of identification test monitoring for the Jacobsen-Skogestad high purity distillation column:: frequency responses and curvefitting (a) with MPC tuning set: PH=35, MH=5, Ywt=[1 1], and Uwt=[0.05 0.03]*0.13 (a) and Small Gain condition for the unweighted and weighted curvefit models (b)

toring procedure. $\bar{\sigma}(S)$ after 5 cycles is only available for the high frequencies (Figure 97b). After 10 cycles, $\bar{\sigma}(S)$ is computed for a wider range but is partly missing in the low frequencies (Figures 98b). All the low singular value plots show good estimation to the true plant (Figures 97d to 98d). Robust stability analysis is improved with increasing test cycles from 5 to 10 cycles (see Figures 99 and 100).

7.4. Identification Testing Stage 3b based on Closed-loop Identification. Taking advantage of the updated model information from Stage 2, we can apply a narrower bandwidth for designing a phase-shifted multisine reference signal for a closed-loop identification test (Figure 101a). As in Stage 3a, we can decide on design parameters $\tau_{dom}^{H} = 67$, $\tau_{dom}^{L} = 15$, $\alpha = 2$, and $\beta = 3$ that lead to a much shorter bandwidth, i.e., $n_s = 27$ and $N_s = 158$. A multisine reference signal ($r = [\pm 0.2 \ \ \pm 0.2]$) is designed with a shift parameter $D = 79$, which produces the shortest signal for this identification test monitoring scenario (Figure 101b). The MPC controller with tuning parameter used in Stage 2 is applied to Stage 3b. Output signals show effective tracking performance in Figure 101b.

Since controller outputs u involve both reference and output signals, the state-space plot shows that they are correlated and closely aligned to [1 1] direction in Figure 102a. The output state-space produces a square spread in Figure 102b, indicating that the closed-loop identification test enhances balanced gain direction information in the data. Using the experimental data of two cycles, frequency responses are computed using spectral analysis using a Hamming window with 64 lags, and then they are curvefitted for nominal MFD models in the curvefitting procedure (Figure 103a). Similar to Stage 2, the Small Gain condition $\rho(E_m\hat{H})$ of the weighted model is less than the unity over the bandwidth (Figure 103b). In a closed-loop setpoint tracking test, the weighted model shows a desirable performance without offset in Figure 104a. As we can expect, the weighted model displays the accurate low singular values to the true plant (Figure 104b).

7.5. Identification Experiment Testing Results. An effective identification test monitoring procedure based on the high purity distillation column was demonstrated using a series of Guillaume-phasing

multisine signal designs. Table 11 shows the design variables chosen during the identification testing. Because of limited *a priori* knowledge, Stage 1 has the widest bandwidth. As we make progress in ensuing stages, the estimate of the high dominant time constant is decreased to narrow down the excitation bandwidth, resulting in shorter testing signal lengths in Stages 2 and 3. From Stage 1 to Stage 3a (Figure 105a), the input magnitudes are increased to improve the low gain directionality contents in data using modified zippered spectrum designs. This also improves the signal-to-noise ratios in the data.

Stage	Type	τ_{dom}^{H}	τ_{dom}^{L}	α	β	ω^{*}	ω_{*}	$\|u\|$ or $\|r\|$	N_s	n_s	1 cycle (hrs)	# cycles
1	Std. Zip.	194	15	2	3	0.1333	0.0017	$\|u\|$=[0.4 0.4]	916	78	122.13	3
2	Mod. Zip.	106	15	2	2	0.1333	0.0031	$\|u\|$=[12 12]	500	43	66.7	3
3a	Mod. Zip.	67	15	2	3	0.1333	0.0050	$\|u\|$=[14 14]	316	27	42.13	14
3b	Phase-shifted	67	15	2	3	0.1333	0.0050	$\|r\|$=[0.2 0.2]	158	27	21.07	2

Table 11. Design information of multisine input signals during identification test monitoring for Stages 1, 2, and 3: $\gamma = 46.57$, v_2 = [-0.7125 -0.7017] for Stage 2 and $\gamma = 69.45$, v_2 =[-0.7070 -0.7072] for Stage 3a with $hf = 0.1$ and $T = 8$ min. Stages 1, 2, and 3a are performed by open-loop identification test. Stage 3b is performed by closed-loop identification test.

At Stage 1, we applied a standard zippered spectrum with the lowest input magnitude due to limited *a priori* knowledge of the distillation column. However, the output responses produced the largest magnitude because the uncorrelated multisine signals correspond predominantly to the high gain direction. Stage 2 used a slightly shorter modified zippered signal with an increased input magnitude; however, its outputs responded in a similar magnitude. The modified zippered input signals produced improved distribution in the low gain direction, resulting in an effective nominal model with desirable setpoint tracking performance. The benefits of the directional multisine input design and control-relevant curvefitting clearly indicate that the weighted model estimated from the modified zippered spectrum always has lower Small Gain condition and accurate low singular values. Stage 3a considers open-loop identification testing to achieve a robust control system at the cost of the large number of testing cycles, whereas Stage 3b takes advantage of an effective nominal model and MPC controller from Stage 2, enabling a stable closed-loop identification test with the shortest signal length.

At Stage 3a, a modified zippered signal design was more refined and considered a much narrower

excitation bandwidth, applying the largest input magnitude (Figure 105a). A reasonable level of additive uncertainty was estimated after 14 cycles, which led to satisfactory robust loopshaping bounds for the set of models. As we met the sufficient and necessary robustness conditions, we could apply a faster set of MPC controller tuning to the weighted model, producing desirable control performance. However, such a robust control design demanded an extended number of testing cycles and high signal-to-noise ratios to count the conservativeness of the uncertainty bounds used in robust stability and performance analysis. As an alternative yet effective identification test, Stage 3b accomplished the identification test monitoring in a more economical consideration, applying the closed-loop identification test (Figure 105b). The output responses properly followed the $\{\min \mathrm{CF}(r)\}$ multisine reference sequences while improving the low gain directional contents in the data. A corresponding robustness analysis for the closed-loop case was not presented but could be performed. A weighted nominal model from Stage 3b with 2 cycle data produced desirable model performance under noisy conditions.

8. Chapter Summary

In this chapter, a novel paradigm for identification test monitoring has been illustrated with a systematic procedure that utilizes improved process knowledge of a system to design inputs suitable for advanced process control applications. The procedure efficiently takes advantage of an integrated framework that includes multisine input design, frequency response estimation, control-relevant parameter estimation, and robust loopshaping. In the case study, process information from a high purity distillation column is systematically refined, progressing step by step in each identification method component and influencing stage by stage experimental designs. The interactive integration of identification methods leads to refined testing input signals and to developing appropriate model estimates with satisfactory control relevance and robustness.

Informative yet control-relevant input designs with narrower bandwidths are achieved during identification testing. A modified zippered spectrum is applied for this distillation column at Stage 2, and we have refined its design specs from Stage 2 to Stage 3. From the benefits of improved gain directionality in the data, the weighted curvefit models show effective model performance in closed-loop setpoint tracking tests using MPC. Such models obtained by a joint approach of control-relevant curvefitting and directional multisine input designs clearly result in accurate estimation of the low gain directionality. Furthermore, improved model knowledge and availability of an *a priori* MPC controller enables the closed-loop identification test.

An iterative procedure is systematically performed to derive a robust control system between control-relevant curvefitting and robust loopshaping when the level of the estimated uncertainty bound is acceptable. A set of models defined by uncertainty descriptions is taken into account of the robust loopshaping procedure. The additive uncertainty estimation procedure is implemented in support of multisine input signal designs and frequency response estimation methods. Robust loopshaping with structured uncertainty descriptions is implemented and performed to provide sufficient and necessary robust stability and performance conditions. As a result, MPC can be tuned more precisely during control-relevant curvefitting to minimize the tedious trial and error of finding a proper tuning set with robustness. However, a robust control system requires a large number of testing cycles to derive applicable robust loopshaping bounds and a suitable level of model uncertainty bounds. This is a topic that merits further study.

It is, therefore, possible to halt an on-going identification test when a set of models satisfies robust stability and performance conditions. The use of the identification test monitoring framework enables the design of a robust control system for multivariable systems while addressing strong interaction, ill-conditioning, and gain directionality with improved effectiveness. The proposed identification test monitoring framework has demonstrated its usefulness through testing scenarios involving both open and closed-loop designs.

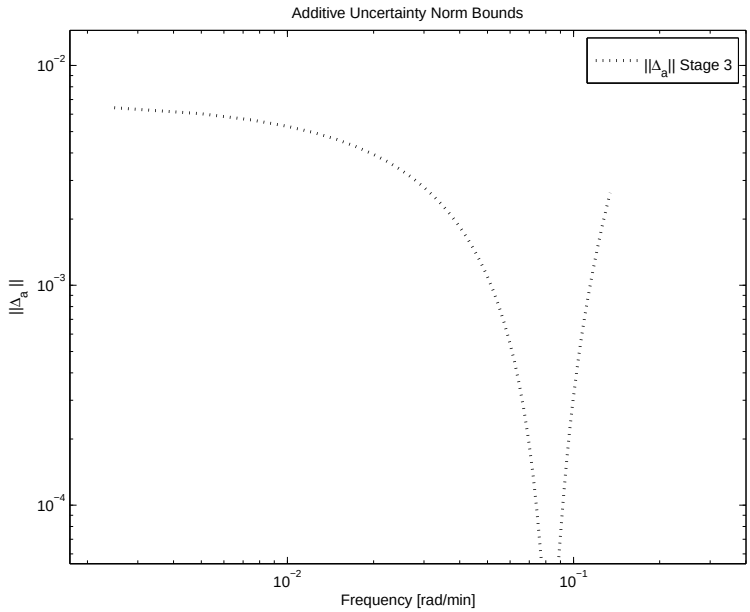

Figure 91. Stage 3a of identification test monitoring for the Jacobsen-Skogestad high purity distillation column: additive model uncertainty norm bound with 14 cycles

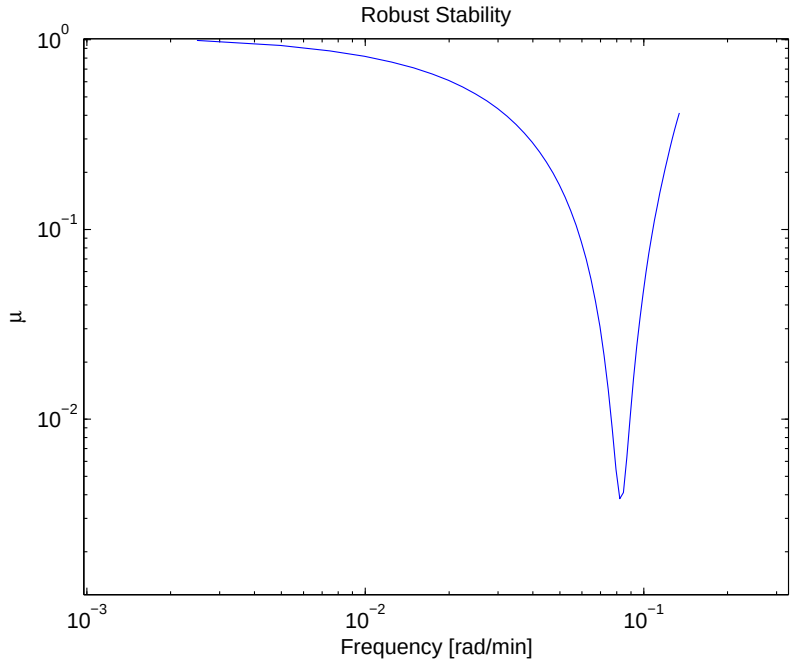

Figure 92. Stage 3a (at 14 cycles) of identification test monitoring for the Jacobsen-Skogestad high purity distillation column: robust stability analysis

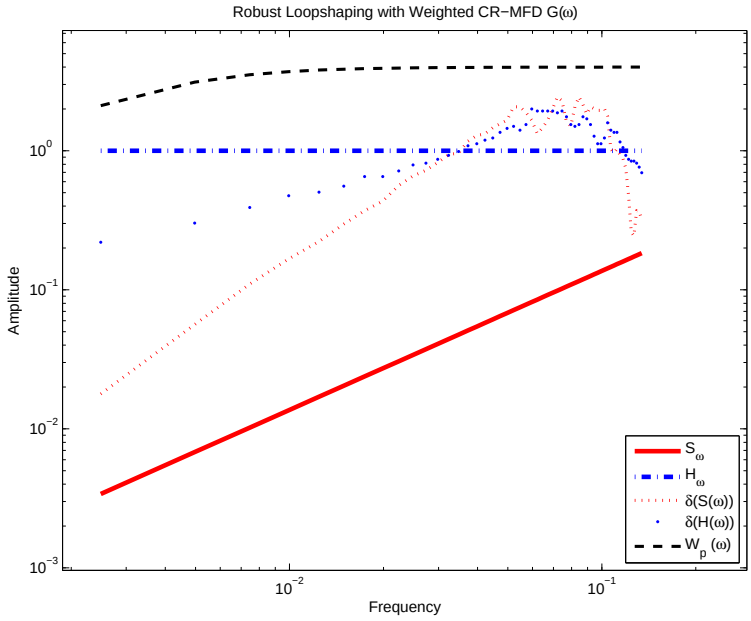

Figure 93. Stage 3a of identification test monitoring for the Jacobsen-Skogestad high purity distillation column: robust loopshaping bounds on $\hat{P}$ with MPC tuning set: PH=35, MH=5, Ywt=[1 1], and Uwt=[0.05 0.03]*0.13

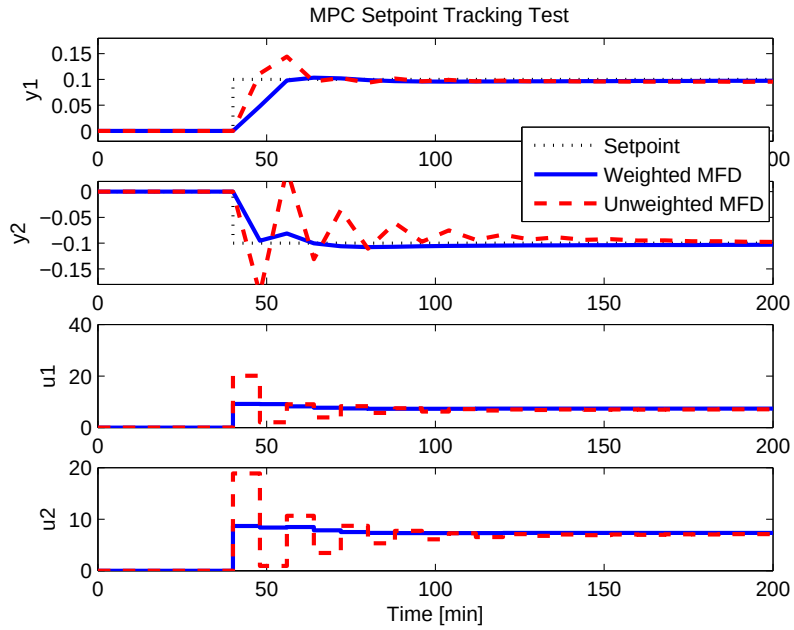

Figure 94. Stage 3a of identification test monitoring for the Jacobsen-Skogestad high purity distillation column: setpoint (r=[0.1 -0.1]) tracking test with MPC, MPC tuning set: PH=35, MH=5, Ywt=[1 1], and Uwt=[0.05 0.03]*0.13

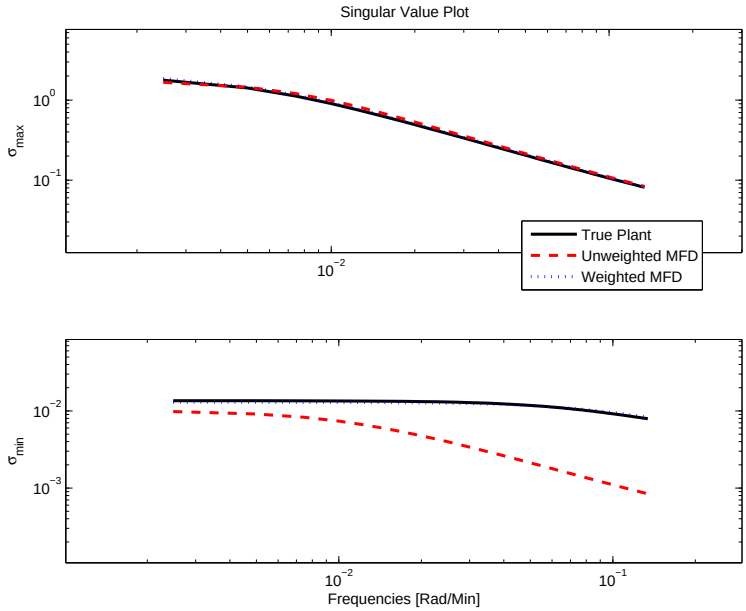

Figure 95. Stage 3a of identification test monitoring for the Jacobsen-Skogestad high purity distillation column: singular values of true plant vs. estimated models in frequency domain, MPC tuning set: PH=35, MH=5, Ywt=[1 1], and Uwt=[0.05 0.03]*0.13

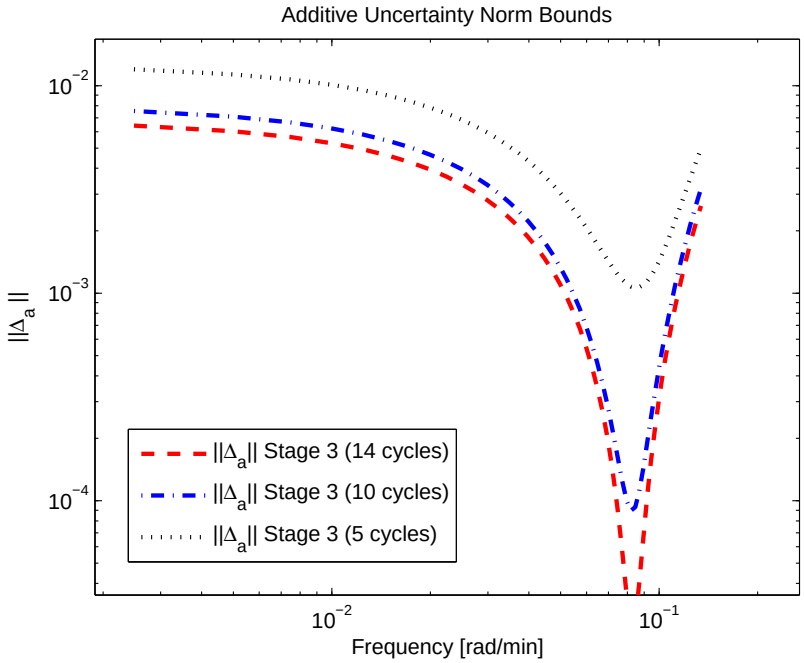

Figure 96. Stage 3a of identification test monitoring for the Jacobsen-Skogestad high purity distillation column: additive uncertainty norm bounds at 5, 10, and 14 cycles

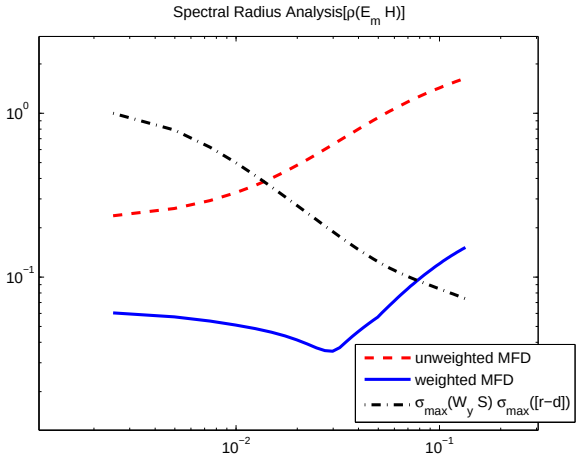

(a) Small Gain condition $\rho(E_m\hat{H})$

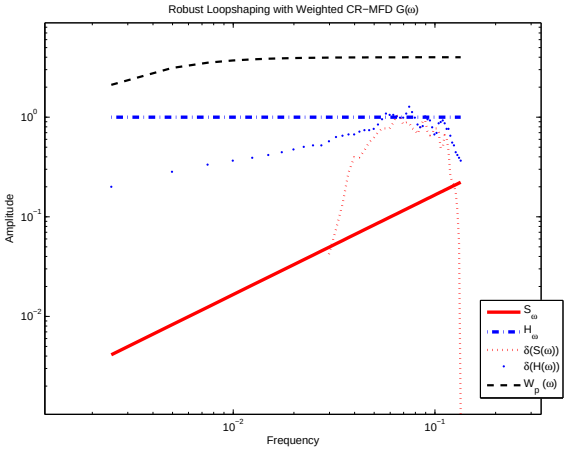

(b) Robust Loopshaping on $\hat{P}$

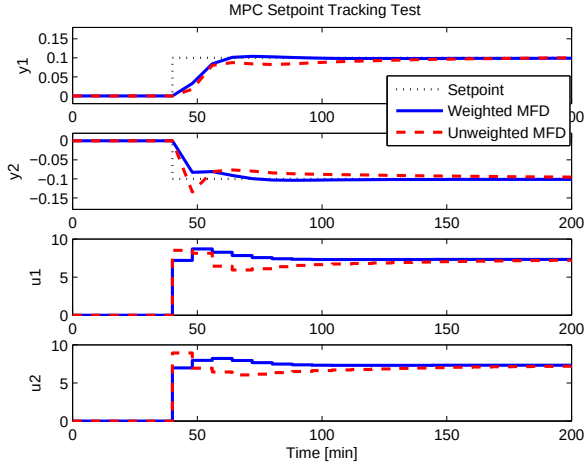

(c) Setpoint Test

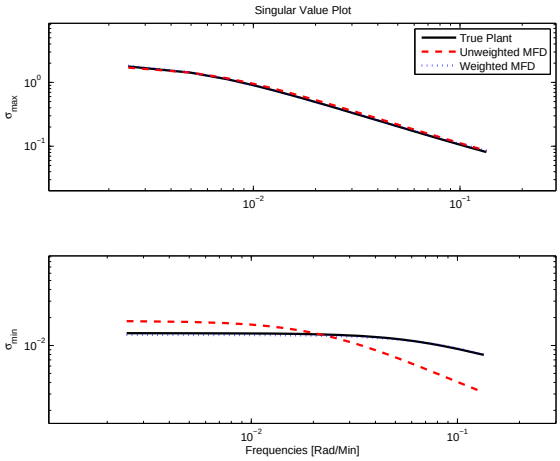

(d) Singular Values

Figure 97. Stage 3a of identification test monitoring (at $n_{cycles} = 5$) for the Jacobsen-Skogestad high purity distillation column: Small Gain condition (a), robust loopshaping (b), MPC setpoint test (c), and singular values (d) with MPC tuning set: PH=35, MH=5, Ywt=[1 1], and Uwt=[0.05 0.03]*0.2

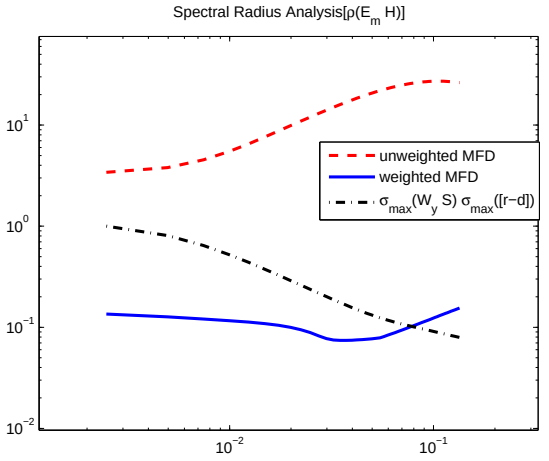

(a) Small Gain condition $\rho(E_m\hat{H})$

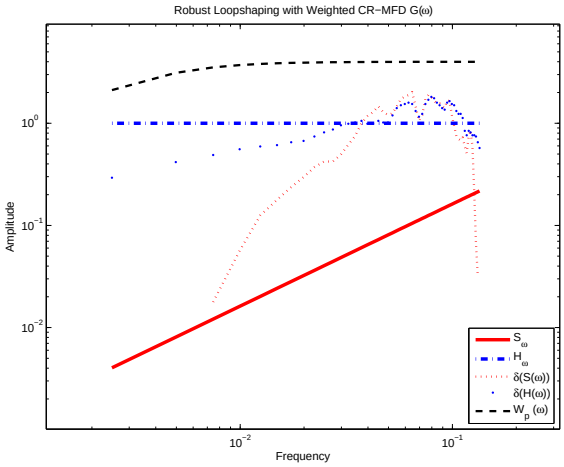

(b) Robust Loopshaping on $\hat{P}$

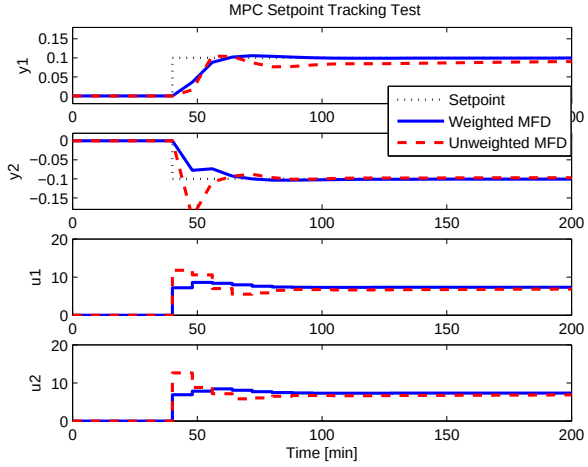

(c) Setpoint Test

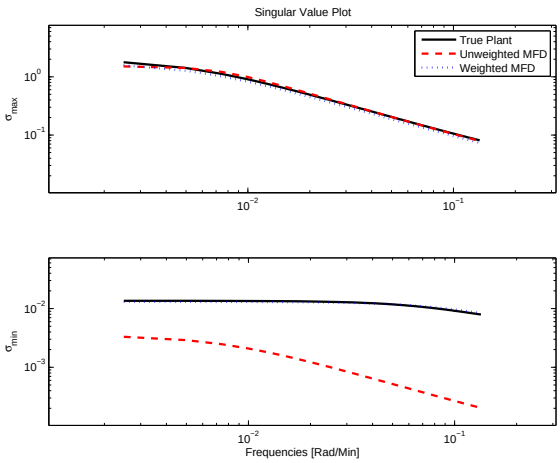

(d) Singular Values

Figure 98. Stage 3a of identification test monitoring (at $n_{cycles} = 10$) for the Jacobsen-Skogestad high purity distillation column: Small Gain condition (a), robust loopshaping (b), MPC setpoint tracking test (c), and singular values (d) with MPC tuning set: PH=35, MH=5, Ywt=[1 1], and Uwt=[0.05 0.03]*0.2

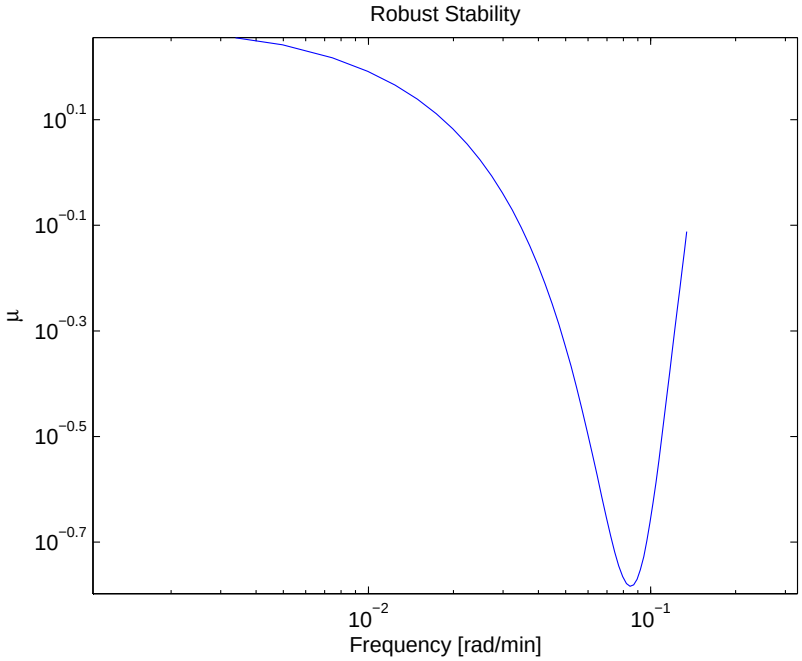

Figure 99. Stage 3a (at 5 cycles) of identification test monitoring for the Jacobsen-Skogestad high purity distillation column: robust stability analysis

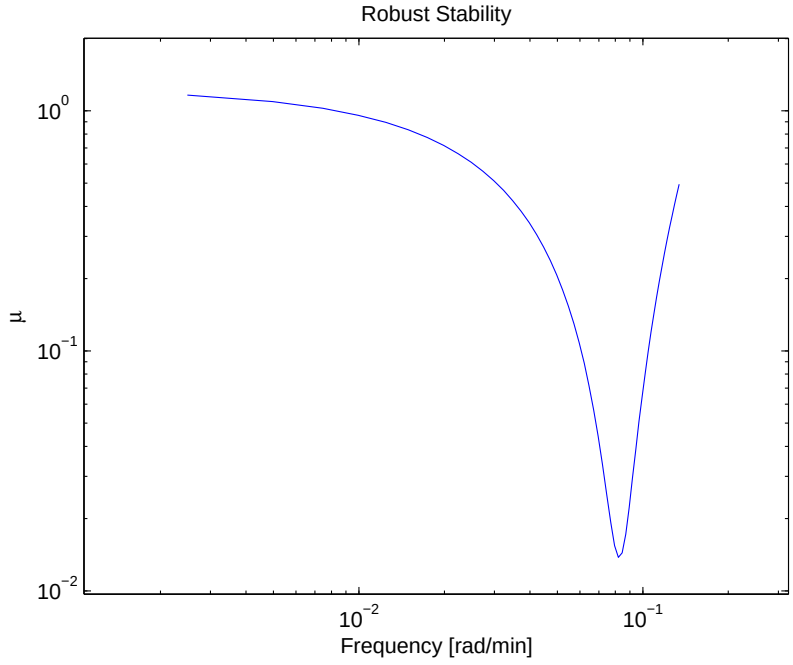

Figure 100. Stage 3a (at 10 cycles) of identification test monitoring for the Jacobsen-Skogestad high purity distillation column: robust stability analysis

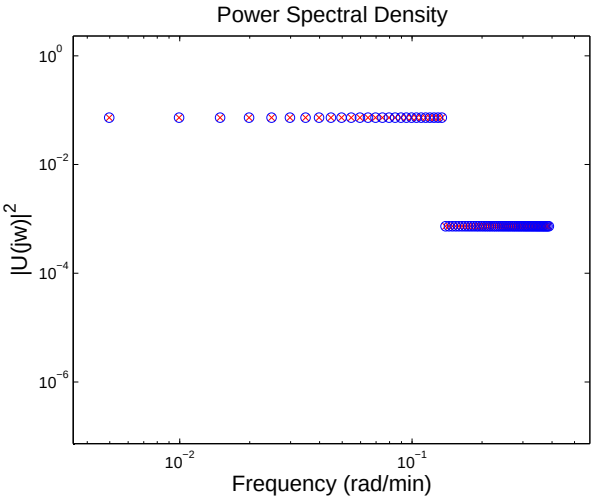

(a) Reference PSD

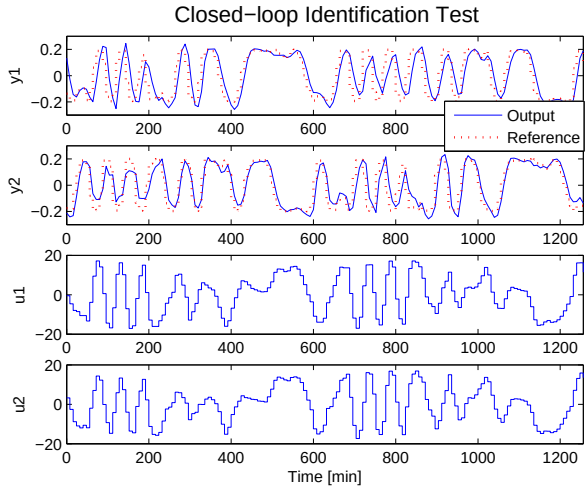

(b) Time Sequences

Figure 101. Stage 3b of identification test monitoring for the Jacobsen-Skogestad high purity distillation column: a phase-shifted multisine design for reference signals in closed-loop identification test (a) and time series of input, output, and reference signals (b)

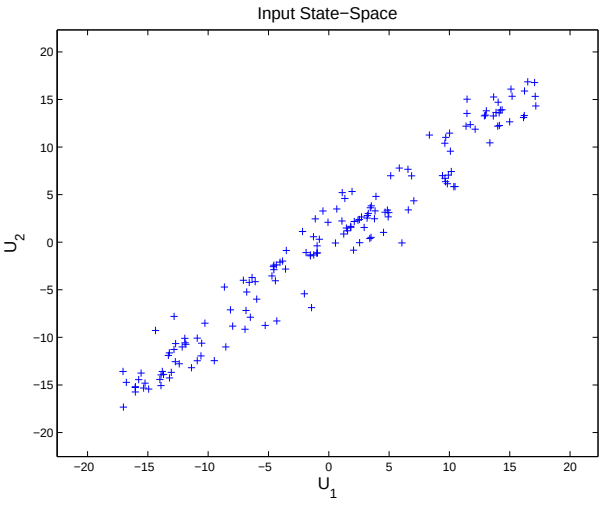

(a) Input State-Space

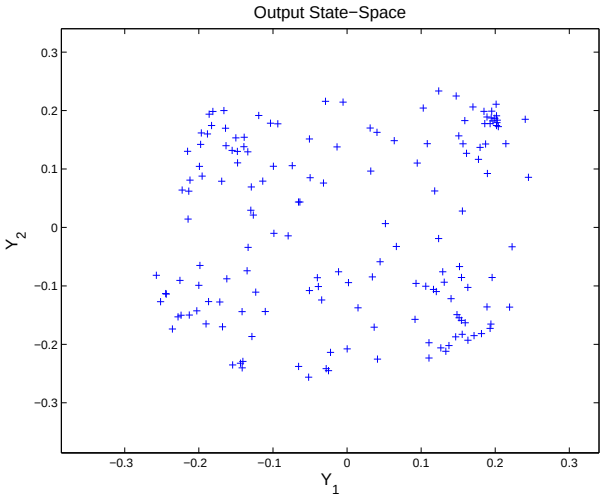

(b) Output State-Space

Figure 102. Stage 3b of identification test monitoring for the Jacobsen-Skogestad high purity distillation column: input (a) and output (b) state-space plots

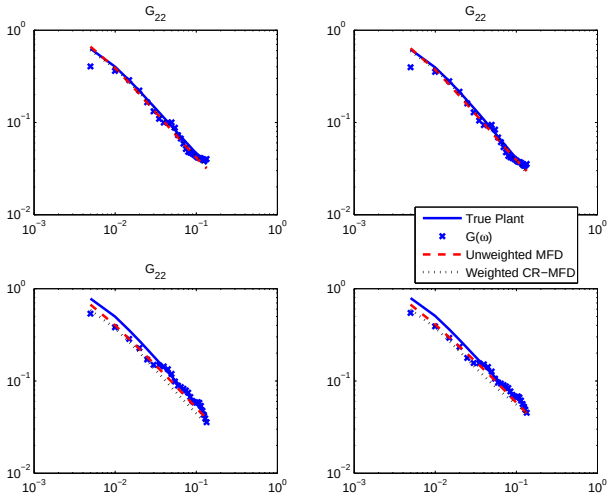

(a) Frequency responses and curvefits

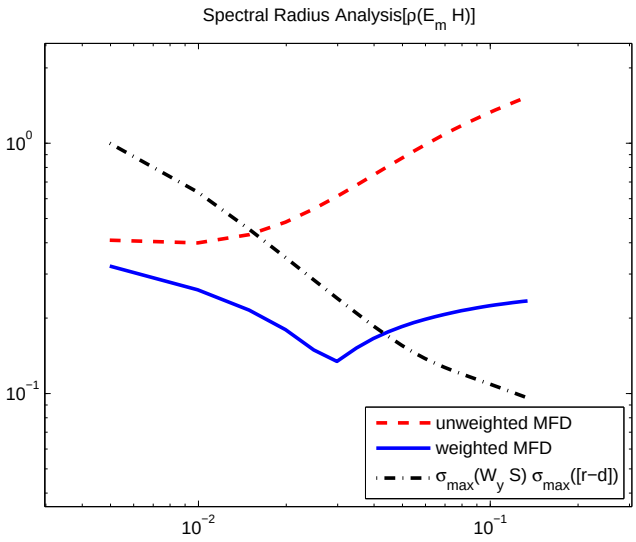

(b) Small Gain condition $\rho(E_m\hat{H})$

Figure 103. Stage 3b of identification test monitoring for the Jacobsen-Skogestad high purity distillation column: frequency response curvefitting (a) and Small Gain condition (b) with MPC tuning set: PH=35, MH=5, Ywt=[1 1], and Uwt=[0.05 0.03]*0.2

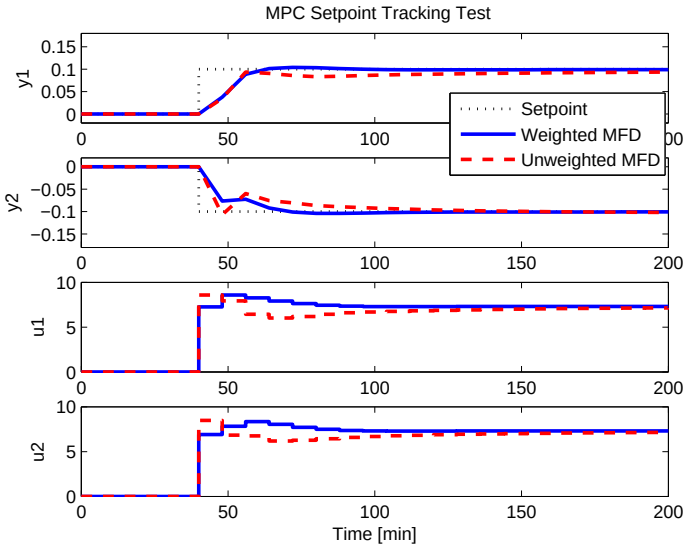

(a) Setpoint Test

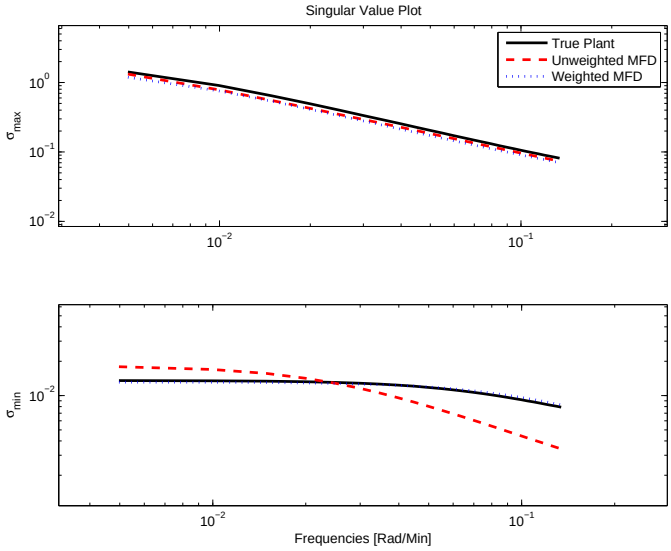

(b) Singular Values

Figure 104. Stage 3b of identification test monitoring for the Jacobsen-Skogestad high purity distillation column: MPC setpoint tracking test (a) and singular values (b) with MPC tuning set: PH=35, MH=5, Ywt=[1 1], and Uwt=[0.05 0.03]*0.2

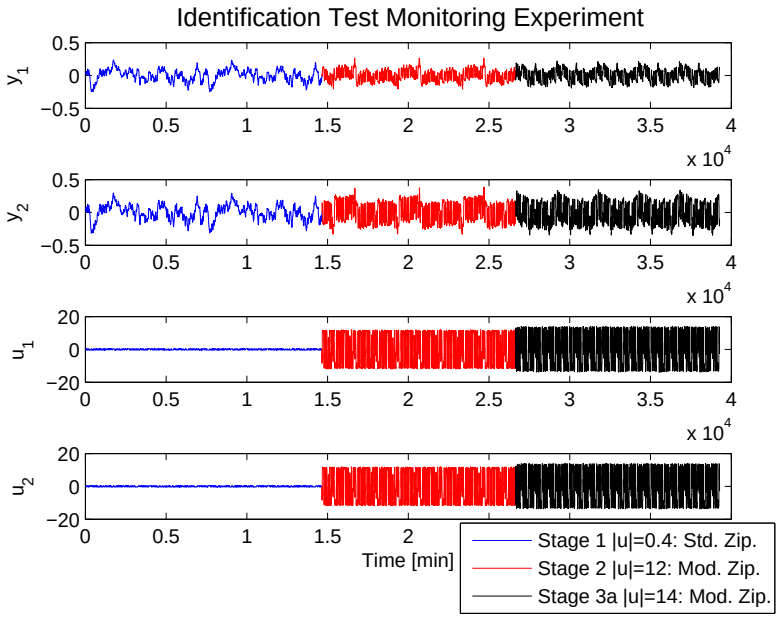

(a) Stages 1, 2, and 3a (five cycles only)

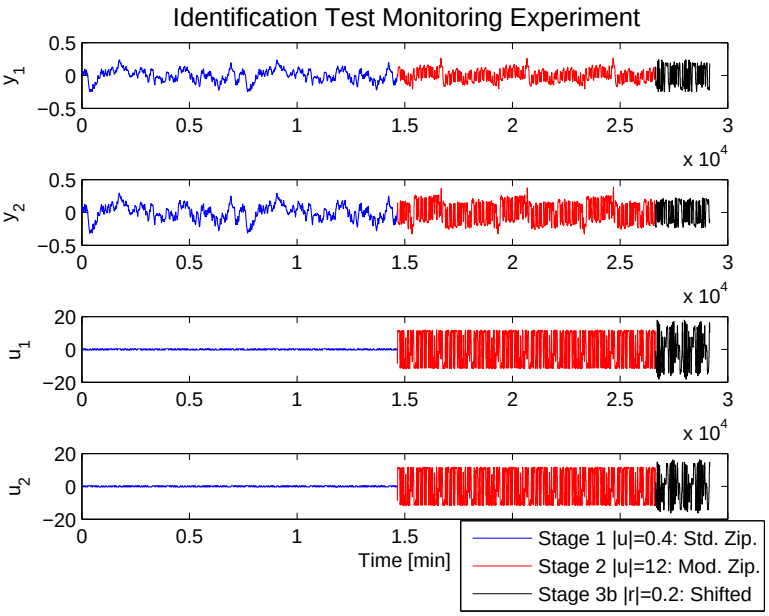

(b) Stages 1, 2, and 3b

Figure 105. Identification test monitoring experiments with Stages 1 (three cycles), 2 (three cycles), and 3a (five of fourteen cycles): open-loop (a) and Stages 1 (three cycles), 2 (three cycles), and 3b (two cycles): closed-loop (b)

CHAPTER 5

DATA-CENTRIC INPUT DESIGN AND MODEL-ON-DEMAND ESTIMATION METHODOLOGY

The flexible design capabilities of the multisine input enable a novel approach to input signal design suited for data-centric modeling algorithms. This chapter will examine the design of constrained, "plant-friendly" multisine input signals based on a geometric discrepancy criterion of Weyl's Theorem. Such signals are meaningful for estimation methods where uniform coverage of the output state-space is critical. The effectiveness of data resulting from a Weyl criterion-based signal is demonstrated for the Weischedel-McAvoy distillation column case study using Model-on-Demand Model Predictive Control, a data-centric multivariable optimization-based control algorithm.

1. Introduction

In recent years, there has been significant interest in data-centric dynamic modeling frameworks such as Just-in-Time modeling (Cybenko, 1996) and Model-on-Demand (MoD) estimation (Stenman, 1999). The appeal of these modeling approaches is that they enable nonlinear estimation while reducing the structural decisions made by the user and maintaining reliable numerical computations. The performance of these methods, however, is highly dependent upon the availability of quality, informative databases, and conse-

quently, good experimental designs are an imperative. An important consideration in experimental design for these estimation methods is to achieve uniform coverage of regressors in the database. This chapter examines the development of multisine input designs that meet this criterion while satisfying plant-friendliness constraints during identification testing.

As a member of the family of data-centric modeling techniques, Model-on-Demand (MoD) estimation provides accurate predictions of nonlinear systems with few user decisions. Furthermore, MoD estimation is achieved without solving a non-convex optimization problem, as is usually the case with global modeling techniques such as neural networks and wavelets (Braun *et al.*, 2001; Stenman *et al.*, 1996; Su and McAvoy, 1997). While the accuracy of such models offers a potentially significant improvement over linear models, the process engineer is faced with the daunting tasks of selecting the model structure, initializing the optimization routine, and subsequent model reduction. However, novel data-centric modeling techniques such as MoD estimation method are focused on accurate predictions of nonlinear systems without such extended effort. Our focus is on generating outputs particularly close to process operating ranges from an informative dataset. As a result, one is able to obtain a local model with sufficiently accurate process dynamics to the specified operating conditions while avoiding complex nonlinear model structures or global modeling procedures. Moreover, a MoD-MPC tool that has been formulated as meaningful for nonlinear process control applications, as developed by Braun *et al.* (2001) and Stenman *et al.* (1996), is examined with the Weischedel-McAvoy nonlinear distillation column in this chapter.

The idea of uniformly distributed experimental designs for system identification relying on multisine signals has previously been examined by Duym and Schoukens (1995), who rely on minimizing an objective function quantifying the real and actual discrepancy from a user-defined grid. A more general approach that we present in this dissertation is to rely on the principles of geometric discrepancy theory (Matousek, 1999) as a means for achieving uniformity of the data in a regressor space. This is accomplished by minimizing a discrepancy function made up of trigonometric polynomials arising from Weyl's Theorem that insure that

the points are equidistant on a state-space. The optimization problem calls for minimizing this discrepancy function on the anticipated outputs of the system, subject to the restrictions of an orthogonal “zippered” spectrum (used to enable multi-channel implementation) and simultaneously enforcing plant-friendliness time-domain constraints on upper and lower limits, move sizes, and rates of change in either (or both) input and output signals. The optimization problem is solved using a state-of-the-art NLP solver (KNITRO 3.1) which uses an interior point trust region method and employs SQP techniques to solve the barrier subproblems.

This chapter is organized as follows: Section 2 presents a brief overview of Model-on-Demand estimation technique as meaningful for data-centric modeling. Section 3 describes the Weyl criterion that defines the geometric discrepancy objective including an example based on a linear highly interactive system per the plant Model0 (2.46). Section 4 illustrates the results of a more demanding case study based on the nonlinear Weischedel-McAvoy distillation column. Finally, Section 5 presents the summary and conclusions.

2. Model-on-Demand Modeling Methodology

Model-on-Demand is a data-centric, nonlinear black-box estimation method which enhances the classical local modeling problem. In MoD, an adaptive bandwidth selector determines the size of data to be used for the local regression. The data is weighted using a kernel or weighting function. A local regression is performed using a linear or quadratic model to estimate the plant output at each time step; all observations are stored on a database and the models are built ‘on demand’ as the actual need arises. Local modeling techniques such as the MoD predictor use only small portions of data, relevant to the region of interest, to determine a model as needed. The variance/bias tradeoff inherent to all modeling is optimized locally by adapting the number of data and their relative weighting. As a consequence, the non-convex optimization problem associated with most global nonlinear modeling techniques is avoided. Moreover, the

user is presented with fewer decisions regarding model structure and can use intuition developed from linear model identification as the basis for obtaining an accurate nonlinear model. MoD estimation consists of two sub-problems: local modeling and database searching; Figure 106 presents a scheme of the MoD estimation.

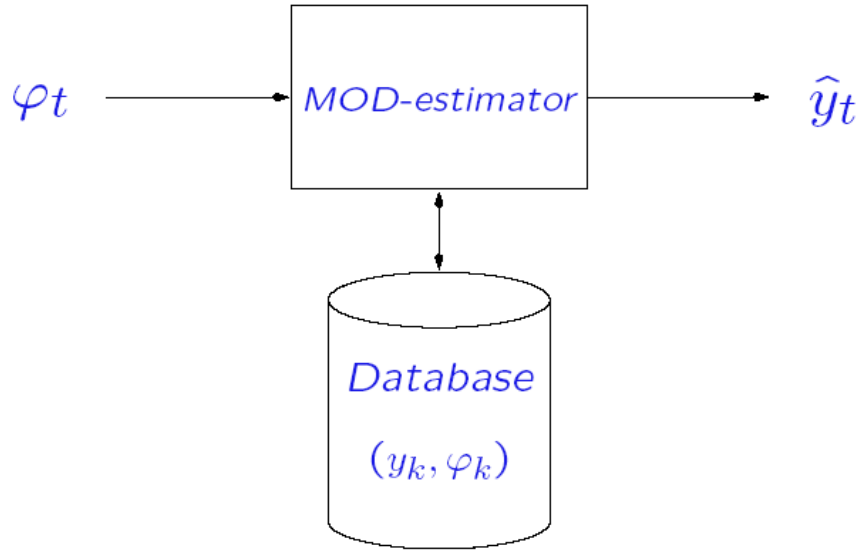

Figure 106. A Scheme of Model-on-Demand Estimator, from Stenman's presentation at CDC, 1999

2.1. Local Modelling. The MoD modeling formulation is described with a SISO process based on the approach of Stenman (1999) and Stenman *et al.* (1996). Consider a SISO process with nonlinear ARX structure, i.e.,

$$y(k) = m(\varphi(k)) + e(k), \qquad k = 1, \ldots, M \tag{5.1}$$

where $m(\cdot)$ is an unknown nonlinear mapping and $e(k)$ is an error term modeled as random variables with zero mean and variance σ_k^2. The MoD predictor attempts to estimate output predictions based on a local neighborhood of the regressor space $\varphi(t)$ (Stenman *et al.*, 1996). The regressor vector is of the form

$$\varphi(t) = [y(t-1) \quad \ldots \quad y(t-n_a) \;\; u(t-n_k) \quad \ldots \quad u(t-n_b-n_k)]^T \tag{5.2}$$

where n_a, n_b, and n_k denote the number of previous outputs and inputs and the degree of delays in the model.

A local estimate $\hat{y}$ can be obtained from the solution of the weighted regression problem

$$\hat{\beta} = \arg\min_{\hat{\beta}} \sum_{k=1}^{N} \ell(y(k) - \hat{m}(\varphi(k),\, \hat{\beta})) \times W\left(\frac{\|\varphi(k) - \varphi(t)\|_M}{h}\right) \tag{5.3}$$

where $\ell(\cdot)$ is a quadratic norm function, $\|u\|_M \triangleq \sqrt{u^T M u}$ is a scaled distance function on the regressor space, h is a bandwidth parameter controlling the size of the local neighborhood and $W(\cdot)$ is a window function (usually referred to as the kernel) assigning weights to each remote data point according to its distance from $\varphi(t)$ (Braun *et al.*, 2002*b*). The window is typically a bell-shaped function with bounded support. These weights can be chosen to minimize the point-wise mean square error of the estimate. Assuming a local linear model structure,

$$m(\varphi(t), \beta) = \beta_0 + \beta_1^T (\varphi(k) - \varphi(t)) \tag{5.4}$$

a quadratic norm, $\ell(e) = e^2$, is used and the model is then linear in the unknown parameters. The estimate can easily be computed using least squares methods. If β_0 and β_1 denote the minimizers of (5.3) using the model from (5.4), a one-step ahead prediction is given by

$$\hat{y}(t) = m(\varphi(t), \hat{\beta}) = \hat{\beta}_0 \tag{5.5}$$

Each local regression problem produces a single prediction $\hat{y}(t)$ corresponding to the current regression vector $\varphi(t)$. To obtain prediction at other locations in the regressor space, the weights change and new optimization problems must be solved. This stands in contrast to the global modeling approach where the model is fitted to data only once and then discarded. However, in a neighborhood around $\varphi(t)$, the local linear model is an input-output linearization. The bandwidth h controls the neighborhood size and has a critical impact on the resulting estimate since it governs a trade-off between the bias and variance errors of the estimate. Traditional bandwidth selectors produce a single global bandwidth; in MoD estimation, a bandwidth is computed adaptively at each prediction.

2.2. Database Searching. It is essential to provide a relevant dataset with the MoD estimator. The relevance of dataset can be interpreted into the closeness to the current operating points of the process. Furthermore, the constraints on the controlled variables invoke a region of data space where local modeling tasks are required. Such a data region can be divided into smaller regions based on operating conditions for the local modeling procedure, as shown in Figure 107.

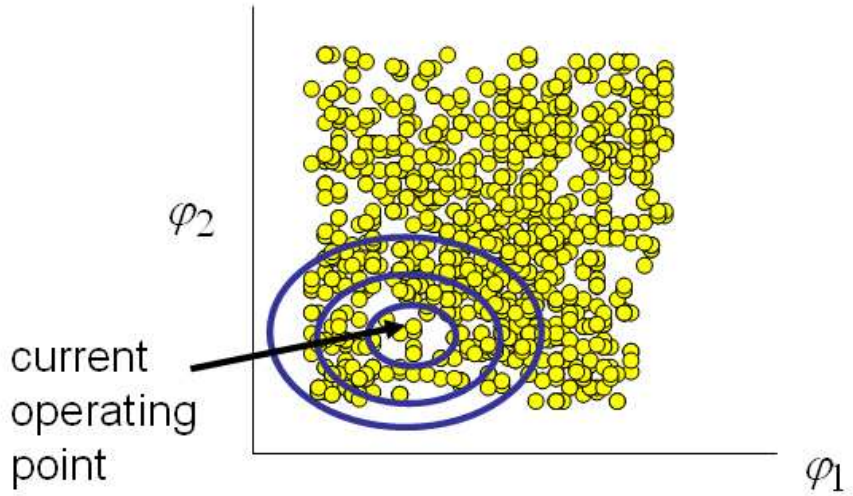

Figure 107. A selection of a data region from the stored database for MoD estimation

The needs of building a relevant database can be solved with multisine input signal design problem formulations subject to constraints on outputs in a manner of plant-friendliness. Objective functions such as the crest factor minimization or geometric discrepancy provide useful datasets for MoD estimations based on process or user specification. The uniformity distribution approach reduces the concerns of model structure dependence on the quality of the dataset. Therefore, a MoD estimator can be implemented as a useful means for local modeling of nonlinear systems by developing plant-friendly optimization problem formulations, leading to data-centric multisine input signal design.

2.3. Model-on-Demand Model Predictive Control. Estimated MoD models can be incorporated into a Generalized Predictive Control (GPC) framework for nonlinear control (aka. MoD-MPC) per the

objective function based on Meadows and Rawlings (1997). A MoD-MPC toolbox in Matlab/Simulink developed by Stenman (1999) and Braun *et al.* (2002*b*) is utilized in this chapter. This in turn makes it possible to evaluate the control peformance of models estimated from the data of the proposed data-centric input signals based on the Weyl-objective approach and the minimum crest factor multisine signals. The detailed information for MoD-MPC formulation is available from Stenman (1999) and Braun *et al.* (2002*b*).

3. Uniform Distribution of Infinite Sequences - The Weyl Criterion

Discrepancy theory deals with the distribution of points in space (Matousek, 1999). The Weyl criterion (Weyl, 1916) gives the necessary and sufficient conditions for a sequence to be uniformly distributed in $[0,1)^d$, the d-dimensional unit interval. The criterion for a two-dimensional sequence can be summarized as follows:

Theorem. (H. Weyl, 1916) A sequence $\{y_1(k), y_2(k)\}$ is equidistributed in $[0,1)^2$ if and only if

$$\lim_{N\to\infty} \frac{1}{N} \sum_{k=1}^{N} e^{2\pi i(l_1 y_1(k) + l_2 y_2(k))} = 0 \tag{5.6}$$

$\forall$ sets of integers l_1, l_2 not both zero.

Decomposing (5.6) into real and imaginary parts we obtain that the sequence $\{y_1(k), y_2(k)\}$ is equidistributed in $[0,1)^2$ if and only if for all sets of integers l_1, l_2 (not both zero) the following conditions hold:

$$\lim_{N\to\infty} \frac{1}{N} \sum_{k=1}^{N} \cos[2\pi(l_1 y_1(k) + l_2 y_2(k))] = 0 \tag{5.7}$$

and

$$\lim_{N\to\infty} \frac{1}{N} \sum_{k=1}^{N} \sin[2\pi(l_1 y_1(k) + l_2 y_2(k))] = 0 \tag{5.8}$$

The Weyl criterion was first applied in this way and adapted to the problems considered in this dissertation from Pendse (2004). The Weyl criterion can be readily extended to higher dimensions, as needed by the requirements of the problem under consideration.

3.1. An Illustrative Example Problem. To illustrate the effectiveness of the Weyl criterion for signal design, we consider a highly interactive system based on the linear distillation column per Equation (2.46) as

$$y(s) = \frac{1}{75s+1}\begin{bmatrix} 87.8 & -86.4 \\ 108.2 & -109.6 \end{bmatrix} u(s) \tag{5.9}$$

where $y(s)$ and $u(s)$ are the Laplace transform of the output and input signals to the system, respectively. When sampled at a T sampling interval, (5.9) becomes

$$y_1(k) = a\,y_1(k-1) + b\,(87.8\,u_1(k-1) - 86.4\,u_2(k-1)) \tag{5.10}$$

$$y_2(k) = a\,y_2(k-1) + b\,(108.2\,u_1(k-1) - 109.6\,u_2(k-1)) \tag{5.11}$$

where $a = e^{\frac{-T}{75}}$ and $b = (1-a)$.

3.2. Constrained Problem Formulation. Our goal is to design an input signal that is uniformly distributed and as such has good directionality information in the output state space of the system; the latter goal is an important requirement when working with highly interactive multivariable systems (Morari and Zafiriou, 1988). This assumes *a priori* knowledge of the plant model as either an equation or a computer program that is available to the optimizer. We introduce two cycles of input each of length N_s and let the transients die out in the first cycle ($k = 0, \ldots, N_s - 1$) of the output. As before, the input $u(k)$ and output $y(k)$ are vectors with two components. To design a plant friendly signal we impose bound constraints on both $u(k)$ and/or $y(k)$ in the second cycle,

$$|z(k)| \le C_z, \qquad k = N_s, \ldots, 2N_s - 1 \tag{5.12}$$

where C_z are user defined constants and z is one of y_1, y_2, u_1, u_2. The restrictions can be imposed on the move size of $u(k)$ and $y(k)$, which is the difference between successive values in $u(k)$ and $y(k)$ such that

$$|z(k+1)-z(k)| \leq \Delta C_z,\ k = N_s-1,\ldots,2N_s-2 \tag{5.13}$$

where ΔC_z are user defined constants. The prediction of the plant output response must be determined from a model estimated from previous identification tests or otherwise obtained *a priori* knowledge. These relationships are:

$$y_1(k) = f_1(u_1,u_2,y_1,y_2),\ k = 0,\ldots,2N_s-1 \tag{5.14}$$

$$y_2(k) = f_2(u_1,u_2,y_1,y_2),\ k = 0,\ldots,2N_s-1 \tag{5.15}$$

f_1 and f_2 indicate the dependence of y_1 and y_2 on the values of the vectors u_1, u_2, y_1 and y_2; these correspond to the sampled data representation for (5.9). The inputs $u_1(k)$ and $u_2(k)$ are chosen per the multisine input signal:

$$u_j(k) = \sum_{i=1}^{(m+1)n_s} \sqrt{2\alpha_{ji}}\cos(\omega_i kT + \phi_{ji}), \quad j = 1,2 \tag{5.16}$$

where $\omega_i = \frac{2\pi i}{N_s T}$, n_s is the number of sinusoids length, and m is the number of input channels.

Fourier coefficients for a modified zippered spectrum are described below:

$$\alpha_{ij} = \begin{cases} \geq 0, & i = j,\ (m+1)+j,\cdots,(m+1)(n_s-1)+j \\ \geq 0, & i = m+1,\ 2(m+1),\cdots,n_s(m+1) \\ = 0, & \text{for all other } i \text{ up to } (m+1)n_s \end{cases} \tag{5.17}$$

In this Chapter, our goal is to uniformly distribute the points $(y_1(k),y_2(k))$ in the output state space region $[-C_{y_1},C_{y_1}) \times [-C_{y_2},C_{y_2})$ based on the Weyl Criterion. Since the Weyl Criterion deals with uniform distributions in $[0,1)^2$, a change of variables is considered

$$\hat{y}_1(k) = \frac{y_1(k)+C_{y_1}}{2C_{y_1}}, \quad \hat{y}_2(k) = \frac{y_2(k)+C_{y_2}}{2C_{y_2}} \tag{5.18}$$

With a finite number of points in the sequences, we choose an integer L and form the set S as follows

$$S = \{x : x \in Z \text{ and } |x| \leq L\} \tag{5.19}$$

where Z is the set of all integers and W corresponds to

$$W = \{(l_1, l_2) : l_1 \in S, l_2 \in S \text{ and } (l_1, l_2) \neq (0,0)\} \tag{5.20}$$

Then, the optimizer minimizes the sum in Equations (5.7) and (5.8) for all elements of the set W considering the "Weyl" constraint on the second cycle ($k = N_s + 1, \ldots, 2N_s - 1$) of the output. The optimization is carried out to estimate the amplitudes and phases $\alpha_{i1}, \alpha_{i2}, \phi_{i1}, \phi_{i2},\ i = 1, \ldots, (m+1)n_s$ of the $m = 2$ multisine input channels. The complete problem statement is as follows:

$$\min_{t, \alpha_{i1}, \alpha_{i2}, \phi_{i1}, \phi_{i2}} t \tag{5.21}$$

s.t.

$$\sum_{k=N_s+1}^{2N_s-1} \cos[2\pi(l_1 \hat{y}_1(k) + l_2 \hat{y}_2(k))] \leq t, \forall\ (l_1, l_2) \in W$$

$$\sum_{k=N_s+1}^{2N_s-1} \sin[2\pi(l_1 \hat{y}_1(k) + l_2 \hat{y}_2(k))] \leq t, \forall\ (l_1, l_2) \in W$$

$$t \geq \varepsilon$$

as well as is subject to constraints per Equations (5.12)-(5.18). The lower bound constraint on t is imposed to promote faster convergence. ε is chosen to be some small positive constant.

3.3. Design Variables for the Weyl Criterion. To better understand the influence of design variables L and ε on the distribution of points in the output state space, we perform two experiments using the example problem per (5.9) with the bound and move sizes shown in Table 12 (Pendse, 2004).

C_{y_1}	C_{y_2}	ΔC_{y_1}	ΔC_{y_2}	ΔC_{u_1}	ΔC_{u_2}
0.5	0.5	0.47	0.47	2.2	2.2

Table 12. Bound and move sizes used for the plant Model0 per Equation (2.46)

3.3.1. *Experiment 1.* In the first experiment, ε is fixed at a value of 10^{-3} and L varies. The distribution of points in the output state space obtained for two different simulations with $L = 2$ and 6 is shown in Figure 108; Pendse (2004) contains simulations for $L = 3$, 4, and 5. It can be seen that by increasing L, the uniformity in the output state space distribution improves dramatically. An increase in the design variable L seems to move the various clusters of points at different places in the state space to achieve an approximation to a uniform distribution.

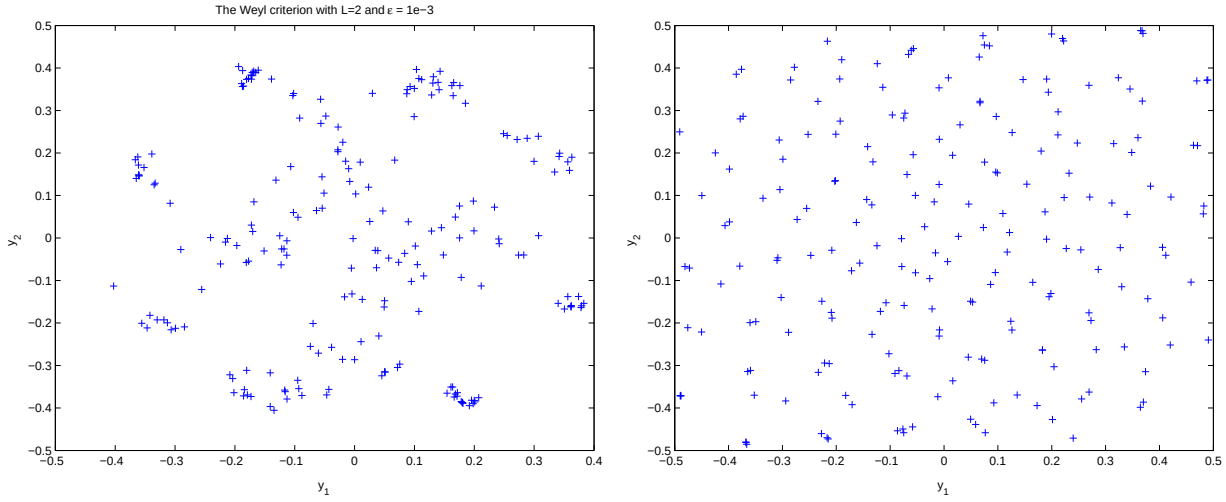

(a) $L = 2$ (b) $L = 6$

Figure 108. Output state space comparison for the plant Model0 per (2.46), $L = 2$ (a) and $L = 6$ (b), $\varepsilon = 10^{-3}$

3.3.2. *Experiment 2.* In the second experiment, $L = 3$ is fixed and ε varies. From Experiment 1, a low value of L gives a relatively poor distribution; the effect of changing ε is then easier to decipher on a relatively poor distribution than with a good distribution. A series of simulations with ε values ranging from $10^{-2}$to 10^{-6} can be found in Figure 109. Decreasing the value of ε tends to keep the various clusters of points in more or less the same position but leads to a redistribution of points within the same cluster. Given this information, there is not much to gain by decreasing ε beyond a certain limit; it is much more advantageous to increase L instead.

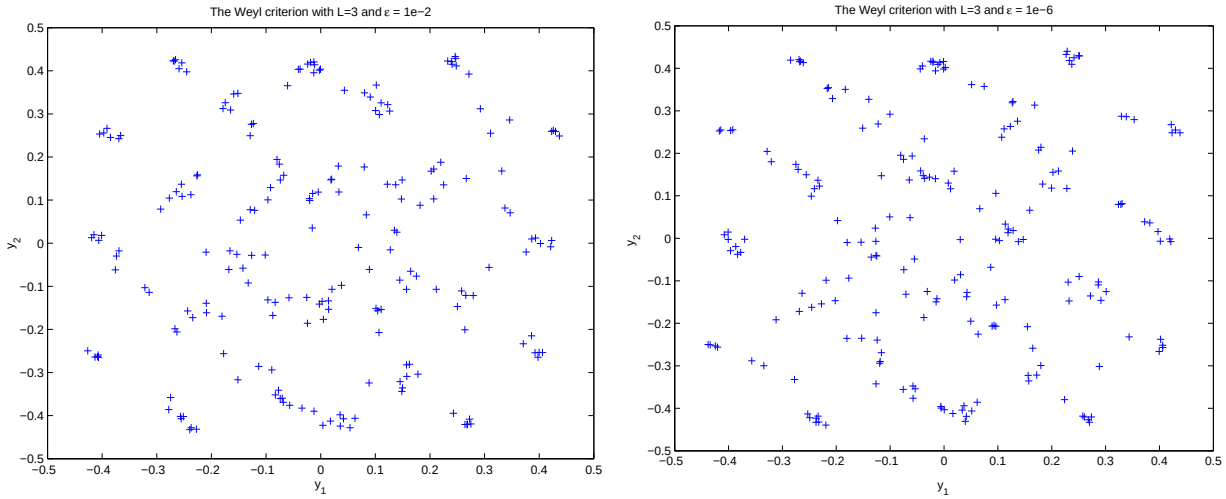

(a) $\varepsilon = 10^{-2}$ (b) $\varepsilon = 10^{-6}$

Figure 109. Output state space comparison for the Example problem, $\varepsilon = 10^{-2}$ (a) and $\varepsilon = 10^{-6}$ (b), $L = 3$

The following can be noted while attempting to satisfy the Weyl criterion under certain limitations:

- *Limited Data:*

  Weyl's theorem has an infinite summation; however, only a finite amount of data is used in the second cycle of the system output. Given this fact, an asymptotic approach can be used to achieve a uniform distribution with the Weyl theorem.

- *Weyl Grid Resolution:*

  The sufficient conditions to ensure a uniform distribution (5.7) and (5.8) should hold true for all sets of integers l_1 and l_2. However, this enforcement is impractical, and a finite implementation is utilized with the sets S and W, respectively, defined in (5.19) and (5.20). There is a considerable amount of flexibility in choosing these sets. It is clear from Experiment 1 that the selection of larger sets S and W would result in a closer approximation to equations (5.7) and (5.8) and therefore a better output space distribution. Increasing L in the set S also increases the size of W at a rate approximately proportional to L^2. It is, therefore, desirable to select a reasonable value of the parameter L. Experiment 1 revealed

that $L = 6$ is a "reasonably good" value.

- *Tolerance Value ε:*

  The Weyl criterion requires the limit on the left hand side of (5.7) and (5.8) to go to zero as $N \to \infty$. Using a finite amount of data, one is only able to make this sum "small enough". Specifically, there is no straightforward way to choose ε. In Experiment 2, decreasing ε does not create new clusters at different locations but leads to a redistribution of points within the same cluster. There is no considerable effect of decreasing ε beyond a certain limit; it is much more advantageous to increase L instead. Nonetheless, a low value of ε can be used in the optimization problem.

4. Case Study: Nonlinear High-Purity Distillation Process

4.1. Input Signal Design and Comparison to Minimum Crest Factor Approaches. A challenging multivariable process system that benefits from judiciously applied system identification techniques is high purity distillation; the methanol-ethanol distillation column model developed by Weischedel and McAvoy (1980) is commonly used as a benchmark problem (Sriniwas *et al.*, 1995). To address the demands of highly interactive systems, one approach is to modify the standard multisine signal to contain correlated harmonics with high levels of power, which improve the low gain-direction content in the data and promote better coverage of the output state-space. The optimization approach per Chapter 2 in this dissertation considers minimizing crest factor (CF), the ratio of the ℓ_∞ (or Chebyshev) norm and the ℓ_2-norm of a signal x (Guillaume *et al.*, 1991). In Chapter 2, a low crest factor indicates that most of the elements in the sequence are distributed near their extremum values. Design parameters for the Weischedel-McAvoy problem determined on the basis of the guidelines in Chapter 2 using dominant time constant estimates ($\tau_{dom}^{L} = 5$ and $\tau_{dom}^{H} = 20$ min) and user choices of $\delta = 0$, $\alpha_s = 2$, and $\beta_s = 3$ lead to parameter settings of $T = 2$ minutes, $n_s = 189$, and $N_s = 378$. A value of the amplification factor $\gamma = 15$ was chosen for a min CF(y) signal with

modified spectrum; the resulting input spectrum for this signal is shown in Figure 110 a. Constraints applied to the problem and salient characteristics of these signals are summarized in Table 13; an output state-space plot is shown in Figure 111 a.

A significant benefit of an optimization-based problem formulation for signal design is that nonlinear model forms can be readily incorporated in the design procedure, which results in an improved ability to both meet plant-friendliness requirements as well as address the directionality and uniform distribution requirements in the output for demanding applications. A polynomial Nonlinear Auto-Regressive with eXternal (NARX) input model with structure as proposed by Sriniwas *et al.* (1995) (see Chapter 2 in this dissertation):

$$\begin{aligned} y(k) &= \theta^{(0)} + \sum_{i=1}^{n_y} \theta_i^{(1)} y(k-i) + \sum_{i=\rho}^{n_u} \theta_i^{(2)} u(k-i) + + \sum_{i=1}^{n_y} \sum_{j=1}^{i} \theta_{(i,j)}^{(3)} y(k-i)y(k-j) \\ &+ \sum_{i=\rho}^{n_u} \sum_{j=\rho}^{i} \theta_{(i,j)}^{(4)} u(k-i)u(k-j) + \sum_{i=1}^{n_y} \sum_{j=\rho}^{n_u} \theta_{(i,j)}^{(5)} y(k-i)u(k-j) + \ldots \end{aligned} \tag{5.22}$$

was estimated for the Weischedel-McAvoy column and used to generate output predictions for the optimizer in both the min CF(y) and Weyl-based signal design scenarios.

The benefits of the Weyl-based formulation over the minimum crest factor signal design in producing a uniform distribution in the output state-space of the data can be clearly seen by contrasting Figures 111 a and 111 b: the use of the Weyl-based criterion results in a much more uniformly distributed coverage of the state-space and a much better suited dataset for data-centric estimation purposes. The uniform distribution of the output within the bounds specified in the problem results in a natural balance between the high and low gain information content in the data. From Table 13 one does notice, however, that the improvement in output state space uniformity is obtained at the cost of higher crest factor, which consequently reduces the signal-to-noise ratio of the data in a noisy data setting. As a result, there is an inherent tradeoff between these objectives that needs to be recognized. One way of addressing this issue in practical input design is to include maximum crest factor bounds as inequality constraints within the Weyl problem formulation; these

can be readily incorporated in the numerical optimization framework described in this paper.

An important difference between these signal designs is observed in the input spectra (Figure 110). In the min CF (y) case, only the phases and a subset of the Fourier coefficients in the high frequency range of the multisine signal are chosen by the optimizer, while for the Weyl-based design, the optimization problem includes a search for *all* Fourier coefficients and phases, including those corresponding to the correlated harmonics; this can be seen in Figure 110 b. Not only do these extra degrees of freedom in the optimizer contribute to the improved performance, they reduce the number of decisions made *a priori* by the user, leading to a more practical design procedure.

4.2. Application to Model-on-Demand Estimation and Predictive Control. From a practical standpoint, MoD estimation allows process engineers to naturally extend insight gained from linear modeling to nonlinear identification and control. Rather than spending time in a difficult structure selection and parameter initialization, the user can focus on developing informative datasets – a common requirement for all nonlinear black-box identification approaches. The user can fully examine the uniformity of coverage the excitation signals produced in the input and output spaces (as done in the previous subsection) and better understand the impact it has on the nonlinear model validation and control problem. MoD can be formulated into a comprehensive methodology for nonlinear identification and predictive control (Braun, 2001; Braun *et al.*, 2000). A Matlab-based tool for MoD estimation and control, developed by ASU's Control Systems Engineering laboratory in collaboration with researchers from the Division of Automatic Control at Linköping University, is available in the public domain (Braun *et al.*, 2002*a*).

First, open-loop Model-on-Demand (MoD) estimation is evaluated for the Weischedel-McAvoy distillation column for estimation purposes using the data arising from the signal designs described in Chapter 2. For validation purposes, a different data-centric signal with lower magnitude bounds was considered, which is shown in Figure 112. For all cases, an implicit Nonlinear ARX structure is used in the MoD estimator,

with k_{min}=20, k_{max}=756, and local polynomial order = 1 as additional MoD estimation parameters (Braun *et al.*, 2001; Stenman, 1999).

Analysis of the results shows that data resulting from the min CF(*u*) signal based on the standard zippered spectrum provides the worst results of all three cases considered. Because the input-output data resulting from this signal lacks information content in the [1 -1] output direction, it results in the poorest prediction on the validation data set (Figure 113). For data resulting from the min CF(*y*) signal with modified spectrum, most of the output sequence is located near its minimum and maximum values, but its corresponding MoD model still seems to produce reasonable predictions in an open-loop sense with a percent unexplained variance of 0.5% (Figure 114). Nonetheless, because of the even state-space distribution, the MoD model estimated from the Weyl-based approach results in the most accurate predictions of all signals considered, with a percent unexplained variance close to 0.09% (Figure 115).

The min CF(*y*) and Weyl-based MoD models are subsequently evaluated in a closed-loop setting using the MoD-MPC Toolbox (Braun *et al.*, 2002*a*); the min CF(*u*) MoD model was not considered in the closed-loop evaluation because a stable controller response could not be obtained. In both cases the tuning parameters are PH=35, MH=15, Ywt=[1 0; 0 1] and Uwt=[7 0; 0 7]. A series of setpoint changes that represent challenges to controller performance for a highly interactive plant, such as high-purity distillation, are shown in Figure 116. While stable responses are obtained in both cases, the MoD-MPC controller relying on the Weyl-based data shows faster settling time, less overshoot, and less interaction than the one resulting from the min CF(*y*) MoD model; these desirable performance features of the Weyl-based MoD-MPC controller point to the effectiveness of this class of signals for closed-loop control purposes in a demanding process application.

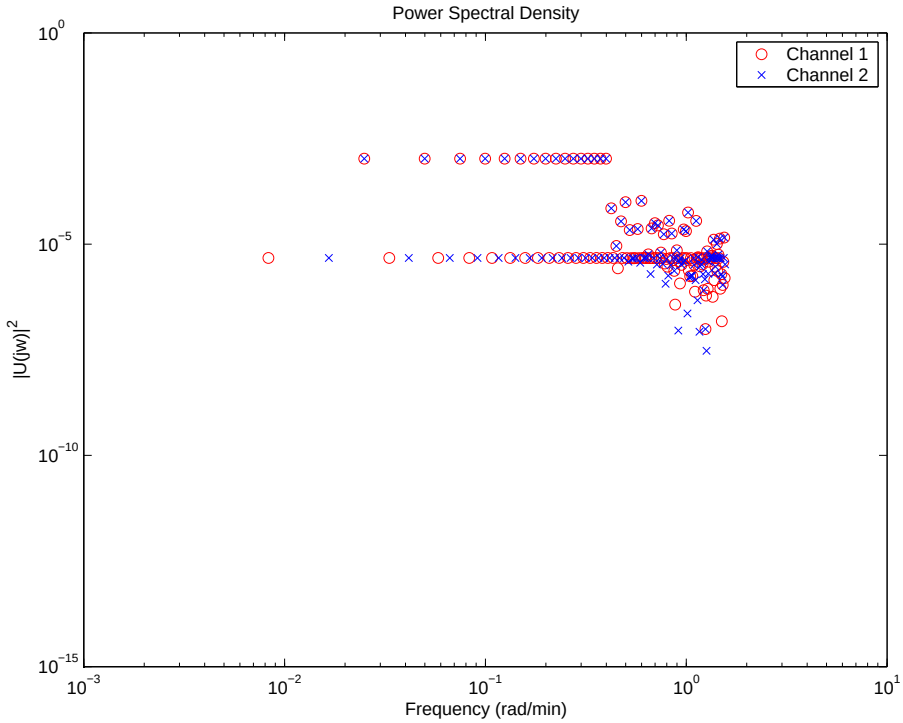

(a) min CF (*y*)

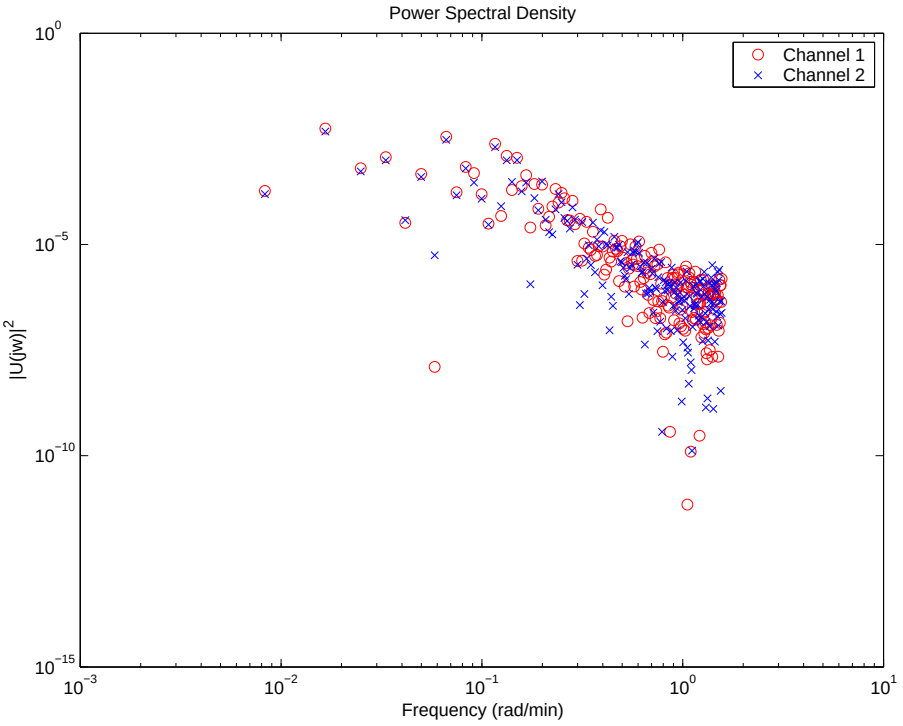

(b) Weyl-based Approach

Figure 110. Input power spectral densities for Weischedel-McAvoy distillation column: min CF(*y*) (a) versus Weyl-based design (b)

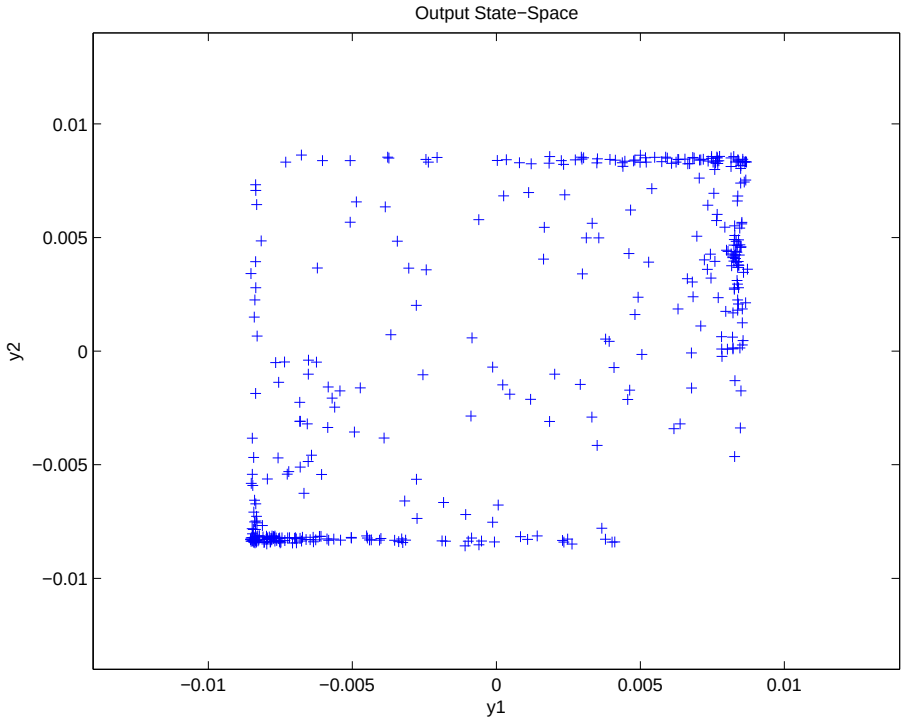

(a) min CF (*y*)

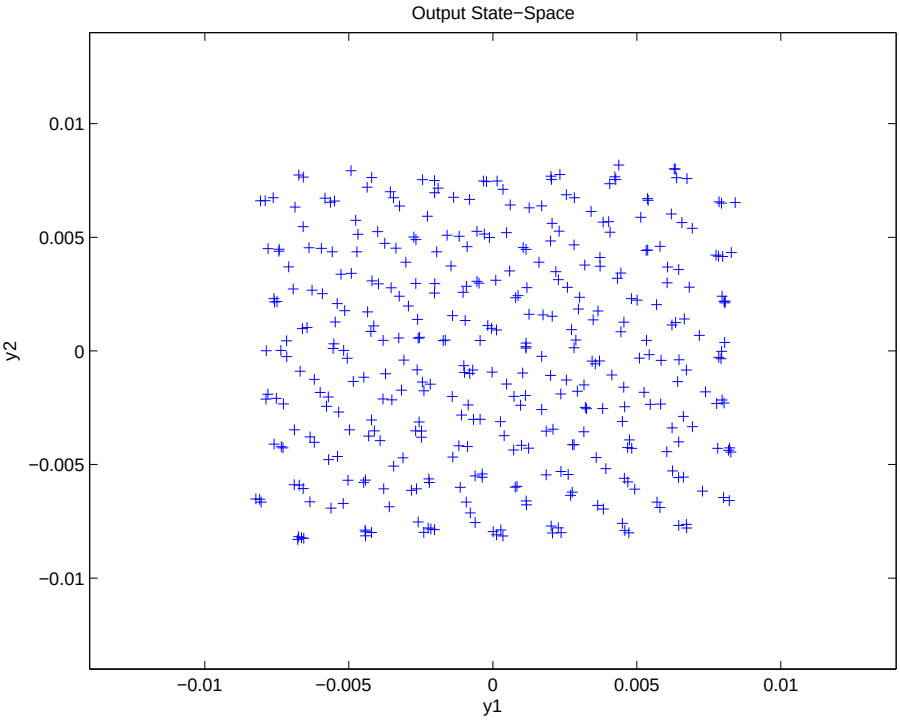

(b) Weyl-based Approach

Figure 111. Output state-space analysis for Weischedel-McAvoy distillation column: min CF(*y*) (a) versus Weyl-based design (b)

Type	Signal (x)	CF(x)	PIPS(%)	max Δx	max x	min x
min CF (u) design; a standard zippered spectrum	u_1	1.21	82.43	0.0025	0.0020	-0.0020
	u_2	1.22	81.77	0.0026	0.0020	-0.0020
	y_1	2.48	48.84	0.0037	0.0325	-0.0211
	y_2	2.19	46.12	0.0031	0.0199	-0.0204
min CF(y) design; a modified zippered spectrum using NARX model prediction $\|\Delta u\| \leq 0.01$, $\|\Delta y\| \leq 0.008$ & $\|y\| \leq 0.0085$	u_1	3.74	31.51	0.0100	0.0365	-0.0254
	u_2	3.25	34.37	0.0100	0.0316	-0.0250
	y_1	1.30	77.45	0.0051	0.0088	-0.0086
	y_2	1.31	77.01	0.0082	0.0087	-0.0086
data-centric experiment using NARX model, subject to $\|\Delta u\| \leq 0.01$, $\|\Delta y\| \leq 0.08$ & $\|y\| \leq 0.0085$	u_1	2.78	37.52	0.0079	0.0292	-0.0268
	u_2	2.50	41.28	0.0076	0.0240	-0.0225
	y_1	1.79	56.54	0.0062	0.0084	-0.0082
	y_2	1.76	57.13	0.0053	0.0082	-0.0083

Table 13. Results summary for signals designed for the Weischedel-McAvoy distillation column Case Study.

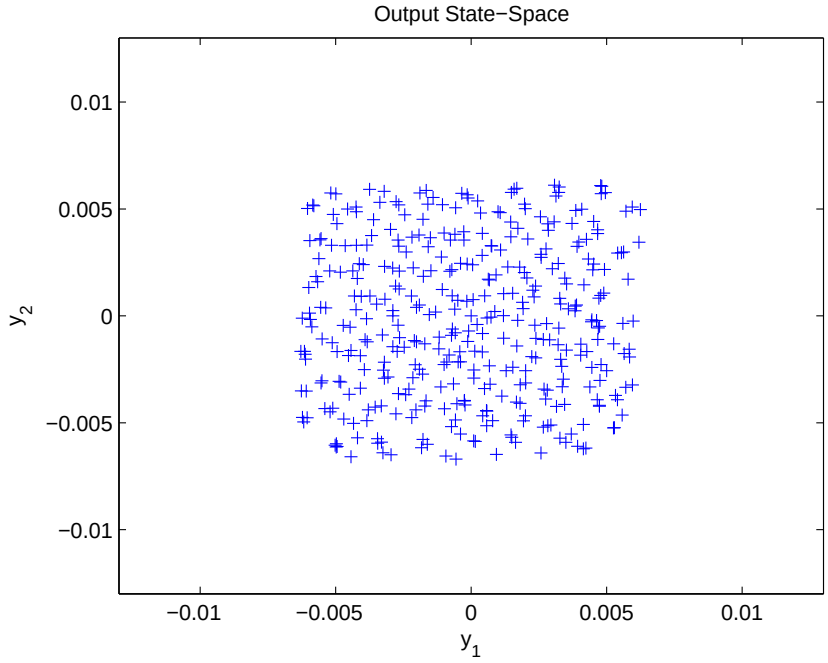

Figure 112. Validation data's output state-space for Weischedel-McAvoy distillation column

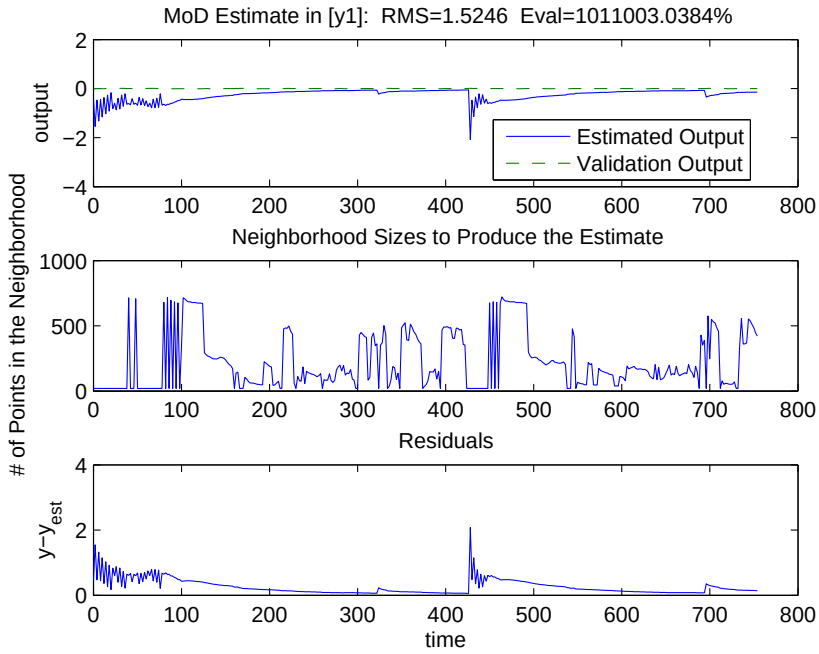

(a) Output 1 (y_1)

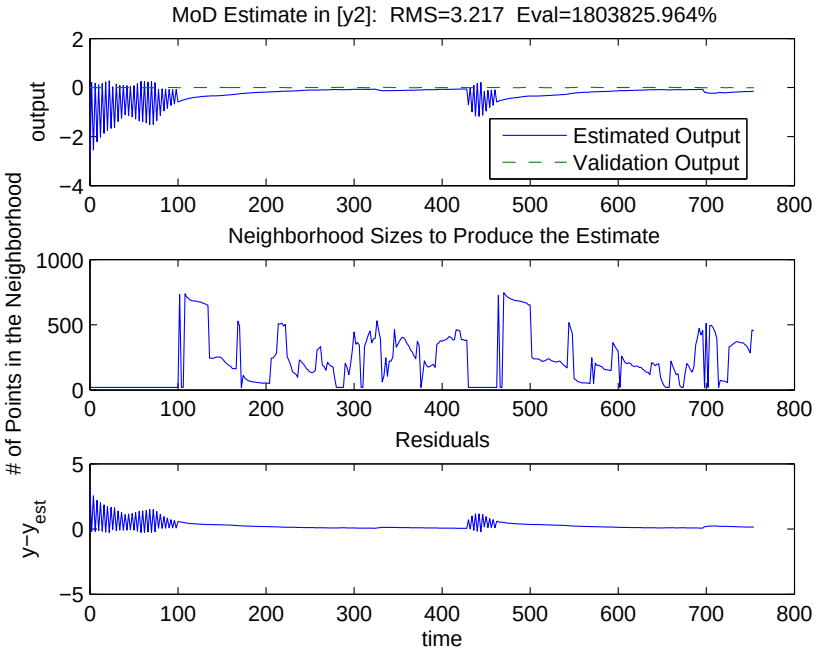

(b) Output 2 (y_2)

Figure 113. MoD estimation and validation results for Weischedel-McAvoy distillation column data arising from a min CF (u) signal using the standard zippered spectrum design

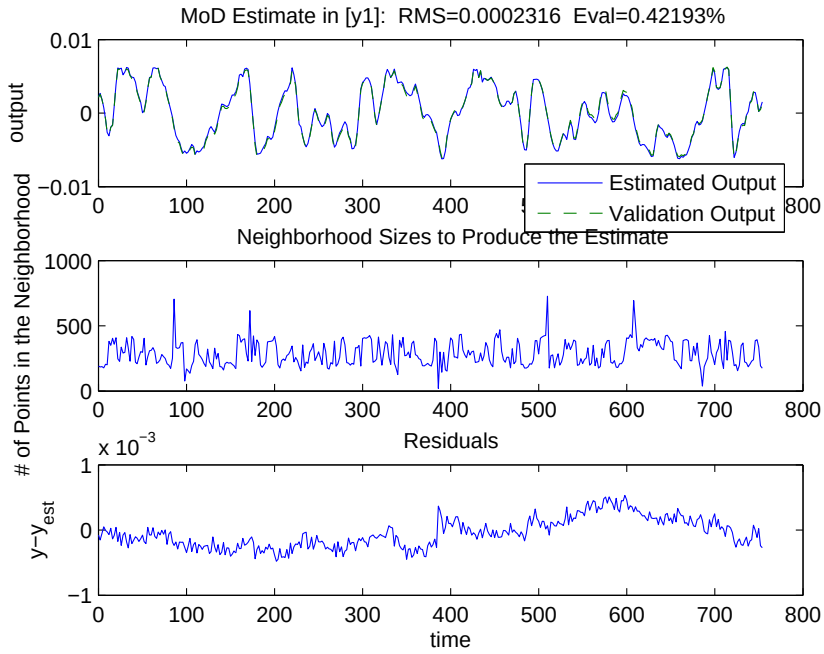

(a) Output 1 (y_1)

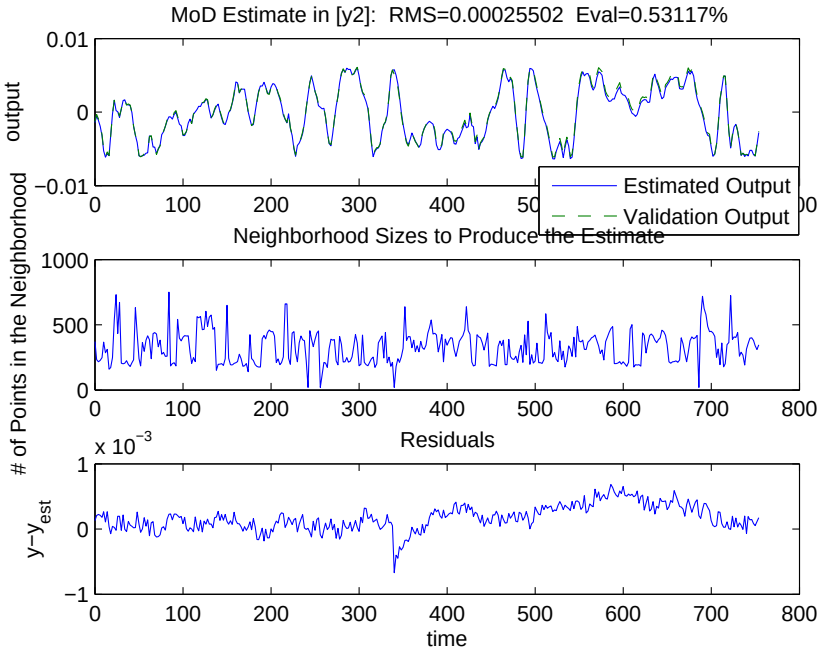

(b) Output 2 (y_2)

Figure 114. MoD estimation and validation results for Weischedel-McAvoy distillation column data resulting from a min CF (y) signal with modified zippered spectrum design

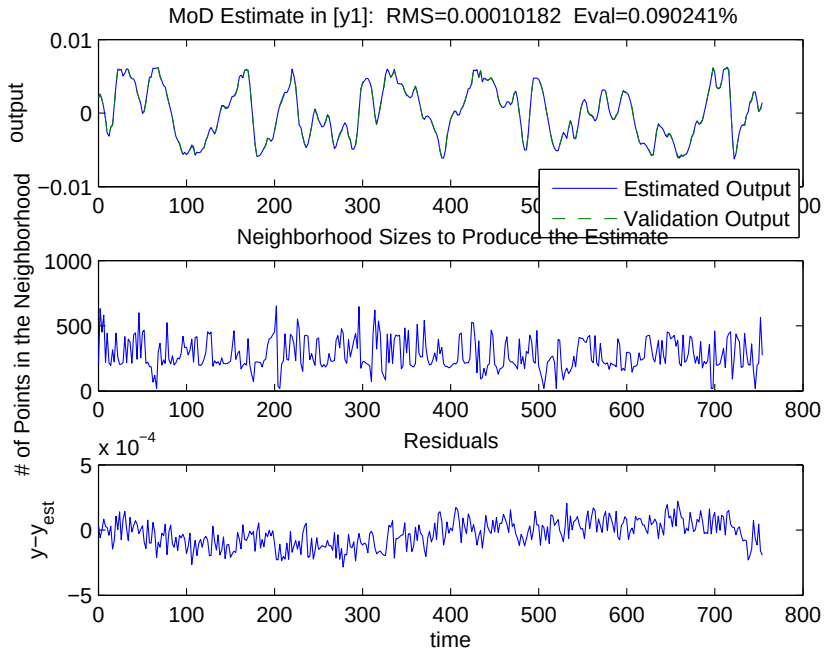

(a) Output 1 (y_1)

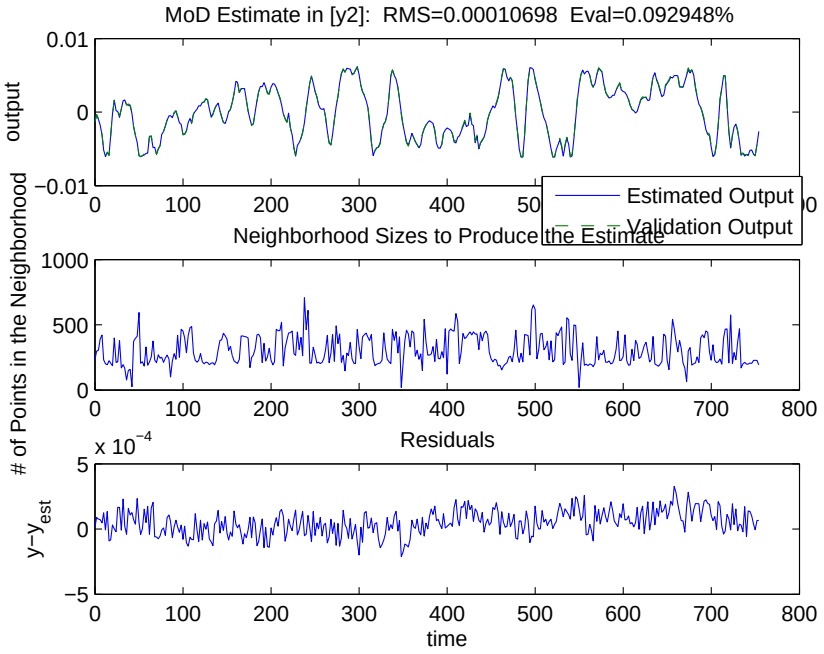

(b) Output 2 (y_2)

Figure 115. MoD estimation and and validation results for Weischedel-McAvoy distillation column data resulting from the Weyl-based signal design.

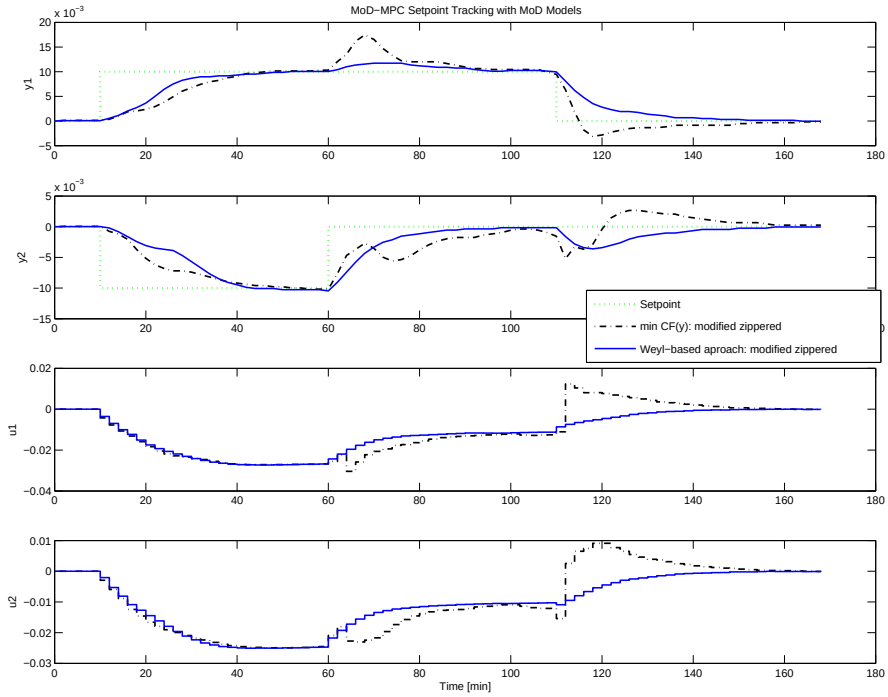

Figure 116. MoD-MPC closed-loop setpoint tracking test on the Weischedel-McAvoy distillation column using MoD Models from the min CF (*y*) signal (dashed) and Weyl-based (solid) signal designs. Controller parameters are PH=35, MH=15, Ywt=[1 0; 0 1] and Uwt=[7 0; 0 7]

5. Chapter Summary

In this chapter, we have presented a novel constrained optimization-based formulation of the multi-sine input signal problem. The objective function arises from the Weyl criterion, which seeks to minimize the geometric discrepancy of the output in the state-space. As a consequence, these signals can be used in support of data-centric estimation algorithms. A problem formulation that helps understand design variables in the Weyl objective is shown and illustrated via a numerical example, culminating in a case study demonstrating the effectiveness of the design procedure for a high purity distillation column, a challenging nonlinear, multivariable process system. Clearly, the power of the proposed framework lies in its flexibility, allowing the user to incorporate both linear and nonlinear models for output prediction, time-domain constraints, and information and control-theoretic frequency domain requirements. The use of state-of-the-art interior-point optimization methods enables the efficient solution of these nonlinear and nonconvex optimization problems.

CHAPTER 6

SUMMARY AND CONCLUSIONS

1. Summary

In this dissertation, we have presented the development of the identification test monitoring framework considering system identification and advanced process control applications targeted on multivariable systems. This framework interactively integrates plant-friendly, constrained minimum crest factor multisine signal design, control-relevant parameter estimation, and robust loopshaping. Such methods can play an important role in a decision tool set that can determine whether further testing is needed or not. The framework allows the user to initiate identification experimental testing based on limited *a priori* information of a system and a subsequent identification test that systematically refines process knowledge until model estimates meet the required control relevance and robustness. As a result, the user can obtain suitable model adequacy for advanced process control applications with shorter test duration in comparison with classical identification approaches.

The multisine input signal presents a flexible design capability, enabling plant-friendliness consideration by use of state-of-the-art constrained optimization techniques. A series of design guidelines for multi-channel multisine signals are derived in Chapter 2, comprising the phase-shifted, standard zippered, and modified zippered designs. The guideline works from single to large number of multiple channels with possible harmonic suppression for identifying nonlinear systems. The multisine input signal in this disser-

tation is able to generate informative inputs signals meaningful to highly interactive systems. The modified zippered spectrum design with the directional and power adjustments improves the gain directional estimation using the conventional open-loop identification test. Directional vectors obtained from a steady-state gain are utilized in the directional and power adjustments in order to amplify the low gain directionality in the output. The MPC closed-loop evaluation test indicates that models estimated from modified zippered designs under noisy conditions show improved control performance compared to models from conventional input designs.

The crest factor is widely used as a measurement of plant friendliness on input and output signals. Lowering the crest factor of a signal implies that it can cause minimal disruption, creating signal sequences located near the extreme values. The signal perturbation energy can increase without increasing the input magnitude span by applying minimum crest factor input signals. Move size, min/max bounds, and other restrictions in the speed of changes in inputs and/or outputs are enforced using constrained optimization techniques, appealing to plant-friendliness and keeping input move sizes small to satisfy actuator limits and minimize “wear and tear” on process equipment. The plant-friendly experimental testing keeps output deviations low to minimize variability in product quality – whenever identification test is in task, it tries not to disrupt the normal operation conditions.

A series of plant-friendly identification experiments are examined with the Weischedel-McAvoy distillation column, known as a strongly ill-conditioned and highly interactive process. Input signals via the modified zippered power spectrum are able to excite both the low and high-gain directions in the output. The models estimated from the open-loop data using modified zippered spectra display noticeable closed-loop control performance, which is less sensitive to model uncertainty under noisy conditions. In addition to linear ARX model estimation, NARX estimation is also examined with the Weischedel-McAvoy distillation column for improving prediction accuracy in the output. This improved accuracy makes it possible for the optimizer to constrain the outputs more precisely, satisfying user-specified time-domain requirements.

A control-relevant parameter estimation algorithm based on frequency response curvefitting is developed, taking advantage of the weighted least-squares method and matrix fractional description approximation. While minimizing the model errors between the frequency responses and the matrix polynomial model, the weights from closed-loop dynamics determine which frequency bandwidth is emphasized. Such control-relevant weights become an important key in redesigning input signals, which supports the concept of iterative identification test monitoring. The curvefitting procedure supports various multisine input designs, e.g., phase-shifted, standard zippered, and modified zippered multisine input signals with possible harmonic suppression frequency grids. It subsequently supports the frequency responses obtained using either ETFEs, spectral analysis, or high-order ARX model estimates. As a result, the nature of control-relevant curvefitting is very comprehensive, involving setpoint/input disturbances, closed-loop dynamics, and control performance requirements.

The process of systematic model refinement is the essence of the proposed identification test monitoring, as demonstrated in this dissertation. The integrated framework utilizes robust loopshaping to determine the model quality and ultimately assess whether to halt or continue experimental testing. Robust loopshaping is a numerical procedure that determines nominal operating conditions based on user-specified performance weights on a set of models with uncertainty descriptions. Naturally, there is an iterative procedure between control-relevant parameter estimation and robust loopshaping until a model estimate is arrived at that can meet robust stability and performance conditions. Specifically, the identification test monitoring procedure helps to accomplish plant-friendliness in identification testing. At the initial stage of modeling, crest factor minimization of inputs is performed with or without input constraints. As testing progresses, the optimizer generates multisine input signals constraining the predictions of the model estimated from the previous data, and this is meaningful for the model-based identification experimental testing. As the model is refined more accurately, the optimizer can more precisely constrain the outputs, improving plant-friendliness. Furthermore, the comprehensive framework of the identification test monitoring conveniently

provides all the necessary tools so that the user can easily perform the systematic model quality refinement. Within the framework, the identification analysis components are selected and connected for refining the process knowledge. Implemented in a GUI software platform (Lee and Rivera, 2006*b*), the framework can deliver its flexibility and applicability directly to the process engineer who seeks efficient methods of modeling for control with ease of use.

The illustration with Jacobsen-Skogestad high purity distillation column demonstrates the modeling effectiveness of identification test monitoring, addressing strong ill-conditioning, high interaction and gain directionality. Three stages of identification experimental testing are used to systematically improve gain directionality in model estimates – designing effective modified zippered signals. Specifically, the testing scenario progressively leads into effective and control-relevant input signals with shorter lengths. A number of testing cycles with a narrower bandwidth are considered to reduce uncertainty bound to a suitable level, applicable for robust loopshaping. In the end, a set of models are obtained that can meet required control relevance and robustness. In addition, a stable closed-loop identification test is performed when a nominally stable models and a controller are avalilable during the identification testing.

A comprehensive approach is considered for plant-friendly, constrained optimization-based input signal generation. A geometrical objective problem based on Weyl's theorem using multisine input signals is derived for data-centric algorithms achieving uniformity distribution in outputs, as needed in data-centric modeling such as the Model-on-Demand estimation method. The Weyl-based designs are shown to be superior to minimum crest factor designs, as illustrated with MoD-MPC control of the Weischedel-McAvoy nonlinear distillation column (1980).

2. Further Research Directions

The following items have been noted throughout this research and can extend current work. Using distillation column simulation models, an identification test monitoring procedure was demonstrated, tak-

ing advantage of standard and modified zippered multisine signals. The testing scenario shows the great applicability to highly interactive processes where the modified zippered spectrum is a powerful means for generating informative input signals. The directional and power adjustments are formulated in the frequency domain for correlated sinusoidal harmonics. Through Chapters 2, 4, and 5, we notice that we can select any arbitrary gain direction at each frequency grid over the bandwidth. Multivariable systems have multiple input gain directions ($u_1, u_2, ..., u_n$) with respect to n-dimension, where $u_1, u_2, ..., u_n$ input gain directions can be sequentially selected at each frequency grid using correlated harmonics with the power and phase adjustments, similar to the use of correlated harmonics in a modified zippered spectrum. This requires a new input power spectrum design since it allows correlated harmonics on all frequency grids. The new input power spectrum can naturally accommodate multiple low gain directions and more uniform output distribution in the state-space because the input signal design tries to balance all the gain directions. Large-scale dynamic systems provide an opportunity to examine the capability of the identification test monitoring procedure and understand pros and cons of the integrated framework.

In the identification test monitoring case study, the robust loopshaping procedure demanded a considerable number of testing cycles for reducing uncertainty bounds in order to satisfy conditions of robust stability and performance. A future research direction could involve addressing the conservativeness of the uncertainty bounds. Under a given noisy condition, uncertainty bounds will converge to a certain level with an increasing number of testing cycles. Improved estimation of uncertainty involving less cycles of data would be advantageous. It would also be advantageous if identification test monitoring could be accomplished without waiting for a full cycle of data.

During the iterative procedure between control-relevant parameter estimation and robust loopshaping, the MPC controller is tuned to satisfy robust loop bounds based on values of PH, MH, Ywt, and Uwt. PH and MH are the prediction and moving horizons, respectively, that can be selected based on time constants, settling time requirements, and process information; Ywt, the output weight, is often set to the unity.

However, Uwt, the input weight, is more critically selected to adjust the loop transfer functions of the system as to satisfy robustness conditions. An algorithm can be developed to automatically search satisfactory Uwt values for the MPC controller. For effective search convergence, the Uwt search should simultaneously meet the requirements of robustness conditions, nominal stability, and closed-loop performance.

The Weyl-based approach presented in Chapter 5 is achieved using a multisine design guideline for a zippered power spectrum. Initially, we tried the Weyl-objective following a modified zippered spectrum but later allowed greater freedom to the optimizer by introducing correlated harmonics at every frequency grid. The following items can be considered extensions from the current approach:

- A Weyl-based design with a phased-shifted multisine spectrum frequency grid. This can utilize the shortest input signal design guideline for a Weyl-based design without requiring the traditional phase-shifting technique among input channels.

- A Weyl-objective formulation for closed-loop identification tests. This requires that a controller transfer function is implemented in the optimizer so that uniform distribution in the output state-space can be achieved for a closed-loop experiment.

- An optimization formulation combining the Weyl-objective function with crest factor bounds on input and/or output signals. The achievement of uniform output distribution causes higher input and output crest factors. However, the user might want to trade-off these competing objectives. A multi-objective problem formulation would be highly desirable under these circumstances.

Examining these problems may demand longer computation efforts, faster computer processors, and more efficient nonlinear constrained optimization solvers. The result, however, is the capability.

The main results of this dissertation have been implemented using a Matlab-based graphical tool called CR-IDENT (Lee and Rivera (2006*b*) and Appendix). The tool takes the user through the various steps of multisine input signal design, frequency response estimation, and control-relevant parameter estimation,

culminating in robust loopshaping. Such a tool can be further interfaced to physical processes from unit operation processes to pilot plants, utilizing its full functionality of identifying multivariable systems.

The general insights from the identification test monitoring framework can be incorporated into more process monitoring tools. By updating a nominal model at a certain interval, we can determine whether the current model is in a set of models with an uncertainty description bound. If a model is not part of the uncertainty set, we may assume there is model variation or physical process change that merits the start of identification test monitoring. Additionally, statistical process analysis can be considered to predict or monitor the failure of a control system before it requires serious attention. We can integrate statistical methods for monitoring control system performance into the identification test monitoring framework. As a result, the framework will be widely acceptable for not only developing initial models but for maintaining models for high-performance control system applications during the life of process operations as well.

REFERENCES

Andersen, H.W. and M. Kümmel (1992). Evaluating estimation of gain directionality Parts 1: Methodology and 2: A case study of binary distillation. *J. Proc. Cont.* **2**, 59–86.

Barker, H. A. (1993). Design of multi-level pseudo-random signals for system identification. In: *Perturbation Signals For System Identification* (K. R. Godfrey, Ed.). pp. 321–347. Prentice Hall. Hemel Hempstead, Herts, UK.

Barker, H.A. and M.H. Al-Hilal (1985). Nonlinear system identification using pseudorandom signals with partillay orthogonal transforms. *Proceedings of the Seventh IFAC/IFORS Symposium on System Identification and System Parameter Estimation* pp. 415–420.

Bayard, David S. (1994). High-order multivariable transfer function curve fitting: Algorithms, sparse matrix methods and experimental results. *Automatica* **30**(9), 1439–1444.

Bayard, D.S. (1993*a*). Statistical additive uncertainty bounds using Schroeder-phased input design. *Applied Mathematics and Computation* **58**, 169–198.

Bayard, D.S. (1993*b*). Statistical plant set estimation using schroeder-phased multisinusoidal input design. *App. Math. and Comp.* **58**, 169–198.

Bayard, D.S. and F.Y. Hadaegh (1994). Multivariable plant set estimation using multisinusoidal input designs. In: *SYSID'94, 10th IFAC Symposium on System Identification*. Vol. 2. Copenhagen, Denmark. pp. 207–211.

Braatz, R.D, M. Morari and J.H. Lee (1991). Necessary/sufficient loopshaping bounds for robust performance. In: *AIChE Annual Meeting, Los Angeles, CA*. paper 154d.

Braun, Martin W. (2001). Model-on-Demand nonlinear estimation and Model Predictive Control: Novel methodologies for process control and supply chain management. PhD thesis. Dept. of Chemical and Materials Engineering, Arizona State University.

Braun, M.W., A. Stenman and D.E. Rivera (2002*a*). Model-on-Demand Model Predictive Control Toolbox. `http://www.eas.asu.edu/~csel/Software.htm`.

Braun, M.W., D.E. Rivera and A. Stenman (2000). Model-On-Demand Model Predictive Control for nonlinear process systems. *2000 AIChE Annual Meeting* **256h**, 1 – 40.

Braun, M.W., D.E. Rivera and A. Stenman (2001). A Model-on-Demand identification methodology for nonlinear process systems. *Int. J. Control* **74**(18), 1708–1717.

Braun, M.W., R. Ortiz-Mojica and D.E. Rivera (2002*b*). Application of minimum crest factor multisinusoidal signals for "plant-friendly" identification of nonlinear process systems. *Control Engineering Practice* **10**, 301.

Briggs, P.A.N. and K.R. Godfrey (1966). Pseudorandom signals for the dynamic analysis of multivariable systems. *Proc. IEE*. **113**, 1259.

Butoyi, F. and Y. Zhu (2002). Case studies on closed-loop identification for MPC. *Control Eng. Practice* **10**, 403–417.

Byrd, R., J.C. Gilbert and J. Nocedal (2000). A trust region method based on interior point techniques for nonlinear programming. *Mathematical Programming* **A(89)**, 149–185.

Byrd, R., M.E. Hribar and J. Nocedal (1999). An interior point method for large scale nonlinear programming. *SIAM J. Optim*. **9**, 877–900.

Callafon, R.A., D. de Roover and P.M.J. Van den Hof (1996). Multivariable least squares frequency domain identification using polynomial matrix fraction descriptions. **2**, 2030–2035.

Chien, I-Lung and B. Ogunnaike (1992). Modeling and control of high-purity distillation columns. In: *AIChE Annual Meeting, Miami Beach, FL*. paper2a.

Chou, C.T., H.H.J. Bloemen, V. Verdult, T.T.J. van den Boom, T. Black and M. Verhagen (2000). Nonlinear identification of high purity distillation columns. ThAM2-2.

Cybenko, G. (1996). Just-in-time learning and estimation. In: *Identification, Adaptation, Learning* (S. Bittani and G. Picci, Eds.). pp. 423–434. NATO ASI. Springer.

de Callafon, R.A. (1998). Feedback Oriented Identification for Enhandced and Robust Control: a fractional approach applied to a wafer stage. PhD thesis. Delft University. Delft, Netherlands.

Doyle, F.J., R.S. Parker, R.K. Pearson and B.A. Ogunnaike (1999). Plant-friendly identification of second-order volterra models. In: *European Control Conference*. Karlsruhe, Germany.

Duym, S. and J. Schoukens (1995). Design of excitation signals for the restoring force surface method. *Mechanical Systems and Signal Processing* **9**(2), 139–158.

Eskinat, E., S. H. Johnson and W. L. Luyben (1991). Use of hammerstein models in identification of nonlinear systems. *AIChE Journal* **37(2)**, 255–268.

Fasol, K.H. and H.P. Jörgl (1980). Principles of model building and identification. *Automatica* **16**, 505–518.

Gaikwad, S.V. and D.E. Rivera (1996). Control-relevant input signal design for multivariable system identification: application to high purity distillation control. *IFAC World Congress,San Francisco, C.A.* **M**, 349–354.

Gaikwad, S.V. and D.E. Rivera (1997). Multivariable frequency-response curve fitting with application to control-relevant parameter estimation. *Automatica* **33**(4), 1169–1174.

Gevers, M.R. (1986). ARMA models, their Kronecker indices and their McMillan degree. *Int. J. Control* **43**, 1745–1761.

Godfrey, K., Ed.) (1993). *Perturbation Signals For System Identification*. Prentice Hall International (UK) Limited. Hertfordshire, UK.

Godfrey, K.R., H.A Barker and A.J. Tucker (1999). Comparison of perturbation signal for linear system identification in the frequency domain. *IEE. Proc. Control Theory Appl.* **146**, 535.

Guillaume, P., J. Schoukens, R. Pintelon and I. Kollár (1991). Crest-factor minimization using nonlinear Chebyshev approximation methods. *IEEE Trans. on Inst. and Meas.* **40**(6), 982–989.

Hjalmarsson, H. (2005). From experiment design to closed-loop control. *Automatica* **41**, 393–438.

Hussain, M.A. (1999). Review of the applications of neural networks in chemical process control-simulation and on-line implementation. *Artificial Intelligence in Engineering* **13**(1), 55–68.

Jacobsen, E.W. (1994). Identification for control of strongly interactive plants. In: *Annual AIChE Metting*. San Francisco, CA. paper 226ah.

Jacobsen, E.W. and S. Skogestad (1994). Inconsistencies in dynamic models for ill-conditioned plants application to low-order models of distillation columns. *Ind. Eng. Chem. Res.* **33**, 631–640.

Jenkins, G.M. and D.G. Watts (1968). *Spectral Analysis and its applications*. Holden-Day. San Francisco, CA.

Kothare, S. and J.A. Mandler (2003). Fast plant testing for model-based control. In: *Annual AIChE 2003 Meeting*. San Francisco, CA. paper 436b.

Koung, C.W. and J.F. MacGregor (1993). Design of identification experiments for robust control: A geometric approach for bivariate processes. *Ind. Eng. Chem. Res.* **32**, 1658–1666.

Koung, C.W. and J.F. MacGregor (1994). Identification for robust multivariable control: the design of experiments. *Automatica* **30**(10), 1541–1554.

Lee, H. and D.E. Rivera (2005). Control relevant curvefitting for plant-friendly multivariable system identification. In: *2005 American Control Conference*. Portland, OR. pp. 1431–1436.

Lee, H. and D.E. Rivera (2006*a*). An integrated input signal design and control-relevant parameter estimation approach for highly interactive multivariable systems. In: *2006 American Control Conference*. Minneapolis, MN. pp. 1665–1670.

Lee, H. and D.E. Rivera (2006*b*). CR-IDENT: a Matlab toolbox for multivariable control-relevant system identification. In: *14th IFAC Symposium on System Identification (SYSID 2006)*. Newcastle, Australia. pp. 708 – 713.

Lee, H., D.E. Rivera and H. Mittelmann (2003). Constrained minimum crest factor multisine signals for plant-friendly identification of highly interactive systems. In: *13th IFAC Symp. on System Identification*. Rotterdam. pp. 947–952.

Li, W. and J.H. Lee (1996*a*). Control relevant identification of ill-conditioned systems: estimation of gain direcionality. *Comp. Chem. Eng.* **20**, 1023–1042.

Li, W. and J.H. Lee (1996*b*). Frequency-domain closed-loop identification of multivariable systems for feedback control. *AIChE* **42**, 2813–2827.

Lindskog, P. (1996*a*). Methods, Algorithms, and Tools for System Identification Based on Prior Knowledge. PhD thesis. Linköping University, Sweden. Dept. of Electrical Engineering.

Lindskog, Peter (1996*b*). A system identification software tool for general miso arx-type of model structures. Technical Report LiTH-ISY-R-1918. Dept of EE. Linkping University. S-581 83 Linkping, Sweden.

Ljung, L. (1999). *System Identification: Theory for the User*. 2nd ed.. Prentice-Hall. New Jersey.

Ljung, L. and T. Glad (1994). *Modeling of Dynamic Systems*. Prentice-Hall. New Jersey.

Mathur, U. and R.J. Conroy (2002). Multivariable control without plant tests. In: *Annual AIChE 2002 Meeting*. Indianapolis, IN. paper 254g.

Matousek, J. (1999). *Geometric Discrepancy: An Illustrated Guide*. Springler-Verlag. Berlin.

Meadows, E.S. and J. Rawlings (1997). *Nonlinear process control*. Chap. Model predictive control, pp. 233–310. Prentice Hall PTR. Upper Saddle Rivera, NJ.

Morari, M. and E. Zafiriou (1988). *Robust Process Control*. Prentice-Hall. Englewood Cliffs, N.J.

Morari, M. and J.H. Lee (1999). Model Predictive Control: past, present and future. *Computers and Chemical Engineering* **23**, 667–682.

Narasimhan, S., S. Rengaswamy and R. Rengasamy (2003). Multiobjective input signal design for plant-friendly identification. In: *13th IFAC Symposium on System Identification (SYSID 2003)*. Rotterdam, The Netherlands. pp. 924 – 928.

Ogunnaike, B.A. and W.H. Ray (1994). *Process Dynamics, Modeling, and Control*. Oxford University Press. New York.

Ortiz-Mojica, Raul (2000). Minimum crest factor input design for plant-friendly identification of process systems. Master's thesis. Arizona State University. Tempe, Arizona, U.S.A.

Parker, R.S., D. Heemstra, J.D. Doyle III, R.K. Pearson and B.A. Ogunnaike (2001). The identification of nonlinear models for process control using tailored "plant-friendly" input sequences. *J. of Process Control* **11**(2), 237–250.

Pearson, R.K. and B.A. Ogunnaike (1997). *Nonlinear Process Control*. Chap. Nonlinear Process Identification, pp. 11–110. Prentice Hall. Upper Saddle River, NJ.

Pearson, Ronald K. (1999). *Discrete-Time Dynamic Models*. Oxford University Press, Inc.. New York.

Pendse, G.V. (2004). Optimization-based formulations using the Weyl criterion for input signal design in system identification. Master's thesis. Arizona State University. Tempe, AZ, U.S.A.

Prett, D.M. and C.E. García (1988). *Fundamental Process Control*. Butterworth. Stoneham, M.A.

Rivera, D.E. and K.S. Jun (2000). An integrated identification and control design methodology for multivariable process system applications. *IEEE Control Systems Magazine* **20**, 25–37.

Rivera, D.E. and M. Morari (1987). Control-relevant model reduction problems for siso h_2, h_∞, and μ-controller synthesis. *Int. J. Control* **46**(2), 505–527.

Rivera, D.E. and S.V. Gaikwad (1995). Systematic techniques for determining modeling requirements for SISO and MIMO feedback control problems. *Journal of Process Control* **5**(4), 213–224.

Rivera, D.E., H. Lee, M.W. Braun and H.D. Mittelmann (2003). Plant-friendly system identification: a challenge for the process industries. In: *13th IFAC Symposium on System Identification (SYSID 2003)*. Rotterdam, Netherlands. pp. 917–922.

Rivera, D.E., J.F. Pollard and C.E. García (1992). Control-relevant prefiltering: A systematic design approach and case study: Special issue on system identification for robust control design. *IEEE Trans. Autom. Cntrl.* **37**, 964–974.

Rivera, D.E., M.W. Braun and H.D. Mittelmann (2002). Constrained multisine inputs for plant-friendly identification of chemical process. In: *15th IFAC World Congress, Barcelona, Spain*. paper T-We-A11.

Rivera, D.E., S. Zong and W.M. Ling (1997). A control-relevant multivariable system identification methodology based on orthogonal multifrequency input perturbations. In: *IFAC Symposium on System Identification (SYSID'97), Fukuoka, Japan*. pp. 595–600.

Sanathanan, C.K. and J. Koerner (1963). Transfer function synthesis as a ratio of two complex polynomials. *IEEE Trans. Autom. Control* **9**, 56–58.

Schroeder, M.R. (1970). Synthesis of low-peak-factor signals and binary sequences with low autocorrelation. *IEEE Trans. Info. Theory* **IT-16**, 85–89.

Skogestad, S. and I. Postlethwaite (1996). *Multivariable feedback control: analysis and design*. Wiley. New York, NY.

Skogestad, S. and M. Morari (1988*a*). LV-control of a high-purity distillation column. *Chem. Eng. Sci.* **43**, 33.

Skogestad, S. and M. Morari (1988*b*). Understanding the dynamic behavior of distillation columns. *Ind. Eng. Chem. Res.* **27**, 1848–1862.

Söderström, T. and P. Stoica (1989). *System Identification*. Prentice Hall, Inc.. University Press, Cambridge.

Sriniwas, G. Ravi, Y. Arkun, I-Lung Chien and B.A. Ogunnaike (1995). Nonlinear identification and control of a high-purity distillation column: a case study. *J. Proc. Cont.* **5**, 149.

Stec, P. and Y. Zhu (2001). Some study on identification of ill-conditioned processes for control. In: *Proc. of the ACC, Arlington, VA*. pp. 1202–1207.

Stenman, A. (1999). Model on Demand: Algorithms, Analysis and Applications. PhD thesis. Linköping University, Linköping University, Sweden.

Stenman, A., F. Gustafsson and L. Ljung (1996). Just-in-time models for dynamical systems. In: *Proceedings of the IEEE Conference on Decision and Control*. Kobe, Japan. pp. 1115–1120.

Stenman, A., F. Gustafsson, D.E. Rivera, L. Ljung and T. McKelvey (2000). On adaptive smoothing of empirical transfer function estimates. *Control Engineering Practice* **8**(2), 1309–1315.

Stoica, P. and R. Moses (1997). *Introduction to Spectral Analysis*. Prentice Hall, Inc.. Upper Saddle Rivera, NJ.

Su, H.T. and T.J. McAvoy (1997). *Nonlinear Process Control*. Chap. Artificial nueral networks for process identification and control. Prentice Hall. Upper Saddle River, NJ.

Varga, E.I. and S.B. Jørgensen (1994). Multivariable process identification: estimating gain directions. In: *1994 AIChE Annual Meeting*. San Francisco, CA. paper 226f.

Van den Hof, P.M.J. (1992). System order and structure indices of linear systems in polynomial form. *Int. J. Control* **55**, 1471–1490.

Van den Hof, P.M.J. and R.J.P. Schrama (1995). Identification for control – closed-loop issues. *Automatica* **31**(12), 1751–1770.

Waechter, A. and L.T. Biegler (2000). Failure of global convergence for a class of interior point methods for nonlinear programming. *Math. Progr.* **88**, 565–574.

Weischedel, K. and T.J. McAvoy (1980). Feasibility of decoupling in conventionally controlled distillation columns. *Ind. Eng. Chem. Fund.* **19**, 379.

Weyl, H. (1916). Über die gleichverteilung von zahlen mod eins. *Math. Ann.* **77**, 313–352.

Worden, K., C.X. Wong, U. Parlitz, A. Hornstein, D. Engster, T. Tjahjowidodo, F. Al-Benderc, D.D. Rizosd and S.D. Fassois (2006). Identification of pre-sliding and sliding friction dynamics: Grey box and black-box models. *Mechanical Systems and Signal Processing* p. in press.

Zhou, K. and J.C. Doyle (1998). *Essentials of Robust Control*. Prentice Hall. Upper Saddle River, NY.

Zhu, Y. (1989). Black-box identification of mimo transfer functions: Asymptotic properties of prediction error models. *Int. J. of Adaptive Control and Signal Processing* **3**, 357–373.

Zhu, Y. (2006). System identification for process control: Recent experience adn outlook. In: *Proc. of the 14th IFAC Symposium on System Identification, Newcastle, Australia*. Newcastle, Australia. pp. 20–32.

Zhu, Yucai (2001). *Multivariable System Identification for Process Control*. Pergamon. Amsterdam.

APPENDIX A

SOFTWARE PACKAGE: CR-IDENT TOOLBOX

This describes CR-IDENT, a Matlab-based toolbox that implements a comprehensive procedure for multivariable control-relevant system identification aimed primarily at process system applications. The toolbox consists of modules for multivariable input signal design (multisine and PRBS), frequency response estimation, control-relevant frequency response curvefitting, and robust loopshaping, leading to models whose end use is the design of high-performance control systems. An important component in the implementation of this design procedure is its reliance on *a priori* knowledge of the system of interest to design input signals meeting both theoretical and practical user requirements. Based on recent research activities in the Control Systems Engineering Laboratory at Arizona State University, CR-IDENT is a Matlab-based toolbox that implements a comprehensive procedure for multivariable control-relevant system identification with these goals in mind.

Although aimed primarily at process system applications, the methodology is broadly-applicable and can be useful in multiple application domains. The modules in the CR-IDENT can be used independently or as part of an integrated procedure of identification test monitoring. This toolbox is designed using Matlab R14 with Service Pack 3 (Version 7.1) and requires the Signal Processing, Control System, System Identification, Model Predictive Control, and Robust Control Toolboxes as well as Simulink. The most updated CR-IDENT toolbox and its documents can be accessed from the ASU-CSEL website using the link: **http://www.fulton.asu.edu/csel/Software.html**.

1. CR-IDENT: A Matlab-Based Toolbox

Invoking the command

```
>> crident
```

calls a general menu (see Figure 117) with options corresponding to each of the three GUIs that comprise CR-IDENT. Salient aspects for each GUI module are briefly described in the following.

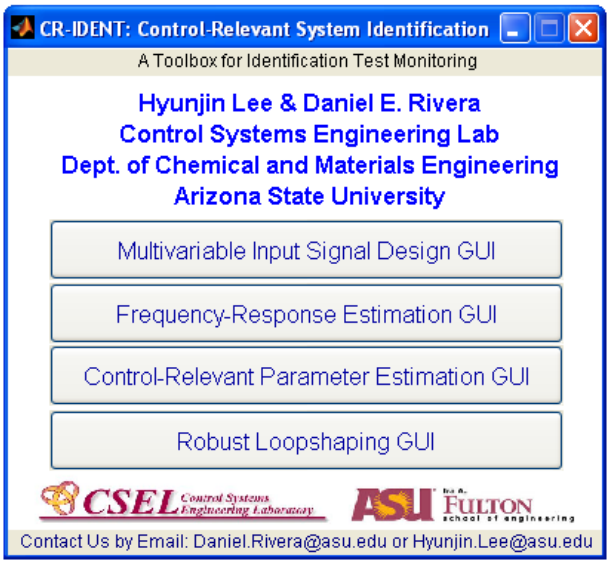

Figure 117. Main GUI for CR-IDENT, a toolbox for multivariable control-relevant identification.

2. Multivariable Multisine Input Signal Design

The principal design guideline implemented in CR-IDENT uses *a priori* knowledge of dominant time constants of the system and speed of the response specifications to define a primary bandwidth for excitation in the signal. This bandwidth is translated into a series of inequalities that determine the number of sinusoids (n_s), sequence length (N_s), and sampling time (T_s). For users not wishing to use these guidelines, the input GUI supports direct parameter specification with a verification routine to insure proper implementation. The input design GUI (Figure 118) offers various options for multi-channel implementation such as phase-shifted, orthogonal ("zippered") spectrum, and modified zippered spectrum designs. For all multisine signal choices shown in Figure 118, the phases can be obtained either through the closed-form formula by Schroeder (1970) or though the iterative *p*-norm optimization approach that minimizes crest factor developed by Guillaume *et al.* (1991).

3. Frequency-Response Estimation

The Frequency-Response Estimation GUI (Figure 119) enables the computation of frequency responses from multisine-generated data using both parametric and non-parametric approaches. The Empirical Transfer Function Estimate (ETFE) and Spectral Analysis (SA) methods are used for non-parametric estimation, while high-order ARX models are utilized for parametric frequency-response estimates. For noisy ETFE responses, a Model-on-Demand curve smoothing algorithm by Stenman *et al.* (2000) is available.

4. Control-Relevant Curvefitting

The goal of the control-relevant frequency-response curvefitting GUI (Figure 120) is to optimally estimate a useful parametric model with satisfactory control-relevance which can be used as a nominal for Model Predictive Control (MPC). The control-relevant curvefitting algorithm approximates frequency-responses into parsimonious discrete-time state-space model representations based on linear Matrix Fractional Descriptions (MFD) by relying on frequency-dependent pre- and post- weight functions meaningful to MPC control (Rivera and Gaikwad, 1995). If a closed-loop Simulink model is available, users can test the estimated model with respect to setpoint tracking directly from the GUI.

5. Robust Loopshaping GUI

The goal of Robust Loopshaping GUI is to design a set of models that can meet the requirements of robust stability and performance for a given set of data. Figure 121 shows the necessary components for this robust loopshaping procedure. The robustness bounds for the sensitivity and complementary sensitivity functions involve performance weight(s) and uncertainty bounds. Those conditions of robust stability and performance are computed using Structured Singular Value analysis. For successful robust control system

design, the users are required to take iterative steps between control-relevant parameter estimation and robust loopshaping while following a procedure of identification test monitoring.

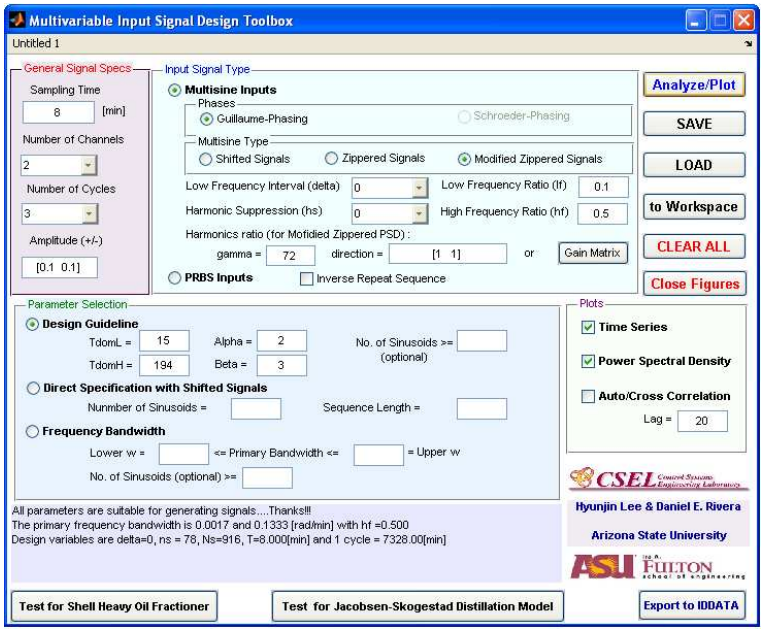

Figure 118. Multivariable Input Signal Design GUI in CR-IDENT.

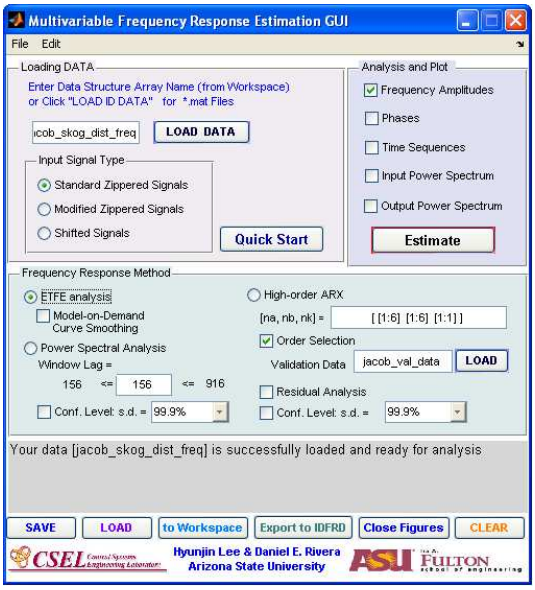

Figure 119. Frequency-Response Estimation GUI.

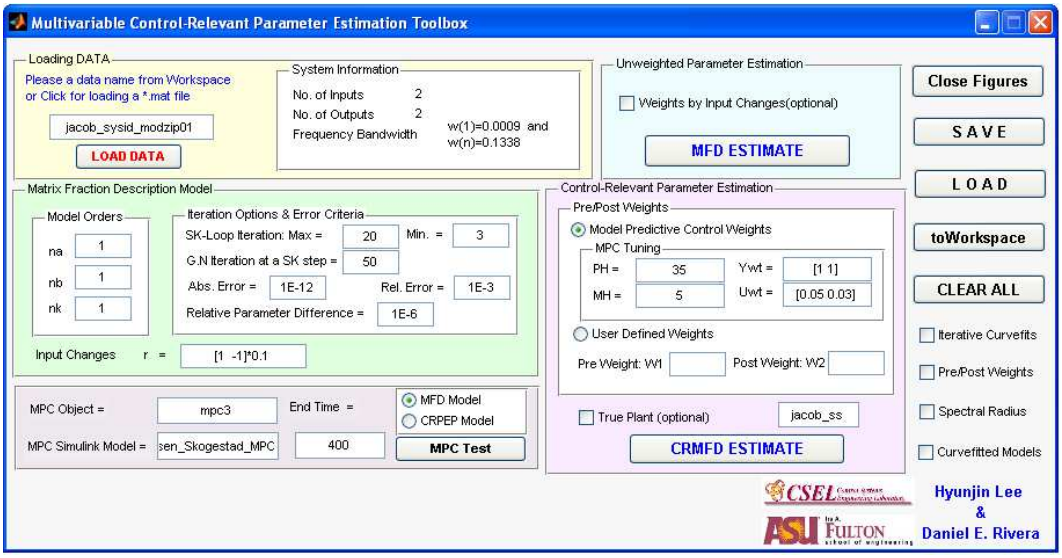

Figure 120. Control-Relevant Parameter Estimation GUI.

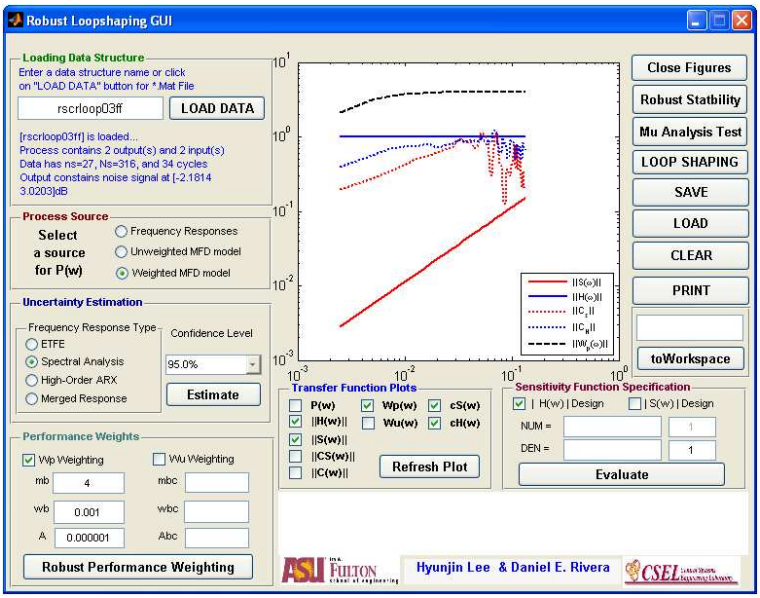

Figure 121. Robust Loopshaping GUI.